

Ground Penetrating Radar Principles, Procedures & Applications

A. P. Annan

Copies of these notes are available on CD in PDF format from Sensors & Software Inc. for a fee of \$50.00 plus shipping and handling. If you wish to obtain copies of these notes, please fill in the information indicated here and send with a cheque, money order or credit card information to Sensors & Software Inc.

PLEASE FILL OUT AND FAX BACK

Name: _____

Company: _____

Address: _____

City: _____ Prov/State: _____ Postal/Zip Code: _____

Phone Number: () _____ Fax Number: () _____

E-mail: _____

Product/Equipment Requested: Ground Penetrating Radar Principles, Procedures & Applications

METHOD OF PAYMENT

  Cheque

Do Not Send Cash By Mail

VISA/MC #: _____

NAME OF PERSON AS IT APPEARS ON CARD:

EXPIRATION DATE: _____

SIGNATURE: _____

(For Credit Card Payments Only)

Table of Contents

1	Introduction	1
1.1	What is GPR?	1
1.2	History	3
1.3	Current Activities & Future Developments	7
1.4	Summary	8
2	Basic Electromagnetic Theory	9
2.1	Overview	9
2.2	Maxwell's Equations	9
2.3	Constitutive Equations	12
2.4	Wave Nature of EM Fields	13
2.5	Low Loss – Damped EM Wave Conditions	17
2.6	Sinusoidally Time Varying Fields	20
2.7	Electromagnetic Impedance	21
2.8	Polarization	23
2.9	EM Fields From Sources	26
2.10	Far Field Approximation	29
2.11	Antenna Patterns, Directivity, Gain	30
3	Physical Properties I	35
3.1	Why are Physical Properties Important?	35
3.2	Conduction Currents	35
3.3	Displacement (Polarization) Currents	37
3.4	Total Current Flow	39
3.5	Magnetic Permeability	40
3.6	Complex Materials	45
3.7	Electrical Properties of Water	50
3.8	Real GPR Examples	52
3.8.1	DNAPL Spill	52
3.8.2	Conductive Contaminant	53

4	EM Wave Properties	55
4.1	Wavefronts and Rays	55
4.2	Wave Properties	55
4.3	GPR Plateau	58
4.4	Material Interfaces	59
4.5	Snell's Law	59
4.6	Critical Angle	60
4.7	Fresnel Reflection Coefficients	61
4.8	Thin Layer Reflection	65
4.9	Plane Wave Model for Finite Sources	68
4.10	GPR Source Near an Interface	71
4.11	Resolution and Zone of Influence	74
4.12	Scattering from a Localized Object	79
4.13	Scattering Attenuation	82
4.14	Propagation Dispersion	84
5	GPR Instrumentation	89
5.1	GPR Measurement Objectives	89
5.2	Fundamental Physics	89
5.3	GPR Timing and Resolution	92
5.3.1	Timing	92
5.3.2	Resolution and Bandwidth	92
5.4	GPR Bandwidth	95
5.5	System Elements & Characterization	97
5.6	GPR Signal Acquisition	98
5.6.1	Correlation Acquisition GPR	99
5.6.2	Frequency Domain Mixer GPR	99
5.6.3	Equivalent Time sampling GPR	101
5.6.4	Common Signal Capture Issues	102
5.7	Real-Time Signal Processing Fundamentals	103
5.7.1	Deconvolution	103
5.7.2	GPR Wavelet Model	104
5.8	System Performance Factor	106

5.9	Signal Amplitude & Recording Dynamic Range	107
5.9.1	Characterizing System Response	107
5.9.2	Dynamic Range	111
5.9.3	Summary	114
5.10	Centre Frequency and Bandwidth	115
5.11	Antennas	117
5.11.1	Dipole Impulse Response or Transfer Function	118
5.11.2	Antenna Directivity	119
5.11.3	Shielding	122
6	Modelling of GPR Responses	127
6.1	The Purpose of Modelling	127
6.2	GPR Modelling Types & Definitions	127
6.3	One-dimensional (1D) Modelling	128
6.3.1	Radar Range Equation (RRE)	128
6.3.2	One-Dimensional (1D) Layered Earth	129
6.4	Two-Dimensional (2D) Modelling	130
6.4.1	Ray Tracing	130
6.4.2	FK 2D Modelling	132
6.4.3	Full Finite Difference (FD) Solutions	133
6.4.4	2½ D Solutions	133
6.5	Three-Dimensional (3D) Modelling	133
6.5.1	3D Ray Tracing	133
6.5.2	3D Finite Difference Modelling	133
6.5.3	Integral Equation – Equivalent source Scattering	135
6.6	Inversion	136
7	Survey Design	139
7.1	Evaluating GPR Suitability	139
7.2	Reflection Survey Design	145
7.2.1	Selecting Operating Frequency	146
7.2.2	Estimating the Time Window	148
7.2.3	Selecting Temporal Sampling Interval	149
7.2.4	Selecting Station Spacing (Spatial Sampling Interval)	149

7.2.5	Selecting Antenna Separation	151
7.2.6	Survey Grid and Coordinate System	152
7.2.7	Selecting Antenna Orientation	153
7.3	CMP/WARR Velocity Sounding Design.	154
7.4	3D Survey Design	156
7.5	Borehole Survey Design	156
8	Data Processing	157
8.1	Data Editing	158
8.2	Basic Processing	159
8.2.1	Dewow	159
8.2.2	Time Gain.	159
8.2.3	Temporal and Spatial Filtering	163
8.2.4	Discussion.	166
8.3	Advanced Data Processing	166
8.3.1	Attributes	167
8.3.2	Deconvolution	168
8.3.3	Background Subtraction.	168
8.3.4	Velocity Analysis from CMP	169
8.3.5	Discussion.	169
8.4	Visual/Interpretation Processing	170
8.4.1	Migration	170
8.4.2	Event Picking	171
8.4.3	Volume Visualization	172
8.5	Discussion	173
8.6	Final Words.	175
9	Interpretation, Concepts & Pitfalls	177
9.1	Gradational Interfaces	177
9.2	Velocity Determination Using Hyperbolic Fitting.	180
9.3	Polarity.	183
9.4	Airwave Events.	185
9.5	X Marks the Spot	188

9.6	Plastic Water Pipe Diameter Determination	190
9.7	Antenna Shielding	193
9.8	Ringling on Radar Records	196
9.9	GPR Time Zero & Depth Estimates	200
9.10	GPR Antenna Elevation	202
9.11	Determining Layer Thickness & Velocity from CMP Data	205
9.11.1	Analysis Procedure	205
9.11.2	Intercept Time & RMS Velocity Conversion to Depth & Interval Velocity ..	209
9.11.3	Direct Air Wave & Ground Wave	210
9.11.4	Summary	210
9.12	CMP Analysis	211
10	Case Studies	213
10.1	Mining & Quarrying	213
10.2	Geotechnical & Environmental	218
10.3	Forensic & Archeology	231
10.4	Buried Utilities	240
10.5	Structure Assessment (NDT)	245
10.6	Military, Law Enforcement & Espionage	262
10.7	Bio Applications	263
10.8	Snow & Ice	264
10.9	Educational material	269
11	References	271

1 INTRODUCTION

Ground penetrating radar (GPR) is a relatively new geophysical technique. The last decade has seen major advances as the technology matures. The history of GPR is intertwined with the diverse applications of the technique. GPR has the most extensive set of applications of any geophysical technique leading to a wide range of application spatial scales and concomitant diversity of instrument configurations.

This document is intended to introduce the physical principles underpinning GPR and provide practical guidance to users of the method.

1.1 WHAT IS GPR?

Before delving into the history, GPR needs definition. GPR uses electromagnetic fields to probe lossy dielectric materials to detect structures and changes in material properties within the materials (Davis & Annan (1989)). Reflection and transmission measurements, as depicted in Figure 1-1, are employed. Most applications to date have been in natural geologic materials, but widespread use also occurs for man-made composites such as concrete, asphalt and other construction materials. In lossy dielectric materials, electromagnetic fields can penetrate to a limited depth before being absorbed. Hence, penetration is always an issue.

With GPR, the electromagnetic fields propagate as essentially non-dispersive waves. The signal emitted travels through the material, is scattered and/or reflected by changes in impedance giving rise to events which appear similar to the emitted signal. In other words, signal recognition is simple because the return signal looks like the emitted signal. Figure 1-2 depicts the general nature of GPR reflection profiling. Figure 1-3 shows the GPR response of two road tunnels.

GPR field behavior occurs over a finite frequency range generally referred to as the GPR plateau where velocity and attenuation are almost frequency independent. The GPR plateau usually occurs in the 1 MHz to 1000 MHz frequency range. At lower frequencies the fields become diffusive in character and pulses are dispersed. At higher frequencies several factors increase signal absorption such that penetration is extremely limited.

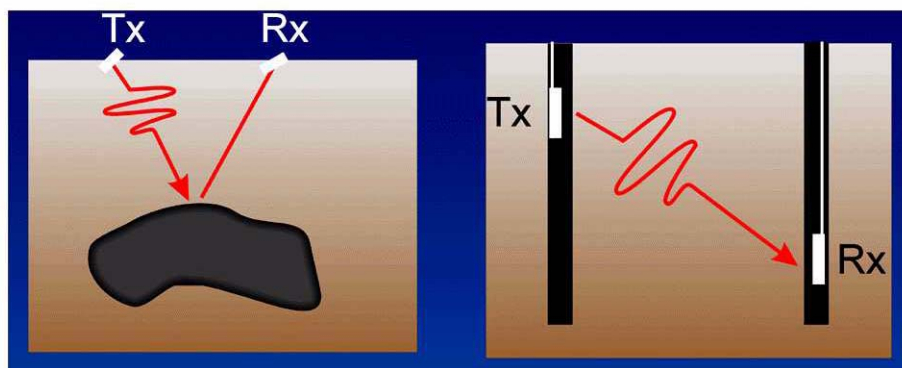


Figure: 1-1 Ground penetrating radar uses radio waves to probe the subsurface of lossy dielectric materials. Two modes of measurement are common. In the first, detection of reflected or scattered energy is used. In the second, variation after transmission through the material is used to probe a structure.

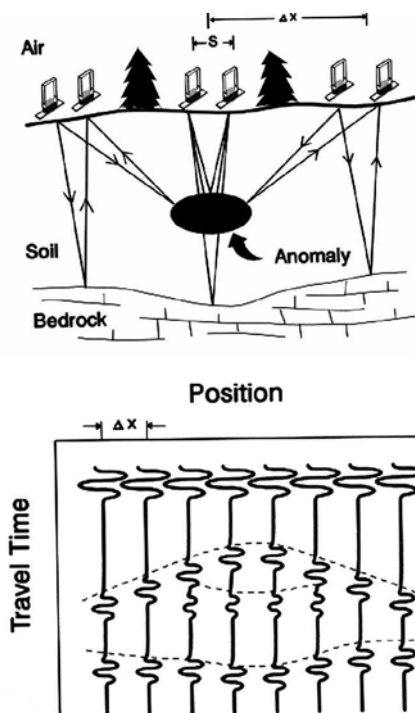


Figure: 1-2 In reflection mode, a GPR instrument is normally moved along a survey line acquiring responses at regular intervals which are used to create a cross sectional image of the ground.

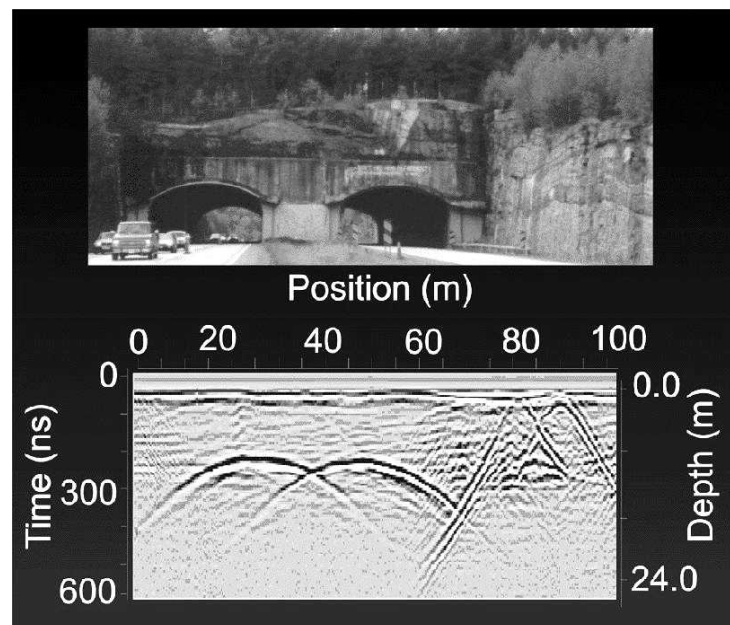


Figure: 1-3 GPR cross section obtained with a 50 MHz system traversed over two road tunnels.

1.2 HISTORY

The following is necessarily brief and intended to give high lights. References lead to other perspectives for those interested in a more extensive understanding of GPR. It is interesting to note that accounts of some activities are published many years later and sometimes not all.

1900 – 1950

During this time a great deal of research on radio wave propagation above and along the surface of the earth occurred. Although several hints at the possibility of using radio waves to probe the subsurface are mentioned, there are no reports of successfully making this type of measurement. Vast number of papers appeared on the subject of communications, direction finding and radar.

1950 – 1955

In this time frame, the first reported attempt at measuring subsurface features with radio wave signals was reported. El Said (1956) attempted to use the interference between direct air transmitted signals and signals reflected from the water table to image the water table depth.

1955 – 1960

The next reported observation of radio frequency sounding of geological materials came about when the USAF reported altimeter errors when attempting to land aircraft on the Greenland ice sheet (Waite and Schmidt (1961)). This was the first time that repeatable indications of penetration into the subsurface through a naturally occurring material were reported. This spawned the era of researchers focused on developing radio echo sounding in ice.

1960 – 1965

The majority of activity during this interval involved the radio echo sounding in ice. Groups, such as the Scott Polar Research Institute at Cambridge, Bailey et al (1964) and the Geophysical and Polar Research Center at the University of Wisconsin, Bentley (1964), Walford (1964) were active in polar regions and also on glaciers.

1965 – 1970

During this time the ice radio echo sounding activity continued. In addition, applications in other favorable geologic materials started to be explored. Cook (1973) explored the use in coal mines since coal can be a low loss dielectric material in some instances. Similarly, Holser et al (1972), Unterberger (1978) and Thierbach (1973) initiated evaluations in underground salt deposits for similar reasons.

This period was the start of lunar science mission planning for the Apollo program. Several experiments were devised to examine the lunar subsurface which was believed to have electrical character similar to that of ice. The work of Annan (1973) reports on some of these developments.



Figure: 1-4 The surface electrical properties experiment carried out on Apollo 17 used a 3 component vector receiver mounted on the lunar rover and a dual axis multi-frequency dipolar antenna laid out on the surface to sound the subsurface.

1970 – 1975

This period saw numerous advances. The Apollo 17 lunar exploration program involved the surface electrical properties experiment (Figure 1-4) which used interferometry concepts similar to the work carried out by El Said (1956) while the work lunar orbiter carried a pulsed radar sounder similar to the ice sounders which made measurements from orbit over the lunar surface (Simmons et al (1973) and Ward et al (1973)).

During the same period Morey and others formed Geophysical Survey Systems Inc. which has been manufacturing and selling ground penetrating radar since that time (Morey (1974)).

In addition a better understanding of electrical properties of geologic materials at radio frequencies started to become available. Work such as that by Olhoeft (1975) led to a much better understanding of the electrical character of natural occurring geological materials and the relationship between electrical conductivity and dielectric polarization of these materials.

1975 – 1980

During this period, applications started to grow because of the availability of technology and a better understanding of geology. The Geological Survey of Canada explored a number of applications, the primary one being a better understanding of permafrost terrain in the Canadian Arctic. A GPR system in operation is shown in Figure 1-5. Proposals for pipelines out of the Arctic to carry oil and gas to southern markets drove a great deal of interest in engineering in frozen soil and environments. GPR was a tool which offered great promise and some of the initial results are reported by Annan and Davis (1976).

During this period the effect of scattering on radio echo sounding in temperate glaciers became better understood. The impact of scattering and the need for lower frequency radars was reported by Watts and England (1976).

Experiments with GPR were reported by the Stanford Research Institute where measurements were made by Dolphin et al (1978) for archeological applications.

Other work carried out in this period which paralleled the Geological Survey of Canada permafrost efforts was lead by Olhoeft at the United States Geological Survey who worked on the Alaska pipeline routes.



Figure: 1-5 GPR system being used to survey potential pipeline routes in the Canadian Arctic (1975).

Extensive work was carried out in potash mines in western Canada. This led to a whole series of ever improving GPR measurements and work in this geological setting by the Geological Survey of Canada. These results were reported by Annan et al (1988). Further coal mine developments were reported by Coon et al (1981).

In addition, the potential for use of borehole radar to investigate rock quality in potential hard rock nuclear waste disposal sites became a topic of interest. The Geological Survey of Canada and Atomic Energy of Canada supported this work (Davis and Annan (1986)).

Commercial instruments were used for most of this work and the number of activities spawned new commercial interest. Geophysical Survey Systems Inc. remained the only supplier at this time but Ensco/Xadar was spawned in an attempt to create an alternate commercial product.

One major issue noted by the Geological Survey of Canada was the great difficulty in using existing equipment in remote areas. Equipment was heavy, bulky and power hungry. In addition, digital data was needed to exploit the digital seismic processing advances rapidly evolving in the petroleum seismic field.

1980 – 1985

During this period, interest in GPR waned to a degree. The initial optimism for the technology gave way to the reality that many environments were not favorable for GPR. Considerable confusion often existed as to whether failures were equipment related or due to natural material responses. In addition, little money was available for technology development.

OYO Corporation of Japan developed a radar product called “Georadar” spawned by association with Xadar developments. This instrument met some initial commercial success in Europe.

A-Cubed Inc. was formed in 1981 in Canada and started development of ground penetrating radars. The low frequency digital GPR developments were reported by Davis et al (1985). This technology development led to the pulseEKKO series of GPR's.

The nuclear waste disposal problem was continually studied and a number of countries funded the Swedish Geological Survey in the development of borehole radar. This work is reported by Olsson et al (1987).

Other applications for GPR such as road investigations and utility mapping met with mixed success. In general, the technology was quite new and not optimized for these applications. Work by Ulriksen (1982) provided a good foundation for some of these applications.

Many non-commercial developments occurred with prototypes that embodied the ideas for portability, digital recording and the use of fiber optics cables.

Other little reported work was conducted by Southwest Research and the U.S. Army on borehole GPR to detect tunneling in sensitive military areas (Owen (1981)).

1985 – 1990

GPR finally started to come into its own during this period. The strengths and weaknesses were becoming better understood and real problems in the near surface created a demand for high resolution mapping. The U.S. Environmental Protection Agency instituted many initiatives to investigate and clean up contaminated land (Benson et al (1984)). GPR was a natural tool to address high-resolution subsurface mapping and as a result a strong commercial driver started to appear.

In addition, many of the previous applications were continually explored and movement to lower frequency GPR's with full digital recording appeared in commercial products. Other applications such as soil classification for agricultural needs appeared (Doolittle & Asmussen (1992)). Adaption of one dimensional seismic modelling occurred in this period (Annan & Chua (1992)).

In 1988, Sensors & Software Inc. was spawned from A-Cubed Inc. and commenced commercialization of the pulseEKKO technology.

1990-1995

The real explosion in the advancement of GPR occurred during this period. Many groups worldwide became interested in the technology.

On the commercial side, Geophysical Survey Systems Inc. exhibited strong commercial success and was bought by OYO Corporation. During this period, Mala Geosciences was spawned from the Swedish Geological Survey roots. ERA in the UK also became more active using its research into unexploded ordinance and landmine detection to create commercial products. Sensors & Software Inc. grew rapidly broadening its pulseEKKO product line.

On the research side, much attention started to be paid by both the geophysical and electrical engineering community. Developments such as multi-fold data acquisition (Fisher et al (1992)), digital data processing (Maijala (1992), Gerlitz et al (1993)), and 2D numerical simulation (Zeng et al (1995), Cai and McMechan (1995)) occurred. Initial three-dimensional numerical simulation was reported by Roberts & Daniels (1996). Advances in applications in archeology (Goodman (1994)), environmental (Brewster and Annan (1994)), geological stratigraphy using radar facies (Jol (1996)) and many other areas expanded. Environmental borehole GPR development was reported by Redman et al (1996).

Ground penetrating radar user meetings became more formalized and were held every 2 years at various locations around the world. This meeting provided a forum for the leading players in this field to meet, present results and discuss problems. These meetings led to proceeding publications which are listed as references. These proceedings provide a great deal of information for new users to the GPR field.

1995 – 2000

In this period, the evolution of the computers drove all of GPR advances. Numerical modelling of full 3D problems became more extensive albeit still with large computers (Holliger & Bergmann (2000), Lampe & Holliger (2000)). The ability to manage the large volumes of information in digital form and manipulate them quickly became routine. As a result, acquisition of data on grids to make maps and grids and 3D visualization became practical (Grasmueck (1996), Annan et al (1997)). The commercial market and demand resulted in a variety of different and simpler systems such as the Noggin from Sensors & Software Inc. (Figure 1-6).



Figure: 1-6 Sensors & Software Inc.'s Noggin Smart Cart.

Strong research groups appeared at a number of universities. ETH led by Alan Green, the University of Texas at Dallas led by George McMechan and the group at TU-Delft led by Jakob Fokema are some examples of groups pushing development of expertise and advancement of GPR frontiers.

The fundamental vector nature of GPR started to become critical. Understanding this full vector nature of the fields became of more interest (Roberts and Daniels (1996)). In addition, there was much more pressure on acquiring accurate positioning of information than historically needed because the need to do data manipulation requires very accurately controlled positioning information (Greaves et al (1996)).

1.3 CURRENT ACTIVITIES & FUTURE DEVELOPMENTS

GPR is now on very solid footing. Research groups with good understanding of the basic physics are developing modelling tools and analysis capabilities. More work is still required on measurement of electrical properties of materials. Electrical properties of mixtures are understood in general but the complexities and interactions in specific instances are still subjects for research.

Digital processing power now exceeds our current capability to make use of it. As a result, development of software and processing algorithms to exploit the computer power available will cause an ever more rapid advance in the manipulation of data to address application needs.

Instrumentation is now stable and reliable. In the early days of GPR, instrumentation was always of marginal capability because of the extremely critical demands placed on the instruments. Designing ultra wideband antennas and electronics to work in close proximity to a variable lossy dielectric media is not a trivial engineering exercise and only now are products becoming stable, reliable and reproducible.

Even now, the amplitude of GPR data is not well controlled. As instruments evolve and designs get better, the amplitude information of the data is becoming more reliable. Historically, the travel time was the most useful part of the GPR record. Relative amplitudes were good indicators but absolute amplitude information was unattainable.

As GPR becomes more sophisticated and stable, reliable quantitative amplitude information will spawn another generation of data analysis and interpretation tools based on inversion to image material properties. Already inversion in various forms to extract electrical properties is being attempted with success at the research level (van der Kruk (2001)).

A major trend already visible is the extraction of “user” information. In the early days of GPR, just acquiring the GPR

cross section image in some form was the end goal of GPR measurement. With full digital data and analysis capability, display information in many forms is mundane and extraction of specific user information much more critical.

1.4 SUMMARY

The future of GPR is bright. The opportunities are still vast and new developments will occur at an every increasing pace. Major points to note at present are as follows.

1. GPR is becoming a mature method.
2. Instrumentation is attaining a high level of quality and dependability.
3. Data processing and advanced presentation of imaging information is easy and is advancing daily.
4. Instruments focused on specific applications and user needs are starting to appear and will be the way of the future.

The following sections are intended to show the basic principles underpinning the technology and the general state of practice at the current time.

2 BASIC ELECTROMAGNETIC THEORY

2.1 OVERVIEW

The foundations of GPR lie in electromagnetic theory. The history of this field spans more than two centuries and is the subject of numerous treatise. The goal in this chapter is to provide the basic building blocks needed to work quantitatively with GPR without reiterating reams of theoretical development. Unfortunately, a minimum set of tools must be established to make later discussions coherent and meaningful. Read the following with this in mind and be prepared to read reference material such as Jackson (1967), Reitz & Milford (1960), and Smythe (1989).

GPR represents a subset of the full electromagnetic field. GPR signals are electromagnetic waves; Maxwell's equations which mathematically describe electromagnetic physics plus constitutive relationships which quantify material properties are the foundations for quantitatively describing GPR signals.

2.2 MAXWELL'S EQUATIONS

In mathematical terms, electromagnetic fields and related properties are expressed as:

$$\bar{\nabla} \times \bar{\mathbf{E}} = -\frac{\partial \bar{\mathbf{B}}}{\partial t} \quad (2-1)$$

$$\bar{\nabla} \times \bar{\mathbf{H}} = \bar{\mathbf{J}} + \frac{\partial \bar{\mathbf{D}}}{\partial t} \quad (2-2)$$

$$\bar{\nabla} \cdot \bar{\mathbf{D}} = q \quad (2-3)$$

$$\bar{\nabla} \cdot \bar{\mathbf{B}} = 0 \quad (2-4)$$

Where:

$\bar{\mathbf{E}}$ - electric field strength vector

$\bar{\mathbf{B}}$ - magnetic flux density vector

$\bar{\mathbf{D}}$ - electric displacement vector

$\bar{\mathbf{H}}$ - magnetic field intensity

q - electric charge density

$\bar{\mathbf{J}}$ - electric current density vector

Maxwell succinctly summarized the work of prior researchers in this compact form.

A pictorial representation of the physics underlying of each equation are presented in Figure 2-1 to Figure 2-4. Equation 2-1 summarizes Faraday's observation that a time varying magnetic field causes electric charges to move implying the presence of a electric field.

Maxwell #1: Faraday Law

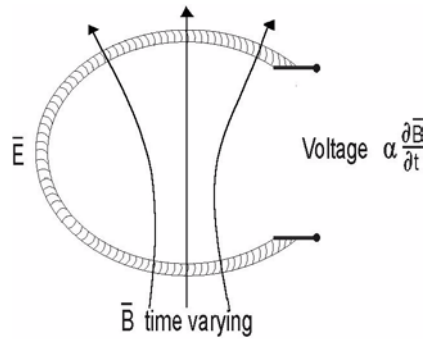


Figure: 2-1 A time varying magnetic field generates a closed loop electric field. A common example is the electric generator where a rotating magnet generates a voltage in a wire loop.

Maxwell #2: Ampere Law

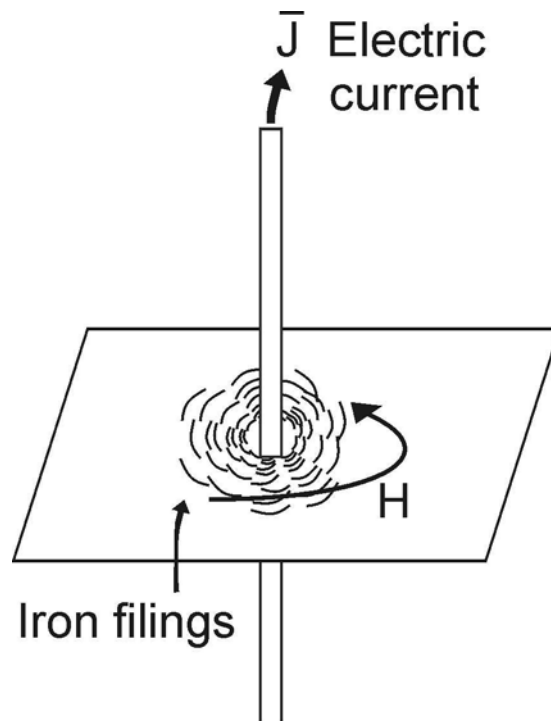


Figure: 2-2 An electric current gives rise to a magnetic field. The classic example to demonstrate this concept is iron filings on a piece of paper forming circles about a current carrying wire.

Maxwell #3

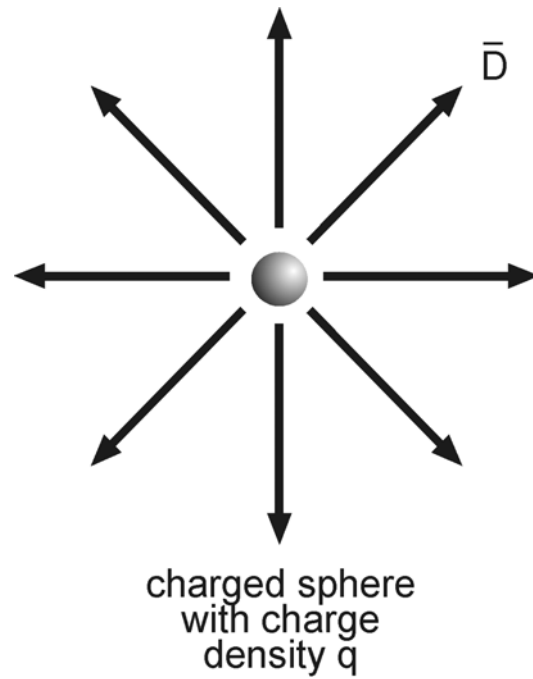


Figure: 2-3 Electric displacement \bar{D} starts (or ends) on an electric charge. Electric fields must form closed loops or terminate on a charge.

Maxwell #4

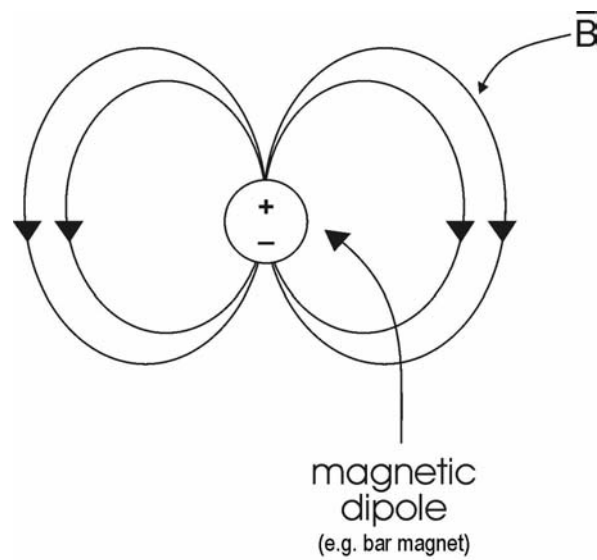


Figure: 2-4 Magnetic flux loops must close on themselves since there are no free magnetic charges.

Ampere's observations that electric currents generate magnetic fields underpin Equation 2-2. Magnetic objects behave the same way when a magnet or an electric current is present. The electromagnet is the common example of this.

Equation 2-3 indicates that electric charges are sources (or sinks) of electric field. Electric fields emanate from electric charges; hence Equation 2-3. Time varying electric fields will be of closed loop form when induction (Faraday's observation) occurs. The electric field will emanate outward (or into) when free charge is the field source. In general both field characters will be present and superimposed for time varying signals. Free magnetic charges have never been observed in nature; as a result, magnetic fields must form closed loops which explains Equation 2-4 and distinguishes magnetic flux behavior from electrical field character.

From these building blocks, all classic electromagnetics (induction, radio waves, resistivity, circuit theory, etc.) can be derived after we characterize material electrical properties.

2.3 CONSTITUTIVE EQUATIONS

Constitutive relationships are the means of quantifying the physical properties of materials. In EM and GPR the electric and magnetic properties are of importance. Constitutive equations provide a macroscopic (or average behavior) description of how electrons/atoms/molecules/ions etc., respond en masse to the application of a field.

For GPR, three quantities are defined, electric conductivity $\tilde{\sigma}$

$$\bar{J} = \tilde{\sigma}\bar{E} \quad (2-5)$$

which describes how free charges flow to form a current when an electric field is present. Dielectric permittivity, $\tilde{\epsilon}$

$$\bar{D} = \tilde{\epsilon}\bar{E} \quad (2-6)$$

which describes how constrained charges are displaced in response to an electric field.

Magnetic permeability, $\tilde{\mu}$

$$\bar{B} = \tilde{\mu}\bar{H} \quad (2-7)$$

which describes how intrinsic atomic and molecular magnetic moments respond to a magnetic field.

In general, $\tilde{\sigma}$, $\tilde{\epsilon}$ and $\tilde{\mu}$ are tensors and can also be non-linear. (i.e. $\tilde{\sigma} = \tilde{\sigma}(E)$). For virtually all practical GPR issues, these quantities are treated as field independent scalar qualities. (In other words, the response is in the same direction as the exciting field and independent of field strength.) While these assumptions are seldom fully valid, the practical world of GPR has yet to be able to discern such complexity except in a few cases.

An additional feature of the properties is that they can depend on the history of the incident field. To be fully correct, we should write Equation 2-5, Equation 2-6 and Equation 2-7 in the form (only Equation 2-5 is written for compactness)

$$\bar{J}(t) = \int_0^{\infty} \bar{\sigma}(\beta) \cdot \bar{E}(t - \beta) d\beta \quad (2-8)$$

We will ignore this issue for now but will return to the topic later. (This more complex form of 2.8 must be used when we deal with frequency dependent or dispersive physical properties.)

For the rest of this chapter we will deal with scalar constant ϵ, μ, σ . Details on electric and magnetic properties will be dealt with in later chapters. For GPR, ϵ and σ are of most importance in the majority of situations.

2.4 WAVE NATURE OF EM FIELDS

In this section the wave character of EM Fields is explored. Only the very simplest uniform medium is considered. Material properties are assumed isotropic, frequency independent and linear.

Maxwell's equations (Equation 2-1 through Equation 2-4) describe a coupled set of electric and magnetic fields when the fields vary with time. Changing electric fields create magnetic fields which in turn induce electric fields, as depicted in Figure 2-5. This continuing succession of one field inducing the other results in fields which move through the medium. Depending on the relative magnitude of losses, the fields may diffuse or propagate as waves. With GPR we are most concerned with conditions where the response is wave-like.

Mathematically, the wave character is seen by rewriting Maxwell's equations to eliminate either the electric or magnetic field. This is achieved by noting that the closed circulation character of the magnetic field can be expressed in terms of the electric field. From Faraday's law (Equation 2-1) one can write:

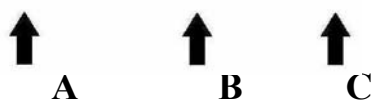
$$\bar{\nabla} \times \bar{\nabla} \times \bar{E} = -\frac{\partial}{\partial t} (\bar{\nabla} \times \mu \bar{H}) \quad (2-9)$$

Using Ampere's Law (Equation 2-2) plus the constitutive relatives one obtains:

$$\bar{\nabla} \times \bar{\nabla} \times \bar{E} = -\mu \frac{\partial}{\partial t} \left(\bar{J} + \frac{\partial \bar{D}}{\partial t} \right) = -\mu \sigma \frac{\partial \bar{E}}{\partial t} - \mu \epsilon \frac{\partial^2 \bar{E}}{\partial t^2} \quad (2-10)$$

which yields what is termed the transverse vector wave equation.

$$\bar{\nabla} \times \bar{\nabla} \times \bar{E} + \mu \sigma \cdot \frac{\partial \bar{E}}{\partial t} + \mu \epsilon \cdot \frac{\partial^2 \bar{E}}{\partial t^2} = 0 \quad (2-11)$$



A
 B
 C

Terms B and C express the fact that currents generate magnetic fields whose time varying circulation create an electric field as expressed by A. The equation represents that all fields must balance.

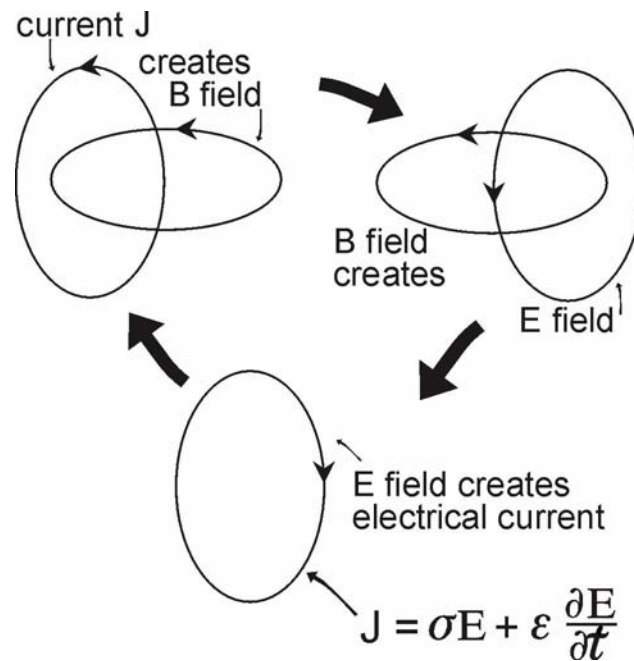


Figure: 2-5 Wave equation formulations express the self-perpetuating field sequences as depicted. A moving charge implies current J which creates a magnetic field which induces an electric field which in turn causes electric charge to move.

Note that we have eliminated the magnetic field in this formulation. If we had chosen to express our fields in terms of magnetic fields only, we would get exactly the same form of equation for H .

The essence of the transverse wave Equation 2-11 lies in its basic solution form. The electric field (or magnetic field) vector must vary in a spatial direction perpendicular to the field vector.

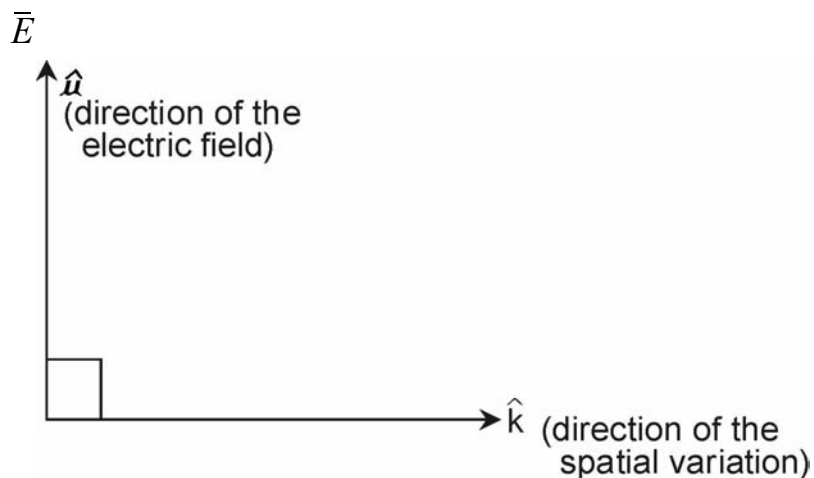


Figure: 2-6 A field satisfying the transverse vector wave equation has the field vector perpendicular to the spatial variation direction.

Mathematically, a position vector and a pair of orthogonal unit vectors ($\hat{\mu}, \hat{k}$) are needed to characterize a simple solution to the EM wave equation. The electric field is

$$\bar{\mathbf{E}} = f(\bar{\mathbf{r}} \cdot \bar{\mathbf{k}}, t) \hat{\mathbf{u}} \quad (2-12)$$

The key lies in understanding what the $\bar{\nabla} \times \bar{\nabla} \times$ operation implies. First we look at

$$\bar{\nabla} \times \bar{\mathbf{E}} \quad (2-13)$$

Defining $\beta = \bar{\mathbf{r}} \cdot \bar{\mathbf{k}}$ as the scalar distance in the direction that the field varies and we see

$$\bar{\nabla} \times \bar{\mathbf{E}} = \hat{\mathbf{k}} \times \hat{\mathbf{u}} \frac{\partial f}{\partial \beta}(\beta, t) \quad (2-14)$$

We see from Farady's law that the time varying magnetic flux

$$\frac{\partial \bar{\mathbf{B}}}{\partial t} = -\bar{\nabla} \times \bar{\mathbf{E}} = -\hat{\mathbf{k}} \times \hat{\mathbf{u}} \frac{\partial f}{\partial \beta} \quad (2-15)$$

is created by the shearing electric field and is in a direction perpendicular to $\bar{\mathbf{E}}$ and $\hat{\mathbf{k}}$ namely $\hat{\mathbf{w}} = \hat{\mathbf{k}} \times \hat{\mathbf{u}}$ (see Figure 2-7).

Continuing we find that

$$\bar{\nabla} \times \bar{\nabla} \times \bar{\mathbf{E}} = \hat{\mathbf{k}} \times (\hat{\mathbf{k}} \times \hat{\mathbf{u}}) \frac{\partial^2 f}{\partial \beta^2} = -\hat{\mathbf{u}} \frac{\partial^2 f}{\partial \beta^2} \quad (2-16)$$

The shearing of the electric field generates a time varying orthogonal magnetic field which in turn creates an electric field in the opposite direction to the original electric field.

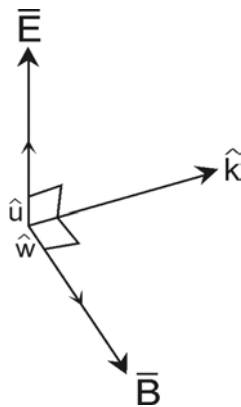


Figure: 2-7 The electric magnetic and field variation direction form a 3D vector space

We find now that our fields in the simple case must have this vector character and the spatial/temporal variation $f(\beta, t)$ satisfies the equation

$$\frac{\partial^2}{\partial \beta^2} f(\beta, t) - \mu\sigma \frac{\partial}{\partial t} f(\beta, t) - \mu\epsilon \frac{\partial^2}{\partial t^2} f(\beta, t) \equiv 0 \quad (2-17)$$

Those versed in wave theory will recognize this as the scalar wave equation.

If we ignore losses (i.e. assume $\sigma = 0$), (Equation 2-17) reduces to

$$\frac{\partial^2}{\partial \beta^2} f(\beta, t) = \mu\epsilon \frac{\partial^2 f(\beta, t)}{\partial t^2} \quad (2-18)$$

which has solutions of the form

$$f(\beta, t) = f(\beta \pm vt) \quad (2-19)$$

where

$$v = \frac{1}{\sqrt{\epsilon\mu}} \quad (2-20)$$

is the wave velocity. The wave nature is indicated by the fact that the spatial distribution of the fields translates in the direction β between observation times as depicted in Figure 2-8.

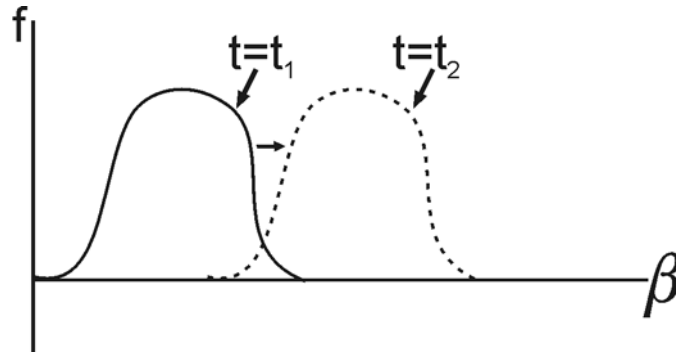


Figure: 2-8 A function of the form $f(\beta \pm vt)$ represents an event which moves spatially at a velocity v . Such functions are solutions to the scalar wave equation.

2.5 LOW LOSS – DAMPED EM WAVE CONDITIONS

For GPR we are most interested in problems where EM fields propagate as waves. All real materials generally exhibit some loss which is primarily attributable to electrical conductivity. We will discuss this subject in more depth in later chapters.

In the previous section we tacitly assumed $\sigma \equiv 0$ for convenience and saw how wave nature of EM fields flowed from Maxwell's equations. The effect of small losses is of great interest in the real GPR world and we deal with this as a perturbation of the derivation of the previous section.

Returning to Equation 2-11, we can get a relative measure of the importance of various contributions to the wave equation by dimensional analysis. For a given spatial scale Δx and time scale Δt , the relative importance of terms in the equation are given by the ratios

$$\left| \frac{B}{A} \right| \approx \mu\sigma \frac{\Delta x^2}{\Delta t} \quad (2-21)$$

$$\left| \frac{C}{A} \right| \approx \mu\varepsilon \frac{\Delta x^2}{\Delta t^2} \quad (2-22)$$

Our criteria for a low loss environment requires

$$\left| \frac{B}{A} \right| \ll \left| \frac{C}{A} \right| \quad (2-23)$$

or regrouping implies that

$$\left| \frac{B}{C} \right| = \frac{\sigma\Delta t}{\varepsilon} \ll 1 \quad (2-24)$$

Electric currents in the material can be viewed as analogous to electric current in a resistor capacity circuit, as depicted in Figure 2-9 (resistance is proportional to $1/\sigma$ and capacitance is proportional to ε). The charging time for the capacitor is expressed as ε/σ . The condition that $|B/C|$ be small requires the time for charge redistribution to be short compared to the time rate of change of the EM fields.

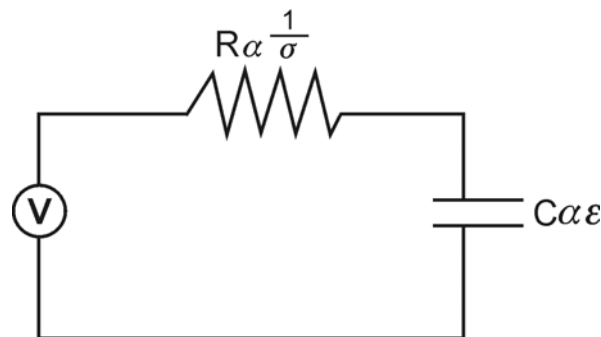


Figure: 2-9 A simple circuit containing a resistor and capacitor is the circuit analog to Equation 2-24. The resistance is proportional to $1/\sigma$ and the capacitance is proportional to ε .

The solution of Equation 2-11 when reduced to the scalar form of Equation 2-17 is approximated by perturbing our wave solution when $\sigma \equiv 0$ by defining

$$f(\beta, t) = p(\beta \pm ut)g(\beta) \quad (2-25)$$

where p is a solution in the zero loss case, namely

$$\frac{\partial^2 p}{\partial \beta^2} = \mu\epsilon \frac{\partial^2 p}{\partial t^2} \quad (2-26)$$

Substituting into Equation 2-11 yields the result that

$$p \frac{\partial^2 g}{\partial \beta^2} + 2 \frac{\partial p}{\partial \beta} \left(\frac{\partial g}{\partial \beta} \pm \frac{u\sigma\nu}{2} g \right) = 0 \quad (2-27)$$

which we can satisfy if

$$\frac{\partial g}{\partial \beta} \pm \frac{u\sigma\nu}{2} g = 0 \quad (2-28)$$

and

$$\frac{\partial^2 g}{\partial \beta^2} = 0 \quad (2-29)$$

In point of fact, we cannot satisfy the second condition but we can show that in the low loss situation this term is negligible.

The first relationship is satisfied if

$$g(\beta) = e^{\pm\alpha\beta} \quad (2-30)$$

where

$$\alpha = \frac{\mu\sigma\nu}{2} \quad (2-31)$$

If we use Equation 2-30 as the solution for g , then

$$\frac{\partial^2 g}{\partial \beta^2} = \left[\frac{\mu \sigma v}{2} \right]^2 g \quad (2-32)$$

Looking at the magnitude of the term

$$p \frac{\partial^2 g}{\partial \beta^2} = \left[\frac{\mu \sigma v}{2} \right]^2 p g \quad (2-33)$$

in Equation 2-27 and comparing it to C in our original Equation 2-11, we find the relative magnitude of this term to be

$$\left| \frac{p \frac{\partial^2 g}{\partial \beta^2}}{c} \right| \sim \left| \frac{\left(\frac{\mu \sigma v}{2} \right)^2}{\frac{\mu \epsilon}{\Delta t^2}} \right| = \frac{1}{4} \left(\frac{\sigma \Delta t}{\epsilon} \right) \ll 1 \quad (2-34)$$

which is indeed negligible compared with all other terms in our original equation when conduction losses are small.

Our solutions are damped waves of the form

$$f(\beta, t) = p(\beta \pm \mu t) e^{\pm \alpha \beta} \quad (2-35)$$

which decay exponentially in amplitude in the direction the wave is travelling. α is called the attenuation coefficient. The EM field translates with shape invariance as a wave but decreases in amplitude as energy is lost to ohmic dissipation in the material. Figure 2-10 illustrates the concept of how the field changes with time and distance.

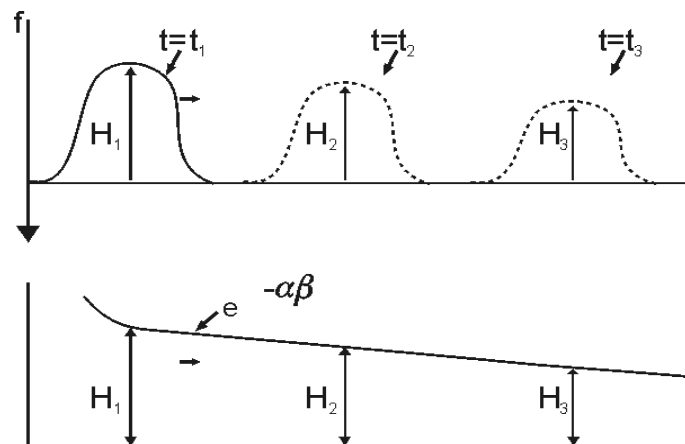


Figure: 2-10 EM fields propagate as spatially damped waves when electrical losses are small. The signal amplitude decays exponentially in the direction of field translation while the field shape remains invariant.

2.6 SINUSOIDALLY TIME VARYING FIELDS

Many EM developments by-pass the discussions given in the previous two sections and deal with EM fields assuming sinusoidal time variation. This approach is in essence the use of a Fourier transform approach to separate time and spatial operators.

In simple terms, the form of f is assumed to be

$$f(\beta, t) = h(\beta)e^{i\omega t} \quad (2-36)$$

and the partial differential Equation 2-11 reduces to the equation

$$\frac{d^2 h}{d\beta^2} - (\omega^2 \epsilon \mu + i\omega \epsilon \mu \sigma)h = 0 \quad (2-37)$$

Defining

$$k = (\omega^2 \epsilon \mu + i\omega \mu \sigma)^{\frac{1}{2}} \quad (2-38)$$

the solution for h has the form

$$h(\beta) = Ae^{\pm ik\beta} \quad (2-39)$$

k is called the propagation constant. Quite often it is convenient to express k in the form

$$k = \frac{\omega}{v} + i\alpha \quad (2-40)$$

where v is the phase velocity (see 2-20) and α is the attenuation. When this is done we have f in the form

$$f(\beta, t) = Ae^{\pm \alpha \beta} e^{i\omega \left(t \pm \frac{\beta}{v} \right)} \quad (2-41)$$

which is exactly the same form of translating and attenuated field behaviour noted in the previous two sections.

The Fourier (or Laplace) transform solutions are necessary in generalized formulations since the sinusoidal excitation solutions are exact. To generate time domain transient solutions the inverse Fourier or Laplace transformation is applied to the frequency domain solution. Often this must be done numerically as analytical solutions are seldom possible.

When losses are low, we find that the two terms in the propagation constant, k , are such that

$$\omega \mu \sigma \ll \omega^2 \epsilon \mu \quad (2-42)$$

or

$$\frac{\sigma}{\omega\epsilon} \ll 1 \quad (2-43)$$

which is called the low loss criteria.

When this condition holds, we find

$$v = \left(\frac{1}{\epsilon\mu} \right)^{\frac{1}{2}} \quad (2-44)$$

$$\alpha = \frac{\mu\sigma v}{2} \quad (2-45)$$

which is the same as our analysis in the previous sections.

2.7 ELECTROMAGNETIC IMPEDANCE

In Section 2.4, the basic solutions of Maxwell's equations were seen to be coupled electric and magnetic fields. The fields are perpendicular to one another and move in a direction perpendicular to both of the fields as depicted in Figure 2-7. As indicated earlier, both the electric and magnetic fields satisfy the same transverse wave equation. Solving for one field allows an immediate solution for the other.

When these prior simple solutions were developed, we worked in terms of the electric field. The amplitude of the magnetic field can be directly related to the electric field and vice versa because of the field coupling. A common term in electrical engineering is the electromagnetic impedance defined as

$$Z = \frac{E}{H} \quad (2-46)$$

From section 2.4,

$$\bar{E} = f(\beta, t)\hat{u} \quad (2-47)$$

and

$$|\bar{H}| = \left| \frac{\bar{B}}{\mu} \right| \quad (2-48)$$

since

$$\frac{\partial \bar{\mathbf{B}}}{\partial t} = \hat{\mathbf{u}} \times \hat{\mathbf{k}} \frac{\partial f}{\partial \beta} = \frac{\hat{\mathbf{u}} \times \hat{\mathbf{k}}}{v} \frac{\partial f}{\partial t} \quad (2-49)$$

we have

$$\frac{\partial}{\partial t} [\bar{\mathbf{B}} - \hat{\mathbf{k}} \times \hat{\mathbf{u}} \frac{f}{v} = 0] \quad (2-50)$$

making

$$\mathbf{B} = \hat{\mathbf{k}} \times \hat{\mathbf{u}} \frac{f}{v} \quad (2-51)$$

Substituting in we find

$$\mathbf{Z} = \mu \mathbf{v} = \sqrt{\frac{\mu}{\epsilon}} \quad (2-52)$$

which states that the relative amplitude of electric and magnetic fields in our solutions (known as plane waves) are determined by the medium properties.

When conductivity is important, we must deal with sinusoidal signals to make math simple and we find that

$$\mathbf{Z} = \sqrt{\frac{\mu}{\epsilon + i \frac{\sigma}{\omega}}} \quad (2-53)$$

In some cases, the inverse of \mathbf{Z} , called the electromagnetic admittance, is used and is expressed as

$$\mathbf{Y} = \frac{1}{\mathbf{Z}} = \sqrt{\frac{\epsilon + i \frac{\sigma}{\omega}}{\mu}} \quad (2-54)$$

These concepts are very useful and will take on significance in later chapters.

In low loss environments, the approximate forms are

$$\begin{aligned}
 Z &\approx \sqrt{\frac{\mu}{\epsilon}} \left(1 - i \frac{\sigma}{2\omega\epsilon} \right) \\
 Y &\approx \sqrt{\frac{\epsilon}{\mu}} \left(1 + i \frac{\sigma}{2\omega\epsilon} \right)
 \end{aligned}
 \tag{2-55}$$

2.8 POLARIZATION

From the intrinsic vector nature of the electromagnetic fields studied, we see the electric and magnetic field vectors are orthogonal to each other and to the direction of translation. From this result, two independent electromagnetic fields can exist for a given propagation direction. Figure 2-11 depicts the concept.

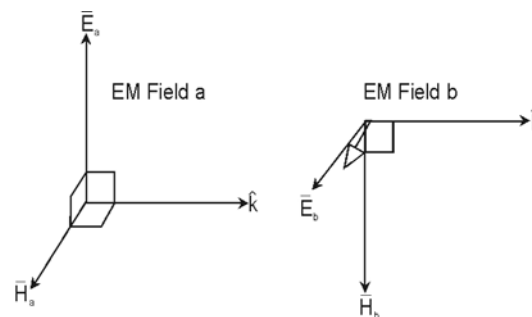


Figure: 2-11 For a given propagation direction \hat{k} , two independent electromagnetic fields, a and b , exist.

By convention, the EM field solutions are characterized by the direction of the electric field vector. Plotting the electric field vector in a plane perpendicular to \hat{k} one observes

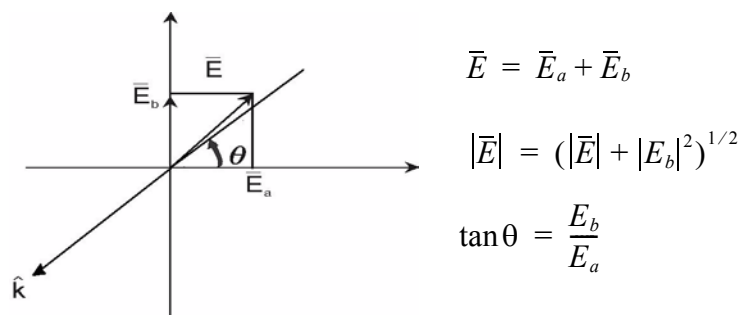


Figure: 2-12 The total observed field, \vec{E} is the vector sum of the two independent fields, E_a and E_b . The polarization direction is in the direction of \vec{E} .

When the time variation of the fields is sinusoidal, the concepts of linear, circular and elliptical polarization arise. The electrical field vector has the form

$$\bar{\mathbf{E}} = E_a e^{i\phi_a} e^{i\omega t} \hat{\mathbf{a}} + E_b e^{i\phi_b} e^{i\omega t} \hat{\mathbf{b}} \quad (2-56)$$

where E_a and E_b are the scalar amplitudes, and ϕ_a and ϕ_b are the phase of each of the components with respect to a common reference and $\hat{\mathbf{a}}$ and $\hat{\mathbf{b}}$ are unit vectors perpendicular to one another.

If $\phi_a = \phi_b$, the electric field is said to be linearly polarized. The vector is fixed in direction (i.e. $\theta = \text{constant}$) and its amplitude varies sinusoidally as depicted in Figure 2-13.

$$|\bar{\mathbf{E}}| = (E_a^2 + E_b^2)^{\frac{1}{2}} \cos \omega t \quad (2-57)$$

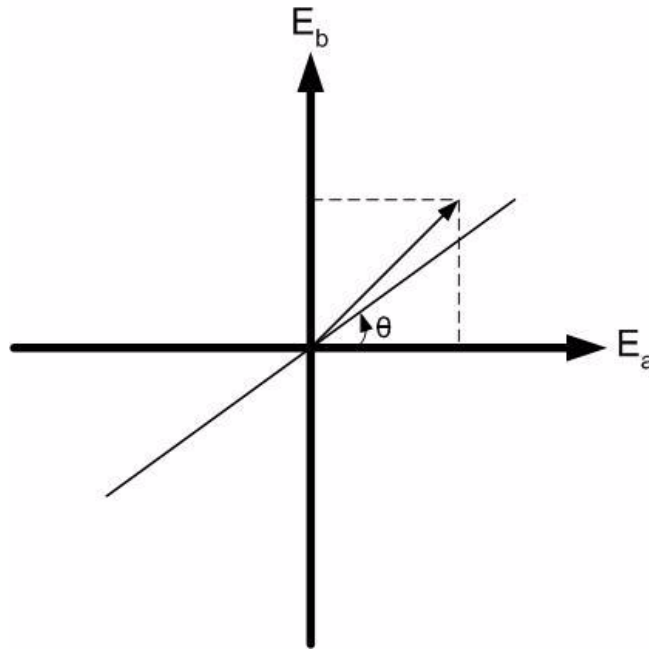
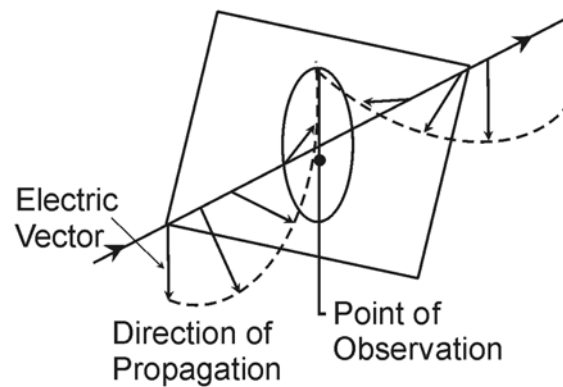
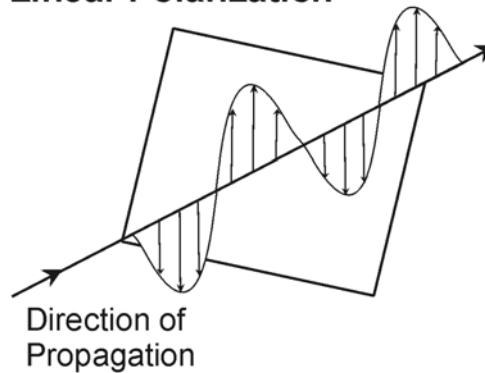


Figure: 2-13 When fields vary sinusoidally with time, linear polarization manifests itself as a total electric field which is in a fixed direction.

Elliptical Polarization



Linear Polarization



Circular Polarization

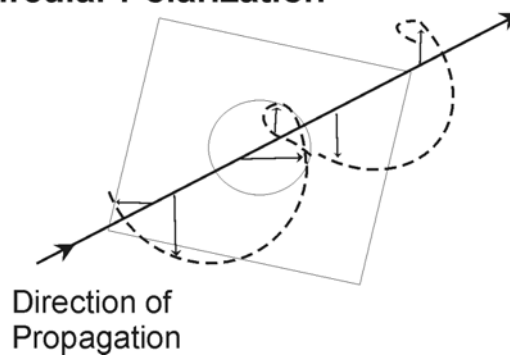


Figure: 2-14 For sinusoidal time varying fields, the fields are, in general, elliptical. Special cases are linear and circular polarization.

In the elliptically polarized case, the amplitude and field direction change with time tracing out an ellipse in the field plane and an elliptical spiral in space, as depicted in Figure 2-14. More discussion of polarized fields can be found in any of the EM texts referenced at the end of the chapter.

Linear, elliptical and circular polarization have limited meaning when dealing with transient fields. In such cases, the field vector may rotate regularly for short durations but generally motion is irregular. Plots of field diagrams showing amplitude and direction for transient events versus time (Figure 2-15) called hodograms - can be very unstructured.

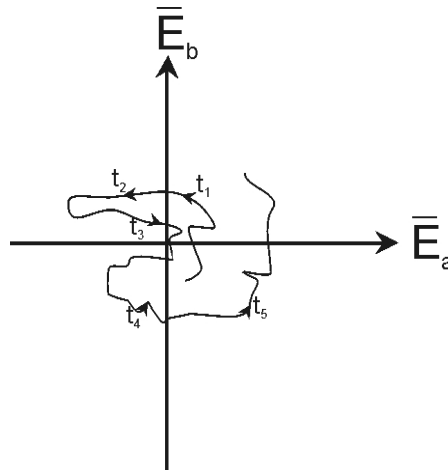


Figure: 2-15 Plotting the total transient electric field vector in a plane versus time creates a hodogram. The arrow traces the vector as a function of increasing time.

2.9 EM FIELDS FROM SOURCES

To this point, our analysis has carefully avoided dealing with sources. This subject becomes mathematically complex. In the following a very cursory view of the subject is given with the objective of establishing fundamental concepts needed for later chapters.

For most GPR applications, we excite electromagnetic fields by causing electrical currents to flow on metal structures (called antennas). In a similar fashion we detect electromagnetic fields by the currents they induce to flow on similar metal structures.

For simplicity, we assume we can separate our electric current in Ampere's law (Equation 2-2) into two parts.

$$\vec{J} = \vec{J}_s + \sigma \vec{E} \quad (2-58)$$

where \vec{J}_s is our source or exciting current and $\sigma \vec{E}$ is the conduction current as defined in 2-5. How \vec{J}_s is created in a controlled fashion is not a trivial issue and one we will skip over for now.

Following on, we find our wave Equation 2-11 is modified to the form

$$\nabla \times \nabla \times \vec{E} + \mu\sigma \frac{\partial \vec{E}}{\partial t} + \mu\epsilon \frac{\partial^2 \vec{E}}{\partial t^2} = -\mu \frac{\partial \vec{J}_s}{\partial t} \quad (2-59)$$

The solution to this equation often requires resorting to numerical calculations. There are some simple instances of analytical solution and one of these we will use for considerable discussion throughout.

The solution for a small current element can be derived in analytical form in a uniform medium. We treat the current density as being concentrated (Figure 2-16) in a line of infinitesimal diameter and length.

Mathematically we describe

$$\bar{J} = I\Delta\ell\delta(x)\delta(y)\delta(z)\hat{e}_2 \quad (2-60)$$

where $\delta(x)$ is the Dirac delta function.

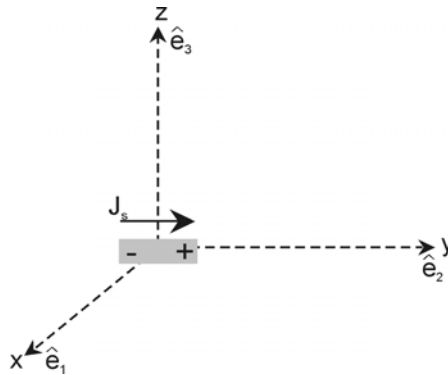


Figure: 2-16 A small electric dipole antenna can be thought of as a small current element.

Aside: Physically we treat \bar{J}_s to exist in a small parallel piped as shown in Figure 2-17.

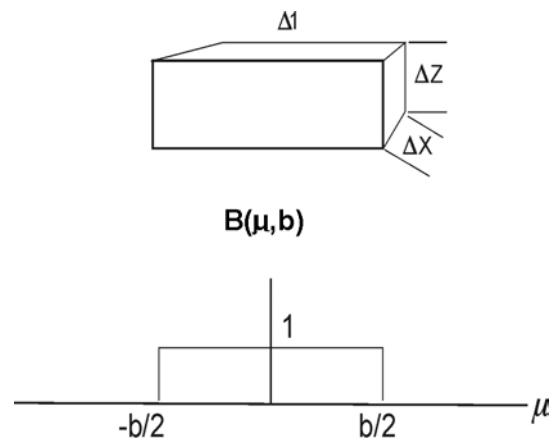


Figure: 2-17 Depiction of a parallel piped of current mode by using boxcar function $B(\mu, b)$.

$$\bar{J}_s = \frac{I}{\Delta x \Delta z} B(x, \Delta x) B(y, \Delta \ell) B(z, \Delta z) \hat{e}_2$$

where

$$B(\mu, b) = 1 \quad \mu > -\frac{b}{2} \text{ to } \mu > \frac{b}{2}$$

$$= 0 \quad \text{otherwise}$$

We let $\Delta \ell$, Δx , Δz approach 0 and in the limiting case

$$\bar{J}_s = \frac{I \Delta \ell}{\Delta x \Delta z} B(x, \Delta x) B(y, \Delta \ell) B(z, \Delta z) \hat{e}_2$$

$$\bar{J}_s \rightarrow I \Delta \ell \delta(x) \delta(y) \delta(z) \hat{e}_2$$

$$\Delta x \rightarrow 0, \quad \Delta \ell \rightarrow 0, \quad \Delta z \rightarrow 0$$

subject to the condition $I \Delta \ell$ remaining finite.

This mathematical trick of taking of the current to an infinitesimal size permits us to ignore details of internal source geometry. This source is called an infinitesimal electric dipole.

Without going into the detailed proof, the solution for \bar{E} field generated for this infinitesimal current source takes the form

$$\bar{E} = \left(\hat{e}_2 g + \bar{\nabla} \frac{\partial g}{\partial y} \right) \quad (2-61)$$

where

$$g(x, y, z, t) = \frac{\mu \Delta \ell \frac{\partial}{\partial t} I(r - vt)}{4\pi r} \quad (2-62)$$

$$r = (x^2 + y^2 + z^2)^{\frac{1}{2}}$$

The kernel, g , is somewhat like our previous solutions to the sourceless case in that signals are shifted (delayed) in time by distance traveled but in this case the signals emanate spherically outward from our source point and decrease with distance. For more extensive discussion see the EM texts on the subject of retarded potentials and retarded field solutions.

As with our previous discussion, when the electrical losses are small, ($\mu\sigma$ small but finite), our expression is modified to read.

$$g(x, y, z, t) = \frac{\mu\Delta l \frac{\partial}{\partial t} I(r - vt)e^{-ar}}{4\pi r} \quad (2-63)$$

Frequently one finds solutions to the finite source problem derived for sinusoidally time varying fields as we have discussed earlier. When the fields are sinusoidal in time, Equation 2-59 becomes

$$\bar{\nabla} \times \bar{\nabla} \times \bar{E} - i\omega\mu\sigma\bar{E} - \omega^2\epsilon\mu\bar{E} = i\omega\mu\bar{J}_s \quad (2-64)$$

and the solutions kernel g takes the 2-63 form

$$g(x, y, z) = \frac{i\omega\mu\Delta l e^{\frac{i\omega r}{v}} e^{-ar}}{4\pi r} \quad (2-65)$$

The time lag becomes a phase shift dependent on distance from the source and the time derivative of the current becomes a multiplication by frequency.

2.10 FAR FIELD APPROXIMATION

When the observer is far from the source, the solutions simplify considerably. Descriptions at a distance are referred to as "far-field approximate" solutions. For \bar{E} (or \bar{H}) the field has a general form

$$\bar{E} = (\mu(\theta, \phi)\hat{\theta} + \nu(\theta, \phi)\hat{\phi})g \quad (2-66)$$

where $\mu(\theta, \phi)$ and $\nu(\theta, \phi)$ depends on the angular position of the observer with respect to the source depicted in Figure 2-18.

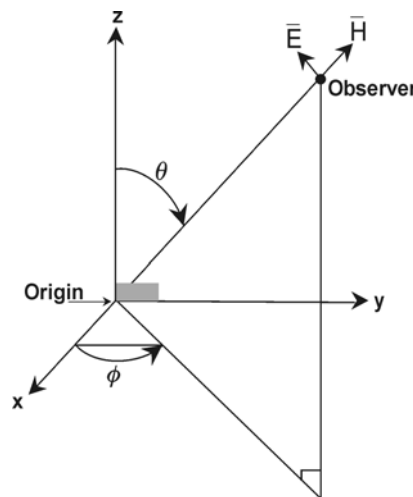


Figure: 2-18 The electric and magnetic field at large distance from the source described using a spherical polar angle notation. \vec{E} and \vec{H} become perpendicular to the radial direction from source to observer.

In the far field, \vec{E} and \vec{H} are orthogonal (perpendicular to one another) and have no radial component. When viewed over a limited spatial volume, the field resembles a "plane wave" discussed earlier. The electric and magnetic fields and the radial vector from the source are mutually orthogonal as depicted in Figure 2-19.

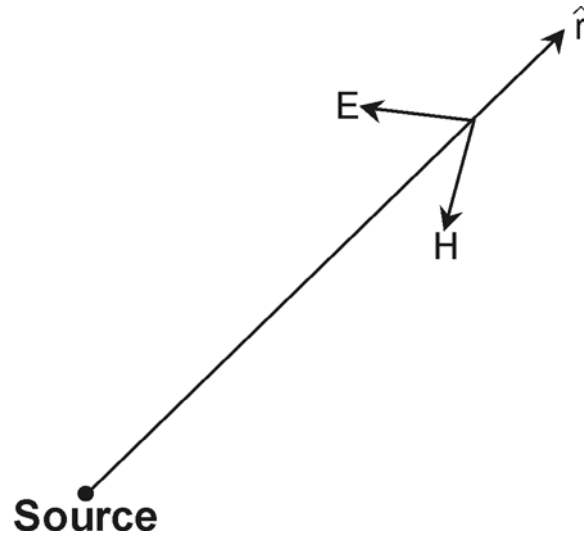


Figure: 2-19 At a large distance from the source, the fields propagate radially outward and resemble plane waves.

In fact,

$$\vec{E} = Z(\hat{r} \times \vec{H}) \quad (2-67)$$

where Z is the electromagnetic impedance as discussed in section 2.9. \hat{r} is the unit vector in the radial direction.

2.11 ANTENNA PATTERNS, DIRECTIVITY, GAIN

All these terms derive from the far field approximation. In physical terms, the far field represents the energy lost from the source as radiated electromagnetic energy. The best way to view far field radiation is to visualize measuring the field at the surface of a large sphere which encloses the source. In theoretical terms the far field approximation becomes exact as the radius of the sphere becomes infinite.

Position on the surface of the sphere is defined by polar (angle) coordinates (θ, ϕ) as depicted in Figure 2-18 and 2.20. (i.e., like latitude and longitude but latitude angles are measured from the north pole rather than the equator).

At any point on the sphere the electric (and magnetic) field is tangential to the surface. The field vector is usually decomposed into components which are in the $\hat{\theta}$ and $\hat{\phi}$ unit vector directions. $\hat{\theta}$ and $\hat{\phi}$ are tangential to the sphere surface and perpendicular to one another. The field vector is then expressed as

$$\vec{E} = E_{\theta}\hat{\theta} + E_{\phi}\hat{\phi} \quad (2-68)$$

The same applies to \vec{H} .

As discussed earlier, the fields are polarized and the direction of \vec{E} is normally used as the polarization direction.

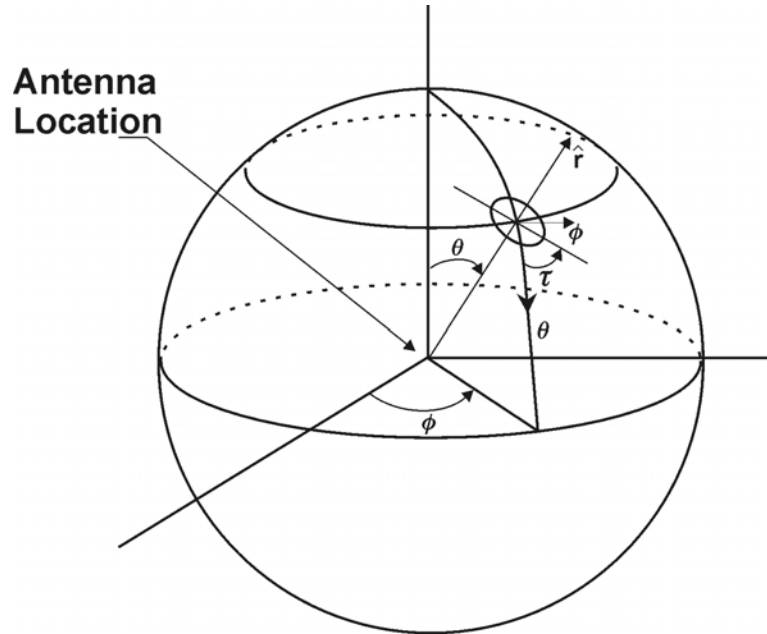


Figure: 2-20 Far field antenna patterns are the fields on a very large sphere. Position on the surface is measured in spherical polar angles as indicated. The power radiated by the source is measured by the energy in the electromagnetic field transported across the sphere's surface.

The power radiated by the source is measured by the energy in the electromagnetic field transported across the sphere's surface. A vector called the Poynting vector \vec{P} is a measure of power crossing the sphere at any point.

$$\vec{P} = \vec{E} \times \vec{H} = \frac{|\vec{E}|^2}{Z} \quad (2-69)$$

\vec{P} is directed radially outward at all points on the sphere. The total radiated power is expressed as:

$$P_T = \iint \vec{P} \cdot \hat{r} dA \quad (2-70)$$

where integration is over the surface area of the sphere.

After this preamble we can get down to some specifics. Sources of electromagnetic radiation seldom emit energy uniformly in all directions. The intensity of the far field varies with position (θ, ϕ) . As the cartoon in Figure 2-21 shows, a highly directional source only emits energy in a small cone.

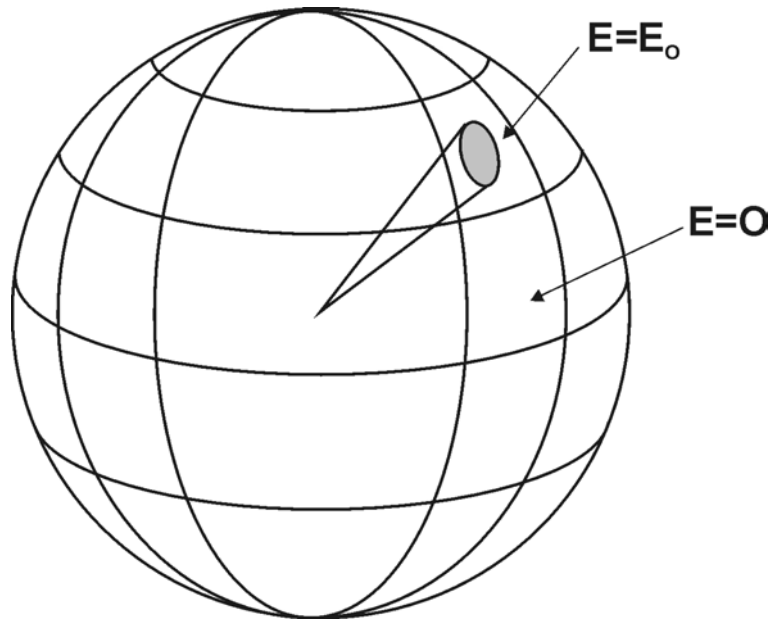


Figure: 2-21 Conceptual illustration of a highly directional source. The radiated energy results in an electric field, E_0 , only in the small shaded area of the far field sphere surface, elsewhere the electric field is zero.

Directivity can be expressed for a specific field component or for total field.

$$D_{\theta}(\theta, \phi) = \frac{|E_{\theta}(\theta, \phi)|}{E_{\text{Ref}}} \quad (2-71)$$

$$D_{\phi} = \frac{|E_{\phi}(\theta, \phi)|}{E_{\text{Ref}}} \quad (2-72)$$

$$D_t(\theta, \phi) = \frac{(E_{\theta}^2(\theta, \phi) + E_{\phi}^2(\theta, \phi))^{\frac{1}{2}}}{E_{\text{Ref}}} \quad (2-73)$$

Generally E_{Ref} is selected so the maximum directivity is 1 and is therefore application and source type dependent. For example, some sources can result in $E_{\phi} \equiv 0$ so that

$$D_t(\theta, \phi) \equiv D_{\theta}(\theta, \phi) \quad (2-74)$$

A related concept is antenna gain. Gain deals with power rather than field strengths. As with directivity it may be component specific. More often gain is related to total power rather than component power. Gain is a most useful parameter in system engineering.

Returning to the Poynting vector discussion, the total energy emitted by a source is

$$\begin{aligned} P_T &= \iint (\bar{\mathbf{E}} \times \bar{\mathbf{H}}) \cdot \hat{\mathbf{r}} dA \\ &= \iint \bar{\mathbf{P}}(\theta, \phi) \cdot \hat{\mathbf{r}} dA \end{aligned} \quad (2-75)$$

If the source radiated uniformly in all directions (called an isotropic radiator source), then

$$P(\theta, \phi) = \frac{P_T}{4\pi r^2} \quad (2-76)$$

would be constant. The fact that P varies in most cases indicates that more energy is sent in one direction than another. In other words, some directions are favored relative to others. Gain (or loss) is a relative measure. Antenna gain is defined as

$$G(\theta, \phi) = \frac{P(\theta, \phi)}{\frac{P_T}{4\pi r^2}} \quad (2-77)$$

which is the ratio of the local power crossing the sphere relative to the power which would be observed if the same source emitted the same power uniformly in all directions (i.e. isotropically).

In practice, $G(\theta, \phi)$ is often expressed in decibels.

$$G_{dB}(\theta, \phi) = 10 \log_{10} G(\theta, \phi) \quad (2-78)$$

Gain, as indicated earlier, is a relative measure of signal enhancement or depletion.

Both directivity and gain have historically been displayed as functions on a cross section of the sphere since plotting data on a spherical surface (translated to a flat page) is difficult.

The antenna pattern is created by drawing a point at a radial distance from the great circle origin proportional to G , G_{dB} or D . The concept is illustrated in Figure 2-22, Figure 2-23 and Figure 2-24.

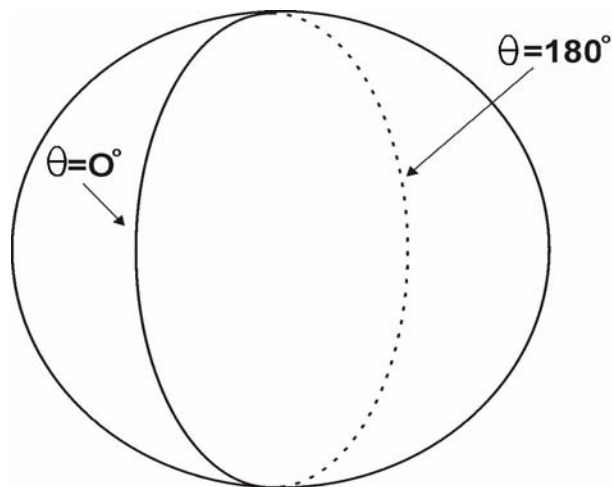


Figure: 2-22 A cut through the center of the sphere is used to generate a circular flat plane for display of signal variations in that cross section of sphere.

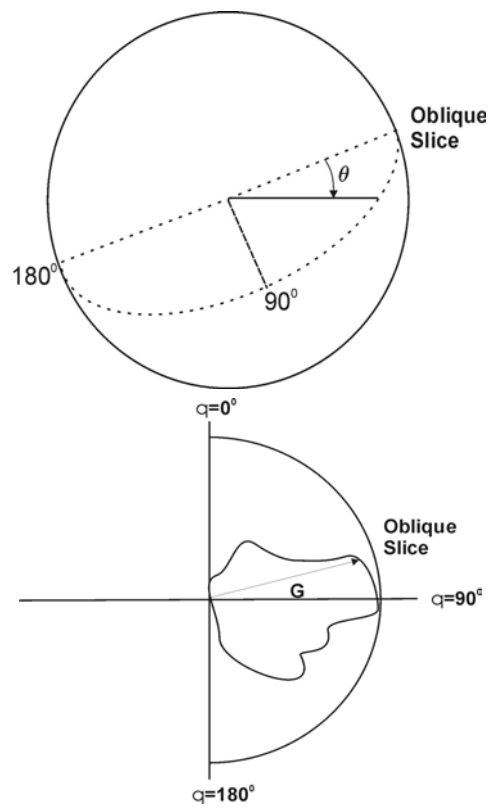


Figure: 2-23 The antenna pattern is created by a vector with length proportional to gain or directivity and in the given direction.

The line that the end of the vector traces as (θ, ϕ) vary defines the pattern.

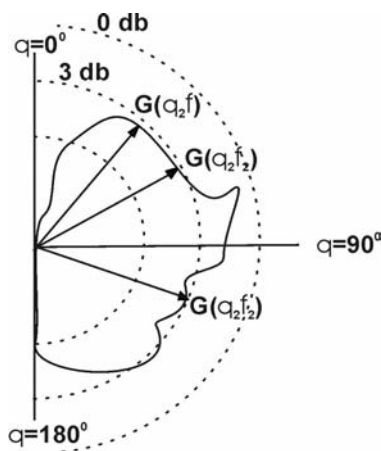


Figure: 2-24 An example of antenna gain pattern.

Antenna patterns (either gain or directivity) are displayed in this fashion. More specific examples will appear later in these notes.

3 PHYSICAL PROPERTIES I

3.1 WHY ARE PHYSICAL PROPERTIES IMPORTANT?

GPR investigates the subsurface by making use of electromagnetic fields which propagate into the subsurface. EM fields which are time varying consist of coupled electric (E) and magnetic (H) fields. As discussed in section 2 the fields interact with the surrounding media. This interaction is macroscopically described by the constitutive equations 2.5 to 2.7. The manner in which the electromagnetic fields interact with natural materials controls how electromagnetic fields spread into the medium and are attenuated in the medium. In addition, the variation in physical properties gives rise to the observed subsurface reflections obtained with a GPR system.

In most geological and NDT (non-destructive testing) applications of GPR, electrical properties tend to be the dominant factor controlling GPR responses. Magnetic variations are usually weak. Occasionally magnetic properties can affect radar responses and GPR users should be cognizant of magnetic effects.

An electric field in a material gives rise to the movement of electric charge, (i.e., electric current). The current flow depends on the nature of the material. There are two types of charge in a material, namely bound and free, which give rise to two types of current flow, namely displacement and conduction. In the following, we will provide a simple overview of the two types of current flow. An in-depth discussion of electrical properties can be found in the text by Von Hippel, (1954).

Magnetic properties are controlled by the electric charge circulation character at the atomic and molecular level. Macroscopic magnetic properties are addressed briefly in these notes. Von Hippel (1954) addresses some of the basic concepts.

3.2 CONDUCTION CURRENTS

Most people are very familiar with electrical conduction currents. Conduction currents are created when unbound (free) charges move in a material. The electrons which flow in a metal wire are an example of conduction current. In a metal, electrons move through the metallic matrix to transfer charge from one point to another. Another common conduction mechanism is the movement of ions in a water solution. The later is much more important in most GPR applications.

Conduction currents arise when free charge accelerates to a terminal velocity (basically instantaneously) when an electric field (E) is applied. As long as the electric field is applied, the charge moves; when the electric field is removed, the charge decelerates and stops moving Figure 3-1 illustrates these concepts.

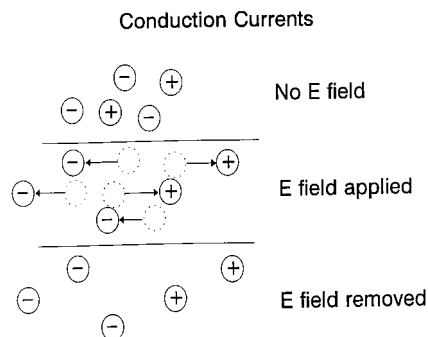
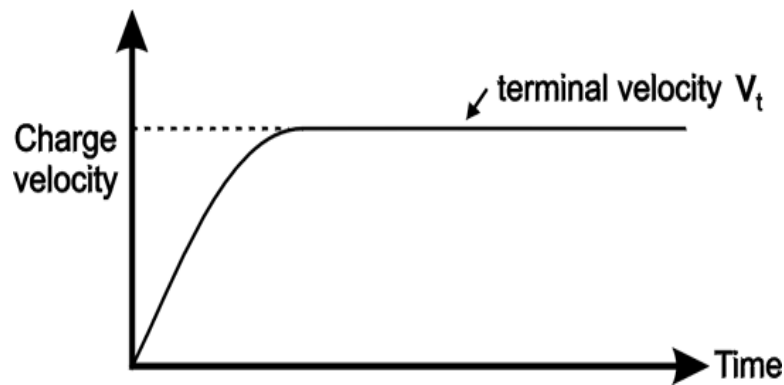
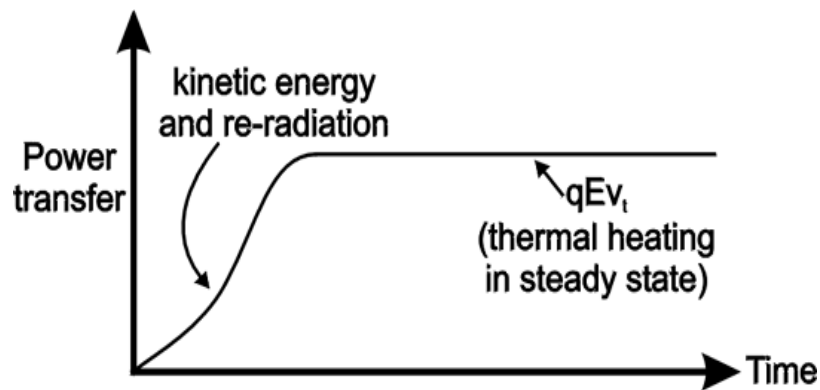


Figure: 3-1 Conceptual illustration of charge movement for conduction currents.



a) Charge velocity versus time after E field applied.



b) Energy is extracted from the applied electric field versus time.

Figure: 3-2 When an electric field is applied, unbound electrical charges accelerate to a terminal velocity. After initial acceleration, velocity becomes constant and a continual transfer of energy to the surrounding material in the form of heat occurs

All the time that charge is moving, the moving charge is working against its surroundings dissipating energy in the form of heat. The moving charge bumps into 'non-moving' objects and transfers mechanical energy which appears in the form of heat in the medium. Conduction currents represent an energy dissipating mechanism for an electromagnetic field. Energy is extracted from the electromagnetic field and transferred irreversibly into the medium as heat.

Mathematically one describes the relationship between conduction current and the applied electric field as indicated in Equation 3-1.

$$\bar{J} = \sigma \bar{E} \quad (3-1)$$

In simple materials, the relationship is linear and the proportionality constant is referred to as the electrical conductivity. Electrical conductivity has units of Siemens per meter (S/m). For many applications, however, it is more useful to work with units of milliSiemens per meter (mS/m). Conductivity is dependent on the charge density and the internal statistical mechanical interaction of the charge with its surroundings. These details are beyond the scope of this discussion.

It should be noted that electrical conductivity and resistivity are directly related. Refer to Figure 3-3 for the relationship and the expression of Ohm's law. Electrical resistivity is the inverse of electrical conductivity.

Conduction Current Density

$$J_c = \sigma E$$

σ = electrical conductivity (Siemens/m)

E = electric field

Ohm's Law

$$E = \rho J_c$$

$$\rho = 1 / \sigma$$

ρ = resistivity (Ohm-m)

Figure: 3-3 Relationship between current and applied field as well as the relationship with Ohm's law and resistivity.

It is important to note that there are simplifications in the above discussion from the general form shown in Chapter 2. The conductivity is shown as being a constant. In fact it can be a function of the rate of change of the electric field, the amplitude of electric field itself, as well as temperature, pressure and many other factors. As a result, one should not be surprised to see both non-linearity and frequency dependent conductivity in real materials. Generally these are second order effects but they must be considered when advanced use of GPR is contemplated. For this basic GPR overview, they will be treated as secondary issues.

3.3 DISPLACEMENT (POLARIZATION) CURRENTS

Displacement currents are associated with bound charges which are constrained to limited distance of movement. Examples of this are the electron cloud around an atomic nucleus, the electrical charge in a small metal object imbedded in an insulating environment, and the redistribution of the molecular dipole moment intrinsic to some molecules. Figure 3-4 depicts the concept. When an electric field is applied, bound charge moves to another static configuration. This transition occurs virtually instantaneously after which the charges no longer move. During the transition, energy is extracted from the electric field and the energy is stored in the material. When the field is removed, the charge moves back to the original equilibrium distribution and energy is released. This type of behavior is typical of what happens in a capacitor in an electric circuit. Energy is stored by the build up of charge in the capacitor and then energy is extracted by the release of that charge from the device.

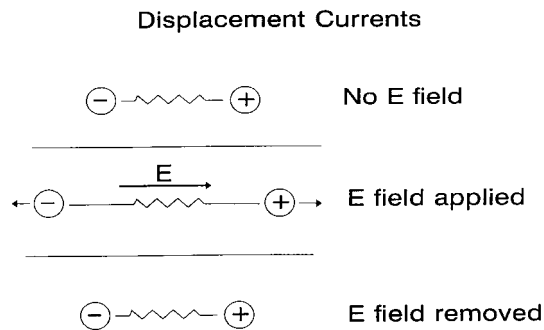


Figure: 3-4 Conceptual illustration of charge movement associated with displacement currents.

Figure 3-5 depicts the characterization of charge separation in a material. When an electrical field is applied, displacement of charge in a bulk material gives rise to a dipole moment distribution in the material. The charge separation is described in terms of a dipole moment density, D . In a more formal derivation, D is called the electric displacement field (see chapter 2). In simple materials, the induced dipole moment density is directly proportional to the applied electric field and the proportionality constant is referred to as the dielectric permittivity of the material and has units of Farads/m (F/m).

Dipole Moment Density

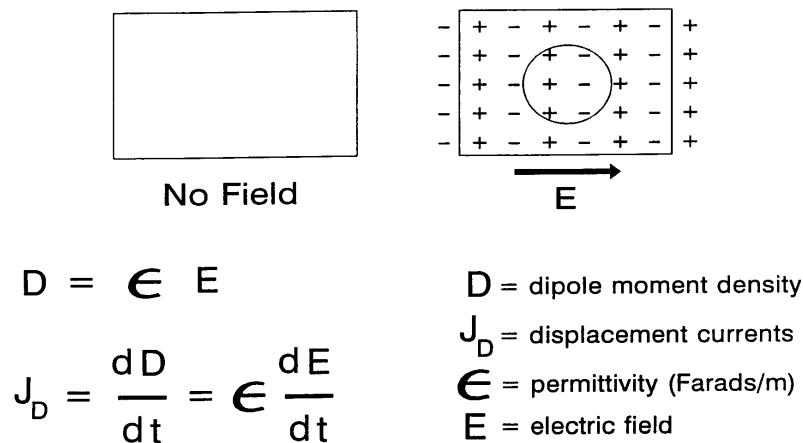


Figure: 3-5 Dipole moment density induced by applied electric field and relation to displacement current.

The creation of a dipole moment distribution in the material is associated with charge movement. The electric current associated with this charge movement is referred to as displacement current. The displacement current is mathematically defined as the time rate of change of the dipole moment density.

The electric permittivity is never zero. Even in a vacuum, the permittivity, ϵ_0 takes on a finite value of 8.85×10^{-12} F/m (Farads per meter). The explanation for this lies in the field of quantum electrodynamics and is far beyond the scope of this discussion.

It is often more convenient to deal with a dimensionless term called relative permittivity or dielectric constant, K . As depicted in Figure 3-6, the relative permittivity is the ratio of material permittivity to the permittivity of a vacuum.

Relative Permittivity / Dielectric Constant

$$K = \frac{\epsilon}{\epsilon_0}$$

$$\epsilon_0 = \text{vacuum permittivity } (8.85 \times 10^{-12} \text{ F/m})$$

Figure: 3-6 Dielectric constant or relative permittivity is the ratio of permittivity of material to that of free space.

3.4 TOTAL CURRENT FLOW

In any natural material, the current which flows in response to the application of an electric field is a mixture of conduction and displacement currents. Depending on the rate of change of the electric field, one or other of the two types of current may dominate the response. Mathematically, the total current consists of two terms; one which depends on the electric field itself and one which depends on the rate of change of the electric field.

$$J = J_c + J_D \quad (3-2)$$

$$J = \sigma E + \epsilon \frac{dE}{dt} \quad (3-3)$$

Quite often it is useful to deal with sinusoidally time varying excitation fields. In this situation, one finds that the displacement currents are proportional to the angular frequency.

$$J = (\sigma + i\omega \epsilon)E \quad (3-4)$$

where ω is the angular frequency.

The displacement currents are out of phase with the conduction currents by 90° which is what ascribing an imaginary $i = \sqrt{-1}$ aspect to the displacement component implies. Those familiar with electrical engineering circuitry terminology will realize that there is a phase shift between the conduction currents and the displacement currents which indicates that one term is an energy dissipation mechanism and the other one is an energy storage mechanism.

A simplified plot of displacement current and conduction currents as well as total current versus frequency is presented in Figure 3-7. Usually there is some frequency above which the displacement currents exceed the conduction currents. In a simple material where the conductivity and the dielectric permittivity are constant, there is a transition frequency, f_t , where the displacement currents and conduction currents are equal. Above this frequency, displacement currents dominate; below this frequency, conduction currents dominate. This factor is important when we deal with EM wave propagation. This frequency defines the onset of the low-loss regime important to GPR.

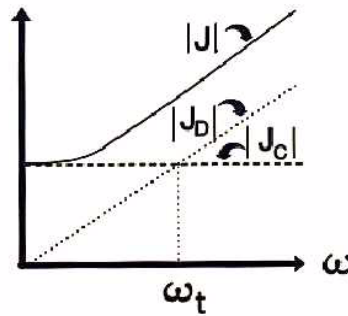


Figure: 3-7 Conduction, displacement and total current versus frequency.

Mathematically the transition frequency is defined.

$$\omega_t = \frac{\sigma}{\epsilon} \quad (3-5)$$

In addition, another term called the loss tangent is defined. The loss tangent is the ratio of conduction to displacement currents in a material.

$$\tan \delta = \frac{|J_C|}{|J_D|} = \frac{\sigma}{\omega \epsilon} \quad (3-6)$$

The term loss tangent tends to be most common in electrical engineering contexts.

Conductivity and permittivity are not independent of the excitation frequency. There is always some variation. This topic is beyond the scope of this chapter of the notes but there is considerable literature (i.e., Olhoeft, 1975) on frequency dependent electrical properties which can be referred to.

3.5 MAGNETIC PERMEABILITY

Magnetic permeability is seldom of major importance for GPR applications. For completeness and to address those exceptional situations where permeability may become important, we review some of the basic aspects of magnetic permeability.

Magnetic permeability is actually related to the intrinsic electrical characteristics of the basic building blocks of physical materials. In simple terms, charged particles, which form atoms, which in turn make molecules, have a quantum mechanical property referred to as spin. When combined with the charge on the particle, spin results in the particle having a magnetic dipole moment. When an electron moves around an atomic nucleus, the charge motion can also create a magnetic moment.

The simple analogy is to have electrical charge uniformly distributed on a spherical ball and then spin ball. The resulting rotating charge appears to be a circular loop of current, which in turn gives on rise to a magnetic dipole. Magnetic properties are essentially the properties of an electrical charge moving around a closed path.

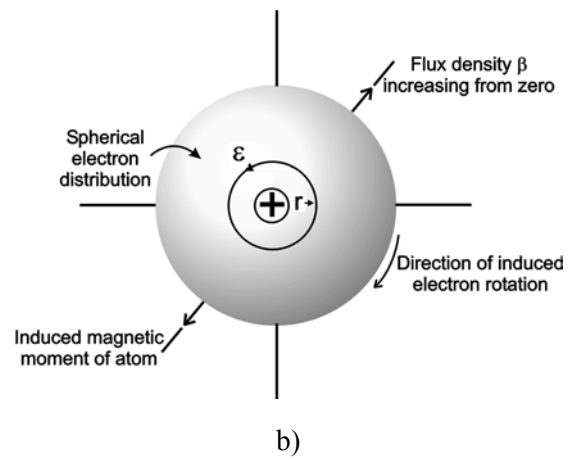
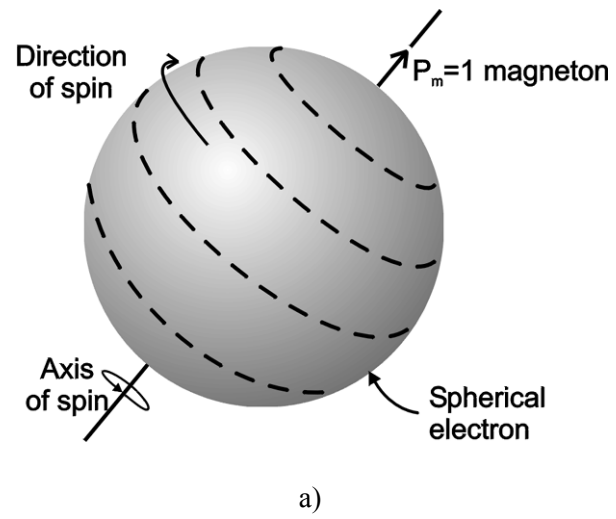


Figure: 3-8 a) A simple picture suggesting the origin of electron spin movement; b) relating the magnetic moment induced in an electron cloud by a change in magnetic field.

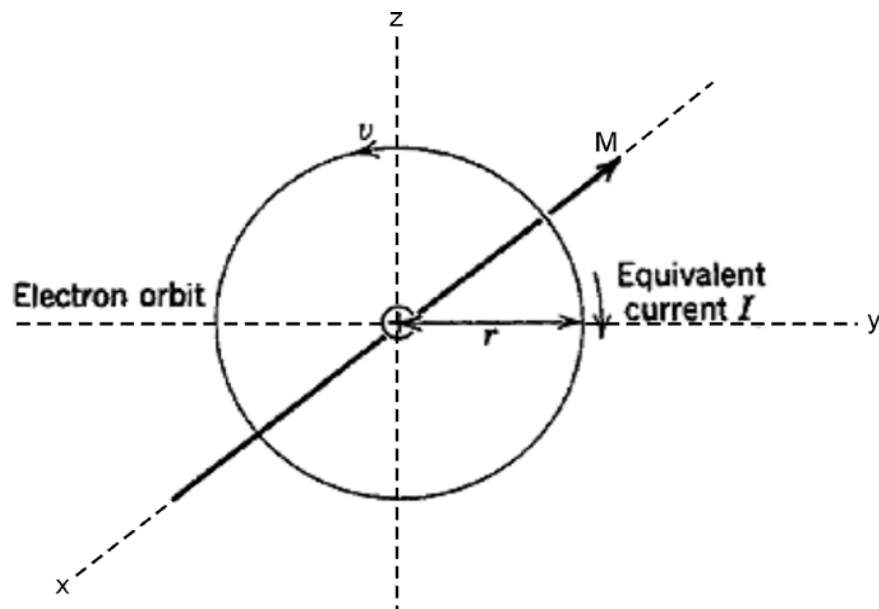


Figure: 3-9 Relating the magnetic moment to a simple electron orbit.

The details are obviously more complex but this provides a simple pictorial model to use. Atoms are formed of electrons and protons plus neutrons. The electrically charged components have intrinsic and orbital spin when they form molecules of a given type of material. The particular orientation of the spin axes of the individual particles can be aligned in random or structured ways and may be altered by an ambient magnetic field. If the molecular structure does not accept random spin orientation but requires a structured crystalline architecture, the material can have a permanent magnetization. If component parts can move to align parallel or anti-parallel to an applied field, an induced magnetization response will arise.

Magnetic permeability measures the degree to which individual dipole moments of the building blocks can be aligned or moved from their normal orientation by an externally applied magnetic field. The more of the individual moments that can be moved into alignment, the more magnetically polarizable the material. The magnetic properties of materials are quantified by magnetic dipole moment density. When an electrical current flows in a closed loop, the magnetic moments is

$$\overline{M} = IA\hat{n} \quad (3-7)$$

where M is the dipole moment, I is the current and A is the area of the loop enclosed by the current filament. M has units of Am^2 . For bulk materials, the material is characterized by dipole moment density

$$\overline{m} = \frac{\overline{M}}{V} \quad (3-8)$$

which has units of A/m . V is volume. When a magnetic field, H , induces a magnetic moment, the amount of moment is expressed as

$$\overline{m} = k\overline{H} \quad (3-9)$$

where k is the magnetic susceptibility (and is a dimensionless quantity). There is considerable similarity between induced magnetic moment and induced electric dipole moment discussed previously in the displacement current section.

In the material, the magnetic flux is expressed as

$$\bar{B} = \mu_0 (\bar{H} + \bar{m}) \quad (3-10)$$

and magnetic permeability is expressed as

$$\mu = \mu_0 (1 + k) \quad (3-11)$$

where

$$\mu_0 = 4\pi \times 10^{-7} \text{ H/m} \quad (3-12)$$

The term relative magnetic permeability is expressed as

$$K_m = \frac{\mu}{\mu_0} = (1 + k) \quad (3-13)$$

in an analogous fashion to relative permittivity. When both magnetic and electric properties vary, relative permittivity is usually expressed as K_e to avoid confusion.

The presence of a magnetic field induces the individual dipole moment to change orientation and line up with the applied field. In some materials the alignment is in the same direction as the applied field, whereas in other materials the alignment may be anti-parallel to the applied field. These two types of behavior referred to as paramagnetism and diamagnetism. Generally these responses are very weak and give rise to small variations in magnetic permeability. Typical values of magnetic susceptibility are less than 10^{-5} .

In some situations, however, the magnetic moments can be aligned in large sections (called domains) of the crystal structure of a material. The moment of domains can be changed by the molecules in the crystal structure behaving in a sympathetic fashion and moving from one domain to another. Such materials are known as ferromagnetic materials.

In ferromagnetic materials, the polarization can be quite large and high values of K_m in the range of tens or even hundreds may be observed in materials such as iron, cobalt, and nickel. With ferromagnetic materials, the behavior is more complex in that the dipole moments when moved, or aligned, remain aligned. This is known as permanent magnetization. In such materials the permeability is very high and the dynamic behavior of the material complex. Such materials seldom form a large volume fraction of soils and rocks but their presence in small amounts can be the dominant factor determining bulk permeability.

Behavior can be very complex. The behavior of dipole moment density is controlled by how domains move, grow and change orientation which can be field dependent, frequency dependent and temperature dependent. The subjects are well beyond the scope of these notes.

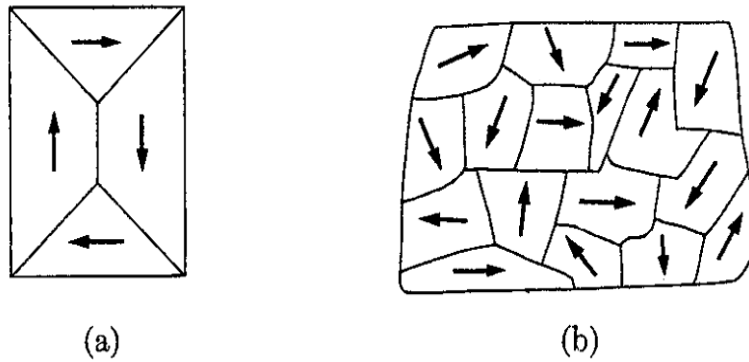


Figure: 3-10 Ferromagnetic domain structures: a) single crystal, b) polycrystalline specimen. Arrows represent the direction of magnetization.

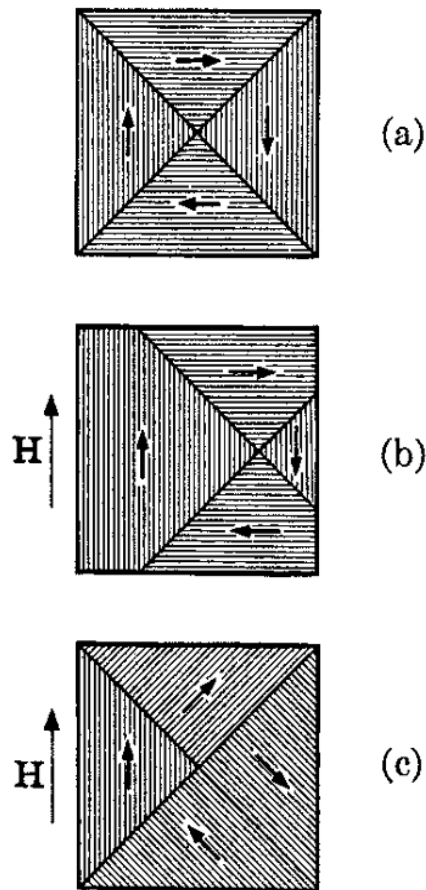


Figure: 3-11 Magnetization of a ferromagnetic material: a) unmagnetized, b) magnetization by domain wall motion, c) magnetization by domain rotation.

In soils and rocks, magnetic behavior is dictated by the amount of magnetite (or similar minerals such as meghemite or ilmenite). The graph (from Grant & West (1965)) in Figure 3-14 shows how susceptibility varies with magnetite volume fraction. The simple approximate formula is

$$k = 3.80 \quad (3-14)$$

where q is the volume fraction of magnetite in the material. To put this result in perspective, 1% by volume magnetite (which is very high in most cases) content yields $K_m=1.038$. Only in rare cases will K_m be significantly different from unity.

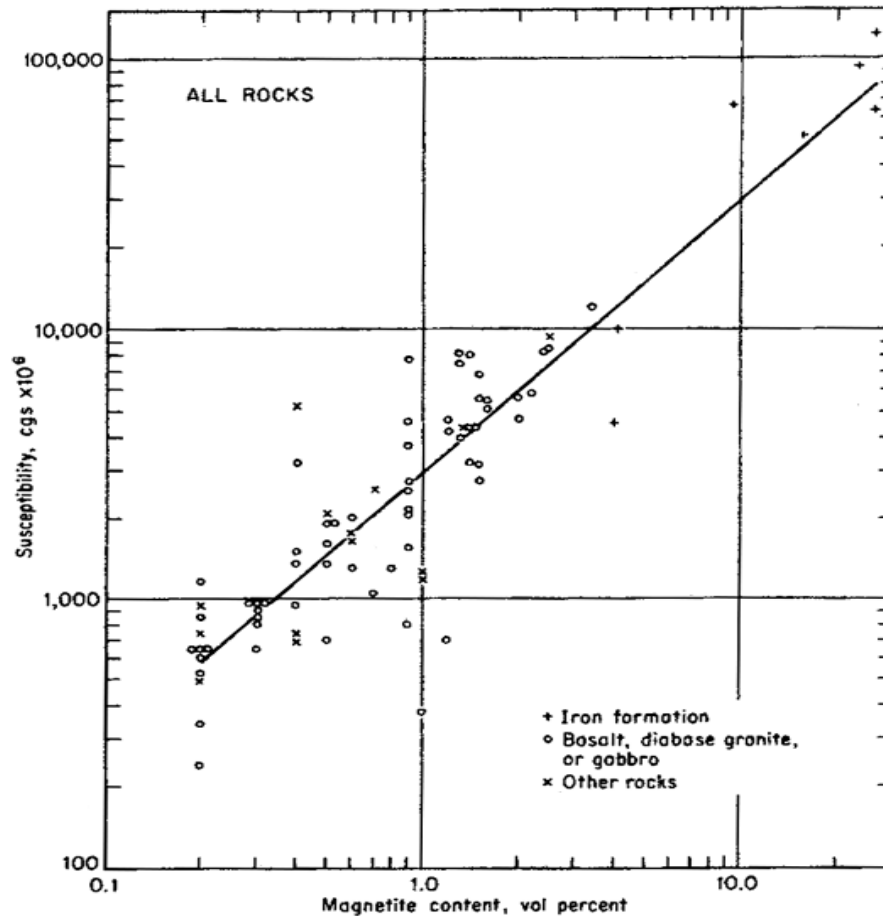


Figure: 3-12 Data from which the empirical formula for susceptibility $k=2.89 \times 10^{-3} V^{1.01}$ was derived. [Mooney and Bleifuss (7).]

3.6 COMPLEX MATERIALS

GPR measurements are seldom carried out in pure elements. Almost all of GPR work is carried out where materials which are composites of many other materials or elements. GPR surveys on water represent one of the few applications on a "pure" single element material.

Table 3-1, Table 3-2 and Table 3-3 show in simple form the composition of some material, which might be encountered in GPR applications. Table 3-1 is a simple quartz sand. This material contains a mixture of soil grains, air, water and ions dissolved in water in variable proportions. Normally soils grains occupy 60 to 80% of the volume.

Table: 3-1 Components of Quartz Soil

quartz grains
air
water
dissolved ions

Table 3-2 summarizes the constituents of hydrocarbon contaminated simple quartz sand such as described in Table 3-1. In addition hydrocarbons in both liquid and vapor form plus a variety of different hydrocarbon compositions will be present as well as biodegraded hydrocarbon derivatives.

Table: 3-2 Components of Hydrocarbon contaminated Quartz& Soil

quartz grains
air
dissolved ions
water
liquid hydrocarbon
bio degradation products

The third example given in Table 3-3 is concrete consisting of cement and aggregate. The aggregate can be any mix of stone materials which are appropriate for mixing with cement and of variable mineralogy. The cement can be full hydrated or partially hydrated. An optimal mix will have very little pore space containing water and/or air. A less than optimal mix will have substantial pore space, which may be connected or disconnected, and which can contain air and/or water.

Table: 3-3 Components of Concrete

aggregate
cement hydrated
cement partially hydrated
air
water
dissolved ions

These are but three simple examples and many more could be cited. Understanding GPR responses and their relationship to electromagnetic properties thus becomes the subject of understanding the properties of mixtures of materials. Mixtures of materials lead to physical property variation which are seldom in proportion to the volume fraction of the constitute components electromagnetic responses. The subject is not simple and is an area of current research. In many respects, this complexity can make quantitative analysis of GPR data impossible without ancillary information.

For example, soil density will have some impact on the GPR response because it will ultimately determine pore space available. Unfortunately density only weakly affects the bulk permittivity whereas the presence of water (the amount of which is controlled by porosity which reflects density) has a large effect on both the permittivity and the conductivity. Using GPR observations to infer soil density requires addition constraints such as full water saturation (i.e. material below the water table).

Table: 3-4 Typical Dielectric Constant, Electrical Conductivity, Velocity and Attenuation Observed in Common Geologic Materials

MATERIAL	K	σ (mS/m)	v (m/ns)	a (dB/m)
Air	1	0	0.30	0
Distilled Water	80	0.01	0.033	2x10 ⁻³
Fresh Water	80	0.5	0.033	0.1
Sea Water	80	3x10 ³	.01	103
Dry Sand	3-5	0.01	0.15	0.01
Saturated Sand	20-30	0.1-1.0	0.06	0.03-0.3
Limestone	4-8	0.5-2	0.12	0.4-1
Shales	5-15	1-100	0.09	1-100
Silts	5-30	1-100	0.07	1-100
Clays	5-40	2-1000	0.06	1-300
Granite	4-6	0.01-1	0.13	0.01-1
Dry Salt	5-6	0.01-1	0.13	0.01-1
Ice	3-4	0.01	0.16	0.01

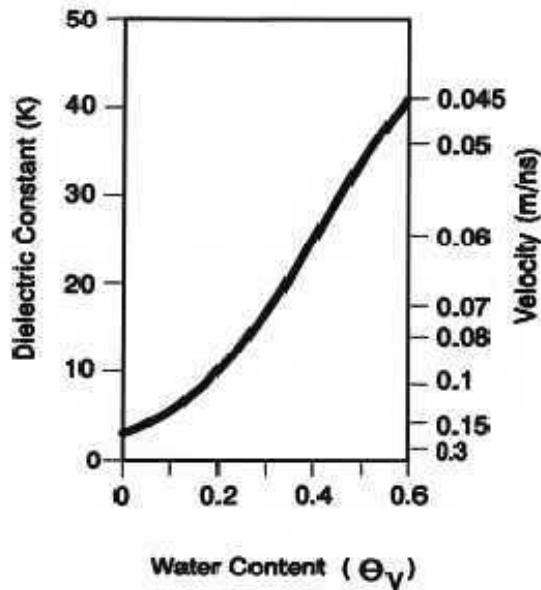
While the subject of mixtures is quite complex, the big picture is not as bad as it sounds. Table 3-4 summarizes the relative permittivity and conductivity for some common materials encountered with GPR (typically in the 10 to 1000 MHz frequency range). The feature that stands out is the presence or absence of water in the material.

A very general picture emerges which the following points summarize.

- Bulk minerals and aggregates in mixtures generally are good dielectric insulators. They typically have a permittivity in the range of 3 to 8 and are usually insulating with virtually zero conductivity.
- Soils, rocks, and construction materials such as concrete, asphalt, etc. have these constituent elements with empty space between the grains (pore space) available to be filled with air, water or other material.
- Water is by far the most polarizable material (in other words it has a high permittivity) naturally occurring.
- Water is invariably present in the pore space of natural (Earth) materials except such unique situations where vacuum drying or some other mechanism assures the total absence of water.
- Water in the pore space normally contains ions and the water conductivity associated with ion mobility is the dominant factor in determining bulk material conductivity.

Empirically derived relationships shown in Figure 3-13 and Figure 3-14 demonstrate the relationship between the permittivity and conductivity of materials with variable volumetric water content. As a general rule the permittivity at zero volumetric water content is in the 3 - 4 range and conductivity is usually very small. As water is added to the mix, the permittivity and conductivity rise until no more water can be squeezed into the available space in the mixture. Obviously porosity of the material dictates the maximum limit on the volume of water that can be placed in the material and ultimately that in turn dictates the maximum permittivity and conductivity of the mix.

Topp Equation



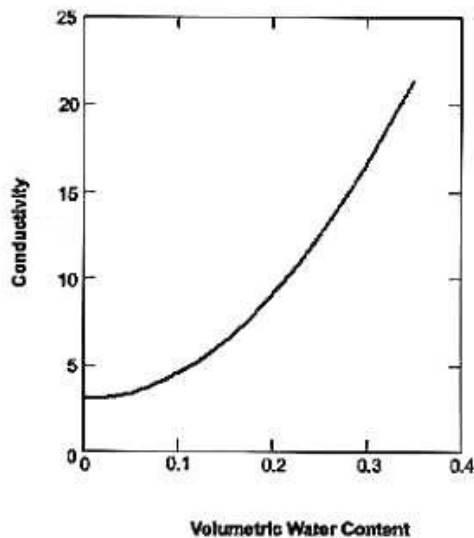
$$K_a = 3.03 + 9.3\theta_v + 146.0\theta_v^2 - 76.6\theta_v^3$$

$$\theta_v = 5.3 \times 10^{-2} + 2.92 \times 10^{-2} K_a - 5.5 \times 10^{-4} K_a^2 + 4.3 \times 10^{-6} K_a^3$$

Figure: 3-13 Variation of dielectric constant and velocity with volumetric water content applicable in the GPR plateau frequency range (see Chapter 4).

These relationships are referred to as mixing relationships. There are a wide variety of theoretical and empirical mixing relationships given for materials. The complexity can be quite enormous depending on the nature of the problem to be addressed. Not only are the material interactions important, some of the interactions have finite response times, which lead to variation of electrical properties with frequency.

Archie's Law



Example of Archie's law for a soil with 1000 ppm TDS groundwater and a surface contribution of 3 mS/m.

$$\sigma = a \phi^m s^n \sigma_w + \sigma_c$$

ϕ - porosity

m - constant 1.3 to 2.5

a - constant 0.4 to 2

s - pore space fraction water filled

n - constant about = 2

σ_w - pore water conductivity

σ_c - soil grain surface conductivity

Figure: 3-14 Summary of Archie's law which relates bulk conductivity to pore water conductivity and porosity.

The Topp equation (Topp et al, 1980) illustrated in Figure 3-13 is an empirically derived relationship which predicts the bulk dielectric constant of soils as a function of volumetric water content. This relationship is most applicable in the 50 MHz to 1000 MHz frequency range. A similar type of empirical relationship applies for conductivity versus water content and its called Archie's Law (Telford et al 1976).

The form of Archie's Law shown is slightly different from the standard one which was originally proposed for use in the petroleum industry at low frequencies of excitation. At GPR frequencies (10-1000 MHz), the pore water is the main contributor to bulk conductivity. An additional mechanism present is surface conduction. Surface conduction is associated with charges which are trapped on the surface of mineral grains in the composite material. The surface area per unit volume in a soil or composite material increases as the grain size of the material decreases. The amount of surface conduction depends on available surface area and the shape of the grains. Generally as grain size becomes finer, as occurs in silts and clays, the electrical conductivity associated with surface conduction contributions increases. Mineralogy also plays a role as evidenced by mineralogical clays which have very large cation exchange capacities (another indicator of large surface area) and exhibit strong surface conduction. As a result, fine grained clay and clay-like materials (such as cement) tend to show higher conductivity at radio frequencies.

Another mixing formula, which is commonly used, is CRIM, which stands for Complex Refractive Index Model (Wharton et al, 1980). This is a totally heuristic mixing formula which weights the relative permittivity based on the volume fraction and the square root of the complex permittivity of the material.

$$\sqrt{K_{mix}} = \sum_i \sqrt{K_i} \theta_i \quad (3-15)$$

where K_i and θ_i are the individual component permittivities and volume fractions.

While heuristic it can be quite helpful for a first order analysis of a problem when trying to get a handle on what one might expect as the changes in permittivity.

Another relationship is the Bruggeman Hanai Sen (BHS) model. This approach uses effective media theory to derive a composite material property from constituents (see Endres and Knight (1992)). Again, there are some basic assumptions about what comprises the host material and what is the additive material when dealing with multiphase media.

3.7 ELECTRICAL PROPERTIES OF WATER

Water is the single biggest factor which determines the bulk electrical properties of materials in most Earth settings. Water is present in all materials to some degree. The reason that water is important is that water is intrinsically a polar molecule. This means that the water molecule has a built-in net displacement of positive and negative elective charges in its molecular structure as schematically depicted in Figure 3-15.

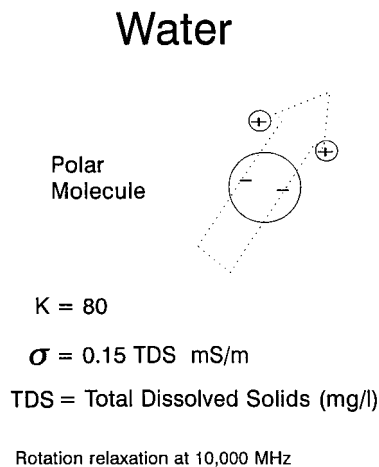


Figure: 3-15 Water plays an important role in determining velocities and attenuation in geologic materials.

Water is highly polarizable because the dipole moment of the water molecule will align itself within an applied electric field. In other words, the dipole distribution in liquid water will redistribute itself to try to align with the applied electric field. This results in a relative permittivity for water in the range of about 80. The permittivity is temperature dependent. Detailed discussions on the properties of water can be found in the informative book by Hasted (1972).

With water being a polar molecule, it will dissolve ionic materials. When ionic substances are placed in water they dissociate forming positively and negatively charged ions which conduct electricity by being mobile in the water. Pure water is a poor electrical conductor. Conductivity is proportional to the numbers of dissolved ions present. Salinity and total dissolved solids (TDS) are measures of dissolved ion concentrations in water.

Water behaves as a polarizable material until frequencies exceed a few thousand MHz. Typically in the range of 10,000 MHz, the water molecule dipole moment can no longer track the applied electric field. The water molecule dipole moment rotation or alignment with an external exciting field is not synchronized which causes energy dissipation in the material. This phenomenon is referred to as a natural relaxation process.

This water relaxation accounts for the utility of microwave ovens. Microwave ovens depend on water being present in the material to be heated. The water relaxation dissipates the electromagnetic energy of the microwaves as heat in the material.

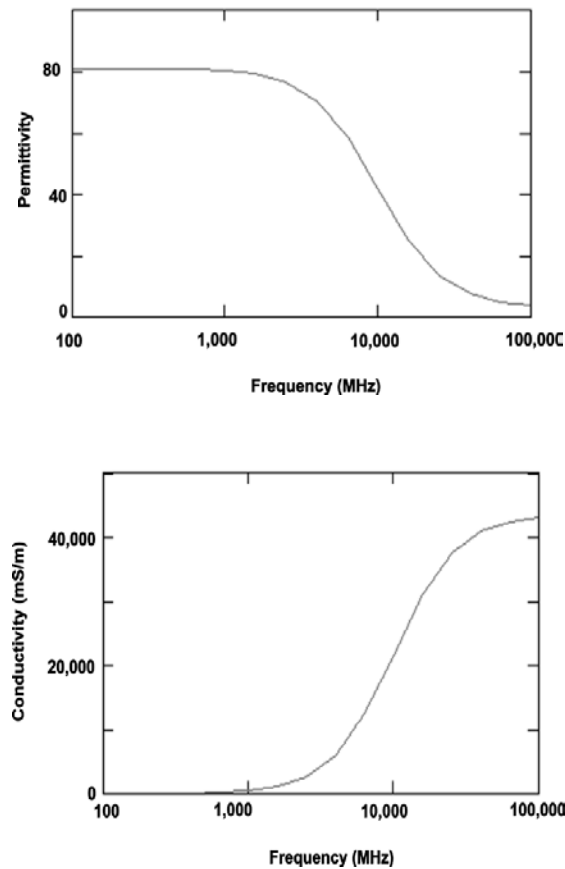


Figure: 3-16 Variation of fresh water permittivity and conductivity with frequency illustration the water molecule dipole moment relaxation response in the 10,000 MHz frequency range.

The relationship between permittivity and conductivity in pure water with frequency is depicted in Figure 3-16. The implications for GPR are that as the GPR frequency exceeds the 500 to 1000 MHz range, the presence of water becomes more and more important as dissipation of energy increases substantially as frequency increases. As a result, only shallow depth sounding applications are practical with GPR at frequencies much above 1000 MHz unless materials are dry (water free). More discussion on frequency dependent properties will be addressed later.

3.8 REAL GPR EXAMPLES

3.8.1 DNAPL SPILL

To illustrate the concept of working with composite materials, two applications of GPR to ground water problems are presented. The first example is the issue of locating DNAPL (acronym for dense non-aqueous phase liquid). A DNAPL represents a hazardous contaminant in the subsurface. A DNAPL when spilled on the ground sinks down into the subsurface. Because it is denser than water, it will tend to displace water from the pore space and sink down through water saturated soils.

DNAPL's are not soluble in water to any large degree. They can be toxic (in some situations) at the part per billion level but soluble at the part per million level. A small pond or pool of DNAPL in the subsurface can contaminate an aquifer for drinking purposes for a substantial period of time.

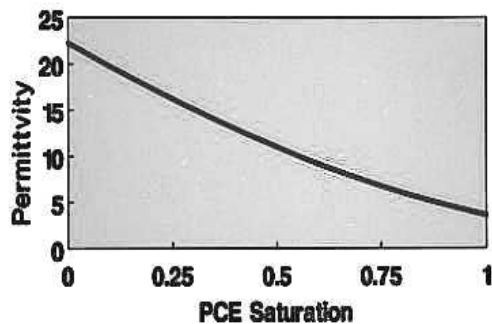
The present example describes a controlled experiment which was carried out to determine whether GPR (and other electric and electromagnetic techniques) could be used to detect the presence of DNAPL's in the subsurface and to track their migration. The experiment is extensively described by Greenhouse et al. (1992) and Brewster et al., (1995).

In this experiment a sandy aquifer at surface was confined using sheet pile walling and a clay aquatard at about a 3 m depth to form a natural cell for the experiment. The composite natural material consisted of beach sand, with some other organic soil present, water, air and DNAPL. For this particular problem the water table was held at surface so that the whole section was water saturated to minimize the air component in the composite mixture. The medium can be considered as a three component mix of soil grains, water and DNAPL.

The soil grains are essentially non-conducting with a permittivity of about 3 to 4. The electrical properties are controlled by the presence of water which, given the soil porosity of about 30 to 35%, creates a bulk permittivity of 25 for the water saturated soil. Similarly, the bulk conductivity is controlled by the ground water conductivity. The bulk saturated soil conductivity is 15 mS/m.

The DNAPL is an insulator with a permittivity in the range of 1.5 and does not conduct on electricity. When it enters the soil, it displaces water from the pore space. Any zone which is substantially penetrated by DNAPL, exhibits a reduction in both permittivity and conductivity. Experimental evaluation of the relationship between electrical properties and DNAPL saturation in the water-saturated material are graphed in Figure 3-17. As the DNAPL displaces water, the permittivity and the conductivity both decrease. These changes in electrical properties define the effectiveness of the experiment.

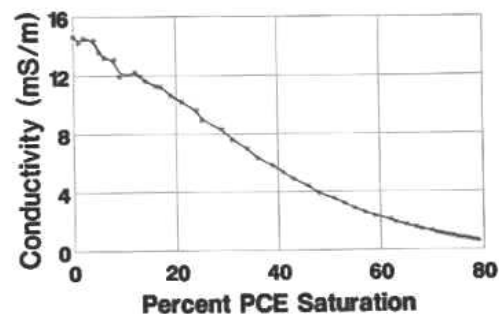
**Relative Dielectric Permittivity
Soil/PCE/Water Mixture - BHS Model**



40% porosity
4.5/2.3/83

(a)

**Conductivity vs PCE Saturation
Lab Observation**



(b)

Figure: 3-17 Illustration of how permittivity and conductivity change when DNAPL replaces water in the pore space of a water saturated sandy soil.

GPR measurements were made at regular time intervals on a grid starting prior to DNAPL injection. The DNAPL penetrated into the subsurface and spread outwards and downwards with time. Changes in the GPR reflection response with time indicate areas of DNAPL concentration build up. As the DNAPL pooled in zones it generated strong reflections of the GPR signal. Figure 3-18a shows the GPR response prior to DNAPL injection. The response at three times after the start of injection are shown in Figure 3-18a, b, c, and d.

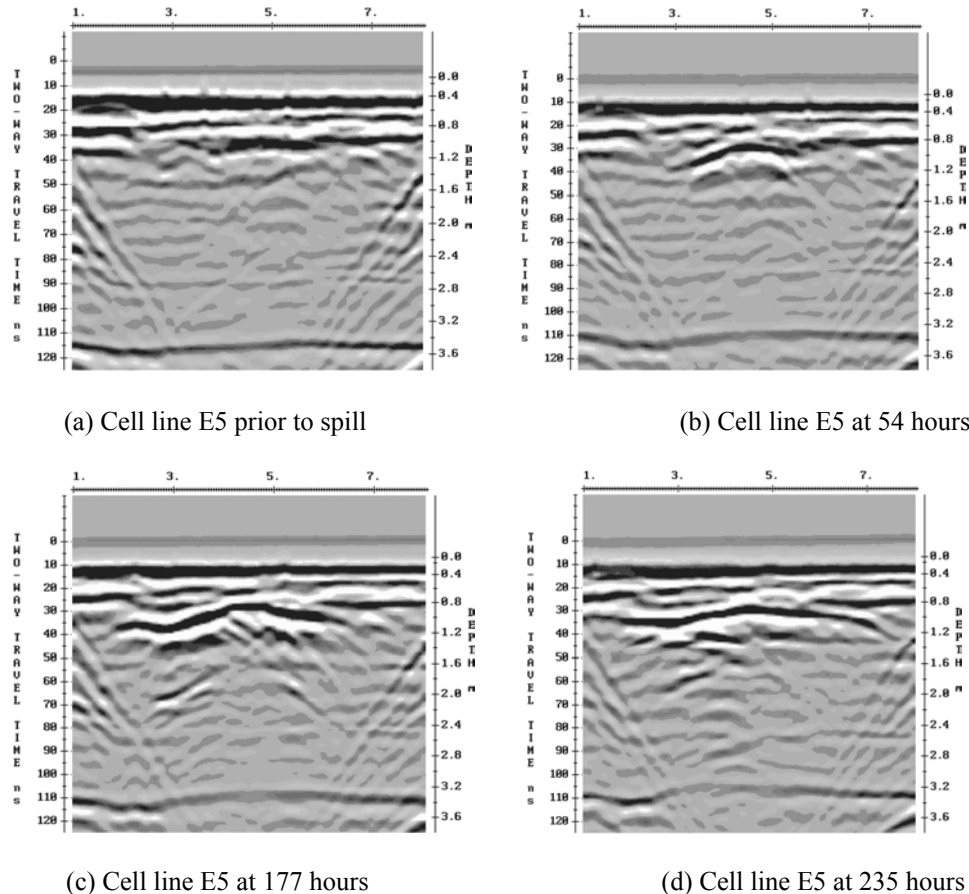


Figure: 3-18 Time lapse GPR cross-sections of an experimental DNAPL spill showing that high concentrations of DNAPL modify electrical properties giving rise to GPR reflections.

The first feature of importance is the strong reflection associated with pooling of the DNAPL at 1 m depth. Second, deeper natural events are affected because the travel time through the DNAPL saturated zone is reduced because of the higher velocity. Third, the reflection amplitude from the aquatard at the bottom is reduced because energy is reflected from the shallower DNAPL pool. These responses are typical manifestations of what one would see at a real site and it illustrates the importance of understanding the interaction of the various constituents in the overall composite mix when evaluating the GPR response.

3.8.2 CONDUCTIVE CONTAMINANT

The second example is that of a leachate contaminate from a landfill percolating through a ground water system. In this case, the landfill has been active for a number of years and the area of testing was in a sand and gravel pit. The sand and gravel have been removed down to the depth of the water table and the pit has been abandoned. The landfill is located up ground water flow direction and generates a leachate. The leachate liquid is chloride ion rich which boosts the pore water conductivity when leachate is present.

The survey area soil consisted of clean sand of glacial/fluvial deposition. The sand is transparent to GPR signals and typically 20 meters of these materials can be penetrated throughout the survey area with one exception. In the area directly down ground water flow direction from the landfill, the radar signals failed to penetrate to the same depth. This effect is caused by changes in the pore water conductivity due to the presence of leachate contaminant from the landfill. An example GPR section down is shown in Figure 3-19. These data clearly show the effect of the leachate-induced change in conductivity of the pore water.

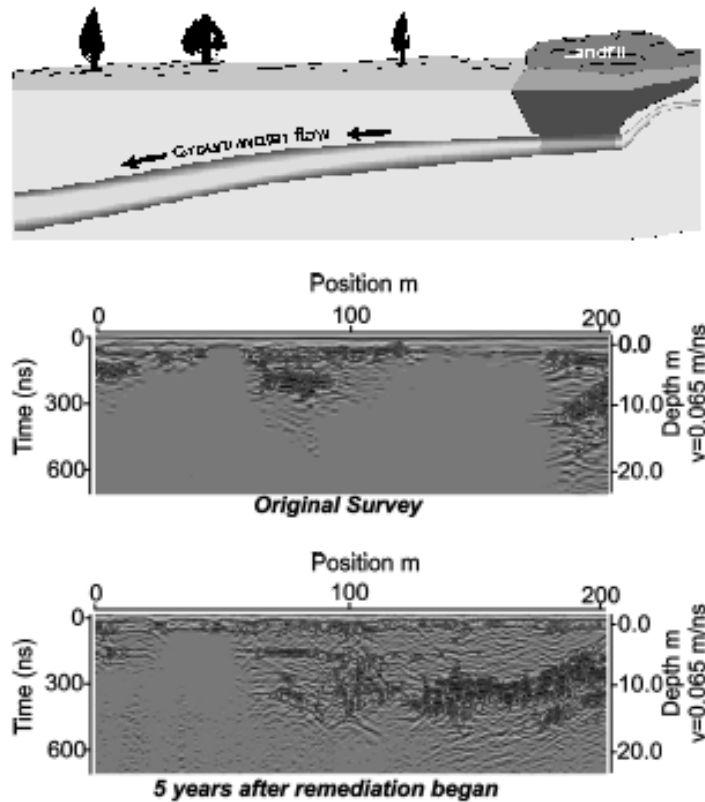


Figure: 3-19 Leachate from a landfill modifies pore water conductivity. The GPR section over the same line at different times illustrate how electrical conductivity affects GPR signals.

From a geologic and a visual observation perspective, the area is uniform; in other words there is water saturated sand throughout the whole survey area. The only thing that changes is the chemistry of the water. The presence of the chloride ion rich leachate boosts the conductivity of the pore water causing the radar signals to be more strongly absorbed and hence the signal penetration depth decreases. This example can be understood using Archie's Law with variable pore water conductivity as the factor controlling the composite mix conductivity.

4 EM WAVE PROPERTIES

4.1 WAVEFRONTS AND RAYS

Electromagnetic fields when propagating as waves can be characterized by wavefronts or by ray paths. Both concepts are depicted in Figure 4-1. The wavefront is the spatial surface on which the signals are all in phase. For a transient signal emitted by a localized source, the equal travel time spatial surface defines the wavefront. The definitions are actually quite a bit more exacting if one studies the subject of geometrical optics (Born and Wolf, 1980) but this simple description suffices for our purposes.

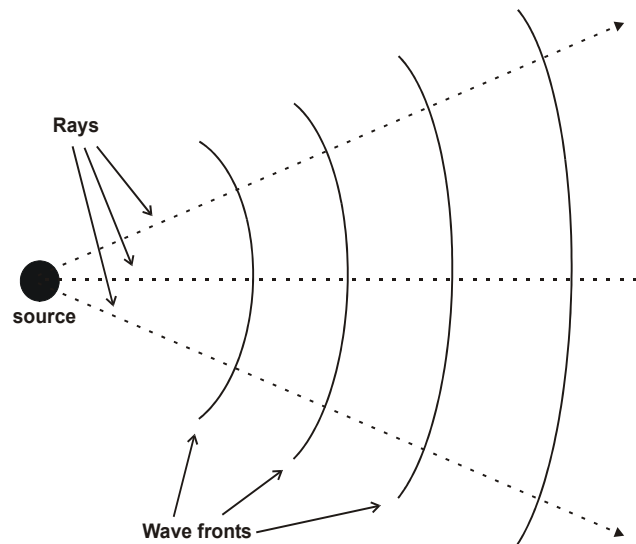


Figure: 4-1 wavefronts are surfaces of equal travel time or phase for waves travelling out from a source. Rays are perpendicular to the wavefronts and sketch out the from trajectory. Both concepts are useful in visualizing GPR signals.

Ray paths are most appropriate when the wavelength or temporal signal duration is very short. Ray paths are perpendicular to the wavefront. The electromagnetic fields when treated as rays conceptually travels along the path defined by the ray. The electric and magnetic fields are perpendicular to the ray path.

Wavefronts and the ray paths are very helpful in visualizing EM fields as they move through a medium. For a more in depth discussion of these topics, the text by Born and Wolf is very helpful; the formal mathematical foundations of these concepts are well presented.

4.2 WAVE PROPERTIES

Wave properties were developed earlier in chapter two. The key EM wave field properties are phase velocity, v , attenuation, α , and electromagnetic impedance Z . The behaviour of these wave properties for a simple medium with fixed permittivity, conductivity and permeability are illustrated in Figure 4-2.

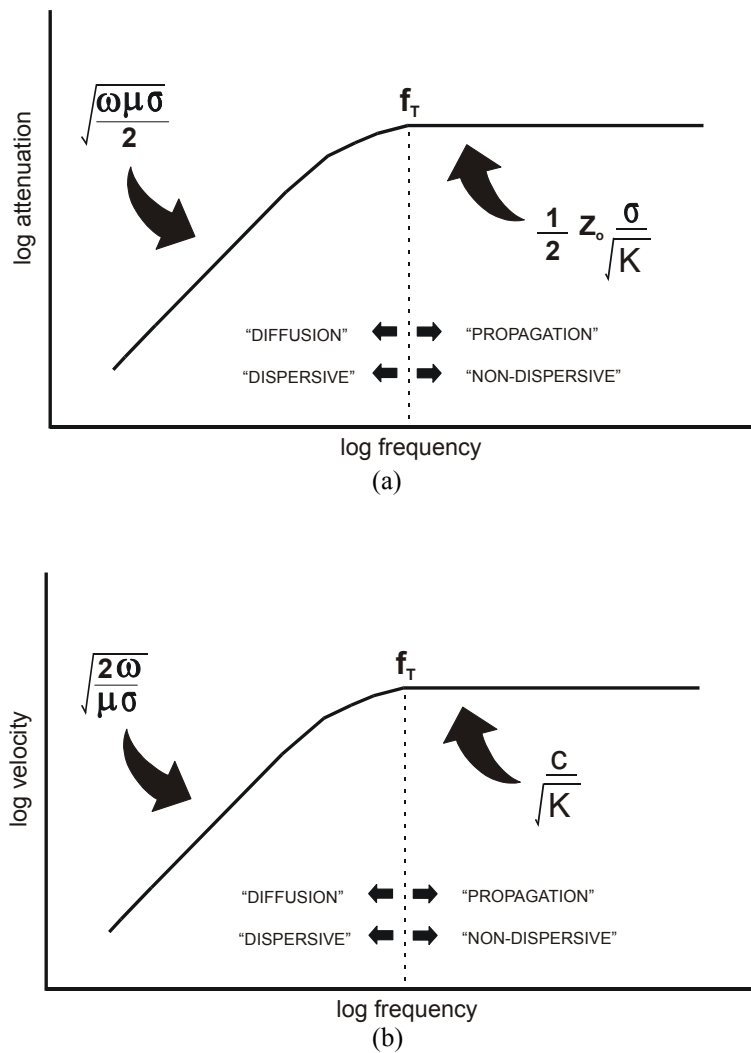


Figure: 4-2 Variation of velocity and attenuation in a simple medium.

The wave properties all show similar behaviour. At low frequencies, all properties depend on $\sqrt{\omega}$. At high frequencies, the properties become frequency independent if ϵ , μ , σ are constant. The high frequency behaviour is the character of most importance to GPR.

At low frequencies, the electromagnetic fields diffuse into the material. The energy distributes itself in the same manner as heat. An impulsive signal gets smeared out (dispersed) because its frequency components are attenuated at different rates and travel at differing phase velocities. The mathematical form for phase velocity, v , attenuation, α , and electromagnetic impedance Z are

$$v = \sqrt{\frac{2 \cdot \omega}{\mu \cdot \sigma}} \tag{4-1}$$

$$\alpha = \sqrt{\frac{\omega \cdot \mu \cdot \sigma}{2}} \quad (4-2)$$

$$Z = (1 + i) \sqrt{\frac{\omega \cdot \mu}{2 \cdot \sigma}} \quad (4-3)$$

At high frequencies, the electromagnetic fields propagate as waves through the medium. All frequency components travel at the same velocity and suffer the same attenuation. An impulsive signal will travel with its shape intact. This is referred to propagation without dispersion (see Annan, 1996). The velocity, attenuation and impedance are expressed as

$$v = \frac{1}{\sqrt{\varepsilon \cdot \mu}} = \frac{c}{\sqrt{K}} \quad (4-4)$$

$$\alpha = \sqrt{\frac{\mu}{\varepsilon}} \cdot \frac{\sigma}{2} = Z_0 \cdot \frac{\sigma}{2 \cdot \sqrt{K}} \quad (4-5)$$

$$Z = \sqrt{\frac{\mu}{\varepsilon}} = \frac{Z_0}{\sqrt{K}} \quad (4-6)$$

with the right most expression being valid where magnetic properties are assumed to be unimportant. Z_0 is the impedance of free space.

$$Z_0 = \sqrt{\frac{\mu_0}{\varepsilon_0}} = 377 \cdot \text{ohms} \quad (4-7)$$

The transition from diffusion to propagation behaviour occurs when the electrical currents change from conduction dominant to displacement current dominant behaviour. For a simple material, the transition frequency is defined as

$$f = \frac{\sigma}{2 \cdot \pi \varepsilon} \quad (4-8)$$

In real materials, the electric and magnetic properties can be frequency dependent as illustrated for water in chapter 3. In this case there will always be a tendency for permittivity to decrease with frequency and conductivity to increase with frequency.

4.3 GPR PLATEAU

Real materials generally behave more as depicted in Figure 4-3. The wave properties will tend to show a plateau, called the GPR plateau, at some frequency range. In some materials this plateau may not exist. Such media are not amenable to traditional GPR measurement methods. The fields will be diffusive in character requiring interpretation of observations using traditional transient electromagnetic induction approaches.

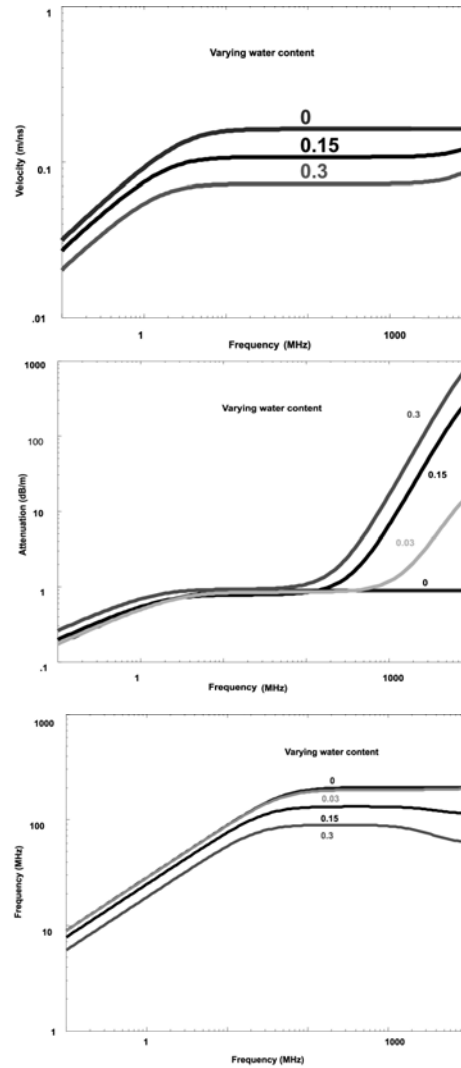


Figure: 4-3 In most geological materials, electrical properties at high frequency will be affected by the presence of free water in the pores and fractures. The water relaxation of 10 GHz causes increased effective conductivity and reduced permittivity. Velocity, attenuation and impedance for materials exhibit a plateau where GPR is a most applicable method.

The “plateau” may still exhibit some gradual increase in velocity and attenuation with frequency. The increase in attenuation is usually the most important as many GPR applications are close to the attenuation limit and any increase can mean the difference between success and failure of GPR. There are two primary factors which induce this increase. One is the presence of water. As discussed in chapter 2, water starts to absorb energy more and more strongly as frequency increases toward the water relaxation frequency of 10,000 MHz. Even at 500 MHz water losses can start to be seen in otherwise low loss materials.

The second factor is scattering loss which are discussed later in this chapter. Scattering losses are extremely frequency dependent and can become more important than electrical losses in many instances.

4.4 MATERIAL INTERFACES

GPR is most frequently used to detect and map features at a distance. To be detectable, the object in question must emit signals. The mechanism for creating such signals is a difference in the electrical properties of the object from those of the surrounding material.

The reflection, refraction and transmission of electromagnetic waves is discussed in the basic EM texts cited previously. The key issues are addressed in the following sections with the concepts most important to GPR and the interpretation of the results.

4.5 SNELL'S LAW

Snell's law expresses how wavefronts change direction as the fields move through materials where velocity is not constant. The concept goes back to the earliest geometrical optics and the bending of light rays. The same law applies with seismic waves.

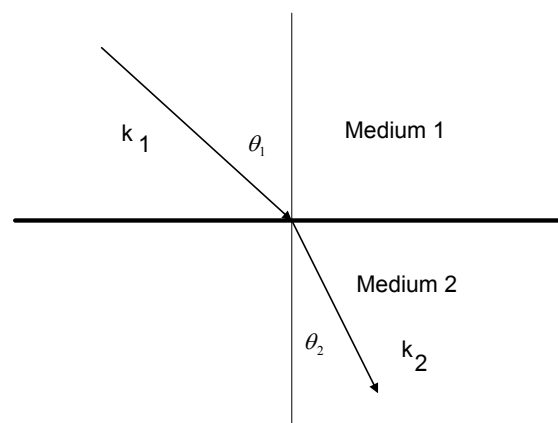


Figure: 4-4 Snell's law predicts that waves change direction of propagation when the waves encounter changes in material properties

The concept is illustrated in Figure 4-4. An EM signal is incident on the boundary between two materials of differing properties. In order for the fields to match at the interface, the horizontal (x direction) movement of the phase must match. From chapter 2, the basic building block is the plane wave and it suffices to illustrate Snell's law. A plane wave incident on the boundary from medium 1 has its propagation vector at an angle θ_1 to the vertical (z axis). When the fields traverse through the interface, the direction of the propagation vector must change. In medium 2, the propagation vector makes an angle θ_2 with the vertical (z axis). Mathematically, Snell's law requires the horizontal component of the propagation vector in each material to be equal.

$$k_1 \cdot \sin \theta_1 = k_2 \cdot \sin \theta_2 \quad (4-9)$$

When the materials are low loss $k=\omega/v$, Snell's law takes the more simple form

$$\frac{\sin \theta_1}{v_1} = \frac{\sin \theta_2}{v_2} \quad (4-10)$$

If multiple interfaces are present, then this rule must be applied at each boundary and the wavefront or rays must bend or change direction at each boundary. If the velocity or materials vary continuously, this relationship still applies.

In GPR, medium 1 can readily be envisioned as the air environment and medium 2 envisioned as the ground or the material to be probed. Since air velocity is always substantially faster than other materials, all signals from the air will bend and travel more vertically downward.

4.6 CRITICAL ANGLE

The critical angle plays a very important role in GPR. It appears in many discussions and interpretations of GPR responses. From the discussion in the preceding section, Snell's law requires the wave fields to bend or change direction in a prescribed manner as velocity changes.

If $v_2 < v_1$ at a simple interface, there a range of angles θ_2 which can not be illuminated from medium as depicted in Figure 4-5.

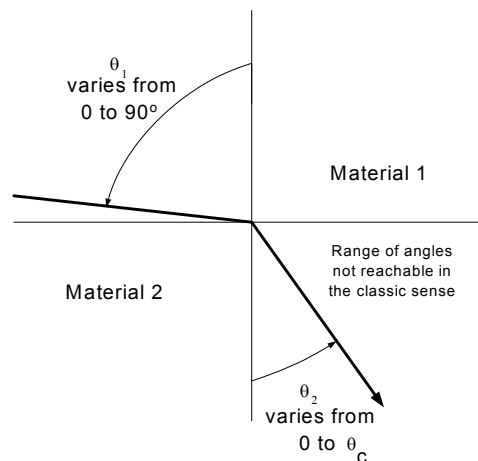


Figure: 4-5 When signals travel from a high velocity (material 1) to a lower velocity (material 2), impinging signals for angles from 0 to 90o only emerge in material 2 between cingles 0 and $\sin \theta_c$. θ_c is normally referred to as the critical cingle.

Incident signals can impinge on the interface between the media at any angle θ_1 from 0 to 90° . The maximum of angle θ_2 is limited to

$$\sin \theta_2 = \frac{v_2}{v_1} \quad (4-11)$$

This value of θ_2 is called the critical angle θ_c . When a signal travels horizontally in medium 1, the signal is refracted downward at the critical angle. In simple ray optics analysis, propagation at angles $\theta_2 < \theta_c$ cannot be energized from

medium 1. As we shall see later, this concept is not completely valid when we deal localized sources near the interface.

When signals travel upward from medium 2 at angles greater than θ_c then these fields require that the angle of propagation in medium take on an counter intuitive character. The details will become more apparent as we deal with waves in layered media later in this chapter. When $\theta_2 = \theta_c$, then $\theta_1 = 90^\circ$. The fields in medium 1 travel horizontally.

When $\theta_2 > \theta_c$ then $\sin \theta_1$ must be greater than 1 which is not possible for normal real physical angles. Mathematically $\sin \theta_1$ can be greater than 1 if θ_1 is a complex number. Physically this means that the horizontal phase velocity must be less than the phase velocity of the material and is only possible if the fields decay exponentially away from the interface in medium 1. Such a wave is called an evanescent wave and only exists at the boundary between materials or in the vicinity of finite field sources.

4.7 FRESNEL REFLECTION COEFFICIENTS

The Fresnel reflection (and transmission) coefficients quantify how the amplitudes of the electromagnetic fields vary across an interface between two materials. Since this topic is treated exhaustively in every EM and optics texts published for the past 100 years, only the essential physics will be reviewed here and the mathematical form presented. See the texts by Jackson (1967) or Born and Wolf (1980) on this topic for details on the mathematical development.

When a plane EM wave impinges on a boundary, it is partially transmitted and partially reflected as depicted in Figure 4-6.

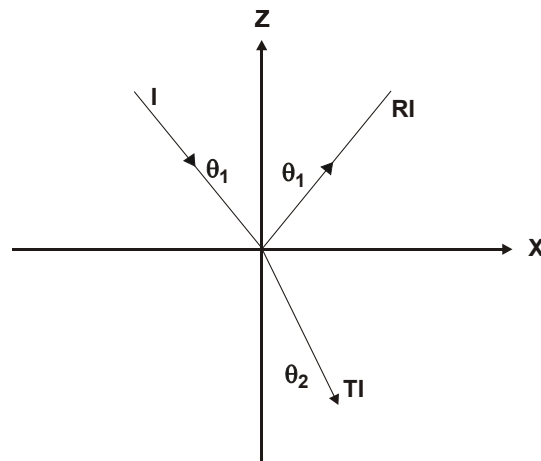


Figure: 4-6 Waves incidence on a planar interface are partially transmitted and reflected. Here the incident signal with amplitude I give rise to a reflected signal RI and a transmitted TI.

The amplitude of the incident field is denoted as I and the reflected signals are denoted as R I and T I where R and T are the transmission and reflection coefficients. At this juncture, we need to get specific about the nature of an EM wave. As we saw in chapter 2, for a given direction of propagation, there can be two independent waves.

When planar boundaries are encountered, it has become traditional to decompose an incident wave into two components whose vector components have a compatible orientation with respect to the boundary. These two wave fields are referred to the TE (transverse electric field) and TM (transverse magnetic field) waves and are depicted in Figure 4-7. The TE wave always has its electric field parallel to the same plane of the interface while the TM wave

has its magnetic field in the plane of the interface. This decomposition is strictly a function of the interface geometry and has nothing to do with the EM fields specifically. By decomposing the field into TE and TM components, the specific mathematical form of R and T can be derived.

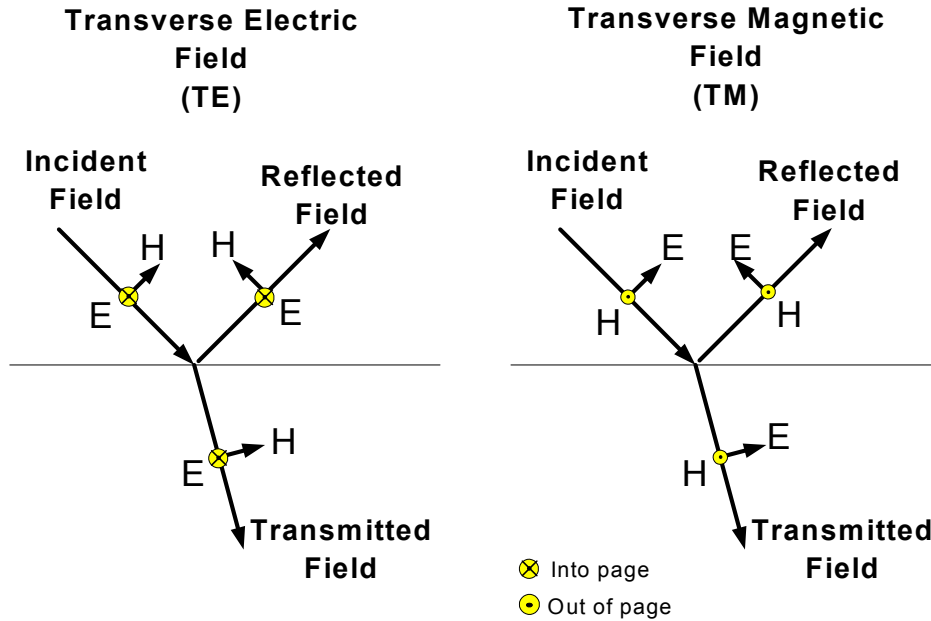


Figure: 4-7 EM waves are transverse vector waves field. For any given propagation direction, two independent fields exist. For planar interfaces, it is tradition to discuss the two waves; one with the electric field in the interface plane called transverse E (TE) and one with the magnetic field vector in the interface plane called transverse magnetic (TM).

The reflection and transmission coefficients for TE and TM waves take different mathematical forms because the field behaviour is different. Formally

$$I_{TE} + R_{TE} \cdot I_{TE} = T_{TE} \cdot I_{TE} \quad (4-12)$$

and

$$I_{TM} + R_{TM} \cdot I_{TM} = T_{TM} \cdot I_{TM} \quad (4-13)$$

where I_{TE} represents the electric field strength for the TE wave and I_{TM} represents the magnetic field strength for the TM wave.

The mathematical forms of R and I are derived by noting two fundamental facts. First, Snell's law must be satisfied. Second, physical behaviour requires electric and magnetic fields in the plane of the interface to be the same on either side of the boundary plus the electric current and magnetic flux density crossing the boundary must be the same on either side of the boundary.

When these conditions are met one finds that

$$R_{TE} = \frac{Y_1 \cdot \cos \theta_1 - Y_2 \cdot \cos \theta_2}{Y_1 \cdot \cos \theta_1 + Y_2 \cdot \cos \theta_2} \quad (4-14)$$

$$R_{TM} = \frac{Z_1 \cdot \cos \theta_1 - Z_2 \cdot \cos \theta_2}{Z_1 \cdot \cos \theta_1 + Z_2 \cdot \cos \theta_2} \quad (4-15)$$

and

$$T_{TE} = 1 + R_{TE} = \frac{2 \cdot Y_1 \cdot \cos \theta_1}{Y_1 \cdot \cos \theta_1 + Y_2 \cdot \cos \theta_2} \quad (4-16)$$

$$T_{TM} = 1 + R_{TM} = \frac{2 \cdot Z_1 \cdot \cos \theta_1}{Z_1 \cdot \cos \theta_1 + Z_2 \cdot \cos \theta_2} \quad (4-17)$$

are the forms for the reflection and transmission coefficients.

It is important to remember that the above expressions apply to the magnetic field in the TM case and the electric field in the TE case. In some instances, the behaviour of the magnetic field in the TE case and the electric field in the TM case are of interest. The reflection and transmission coefficients for the field components are expressed as follows where the superscripts indicate the field component.

$$R_{TE}^H = -R_{TE}^E \quad (4-18)$$

$$R_{TM}^E = -R_{TM}^H \quad (4-19)$$

$$T_{TE}^H = \frac{Y_2}{Y_1} \cdot T_{TE}^E \quad (4-20)$$

$$T_{TM}^E = \frac{Z_2}{Z_1} \cdot T_{TM}^H \quad (4-21)$$

When the EM wave is vertically incident on the interface ($\theta_1 = 0^\circ$), there is no distinction between a TE and TM wave and the TE and TM reflection coefficients become identical (for the field components). For none vertical incidence, the coefficients are different. Two examples are shown graphically in Figure 4-8 for the case when electrical losses are small enough to be ignored. In the first, the velocity decreases at the interface while in the second the velocity increases. Behaviour impedance contrasts for 2:1 (dry soil) to 9:1 (water) are depicted.

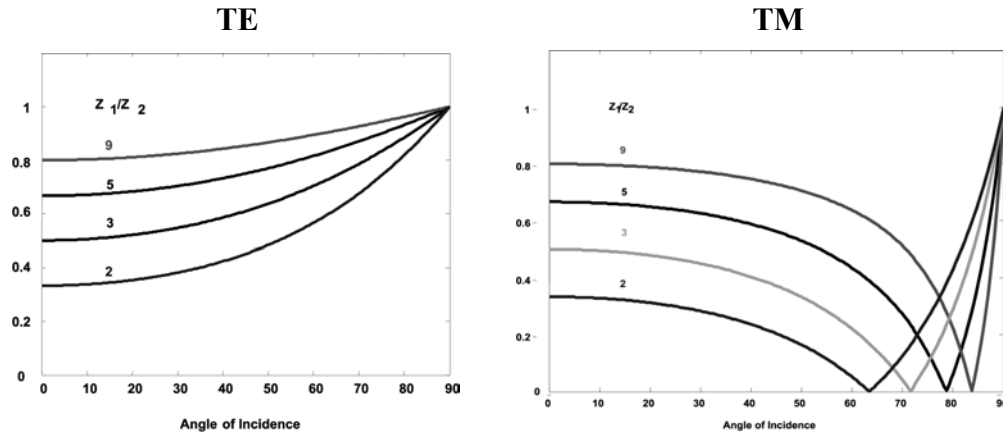


Figure: 4-8 TE and TM reflection coefficients as a function of incidence angle.

These results show the 4 important points that should be remembered when evaluating and interpreting GPR data. First, the reflection magnitude becomes larger at large angles.

Second, the TM reflection coefficient can show a null or a reduction to a minimum as the angle of incidence increases. The angle of the minimum is known as the Brewster angle. At the Brewster angle, maximum transmission through interface occurs. For TE waves, the admittance must decrease at the interface for Brewster angle to exist; for TM waves, the impedance must decrease crossing the interface.

Third, when the waves are travelling from a low velocity to higher velocity medium, the magnitude of the reflection coefficients becomes unity for angles greater than the critical angles. The waves are totally reflected but as mentioned in the previous section, fields do exist in the other material but behave as evanescent signals which decay exponentially with distance from the interface.

Fourth, the sign of the reflection coefficients can be either positive or negative. A positive reflection coefficient means the reflected field (E for TE and H for TM) are in the same direction as the incident field vector while a negative coefficient means the reflected field is in the opposite direction to the incident field direction such as depicted in Figure 4-9.

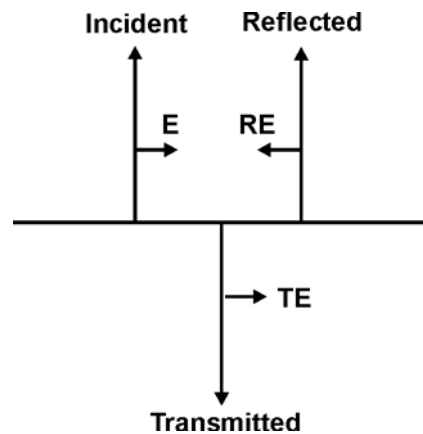


Figure: 4-9 Illustration of polarity of signals for normal incidence. Note R can be either positive or negative which can prove a very powerful interpretation diagnostic.

In order to provide a frame of reference, the normal incidence reflection coefficients for some common interfaces that might be encountered in GPR are tabulated in Table 4-1.

Table: 4-1 Example of normal incidence reflection coefficient for some common GPR interfaces assuming conductivity is negligible.

Boundary	K_1	K_2	Z_1	Z_2	R
Air-dry soil	1	4	377	188	- 0.05
Air-wet soil	1	25	377	75	- 0.67
Dry soil - wet soil	4	25	188	75	- 0.43
Dry soil - rock	4	6	188	154	- 0.01
Wet soil - rock	25	6	75	154	+ 0.34
Ice - water	3.2	81	210	42	- 0.67
Moist soil - water	9	81	126	42	- 0.5
Moist soil - air	9	1	126	377	+0.5
Soil - Metal	9	∞	126	0	-1

4.8 THIN LAYER REFLECTION

A common GPR target is a layer of different material sandwiched in a uniform background. There are many examples – a crack in concrete, a fracture in rock, a thin clay layer in a sand deposit, a DNAPL spreading an impermeable soil horizon. The question that often arises is “Can a layer of a given thickness be detected?”. Since the mathematical solution is relatively simple, it is provided here as a guide for many later discussions.

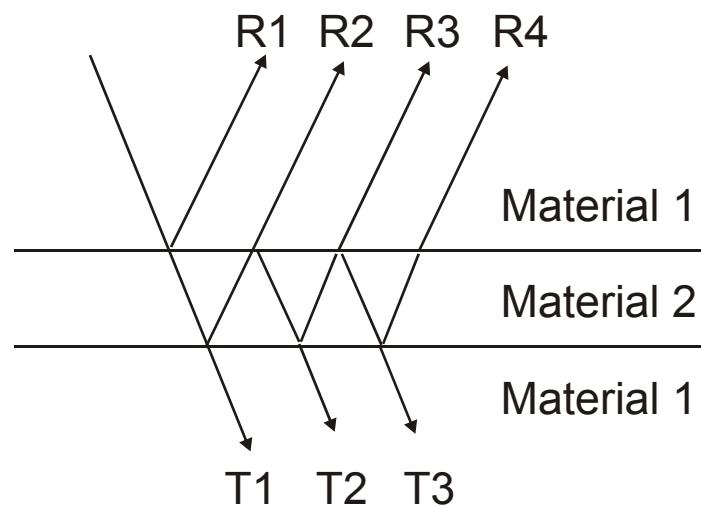


Figure: 4-10 When a signal is incident on a layer embedded in a medium, signals are partially transmitted and reflected. Signals entering the layer bounce back and forth between the interfaces re-emitting reflected and transmitted signal replicas which occur at fixed time delays (or with fixed phase shifts).

Figure 4-10 depicts the nature of the problem and how the response can be heuristically derived by following ray paths. The response is not a single event but a host of events representing the reverberation of the signal back and forth in the layer. Mathematically, the reflection coefficient is expressed

$$R = R_{12} + T_{12}T_{21}R_{21}\beta + T_{12}T_{21}R_{21}^3\beta^2 + T_{12}T_{21}R_{21}^5\beta^3 + \dots \quad (4-22)$$

where R_{pq} and T_{pq} are the previously defined fresnel reflection and transmission coefficients at the boundary between medium p and medium q. The factor β represents the time delay or the phase shift the signal encounters on travelling down and back through the layer. For a normal incident monochromatic (i.e. sinusoidal excitation) wave

$$\beta = e^{i2k_2d} \quad (4-23)$$

where k_2 is the propagation in the layer and d is the layer thickness.

A similar formulation can be developed for the transmitted signal but this will not be explored here.

This expression for R is just a geometric series which can be summed with the result that

$$R = R_{12} + \frac{T_{12}T_{21}R_{21}\beta}{1 - R_{21}^2\beta} \quad (4-24)$$

To understand the behaviour of this reflection coefficient, the result for zero loss as of function of sinusoidal excitation frequency is depicted in Figure 4-11a). The horizontal axis is d/λ_2 since

$$k_2d = \frac{2\pi d}{\lambda_2} = \frac{2\pi fd}{v_2} \quad (4-25)$$

where f is excitation frequency, v_2 is the velocity in the layer and λ_2 is the wavelength in the layer.

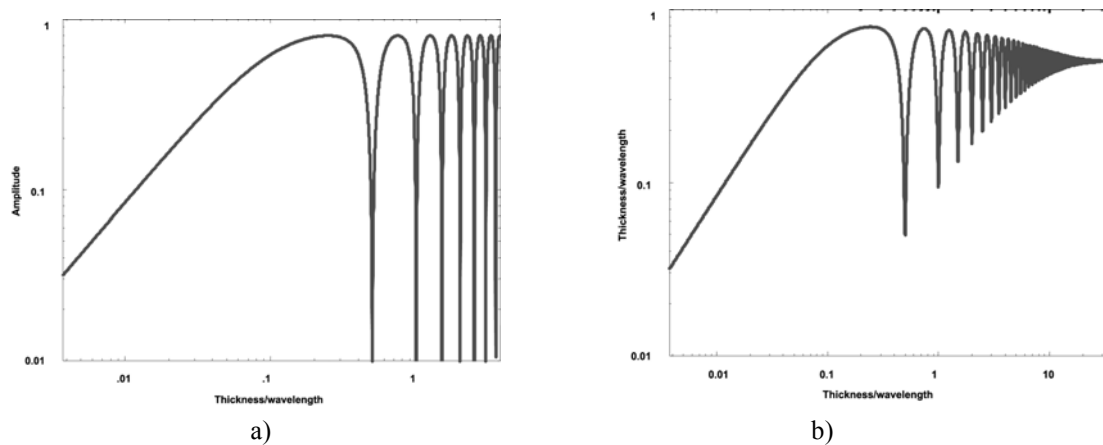


Figure: 4-11 The embedded thin layer reflection coefficient magnitude for sinusoidal excitation. The reflection amplitude varies as the ratio of layer thickness to wavelength. For a lossless layer the magnitude oscillates between 0 and a maximum value. If the layer has some loss, the oscillations damp out as the layer becomes thick.

The reflected response goes to zero at zero frequency ($d/\lambda_2 \rightarrow 0$) and oscillates with maximum at

$$\frac{d}{\lambda_2} = \frac{1}{4} + \frac{n}{2} \quad (4-26)$$

where n is an integer. The maximum value is

$$R = R_{12} \left(\frac{2}{1 + R_{12}^2} \right) \quad (4-27)$$

and minimum is

$$R = 0 \quad (4-28)$$

If the layer has some finite high-frequency loss, R has less extreme variations that die out as d/λ_2 increases as shown in Figure 4-11b). The maxima and minima just indicate when the reflections from the top and bottom of the layer add together constructively or destructively.

Of interest in many situations is the behaviour when d/λ_2 is small. In this case

$$\beta \approx 1 + i2k_2d \quad (4-29)$$

and

$$R \approx \frac{R_{12}}{1 - R_{12}^2} i2k_2d \quad (4-30)$$

Regrouped one has

$$R = \left(-\frac{R_{12}}{1 - R_{12}^2} \frac{2d}{v_2} \right) i\omega \quad (4-31)$$

The expression has two important consequences. First, R depends linearly on the layer thickness which has many uses in the interpretation of GPR responses. Secondly, for traditional finite bandwidth GPR systems, all the excitation frequencies in the pulse can be such that $k_2d \ll 1$. In other words, the excitation spectrum $S(\omega)$ of the incident signal is small (zero) when k_2d gets large. In this case, the transient response of the thin layer has the form

$$R(\omega) = i\omega CS(\omega) \quad (4-32)$$

where $S(\omega)$ is the band limited excitation and C is the bracketed component of Equation (4-31). When transformed to a temporal response, the reflected signal becomes

$$r(t) = C \frac{d}{dt} s(t) \quad (4-33)$$

In other words, the temporal shape of the reflected signal is the time derivative of the incident pulse multiplied by a constant that depends linearly on layer thickness. The result is depicted graphically in Figure 4-12.

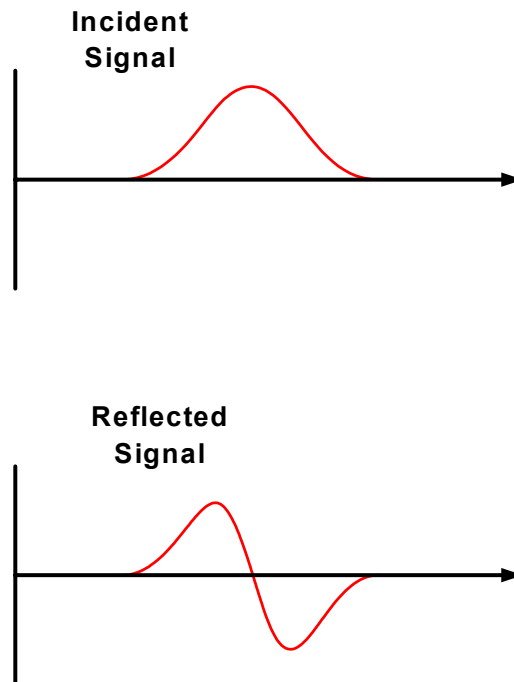


Figure: 4-12 When a layer is very thin compared to all wavelengths in a pulse, the reflected signal looks like the time derivative of the incident signal.

The thin (and finite thickness) layer response discussed here contain many of the essential characteristics of all GPR targets. The simple model is also useful in addressing the issue of resolution versus detection of a feature. Resolution requires layer thickness to be on the dimension of a wavelength (λ_2) or the travel time through the layer to be comparable or greater than the pulse duration. Detection only requires the thin layer reflection to be detectable above the noise level.

4.9 PLANE WAVE MODEL FOR FINITE SOURCES

One of the critical aspects of GPR is the behaviour of the antennas when placed on the ground. This topic can become quite mathematical to quantify the behaviour in even the simplest cases. Again, we will follow the heuristic

approach giving the essential results without resorting to full mathematical formalism.

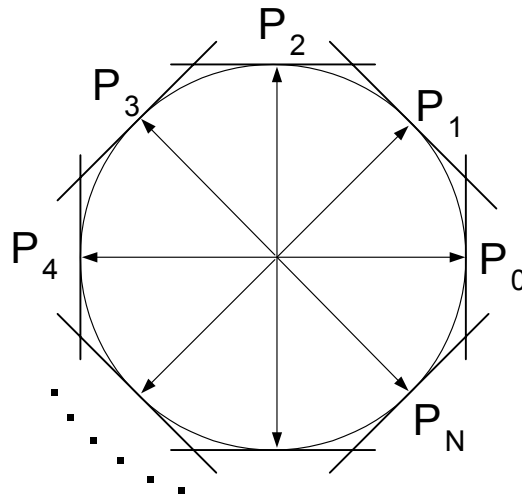


Figure: 4-13 A spherical (in general curved) wavefront can be synthesized as a superposition of planar wavefronts.

The behaviour of a small (by which we mean $d/v \ll 1$ in all materials where d is the source dimension) current element can be treated as a source of spherical wavefronts as we discussed in chapter 2. The spherical wavefront can be envisioned as being built up of planar wavefronts which are tangential to the spherical wavefront as depicted in Figure 4-13. The spherical wave S is thus expressed as

$$S = f_0 P_0 + f_1 P_1 + f_2 P_2 \dots$$

$$\sum_{n=0}^N f_n P_n \quad (4-34)$$

where f_n are the relative wave amplitudes. In the simple two dimensional case, the plane waves travel in the θ directions between 0 and 2π and P_n have the form

$$P_n = e^{ik\vec{r} \cdot \hat{d}(\theta_n)} = e^{ik(z \cos \theta_n + x \sin \theta_n)} \quad (4-35)$$

where \hat{d} is a unit vector in the direction $\theta_n = i \left(\frac{2\pi}{N+1} \right)$.

Writing $k\hat{d}$ out as its geometric components.

$$P_n = e^{i(k_z^n z + k_x^n x)} \quad (4-36)$$

where

$$\begin{aligned} k_z^n &= (k^2 - k_x^{n2}) \\ k_x^n &= k \sin \theta_n \end{aligned} \quad (4-37)$$

While the derivation here is simplistic, in fact the outgoing fields from a localized source can be represented with full accuracy with the limit of letting $N \rightarrow \infty$ and letting k_x range from $-\infty$ to ∞ . The mathematical form becomes

$$s(x, z) = \int_{-\infty}^{\infty} F(k_x) e^{ik_x x} e^{ik_z z} dk_x \quad (4-38)$$

which is just a spatial fourier transform for those familiar with fourier analysis. When the full 3D problem is addressed we have to introduce the y dimension and the resulting form is

$$s(x, y, z) = \int_{-\infty}^{\infty} \int_{-\infty}^{\infty} F(k_x, k_y) e^{i(k_x x + k_y y + k_z z)} dk_x dk_y \quad (4-39)$$

where

$$k_z = (k^2 - k_x^2 - k_y^2)^{1/2} \quad (4-40)$$

This basic type of mathematical formalism has been known and used for over a century. One can refer to the work of Sommerfield (1949), Banos (1962), Wait (1962) and Brekhovskikh (1962).

From this formalism, although very simplified, it is possible to understand the first order behaviour of a GPR system which is addressed in the next section.

A slight of hand here was to allow k_x to range from $-\infty$ to ∞ instead of just $-k$ to k . Physically this means that the angle of incidence range is beyond the physically observable range of 0 to $\pi/2$ (90°). If one carries out the full formal solution, one must mathematically include waves for which $k_x > k$. The meaning of such a wave is seen by noting that k_z becomes imaginary (complex or square root of a negative number). This rather odd result is called an evanescent wave. The 2D plane evanescent wave has the form

$$e^{i(k_x x + k_z z)} \quad (4-41)$$

and, if $k_x > k$, the $k_z = \pm i(k_x^2 - k^2)^{1/2}$ and the plane wave is expressed

$$e^{\pm (k_x^2 - k^2)^{1/2} z + i k_x x} \quad (4-42)$$

A reference horizon is always involved (i.e. $z =$ source position). The sign of z dependence is picked to yield a physically correct field (that is one where the field decays away from the reference plane). The result is sketched in Figure 4-14.

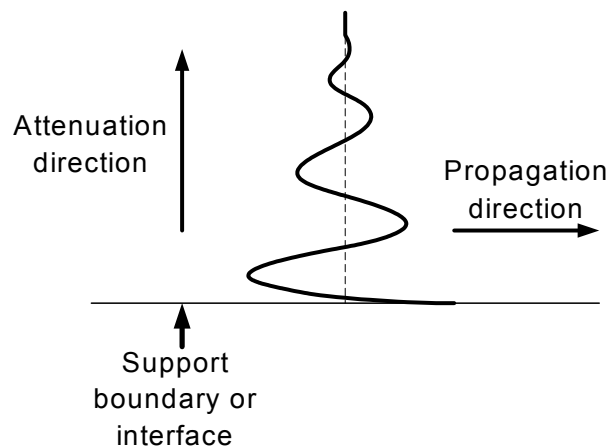


Figure: 4-14 An evanescent wave is one tied to a reference surface. The wave propagates parallel to the surface and decays exponentially with distance away from the surface.

4.10 GPR SOURCE NEAR AN INTERFACE

To continue with our exploration of GPR sources over the ground, the afore discussed wave model describing fields spreading out from the source leads to the visualization in Figure 4-15. When our localized source is above the ground, the signals spread out as depicted in Figure 4-15. The spherical wavefront impinges on the ground. Ignoring finite source dimension and wavelengths, the field at any point along the ground interface can be visualized locally as a planar wave impinging on the boundary at a specific incidence angle defined by geometry (source height and lateral distance). Locally the signal is reflected and refracted according to Snell's law and the fresnel reflection coefficient.

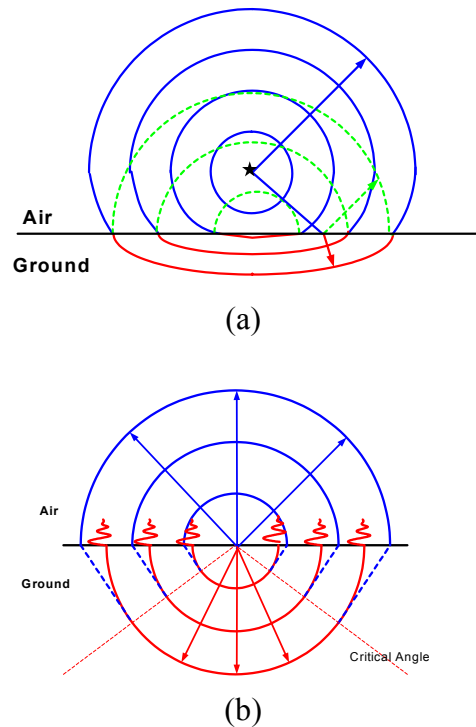


Figure: 4-15 wavefronts spreading out from a localized source a) located above the ground and b) located on the air-ground interface.

If one examines the wavefront in the ground, it is no longer spherical as bending occurs with differing degrees depending on the varying incidence angle. To understand what is happening in the ground and near the interface, the limiting case of the source right at the interface is informative (see Figure: 4-15b). The incident and reflected waves in the air coalesce into an outgoing spherical wave. In the ground, the transmitted signal divides into two parts, a spherical wave and a planar wavefront travelling at the critical angle which links the direct spherical air wave and the spherical ground wave. Near the interface, the spherical ground wave extends into the air as an evanescent field.

The derivation of the mathematical form is based on the plane wave field expansion discussed in the previous section. For those interested, references such as Sommerfeld (1949), Wait (1962), Brekhovskik (1960) and Annan (1973) have discussions. The various wave fields are clearly visible at large distances from the source and/or very short wavelengths. For short distances from the source or long wavelengths, the separation of the events is blurred but the essential concepts are valid.

For a localized target in the ground, there can be several possible paths that energy can travel from a transmitter to the receiver. The concepts are depicted in Figure 4-16 and the ray paths are shown in Figure 4-17.

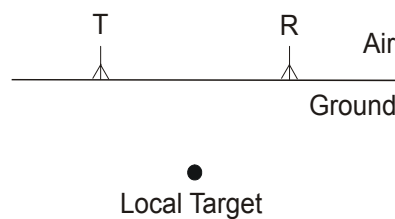


Figure: 4-16 Concept drawing of a localized target beneath the ground with a transmitter and receiver located at the air ground interface.

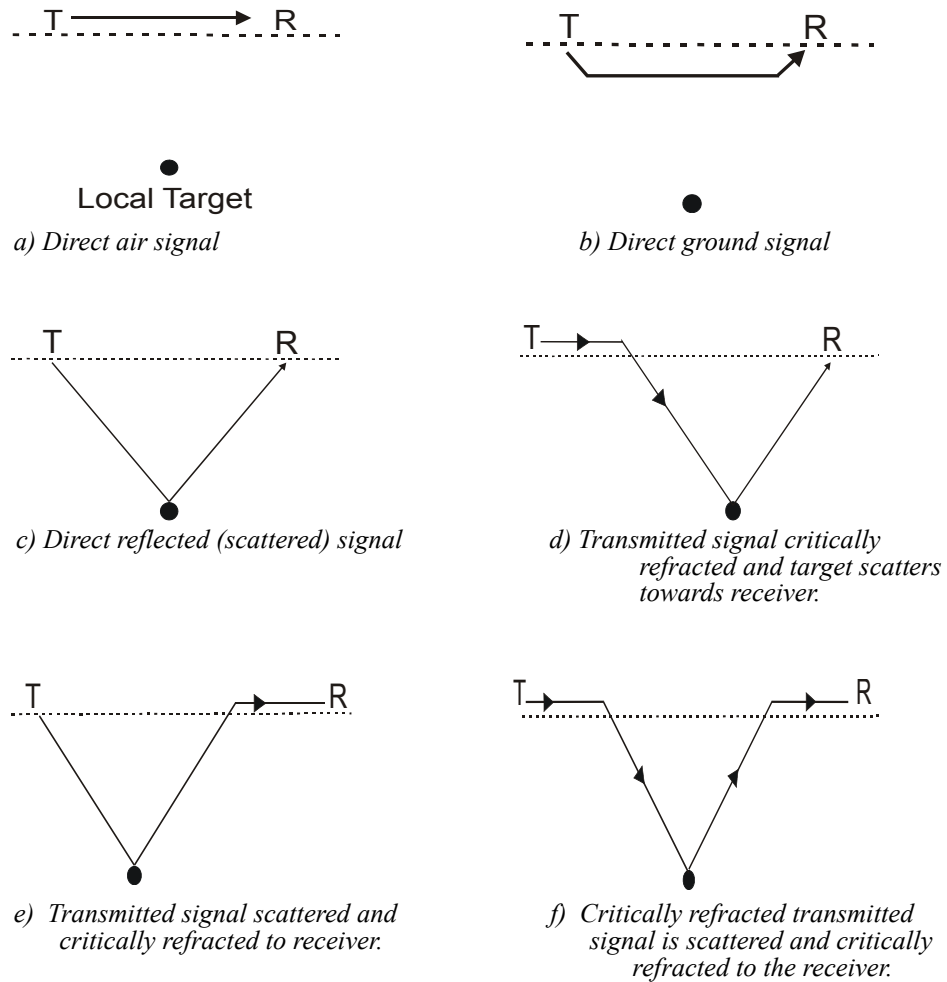


Figure: 4-17 For the simple model in Figure 4-15, there are many paths that signals can travel between a transmitter and a receiver.

The relative importance of each path depends on the target depth, the separation between the transmitter and receiver and elevation of the transmitter and receiver. One should also note that one can not distinguish between d) and e).

In most GPR cases, the transmitter receiver separation is small and the predominant paths are a), b) and c). Paths d) and e) can still be important if both the transmitter and receiver are a substantial distance from the target even if the transmitter and receiver are close together.

The wavefronts are most commonly represented as ray paths as these are simpler to draw. For the source on the ground, the ray paths to a receiver at separation x and associated signal travel times are depicted in Figure 4-18.

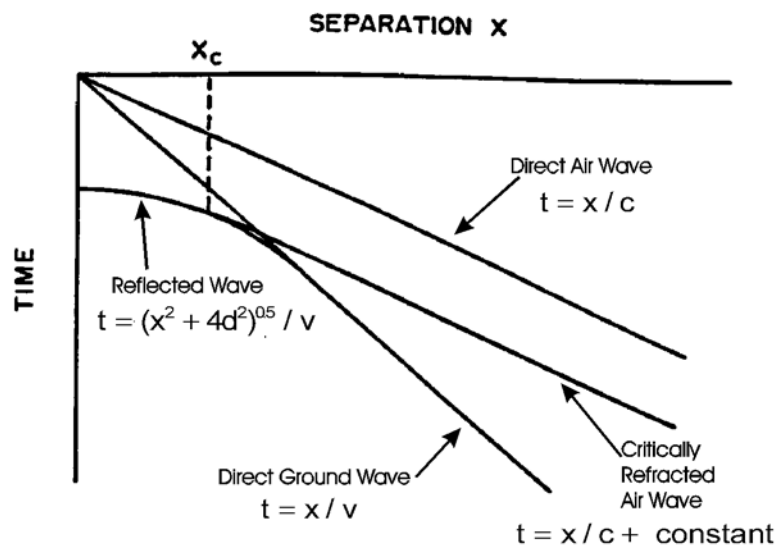
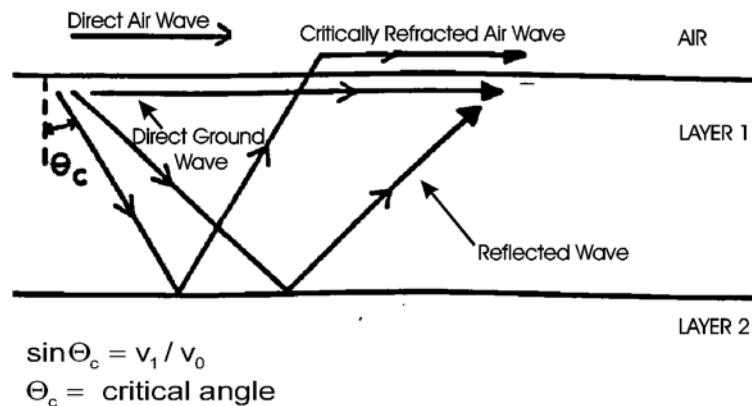


Figure: 4-18 The wavefronts about a source on the ground (Figure 4-15) are often represented as ray paths as depicted. d is the layer 1 thickness, v is the layer 1 velocity and c is the speed of light in the air. The arrival time of these rays versus source-receiver separation provide a means of determining ground velocity structure.

As indicated earlier, the intent here is to provide a basic overview. For the curious, dig into the references. Many of the ideas will be revisited in later discussions where some aspects are explored in more detail.

4.11 RESOLUTION AND ZONE OF INFLUENCE

Since GPR detects objects at a distance, the question that always arises is how accurately can the object be located and what detailed information can be extracted about the geometry of the object. Resolution indicates how precisely the position can be determined. Closely related to the question of resolution is the question of what geometrical attributes of the target can be extracted. Geometrical attributes include such factors as the size, shape, thickness, etc.

Resolution divides into two topics; there is longitudinal (range or depth) resolution and there is the lateral (or angular) resolution. The basic concepts are depicted in Figure 4-19.

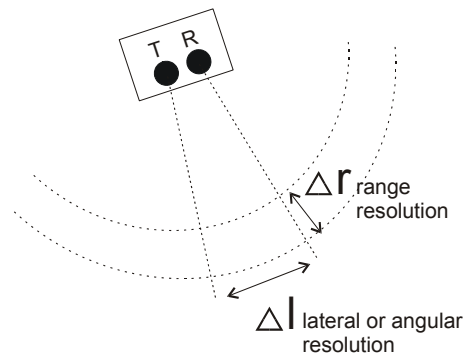


Figure: 4-19 Resolution for GPR divides into two parts; namely range resolution and lateral (or angular) resolution.

Understanding resolution gets into the fundamental issues of GPR detection concepts. These concepts are also common to seismic measurements and in fact they are applicable to any technique where wave phenomenon are used to detect objects at a distance.

In the current discussion we will work in the time domain. We will be considering systems which generate a pulse and detect the echoes from distant targets. Echoes may arrive simultaneously, overlap or be separated in time as depicted in Figure 4-20.

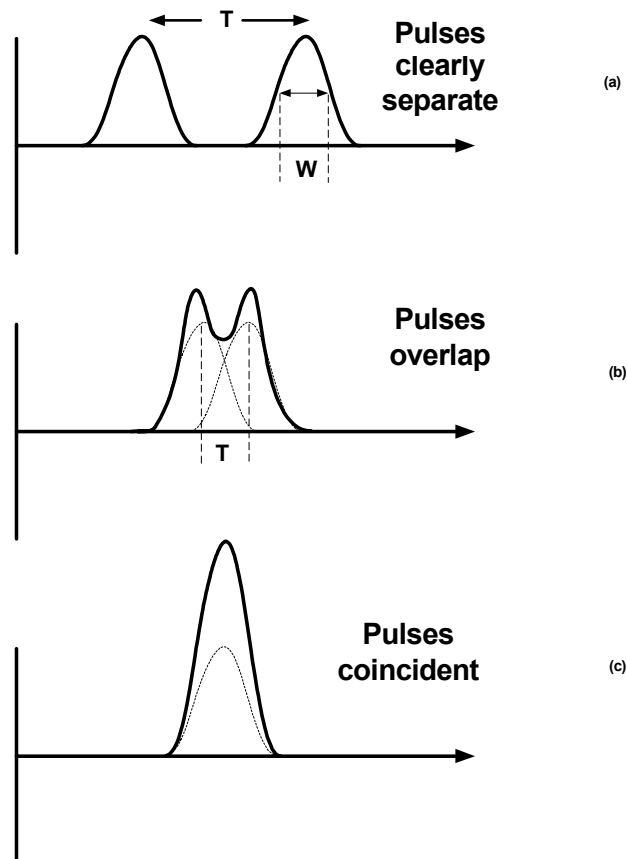


Figure: 4-20 Temporal pulses with $1/2$ width of W . Pulses are clearly separable when $T \gg W$ (a). Two pulses are said to be distinguishable until $T \approx W$ (b). When $T \ll W$ then two events are not distinguishable (c).

When two responses are present, how closely spaced in time can they be and still be discerned as distinct separate events. If two pulses are coincident in time, the amplitude will be enhanced. The result will be one event with a larger amplitude. As time separation between the events increase they can be recognized distinctly as two events when they no longer overlap. This subject is raised again in chapter 5 when we talk about system bandwidth and resolution.

Generally speaking a pulse is characterized by its width at half amplitude, W . While there are many definitions of resolution, the widely accepted definition of resolvable pulses requires that the two pulses be separated by half their “half width” in order to be distinguishable as two events. If they are separated in time by less than this amount then they will most likely be interpreted as a single event.

These temporal pulse concepts must be translated into the spatial domain to define spatial resolution. The approach is best understood by examining the response of two point targets as illustrated in Figure 4-21.

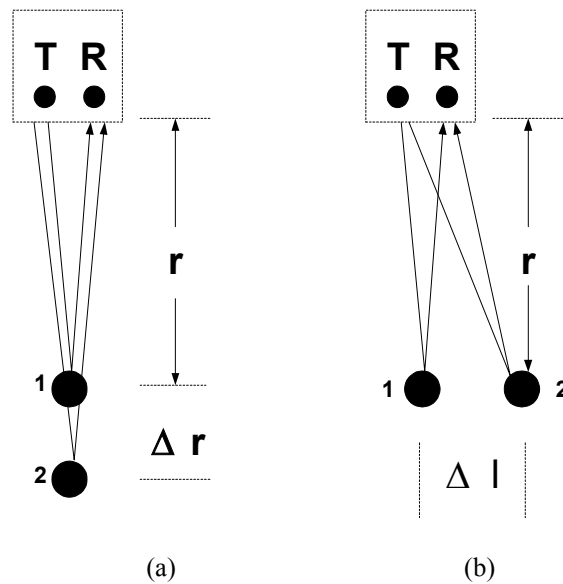


Figure: 4-21 Range and lateral resolution can be determined by considering the response of two localized targets either in-line (a) or side-by-side (b).

For two targets denoted 1 and 2, as shown in Figure 4-21, the longitudinal difference in travel time (which is observed on a GPR record) is directly related to the difference in radial or longitudinal distance between the targets. The travel time for the first target will be

$$t_1 = \frac{2r}{v} \quad (4-43)$$

and the travel time for the second target will be

$$t_2 = \frac{2r + 2\Delta r}{v} \quad (4-44)$$

where v is the propagation velocity of the signal.

The differential time is expressed as

$$\Delta t = t_2 - t_1 = \frac{2\Delta r}{v} \quad (4-45)$$

and this time difference must be greater than half the pulse half width in order that the responses be detected as two events. The spatial separation of targets in the radial direction from the system must be greater than or equal to

$$\Delta r \geq \frac{Wv}{4} \quad (4-46)$$

One can see from this analysis that the pulse width and the velocity in the material combine to dictate the radial resolution. The radial resolution is essentially independent of distance from the source in an ideal world.

The lateral resolution is analyzed in a similar fashion. Following along from the geometry in Figure 4-21, the travel time for target 1 is

$$t_1 = \frac{2r}{v} \quad (4-47)$$

and the travel time for target 2

$$t_2 = \frac{2(r^2 + \Delta l^2)^{1/2}}{v} \quad (4-48)$$

The time difference between the two events is expressed as

$$\Delta t = \frac{2[(r^2 + \Delta l^2)^{1/2} - r]}{v} \quad (4-49)$$

In most situations the target is a substantial distance away from the measurement system permitting the use of an approximation. When this approximation is employed, the time difference is the square root in Equation (4-49).

$$\Delta t \approx \frac{\Delta l^2}{vr} \quad (4-50)$$

The lateral resolution (minimum separation of two side-by-side targets to be distinguishable) must be

$$\Delta l \geq \sqrt{\frac{vrW}{2}} \quad (4-51)$$

From this result one can see that the lateral resolution depends on the velocity and the pulse width as well as the distance from the system. The larger the distance to the targets, the lower the lateral resolution.

The lateral resolution is closely related to the Fresnel zone concept which expresses the resolution concepts for interference of monochromatic (sinusoidal) signals.

With GPR, the pulse width, W , in time is directly related to the bandwidth, B , which is normally related to the center frequency, f_c . Using the relationship

$$W = \frac{1}{B} = \frac{1}{f_c} \quad (4-52)$$

and

$$\lambda_c = v/f_c \quad (4-53)$$

where λ_c is the wavelength of the GPR center frequency, one finds that the lateral resolution can be expressed as

$$\Delta l = \sqrt{\frac{d\lambda_c}{2}} \quad (4-54)$$

This result is identical to the expression for the Fresnel zone for monochromatic signals.

Lateral resolution actually defines an area or zone of resolution since all targets encompassed by a radius of $\frac{\Delta l}{2}$ perpendicular to r can not be resolved.

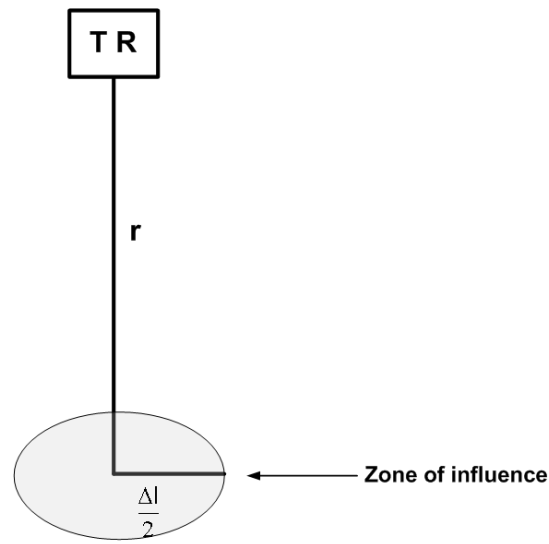


Figure: 4-22 The zone of influence is defined as the area which can contain a second target that can not be uniquely resolved.

The zone of influence extends into a “tube” of influence when the concepts are extended to transillumination GPR techniques. These concepts are not unique to GPR and an excellent discussion of these same concepts from a seismic perspective is presented by Knoll (1991).

4.12 SCATTERING FROM A LOCALIZED OBJECT

Time and again with GPR, one has to address the issue of energy returned from a localized feature in the subsurface. Trying to quantify this behavior is complex and full analysis is beyond the scope of this introductory set of notes. In general, one can visualize the problem as depicted in Figure 4-23. An electromagnetic field is incident on a localized object which gives rise to a secondary field being scattered outward from the object. The source of the secondary field is a movement of the electrical charges in the structure in response to the incidence fields impinging on the object.

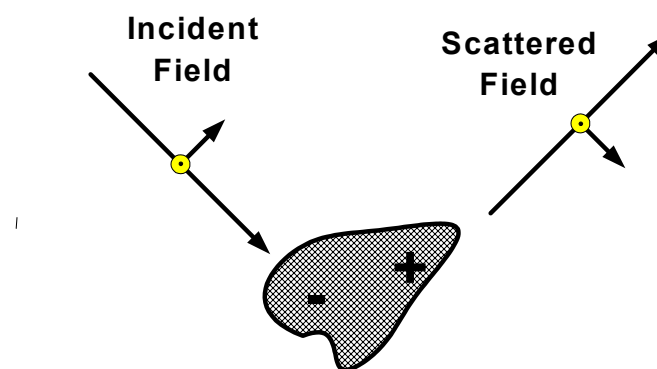


Figure: 4-23 A localized object interacts with an incident electromagnetic field. The field causes movement of electrical charge which gives rise a re-emitted (scattered) electromagnetic field.

Full analysis in even the simplest case in quantitative form is a very involved mathematical problem. The essential

physical behavior is discussed here and readers should refer to other texts on electromagnetics to get more details on the subject.

For most analysis one can view the incidence field as a field which carries a certain amount of power per unit area P_I . The object acts like a mask which absorbs energy and casts a shadow behind it as depicted in Figure 4-24. In essence the object can be treated optically to first order with the incidence signal power being extracted. This extracted power may be absorbed internally into the object or it may give rise to re-radiated energy which makes it detectable at some distance (the GPR goal).

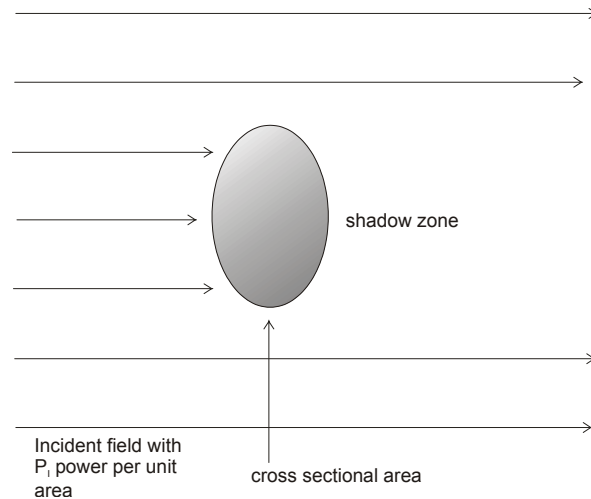


Figure: 4-24 An incident field illuminates a target with a finite amount of power per unit area. The cross section of the target interrupts the power flow. If the target absorbs the power intercepted it will cast a shadow.

In general, one defines the power extracted from the incident field from the object as follows

$$P_{\text{extracted}} = AP_I \quad (4-55)$$

where A is the cross sectional area for the target.

To first order, A is the physical area cross section presented to the field. In practice, however, the area is only a way of representing the effect and is not always equal to the geometrical cross section of the object. Only in the optical limit of infinitely short wavelengths will the geometrical and target cross section be equal. When the object is finite compared to the wavelength then A is called the effective cross section, A_e .

The target may re-emit some or all of the power which it extracts from the incident field. Mathematically the re-emitted signal, P_s , is expressed as

$$P_s = \xi A_e P_I \quad (4-56)$$

where ξ indicates the fraction of the power which is reemitted ($0 \leq \xi \leq 1$). The combination of ξA_e is called the scattering cross section for the target.

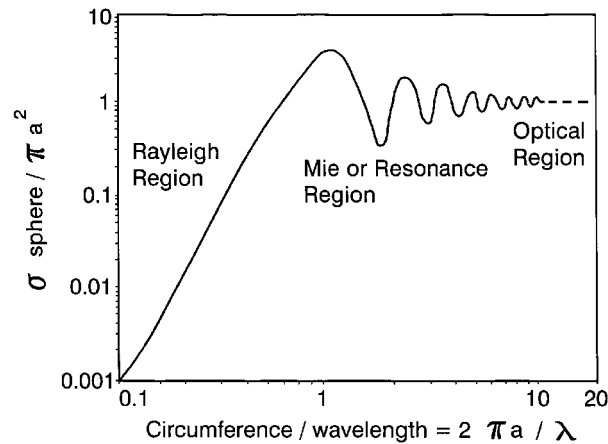


Figure: 4-25 Variation of the scattering cross section of a spherical target as a function of dimension normalized against wavelength (Skolnik (1970)). While specific to a sphere, similar behaviour is displayed by any object of finite dimension. The response increases until the object is on the same order of size as the wavelength. For GPR to penetrate through a heterogeneous material, it is highly advantageous that the GPR wavelength be large compared to the scale of heterogeneity.

Perhaps the most informative study of a scattering object is the work by Mie described in Skolnik (1970) who studied the behavior of a perfectly conducting sphere of arbitrary dimension for monochromatic (sinusoidal) excitation. The basic result is depicted in Figure 4-25. Here the cross section is normalized to the geometric cross section

$$A_e^N = \frac{A_e}{\pi a^2} \quad (4-57)$$

and is plotted against the normalized dimension

$$D^N = \frac{2\pi a}{\lambda} \quad (4-58)$$

where the factor a is radius of the sphere and λ is the wavelength of the excitation signal.

The characteristics of the plotted cross section versus dimension are shown in Figure 4-25. When the dimensions of the object are small compared to the excitation wavelength, the response is called the Rayleigh response. This represents the response of a small object and the response varies as the fourth power of the excitation frequency. When the object dimension approaches the same size as the excitation wavelength, the response is called the Mie or the resonance response. Here effective area can exceed unity and will oscillate in amplitude. Physically the charges (currents) on the sphere have transit times which are comparable to the transit time or the period of the excitation signal. As a result, a response enhancement through resonance or a response suppression when anti-resonance can occur. As the dimension of the object gets larger, the normalized cross section approaches unity. At this point the response is referred to as the optical response and the geometrical cross section essentially matches the scattering cross section. The object is much larger than the wavelength and the sphere has a cross section equal to that of a disc with the same diameter.

It is interesting to compare the Mie scattering response with the behavior of the thin layer reflection coefficient discussed in section 4.8. The behavior is quite similar which is not surprising given that the same basic physics and phenomena are involved.

Of much interest in GPR and many other physical problems is the case where the object is small compared with the wavelength which is referred to as the Raleigh scattering regime. The strength of the scattered signal and hence the scattering cross section very strongly with frequency. Typically the scattering cross section can be expressed as

$$\xi A_e = C a^6 f^4 \quad (4-59)$$

where C is a constant, a is the radius of the object and f is the excitation frequency. One can see the scattering cross section increases rapidly with frequency and slight changes in GPR frequency will give rise to much more intense response from a localized object.

4.13 SCATTERING ATTENUATION

GPR signals are invariably transmitted through complicated media. The signals encounter heterogeneous electrical and magnetic properties on many scales. GPR survey design requires EM wavelengths to be comparable in scale to the objects to be detected. Smaller scale heterogeneities generate weak or undetectable responses but their presence has an impact on the signals as they pass by. The heterogeneities extract some energy as the EM field passes and scatter it in all directions and may absorb some through ohmic dissipation. The best although imperfect analogy is a light bulb being viewed on a foggy night. On a clear night, the light may be visible at distances of many kilometers. When fog (water droplets) are present, the light may only be visible at a few meters. While the water droplets are likely larger than the light wavelength so the analogy is not perfect, the essence of the illustration is that the direct signal is so disrupted on its path from the light to the observer that it never reaches the observer.

When GPR signals travel through complicated non-uniform media, the direct signal is constantly losing energy. It is impossible to quantify the energy loss unless a specific model is used. Considerable research has been carried out on this topic in other EM application fields under the general topic of “propagation in random media”. In this section, a rough idea of the magnitude of the effective and how to quantify scattering attenuation is presented in a very rudimentary fashion.

The GPR signal carries power through the medium. The Poynting vector as discussed in chapter 2 can be used to quantify power transfer. Figure 4-26 illustrates how scattering can be viewed from an energy viewpoint. At any point on the wavefronts, the incident signal with power per unit area impinges on local small scale scatters which are characterized by a spatial size, a, and number per unit volume, N.

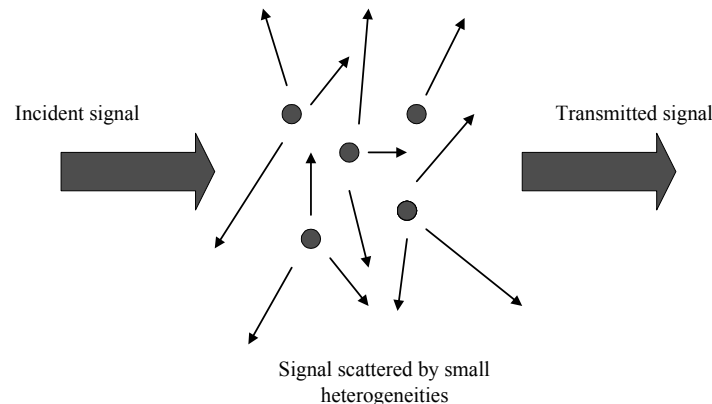


Figure: 4-26 GPR signals are scattered by small heterogeneities in material properties which reduce the transmitted signal

If the power incident is P_i , over a path length dL , the incident field will encounter $N \cdot dL$ scatterers per unit area. Mathematically, the transmitted signal P_T is expressed as

$$P_T = P_i - dP \quad (4-60)$$

where dP is the power extracted per unit area by the scatters in the path length dL . The details of explicitly computing dP can become very complicated. To keep the discussion simple, the scatters can be viewed as having a scattering cross sectional area, A . Following a simple optical analogy, the area the scatter presents to the incident signal indicates the power the scatterer extracts from the incident signal. The scattered power is then expressed as

$$dP = N \cdot A \cdot P_i \cdot dL \quad (4-61)$$

which immediately means that the power will decline exponentially as the fields travel through the material. Re-grouping one has the differential equation

$$\frac{dP}{P} = d \ln P = -N \cdot A \cdot dL \quad (4-62)$$

which has the solution

$$P = P_0 \cdot e^{-N \cdot A \cdot L} = P_0 \cdot e^{-\alpha_s^P \cdot L} \quad (4-63)$$

where α_s^P is the power scattering attenuation coefficient.

Since the EM field power depends on the square of the electric or magnetic field, the fields will attenuate with a scattering attenuation coefficient $\alpha_s = \alpha_s^P / 2$. In other words, the electric (magnetic) field will decrease as

$$E = E_0 \cdot e^{-\alpha_s \cdot L} \quad (4-64)$$

where

$$\alpha_s = \frac{N \cdot A}{2} \quad (4-65)$$

To provide a quantitative measure of this and to stress what role frequency plays, the special case of very small scatterers which can be treated as rayleigh scatterers is analyzed. As indicated in the previous section, scattering from an object can be extremely complex. Even a simple spherical object (normally discussed as Mie scattering) is mathematically difficult.

The rayleigh scattering cross section can be expressed as

$$A = C \cdot a^6 \cdot f^4 \quad (4-66)$$

where C is a constant with units of $m^{-4} \text{ Hz}^{-4}$, a is the sphere radius and f is frequency. The critical point to note is that

scattering cross sectional area is very strongly dependent on the scatterer's radius and the excitation frequency. For small metallic spheres, an approximate value for C is

$$C = 2 \cdot 10^{-6} \cdot K_h^2 \quad \text{m}^{-4} \text{Hz}^{-4} \quad (4-67)$$

where K_h is the relative permittivity of the host medium.

To illustrate the magnitude of the attenuation, two cases are computed and tabulated. The first might represent aggregate pebbles in concrete; the second stones in coarse till. (Note that the attenuation is expressed in dB/m which is equal to 8.69 times the attenuation coefficient above which has the units m^{-1} .)

Table: 4-2 Scattering Attenuation in dB/m

	Case 1	Case 2
Frequency (MHz)	N=1000/m ³ and a=0.02m	N=10/m ³ and a=0.1m
1	1.6 x 10 ⁻¹³	1.6 x 10 ⁻⁹
10	1.6 x 10 ⁻⁹	1.6 x 10 ⁻⁵
100	1.6 x 10 ⁻⁵	1.6 x 10 ⁻¹
1000	1.6 x 10 ⁻¹	1.6 x 10 ³

At the higher frequencies, the small object assumption becomes dubious but the essential points to note are that scattering attenuation is strongly frequency dependent and it increases rapidly with frequency

One last point to note is that scattering attenuation must be added to the ohmic or material loss attenuation to determine the full attenuation the GPR signal will see as it travels through a heterogeneous lossy dielectric medium!!

$$\alpha_{total} = \alpha_{ohmic} + \alpha_{scattering} . \quad (4-68)$$

Scattering losses will invariably be present. The current discussion is intended to provide an understanding of the basic physics. The subject can be dealt with in a lot more depth and still requires more study in the GPR context. The effect of volume scattering was recognized very early by the radio echo sounding community (see Davis (1972), Watts and England (1976)) as a limiting factor in temperate ice sounding. Its effect was more important than for most soil, rock and NDT type GPR surveys because ohmic attenuation is very much smaller in ice. Scattering attenuation quickly became the limiting factor in temperate glaciers where water pockets formed strong scattering centers and radar sounding required reduction of the radar frequency to get deep penetration.

4.14 PROPAGATION DISPERSION

An important concept for GPR is that of propagation dispersion. As we saw in the previous section the attenuation of GPR signals can be frequency dependent. When a pulse travels through electrically lossy ground material, both attenuation and velocity can vary with frequency (see Annan, 1996).

A GPR pulse has a finite bandwidth over which energy is distributed as depicted in Figure 4-27. If the velocity and attenuation vary with frequency, different spectral components will travel at different distances in the same time and

will have different changes in amplitude when they travel over the same distance.

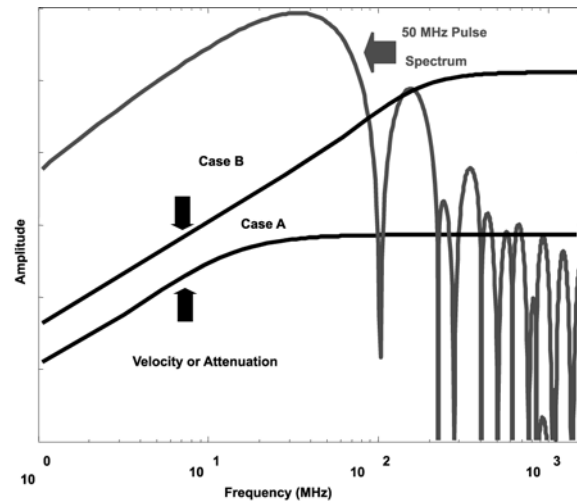


Figure: 4-27 A GPR pulse contains a broad range of frequencies. If velocity and attenuation vary with frequency, the pulse will change its shape as it travels.

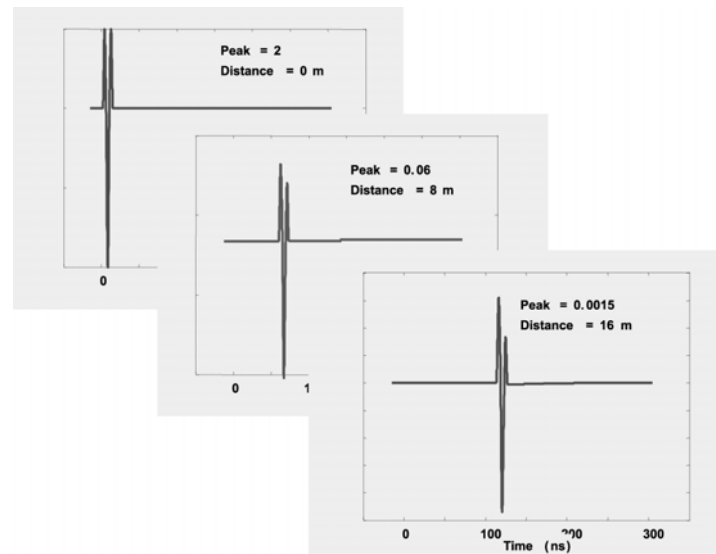
Quantitatively one could view the attenuation and velocity as functions of frequency which vary slowly in many situations. If one makes the assumption that the radar pulse spectrum contained is between frequencies ω_1 and ω_2 , one can understand the effect of propagation dispersion by the following approximate description of attenuation velocity (essentially a local Taylor expansion).

$$\alpha \approx \alpha(\omega_1) + \Delta\alpha(\omega - \omega_1) \quad (4-69)$$

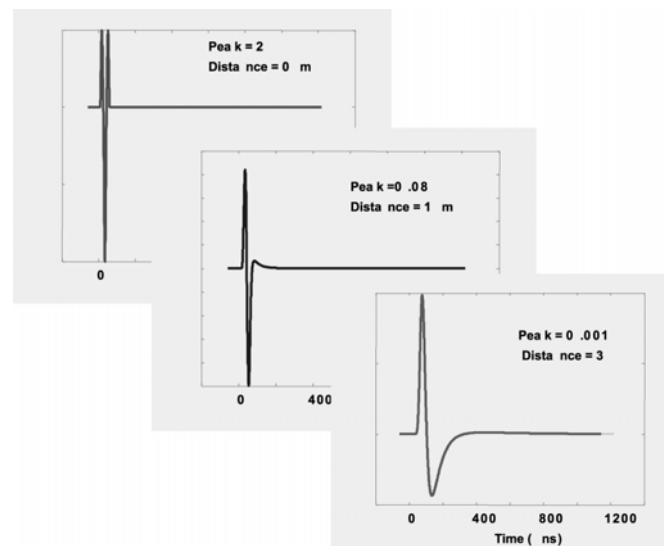
$$v = v(\omega_1) + \Delta v(\omega - \omega_1) \quad (4-70)$$

In all physical situations velocity and attenuation will increase with frequency. Further for the vast majority of GPR problems, changes in attenuation are far more significant than changes in the velocity.

The effect of changing attenuation or velocity is to have higher frequency signals travel faster but suffer more attenuation. This causes a pulse which appears to travel somewhat slower and contains lower frequency content as it moves away from the source. Figure 4-28 shows how the typical GPR pulse can change shape with distance.



(a)



(b)

Figure: 4-28 GPR pulses travel with little change in shape in low loss environments such as a). In higher loss materials (b), the pulse decreases in amplitude rapidly and exhibits strong change in shape.

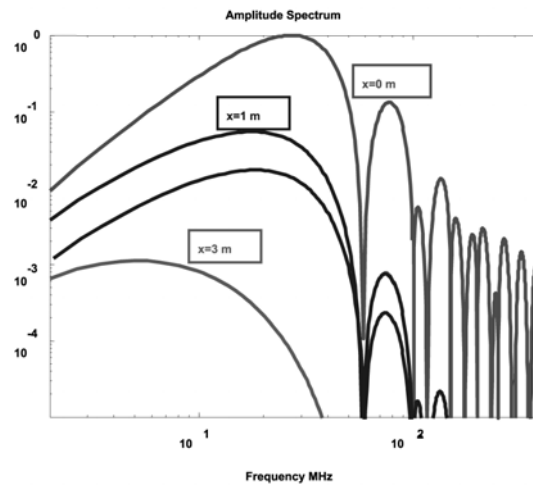
The impact can be viewed as filtering the pulse. If there is no dispersion, Δv and $\Delta \alpha$ are zero and the pulse will travel with the velocity $v(\omega_1)$ and reduce equally in amplitude at all frequencies as

$$e^{-\alpha(\omega_1)x} \quad (4-71)$$

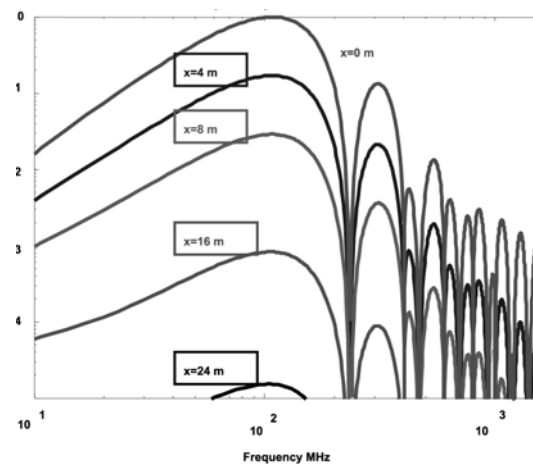
The dispersion can be viewed as applying a filter to the pulse. The filter function will be

$$e^{-i\left(\frac{\omega\Delta v}{v^2}(\omega - \omega_1)\right)} e^{-\Delta\alpha(\omega - \omega_1)\Delta x} \quad (4-72)$$

The velocity change induces a phase advance relative to the constant velocity $v(\omega_1)$ while the attenuation decreases the high frequency amplitude. The effect on the spectrum of a pulse is sketched in Figure 4-29.



(a)



(b)

Figure: 4-29 The effect of frequency dependent velocity and attenuation changes the GPR spectral distribution. In low loss conditions (minimal frequency dependence) the spectral amplitudes reduce uniformly as in (b). In higher loss conditions, low frequencies are less attenuated compared to high frequency spectral components as in case (a).

In the past, this translation of GPR signals to lower frequencies has been noted but seldom explained in terms which provide the insight given above. Often practitioners have referred to the pulse as being shifted in frequency. The pulse does not change its frequency, just that the relative amount energy versus frequency is changed. This is more correctly called ‘colouring’ the spectrum; the spectrum with more red or longer wavelengths will penetrate further through the material.

5 GPR INSTRUMENTATION

5.1 GPR MEASUREMENT OBJECTIVES

In order to put the specifics of instrumentation related to ground penetrating radar (GPR) systems into perspective, it is important that we understand the measurement objectives. GPR as it is known today has developed as a tool for mapping the internal structure of materials, primarily the ground but not necessarily limited to that. In general we are dealing with lossy dielectric materials which quickly absorb the radio wave energy as the signals traverse through the medium.

The requirements for GPR instrumentation are vastly different from those required for airborne tracking and surveillance radars. About the only similarity is that we use the travel time of the signal in order to estimate a distance to the target. Unfortunately the term "radar" brings certain connotations to mind, particularly among lay people and also to electrical engineers versed in the conventional uses of radar. As a result, clearly defining the measurement objectives is required before the specific nature of the ground penetrating radar instrumentation needs can be understood. The following is an attempt to present how the instruments work in principle without overwhelming detail.

5.2 FUNDAMENTAL PHYSICS

Radar is an acronym for "**R**adio **D**etection and **R**anging". The acronym implies that we use radio waves which are emitted from a source to detect an object at a distance and determine the direction to the object as well as the distance to the object. In order to detect an object, the object must re-emit some of the radio wave energy that impinges on it. This requires there be a change in the electrical properties from the surrounding host material. As discussed previously, changes in dielectric permittivity and electrical conductivity cause scattering of radio waves (electromagnetic energy). By detecting this scattered energy, it is possible to detect and position the sources of the scattered energy.

Implicit here is the return signal and the fact that there is a return signal. The magnitude and character of the return signal are controlled by the geometry and the impedance contrast of the object generating the return signal. Unfortunately the return signal is not necessarily unique and trying to uniquely identify the target on this basis alone is sometimes impossible. Even advanced military radars have great difficulty identifying metal objects in a uniform environment. For the GPR application, the problem is orders of magnitude worse because of the highly variable host medium electrical property conditions that can be encountered.

Figure 5-1 illustrates the general concept of how this detection is carried out. We have an object with certain electrical properties immersed in another medium which has a different set of electrical properties. A source of electromagnetic energy, which transmits its signals in the form of radio waves, sends out energy towards the target and scattered energy is detected by a receiver.

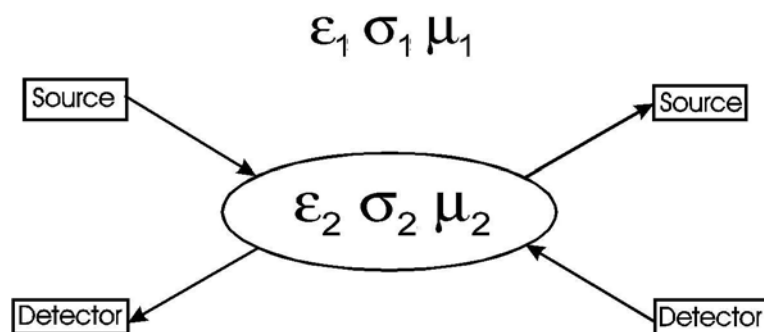


Figure: 5-1 Concept of using reflected or scattered signal to detect and define an object. The distance to the object and some information on its composition can be obtained from reflected signal. Implicit in the full three dimensional positioning is the ability to sense or detect the signals in or from specific directions or make measurements in a number of different positions.

The physical items and procedures involved are as follows.

- a. An electrical circuit is required to generate time fluctuating voltages in the desired frequency range in some controlled and monitorable manner is required.
- b. An efficient means of translating this electrical signal into a electromagnetic wave field which can traverse (without cabling or connections) through the host medium to the target is required. The transducer which does this is normally referred to as an antenna. An antenna transforms electrical voltage signals into outward propagating electromagnetic wave energy and vice versa. The source(s) and antenna are normally referred to as the transmitter.
- c. The target must generate scattered energy. As discussed in a previous chapter, this requires a contrast in electrical properties and suitable geometrical sizes compared to the wavelength and distance from the source such that some detectable signal can be returned to a measurement device.
- d. A detection system (receiver) normally consisting of an antenna and electronic circuitry which can detect electromagnetic waves and transform this information into an electrical voltage or current which can be recorded and viewed.

The fundamental physical behavior is the propagation delay between the time that the source emits its signal and the time at which any echoes return back to the detector. This time delay is determined by the distance to and from the target divided by the speed with which the waves propagate through the host material. The essence of GPR (and all radars) is to measure this time delay. The larger the time delay the greater the distance to the target, assuming uniform velocity conditions.

No matter how the radar data are acquired, the most common display is one of showing the signal amplitude versus time. Figure 5-2 illustrates the basic concept. The data display is one which shows the amplitude of the return signal versus delay time. Detection presupposes the return signal from the target is bigger than background signals. While not usually stated, this detected signal contains responses from a range of spatial directions as well as differing distances. The real world is three dimensional - not one dimensional.

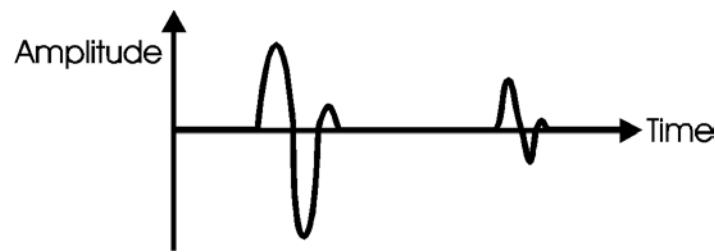


Figure: 5-2 Typical data recorded by a GPR for analysis is an amplitude versus delay time. Events from three dimensional space are mapped into a one dimensional time record.

The preceding discussion addresses the measurement of distance to a target. In addition to knowing the distance of the target, it is also important to know the direction to that target. Two approaches are used to measure direction as depicted in Figure 5-3. When the direction in which the source emits its energy and the direction from which energy is detected with the receiver are controllable, a beam steering process is used to angularly position the target. In other words, the antennas are pointed at the target and antenna orientation is measured.

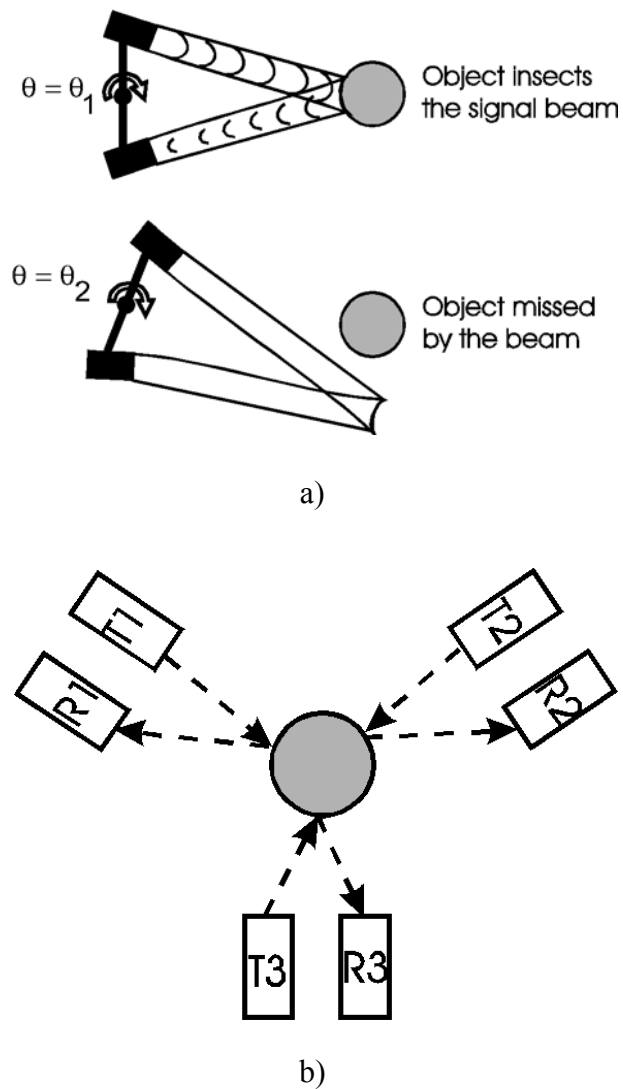


Figure: 5-3 a) Source receiver signal directionality used to obtain angular position information. b) Multiplicity of measurement positions used to define position.

If the source and detector directivity are low or non-existent, then moveable source and detector or multiple source and detectors can be used to locate a target by triangulation. From the basic physics, what we need in instrumentation is as follows.

- a. a means to generate the signal;
- b. a means to emit the signal in the form of radio or EM waves;
- c. a means to detect and measure the delay time of these return signals;
- d. a means to record and display detected signal and delay time;
- e. a means for controlled movement or aiming of the signal sources.

5.3 GPR TIMING AND RESOLUTION

The next step in instrumentation assessment is to define the timing and the frequency bandwidth requirements for GPR instrumentation. In general terms, GPR is used for looking at objects which can be as shallow as one centimeter and as far off as hundreds of meters. If we choose 0.01 to 100 meters as extremes for typical GPR exploration, then these provide an indication of frequencies, times and resolutions that are important in instrumentation.

Obviously there may be exceptions to these minimum and maximum depths of exploration, but these can be handled by the same type of analysis as we are discussing here. What we are trying to do is get a typical range of values for the parameters which have to be considered.

5.3.1 TIMING

If we take the minimum and maximum distances and combine these with the minimum and maximum velocities typically encountered in most geologic or man-made materials explored by GPR, then we have minimum and maximum time ranges for the objects that we may wish to detect. Table 5-1 summarizes this information and we can see that the extremes for the travel time of our signals will be somewhere between 67 picoseconds and 6,700 nanoseconds. These are very small times on an every day scale.

Table: 5-1 Computation of Maximum & Minimum Delay Times

$$\text{Delay time} = \frac{2 \times \text{Distance}}{\text{velocity}}$$

$$\text{Maximum time} = \frac{2 \times \text{maximum distance}}{\text{minimum velocity}}$$

$$\text{Minimum time} = \frac{2 \times \text{shortest distance}}{\text{maximum velocity}}$$

Maximum distance	100 m
Minimum distance	.01 m
Maximum velocity	0.3 m/ns (air)
Minimum velocity	0.033 m/ns (water)
Maximum time	= 6060 ns
Minimum time	= 67 ps

5.3.2 RESOLUTION AND BANDWIDTH

In addition to the travel times we also have to consider how we are going to discriminate whether or not more than one target is present. This aspect of the problem leads to the concept of system bandwidth. Discrimination of more than one target is summarized in Figure 5-4. If two events occur on a record then they have to be sufficiently separated in time so that the two events are clearly seen as distinct entities rather than one larger event (Berkhout (1984), Knapp (1991), Kallweitt & Wood (1982)).

Resolution is most easily understood by considering two pulses which occur as amplitude oscillations versus time. The pulse envelope, as depicted in Figure 5-4, is the dotted line which encloses the oscillatory radar pulse. If the travel time to two individual targets is similar the pulses (and the envelopes) overlap. It is generally accepted that the two events can be distinguished as opposed to having one large event if the targets are separated in time by a time difference of half the envelope width.

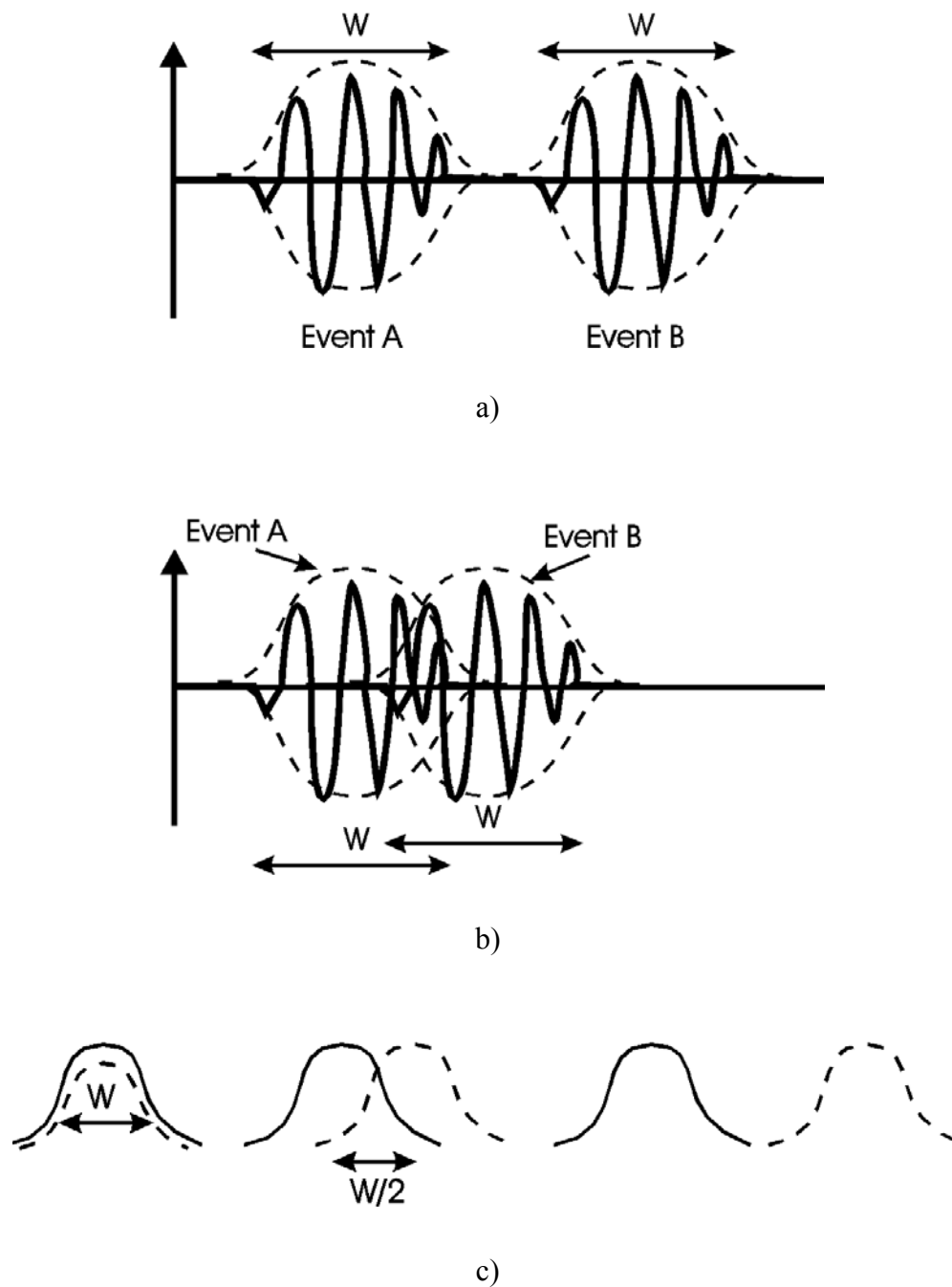
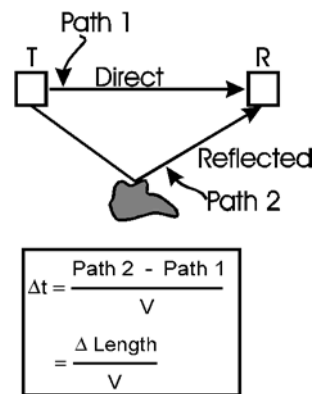
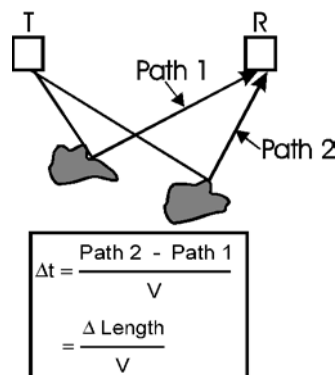


Figure: 5-4 a) Two radar return events are well resolved if the two transient signals are clearly separated in time as depicted here. The dotted lines, called the pulse envelope, are totally separated. b) When two events overlap each other in time, the question arises as to whether one or two events are present. c) Examining pulse envelopes only, two events are said to be resolved when separated by a time $w/2$.

For GPR, there are two aspects of resolution which have to be considered. The first is referred to as "transmitter blanking", and the second is referred to as dual target separation and discrimination. The two concepts are illustrated in Figure 5-5.



a)



b)

$$\Delta \text{Length} > \frac{w}{2} \times \text{velocity}$$

c)

Figure: 5-5 a) Transmitter blanking occurs when the direct signal travelling from the transmitter to the receiver overlaps in time reflected signals. b) If two targets yield similar path lengths the differences in travel time can be small causing reflected pulses to overlap. c) To resolve two events, the path length difference must exceed half the pulse width multiplied by the velocity.

Transmitter blanking is the phenomenon known as the inability of a receiver to detect signals until after the transmitter has finished transmitting. The transmitting source usually emits a very large signal and, if the receiver is in close proximity to transmitter as is usually the case, then the receiver will see the very large direct transmitted signal. If this signal is sufficiently large that the receiver electronics are overloaded the receiver will not detect any reflected signals until after the transmitter has ceased emitting its signal.

The second aspect of resolution is separating responses from two closely spaced scattering targets. In this case the separation in time is proportional to the difference in distances to the targets divided by the propagation velocity in the medium.

This discussion supposes that the radar signal has been processed to make W as small as possible. The envelope width in time, W , is obviously important and measures the spatial resolving capability of the radar.

The envelope width is usually the half width of the envelope. (i.e. it is the time between the points on the envelope where the envelope is greater than 2 of its peak amplitude or 6 dB points). Sometimes other definitions are used such as -3 dB or -10 dB points.

Considerable time has been expended here in discussing resolution because resolution is a very critical aspect of system design. The resolution needs of a system translate directly into the frequency content or bandwidth required in the transmitter and the detection system.

In practical GPR applications resolution is dictated by the depth of exploration. Realistically one does not require the same resolution needed for targets at one centimeter as for targets at depths of a hundred meters. A rough guide is that the resolution should be on the order of the maximum depth of exploration divided by 100.

$$\Delta r \approx \frac{d_{\max}}{100} \quad (5-1)$$

The above relationship is reasonable representative of modern commercial systems and shallow sounding applications. While for very shallow depths the 100 factor is appropriate, for larger depths the resolution available with modern systems can approach 1/1,000 of the depth of exploration.

Taking this basic analysis, we can then say that the time between events is roughly given by the maximum depth divided by the minimum velocity divided by 100.

$$\Delta t \approx \frac{2}{v_{\min}} \times \frac{d_{\max}}{100} \quad (5-2)$$

From this analysis we have guidance as to what values of W (pulse width) are likely to be useful. The results are summarized in Table 5-2.

Table: 5-2 Summary of depth, resolution, and bandwidth typically needed in GPR systems

Maximum Depth (m)	Resolution Required(m)	Envelope Width in (ns)	Required Bandwidth (MHz)
0.1	0.001	0.02	50000
1.0	0.010	0.20	5000
10.0	0.100	2.00	500
100.0	1.000	20.00	50

$$\text{Bandwidth} = \frac{1}{\text{Pulsewidth}}$$

**Note: A material with a permittivity of 9 is assumed in calculated envelope width and bandwidth.*

5.4 GPR BANDWIDTH

Instrument bandwidth determines a systems minimum response time (for a GPR this translates into resolution). Bandwidth and response time (i.e. radar envelope width) are inversely depicted in Figure 5-6.

At one extreme, a narrow bandwidth amplitude modulated sine wave has a very oscillatory pulse which has a finite time duration. In the frequency domain, the frequency bandwidth of the signal is quite small. In radar jargon, this is referred to as a pulsed CW (continuous wave) signal.

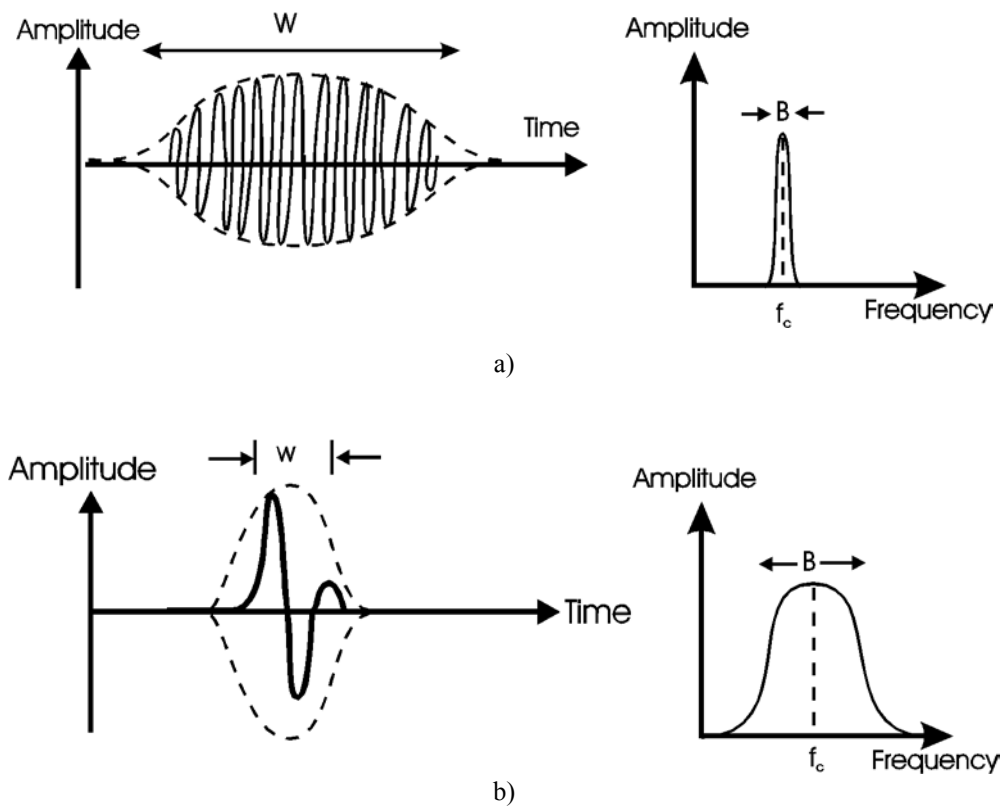


Figure: 5-6 a) A narrow bandwidth signal is a long oscillatory pulse characterized by single dominant frequency, f_c .
 b) A wide band signal has few if any oscillations, a short time duration and broad frequency content which can at best be said to be centred at a frequency, f_c .

The other extreme is the ultra wide band monocycle pulse. In this case, a single cycle of a sine wave is the signal. The bandwidth and the centre frequency are about equal.

GPR pulses are characterized by the bandwidth to centre frequency ratio

$$R = \frac{B}{f_c} \quad (5-3)$$

Every effort is made to make R as large as possible for GPR. The goal is always to maximize B and minimize f_c . The practical limiting value of R is about unity.

A surge of interest in impulsive source devices has created a great deal of interest in ultra wide bandwidth technology. A more general form of R is

$$R = \frac{2(f_{\max} - f_{\min})}{f_{\max} + f_{\min}} \quad (5-4)$$

where f_{\max} and f_{\min} are the maximum and minimum cutoff frequencies in the spectrum. The definition avoids having to specifically identify centre frequency, f_c .

When constructing radio frequency instruments and antennas, keeping R small has been desirable because it makes the job easier. If a desired resolution is set, then R can be kept small by increasing f_c . Unfortunately this is not desirable for GPR applications.

The reason for this is the high attenuation radio waves encountered in soils, rocks and man-made materials. In general, attenuation increases as frequency increases. The attenuation in natural materials is a combination of electrical losses and considerable scattering loss which both decrease with decreasing frequency. Since attenuation can be very severe, the lower the frequency the more likelihood of obtaining signal penetration into the medium. Figure 5-7 shows the general characteristic of attenuation versus frequency typical for lossy materials. As a result, GPR systems attempt to operate with as low a centre frequency as possible. The result has been that most GPR's try to achieve a monopulse type character (i.e. $R=1$) and are most appropriately referred to as ultra wide band radars or impulse radars.

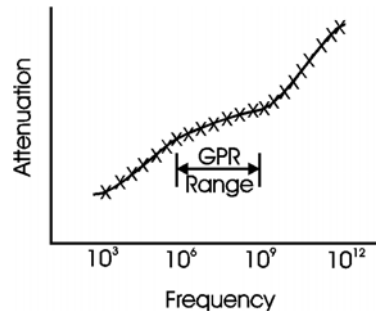


Figure: 5-7 Attenuation of radio frequency signals in soils, rocks and man-made materials always increases with frequency, forcing GPR's to operate at as low a frequency as practical given bandwidth requirements.

There are obviously some situations where the carrier frequency shouldn't be taken too low. If the bandwidth requirements suggest that the carrier frequency should be below the transition frequency of the host medium (see chapters 2 & 3), then one will be operating in a diffusive environment for the EM signals rather than a propagating environment (Annan, 1996). In this situation, one should be more careful about system selection and design.

5.5 SYSTEM ELEMENTS & CHARACTERIZATION

A GPR system is conceptually very simple. A block diagram depicting a GPR system is shown in Figure 5-8. The heart of the system is the timing unit which controls the generation of the radar signal and then the detection of receive signals as a function of time.

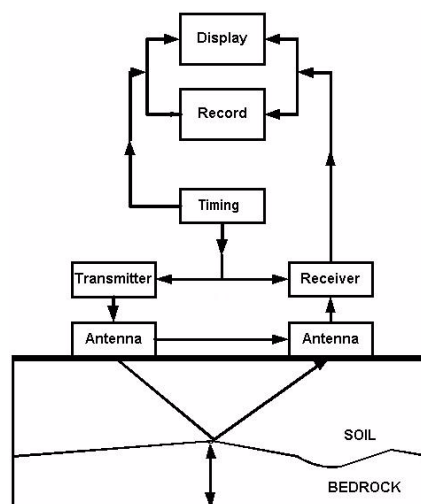


Figure: 5-8 Block diagram depicting main components of a GPR system.

Characterization of a radar system is an extremely complex task. A simple block diagram of a GPR system is shown in Figure 5-8. There are many elements in the system which, although not apparent on the surface, impact the operation and use of the system. The major factors which govern GPR classification and characterization are summarized in Figure 5-9. The following is a brief summary of the impact of each of these items.

SYSTEM CHARACTERISTICS

- Signal capture method
- Signal Processing
- Performance factor
- Centre Frequency and Bandwidth
- Antenna Patterns

Figure: 5-9 Characteristics which define a ground penetrating radar system.

5.6 GPR SIGNAL ACQUISITION

Few users of GPR delve into the details of GPR signal acquisition and real time processing. Numerous issues at the technical core of GPR systems can generate misleading concepts. The ideal GPR system is shown in Figure 5-10. In this system, the transmitter electronics deliver an electronic signal to a transmitting antenna which energizes the surroundings. The receiving antenna detects the transmitted fields and returns an electrical signal.

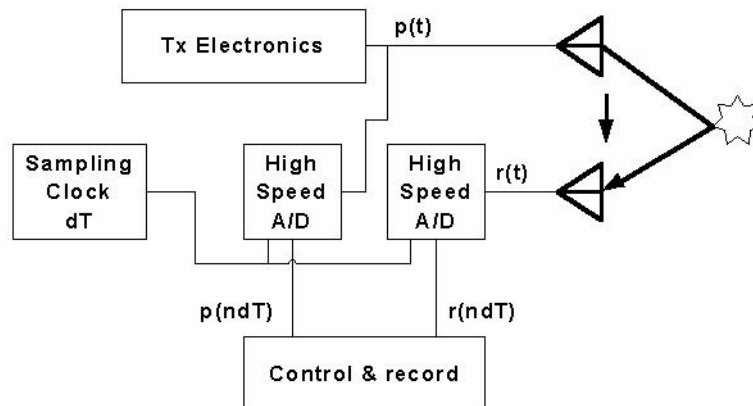


Figure: 5-10 Ideal GPR system with full capability and digital output.

In this perfect system, the output signal from the transmitter electronics, $p(t)$, being fed to the transmitting antenna and the signal returned from the receiving antenna, $r(t)$, would be digitized at a rapid rate through a high dynamic range analog-to-digital (A/D) converters and recorded, processed and displayed.

Unfortunately this ideal system while practical for audio frequency signals and the basis of modern seismic systems is impractical at the frequencies of GPR systems. The reason for this is that A/D converters having sufficiently high sampling rates with sufficient dynamic range do not exist. Specialized transient samplers with 500 to 1000 MHz conversion rates have been implemented (Wright et al, 1994) but with high power demands and limited dynamic range unless stacking is employed. Alternate techniques, which have been used for many years, are still the mainstay of signal acquisition in GPR systems. The objective in these designs is to measure the ground response without having to directly digitize or record the high radio frequency signals. A combination of repetitive transmissions and specialized analog circuitry are used. The following is a very abbreviated discussion of the approaches employed.

5.6.1 CORRELATION ACQUISITION GPR

One technique for creating a lower signal rate GPR acquisition is to use a correlation based signal detection process. This approach is depicted in Figure 5-11. In such a system, the transmitter electronics generate a wideband (usually random) signal. This signal could be noise or a digitally generated pseudo-random binary sequence.

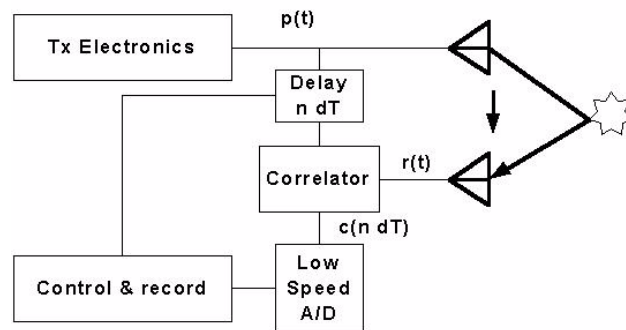


Figure: 5-11 Simple correlation based GPR system.

The detector is a correlator which is an analog signal multiplier and integrator. In this case, the correlator multiplies a reference signal (i.e. the transmitter drive signal) and the input signal together and integrates the output. The result is a low frequency (essentially DC) signal which can be sampled with a high dynamic range, low speed A/D converter and then recorded.

In the simple system shown here, the control system varies the delay of the transmitter signal with respect to the received signal. This delay, which is the GPR time delay, causes the correlator output to change. A good summary of an implementation of such a system is described by Wills (1992).

The sampled correlator output versus delay is the impulse response of the ground convolved with the antenna characteristics and the auto correlation of the excitation (transmitter drive) signal. The benefit of this style of system is low speed signals and simplicity. Data acquisition speeds can be too slow for many applications.

5.6.2 FREQUENCY DOMAIN MIXER GPR

Another technique for acquiring GPR high frequency signals without having to deal with the high frequency signals directly is depicted in Figure 5-12. In this style of system a mixer is used. A mixer is very similar to a correlator. Another term for mixing signals is heterodyning.

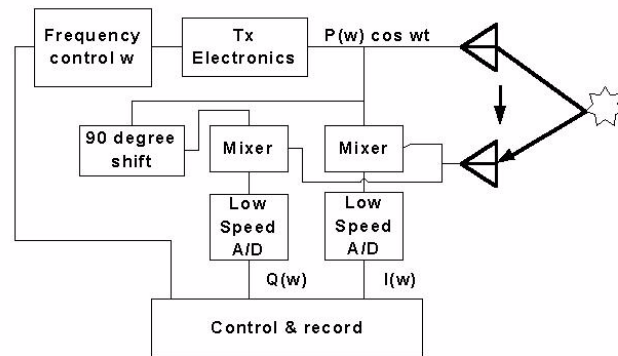
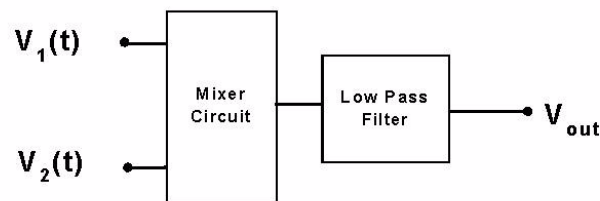


Figure: 5-12 Frequency domain mixer approach to GPR system.

A mixer is an analog circuit designed to multiply sinusoidally varying signals. As depicted in Figure 5-13, a mixer combined with a low pass filter outputs a resulting signal which varies sinusoidally at the frequency difference between the inputs. If the two signals have the same frequency, the output is a DC voltage proportional to the amplitude of the input signals. This low frequency (DC) voltage can be sampled with a low speed high dynamic range A/D converter and recorded.



$$V_1(t) = A_1 \cos \omega_1 t$$

$$V_2(t) = A_2 \cos \omega_2 t + \Theta$$

$$V_{out} = A_1 \cdot A_2 \cdot \cos(\omega_1 - \omega_2)t + \Theta$$

Figure: 5-13 Mixer is a circuit which multiplies sinusoidally varying signals

In the frequency domain approach, the frequency output of the transmitter electronics (which is a sinusoidal) is controlled. The output of the transmitter electronics is mixed with the input from the receiving antenna. By filtering the transmitter signal through a 90° phase shift it is possible to measure the received signals that are both in-phase with the transmit. This technique (which has been used in the majority of commercial GPR systems to date) is called the equivalent time sampling (ETS) approach. Figure 5-14 depicts an equivalent time system.

By appropriately changing the oscillation frequency, one can measure the ground transfer function multiplied by the antenna characteristics over a frequency range. This transfer function can then be Fourier transformed to provide the transient response of the earth. The transient response is the impulse response of the ground convolved with the antenna impulse response. Good examples and discussions of this style of GPR system implementation are given by Stickley et al (1998) and Noon et al (1994)

5.6.3 EQUIVALENT TIME SAMPLING GPR

This technique (which has been used in the majority of commercial GPR systems to date) is called the equivalent time sampling (ETS) approach. Figure 5-14 depicts an equivalent time system.

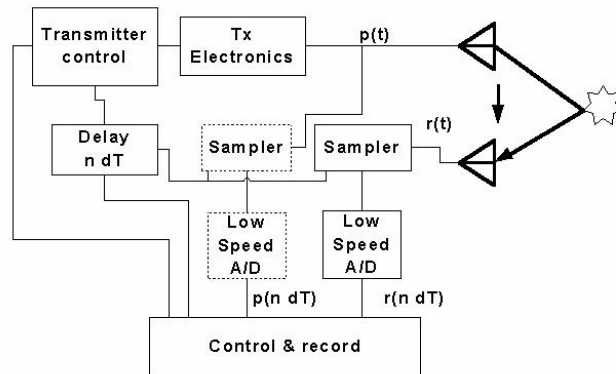
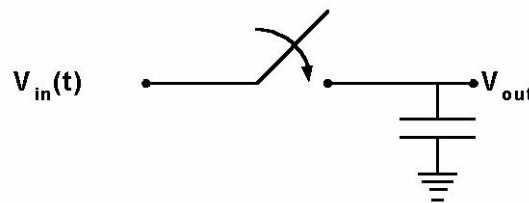


Figure: 5-14 Time domain approach to a GPR system.

In an ETS system design, the transmitter generates a controlled output pulse with a specified temporal shape (and frequency content). The excitation pulse is fed to the transmitting antenna and to a signal acquisition circuit (if so desired).

The sampler is very fast switch. The switch is linked to the transmitter control. The transmitter control clock is delayed by a time $n dT$ and used to toggle the sampler.

The sampler, shown in Figure 5-15, is a high-speed analog switch which closes for a very short duration. When the switch is closed, the input voltage charges a capacitor. The resulting output voltage is proportional to the integral of the input signal over the time interval of switch closure. If the time window is very short compared to the rate of change of the input signal, then the output voltage is a measure of the input voltage at the time delay $n dT$.



$$V_{\text{out}} = \int_{n dT}^{\Delta + n dT} V_{\text{in}}(t) dt \approx C \cdot V_{\text{in}}(n dT)$$

where C is a constant

Figure: 5-15 Sampler is just a fast opening and closing switch.

The equivalent time sampling approach uses the transmitter control and an adjustable delay time to sample successive points along a transient wave form. The V_{out} result is a slow varying replica of the high frequency signal which can be sampled by a low speed analog converter. This process is the electronic equivalent of the stroboscope concept which is used to slow down or freeze repetitive motion. Original discussion of ETS signal capture is given by Hansen (1942). ETS has been part of high frequency signal capture oscilloscopes for decades and has advanced to a very high level with constant improvement and evolution.

In the majority of time domain GPR systems, the transmitter electronics and antennas are designed to be as invariant as possible. The objective is to make these components stable so that a second sampler to record the transmitter output signal is not required.

The resultant signal $r(n \Delta T)$ is the sampled version of the transient response of the transmitter output convolved with the impulse response of the ground and the impulse response of the antennas. In the ideal system, the transmitter electronics would output a perfect δ function (spike) and the received signal would be the impulse response of the ground convolved with the antenna system impulse response.

5.6.4 COMMON SIGNAL CAPTURE ISSUES

The preceding discussion provides a simple conceptual view of how GPR's acquire signals. When faced with the discussion of electronic implementation, the average user can quickly be overwhelmed by electrical engineering jargon. Generally, commercial radars have been of the ETS type. These radars have often been referred to as impulse or base and radars because the driving signal is usually an impulse.

Recent electronics developments have made sinusoidal synthesizers and mixers more robust and inexpensive. This has led to researchers implementing step frequency systems. The step frequency systems are based on the frequency domain approach depicted in Figure 5-12.

In an ideal world, all of the systems presented will generate equivalent results. The differences lie in the electronic embodiment of the circuitry. Issues such as the degree of linearity in the analog components, component stability and circuit complexity all affect which approach may be better than the other in a particular application.

To date, the time domain systems have been preferred because the raw signal acquired is representative of the ground response with no (or minimal) signal processing required. As computers in small packages become available, step frequency systems using the frequency domain approach have started to appear. Computer implemented fast fourier transforms can generate transient output in these systems. In general, the ETS time domain approach is more tolerant of non-linearity in system elements.

There are some common fundamental issues which have not been addressed in the discussions so far.

- a. The antennas of a GPR system need to be close to the ground so that good ground coupling will occur and emissions into the air are minimized.
- b. When GPR antennas are close to the ground there is a considerable degree of variation in the ground impedance which has an impact on the transfer function (impulse response) of the antennas. As a result, the antenna response can not be assumed as invariant but will vary from place to place. The measurements in all the GPR systems are contaminated to some degree because the transfer function of the antennas is a variable which is difficult to control and even more difficult to measure.
- c. Modern GPR system designs have placed major emphasis on minimizing the antenna variability with ground impedance conditions. The quality of a GPR system is directly proportional to how well the engineering of the antenna (and associated electronics) minimizes this variation.
- d. Antennas that are mismatched or vary with ground conditions will generally exhibit reverberations (commonly called "ringing"). Instead of an ideal impulse being emitted or synthesized post acquisition, the antennas will generate a repetitive train of emissions that are spread out in time. This reverberation masks the ground response and makes it difficult to interpret the GPR response.

- e. In systems where mismatch is common, users resort to “background” subtraction for reverberation removal to see the raw ground response. Background subtraction measures the primary or direct signal and attempts to subtract or filter it out in some manner. Systems that depend on this process suffer from the fact that a part of the ground response will often be removed in the process.

5.7 REAL-TIME SIGNAL PROCESSING FUNDAMENTALS

The simplest model for the received signal is the transmitter electronics output convolved with the antenna system impulse response, $a(t)$, and the impulse response of the ground, $g(t)$. Note that this simple model assumes that the antenna directivity is independent of frequency which is definitely not true for most antennas!! Despite this limiting reality, the model is reasonable valid for most GPRs which use small dipolar antennas.

$$r(t) = g(t) ** a(t) ** p(t) \quad (5-5)$$

Note that ** means convolution in this discussion.

When a correlating GPR architecture is used, $p(t)$ represents the auto correlation function of the excitation signal. In the frequency domain, obtained by fourier transform, the convolution operator becomes a simple multiplication of the transfer functions.

$$R(\omega) = G(\omega) \cdot A(\omega) \cdot P(\omega) \quad (5-6)$$

Note that ω represents angular frequency. Capital letters indicates transfer functions while lower case letters represent impulse response functions.

In a frequency domain style system architecture, one has

$$R(\omega) = I(\omega) + i \cdot Q(\omega) \quad (5-7)$$

where I and Q are the in-phase and quadrature part of the received signal.

5.7.1 DECONVOLUTION

In GPR, the obvious measurement goal is to recover the impulse response or transfer function of the ground ($g(t)$ or $G(\omega)$). A scheme is needed to remove the antenna response and transmitter (source) excitation characteristics to leave the pure ground response. The extraction of $g(t)$ is referred to as “deconvolving out” the measurement system response. This is never possible in the pure GPR context since nulls occur in the antenna transfer function at 0 frequency and possibly at other frequencies. Similarly, the transmitter output may have nulls in its spectrum .

Ignoring these very real issues for now, the ground impulse response can be mathematically expressed as

$$g(t) = \text{IFT} \left[\frac{R(\omega)}{A(\omega) \cdot P(\omega)} \right] \quad (5-8)$$

where IFT stands for inverse fourier transform. The fact that $A(\omega)$ and $P(\omega)$ have nulls represents a numerical problem that must be addressed in real systems. At the spectral nulls, the ground response is undefined and the computed result will be determined by the relative character of the error (noise) in the measurements of R, A and P. Blindly carrying out the above “deconvolution” usually generates a result which is random garbage signal bearing little or no relationship to the true ground response.

In the early days of GPR, attempting such a process was not realistic given the limited and analog-only processing capability available. With the advent of powerful microprocessors and DSP devices, such processing can be implemented in real-time. Since GPR has been a useful device for many years, it is useful to review the compromise solutions which give useful results.

The most obvious solution is make the combined antenna and excitation signal mimic a perfect impulse (δ function mathematically). The resulting devices are called impulse or baseband radars in radar jargon. Now-a-days such radars are called ultra wideband (UWB) radars.

When this occurs, then

$$r(t) = g(t) \quad (5-9)$$

Physical reality limits how well this can be achieved as the discussions of the nulls in the antenna transfer function previously suggest.

By suitable electronic design and antenna construction, the system response can be reduced to a short time-duration wavelet, $w(t)$. The received signal then has the form

$$r(t) = g(t) ** w(t) \quad (5-10)$$

For the most part, this is the approach taken by GPRs today. Engineering design to make $w(t)$ a very compact time duration signal is the prime focus of system developers. All current practical GPRs use $r(t)$ (or possibly some enhanced form thereof) and not $g(t)$. For many applications this is not a great limitation and very useful results are obtained.

In conventional radar, the need to make $w(t)$ compact is not so critical and can often be achieved by increasing the operating frequency while maintaining a constant bandwidth. GPR always needs the maximum bandwidth at the lowest possible frequency.

Considerable effort has been devoted in recent years to post-processing of GPR to deconvolve the data by a variety of processing techniques (Turner (1992), Majala (1992)). In general these attempts have produced marginal benefit for data obtained with well engineered systems where $w(t)$ has been refined to be very compact by the system hardware designers.

There are many ways of carrying out deconvolution (weiner, least squares, parametric, spectral whitening, etc.) in a more sophisticated manner than that suggested mathematically above. The seismic processing industry has refined these concepts to a very high level. An excellent overview of the seismic advances and techniques which also apply to GPR is given by Yilmaz (1987). Simple stabilization of the above operation can be achieved (in Equation 5-11) by adding a whitening contribution to the denominator which can be adjusted to make the deconvolved output

$$g(t) = \text{IFT} \left[\frac{R(\omega)}{A(\omega) \cdot P(\omega) + \beta} \right] \quad (5-11)$$

By adjusting empirically β , the output can be shaped. In some instances improvements in estimating $g(t)$ can be achieved. Unstated here is the need to measure $p(t)$ and $a(t)$ or $A(\omega)$ and $P(\omega)$ which is not a trivial matter.

Since most GPRs use a form of $r(t)$ rather than attempting to get to $g(t)$. The form of $w(t)$ is of considerable interest. There is no specific form that fully represents the full antenna behavior but a good approximate model for modelling and simulation is as follows.

5.7.2 GPR WAVELET MODEL

The radiated wavelet from a GPR system is a complicated function of the antenna construction and the electronics drive circuitry. For impulse style ultra wideband systems a simple mathematical model is available for helping with numerical simulation.

The form of signal is

$$s(t, q, T) = v(t) - (2 - q)v\left(t - \frac{T}{2}\right) + (1 - q)v(t - T) \quad (5-12)$$

where $0 < q < 1$ (damping factor)

q – damping factor (0 to 1)

f_c – center frequency

and

$$T = \left(\frac{2}{3} + \frac{(1-q)}{7} \right) \frac{1}{f_c} \quad (5-13)$$

and

$$v(t) = \frac{1}{2} \left(1 + \cos \pi \frac{t - \frac{T}{2}}{\frac{T}{2}} \right) \quad 0 < t < T$$

$$= 0 \text{ otherwise} \quad (5-14)$$

The damping factor q depends on system design. As q varies from 1 to 0 the wavelet $\omega(t)$ varies between one cycle and one and a half cycle shape as shown in Figure 5-16. The amplitude spectra for various values of q are shown in Figure 5-17.

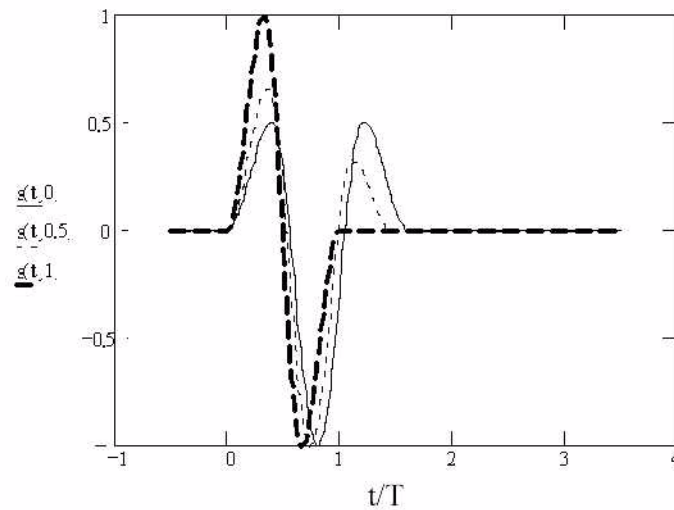


Figure: 5-16 Typical GPR model wavelets for a range of damping parameters.

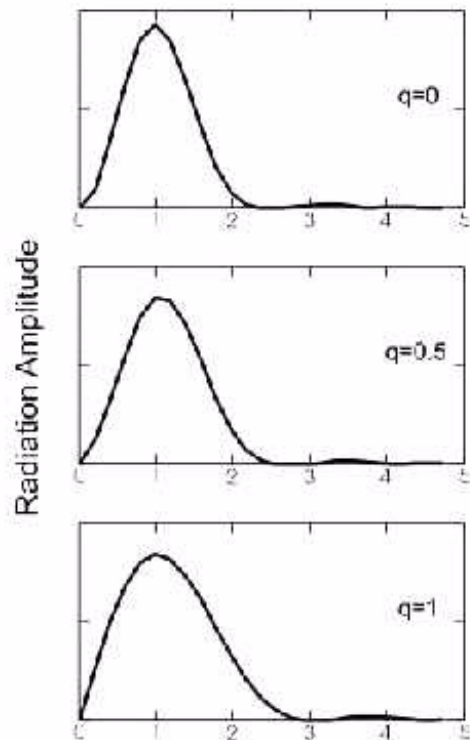


Figure: 5-17 Amplitude spectra of GPR pulses for varying damping factors

5.8 SYSTEM PERFORMANCE FACTOR

System performance factor, Q , is a measure of the ratio (usually expressed in decibels) of the source power to the receiver noise power. The basic ideas are summarized in Figure 5-18. The reason the system performance factor is so important, is that it is the primary factor which determines the range to which the radar can see and the size of objects the radar can detect.

System Performance Factor

$$Q = 10 \log_{10} \left[\frac{\text{Source power}}{\text{Receiver noise power}} \right] \text{ dB}$$

$$Q = 20 \log_{10} \left[\frac{\text{Transmitter voltage}}{\text{Receiver voltage}} \right] \text{ dB}$$

Figure: 5-18 The system performance factor Q provides a readily measured GPR parameter.

In order to understand the impact of the system performance factor, it is best to refer to the radar range equation. Figure 5-19 gives a block diagram of the radar range equation. It shows the sequence of events from the point where the transmitter electronics generate a signal, (i.e., referred to as the source power) through to the signal which the receiving electronics present to the display unit, (i.e., the received power). In order for a feature to be detectable the received power must be in excess of the noise level in the receiver.

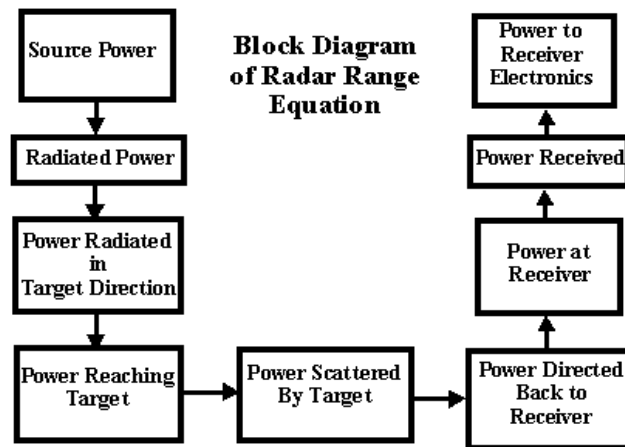


Figure: 5-19 Block diagram showing the major steps in the radar range equation.

Analyzing particular situations with the radar range equation allows one to anticipate the range to which a target can be detected. For a given system performance factor value, the sum of all the losses of energy along the various paths that the signal will travel must not exceed the system performance factor; otherwise, the target will not be detectable. Detailed implementation in a GPR context is described by Annan & Davis (1977) and Annan & Chua (1992).

5.9 SIGNAL AMPLITUDE & RECORDING DYNAMIC RANGE

While GPR data can be acquired in a number of different ways using different recording procedures, the data are almost invariably reduced to an amplitude versus time output for evaluation and display. The response is in a form that approximates the impulse response of the system and the ground.

Systems are never perfect. There are a number of factors in the electronics and the actual physical antenna structure and support systems which will invariably cause the impulse to be blurred in time. There are two major issues which must be addressed. First, the question arises as to how well does the system approximate an impulse response and what does this do to the recorded ground response. Second, how does the dynamic range of recording impact measuring the ground response.

5.9.1 CHARACTERIZING SYSTEM RESPONSE

The system response should generally respond as shown in Figure 5-20. The transmit signal has an onset at 0 time and lasts for a duration of W . In a perfect world, all system signals would vanish after W . The signal during the interval 0 to W represents the excitation impulse.

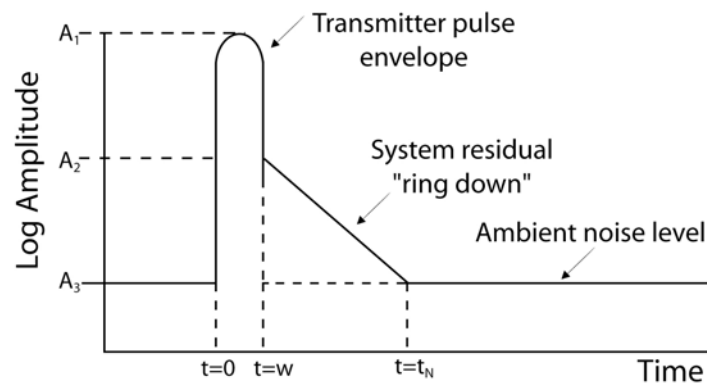


Figure: 5-20 Idealized GPR impulse response envelope amplitude (log) versus time. The key parts of the response are the ambient noise level A_3 (before pulse and at late time), the peak signal A_1 and initial residual system response, A_2 .

With real electronic components, responses will linger in time after the ideal signal has terminated. In addition, with a GPR system, the actual emitted signals and detected signals are launched and retrieved using an antenna structure. The antenna structure has (intrinsic to its character) a finite time delay for currents to move around the structure to achieve efficient launch and detection of signal.

In addition to the antenna, the antennas have to be carried, mounted and interconnected using cables and other mechanical structures. These ancillary structures can also have electrical currents induced upon them which in turn generate re-radiated fields that occur at a time delay.

The standard GPR approach is to denote the signal which appears after the transmit pulse should ideally have turned off as the residual system response. This system response normally will “ring-down” or decrease with time after the transmit pulse and fall below the noise level.

Echoes from the ground will return during this “ring-down” period. If the residual signal from the system is larger than the ground response, then the ground response will be masked and not visible. In general, the ground response will be largest at an early time and get successively smaller as time increases. Quite often a mathematical model which describes signal amplitude, $G(d)$, from the ground versus depth, d , is useful for discussion.

$$G(d) = G_0 \frac{e^{-\alpha d}}{d} \quad (5-15)$$

$$t = \frac{2d}{v} \quad (5-16)$$

$$G(t) = G_0 \frac{2}{vt} e^{-\alpha vt/2} \quad (5-17)$$

In this model, the ground response amplitude for a target at depth d is re-expressed in terms of attenuation, α , and the velocity, v . If one assumes that time is equivalent to depth as in Equation 5-16, the ground response amplitude versus time can be expressed in Equation 5-17. In other words, the ground response on average will decay inversely and exponentially with time and be dictated by the velocity and attenuation in the ground.

For the basic design and analysis, the GPR response (no ground present) can be characterized by a simple model. The character of the system amplitude response versus time as shown in Figure 5-20 is expressed as follows.

$$A = A_3 \quad t < 0 \quad (5-18)$$

$$A = A_1 \quad 0 < t < W \quad (5-19)$$

$$A = A_2 - B(t - W) \quad W < t < t_n \quad (5-20)$$

$$A = A_3 \quad t > t_n \quad (5-21)$$

where

$$t_n = \frac{A_2 - A_3}{B} + W \quad (5-22)$$

and

$$A_1 \text{ - peak signal during the transmit pulse} \quad (5-23)$$

$$A_2 \text{ - residual signal amplitude at time } W \quad (5-24)$$

$$A_3 \text{ - noise level of the measurement} \quad (5-25)$$

$$B \text{ - residual "ring-down" rate (normally in dB/ns)} \quad (5-26)$$

Figure 5-21 through Figure 5-25 depicts the ground response superimposed on a typical GPR system response. Here the ground response initial amplitude and time delay rate ($\alpha v/2$) from Equation 5-17 are shown superimposed on the system response. In the example shown in Figure 5-21, the ground response is larger than the system residual response and decays slower. This is the ideal situation and the system residual has a negligible impact on the measurement of ground response over all delay times.

Ground conditions can impact both the ground response as well as the system residual response. As a result, a wide variety of conditions can occur depending on ground conditions. Some of these behaviors are depicted in Figure 5-22 through Figure 5-24. The system residual response can mask some or all of the ground response over some time periods.

In some situations, the system residual response may be predictable; if it can be estimated and subtracted, the system residual response can be reduced with respect to the ground response and the ground response made visible such as depicted in Figure 5-25.

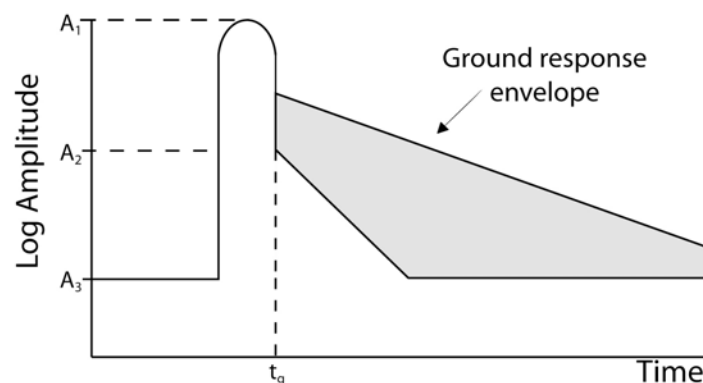


Figure: 5-21 Case where signals from the ground are larger and decay more slowly than system "ring down". Ground response is always visible.

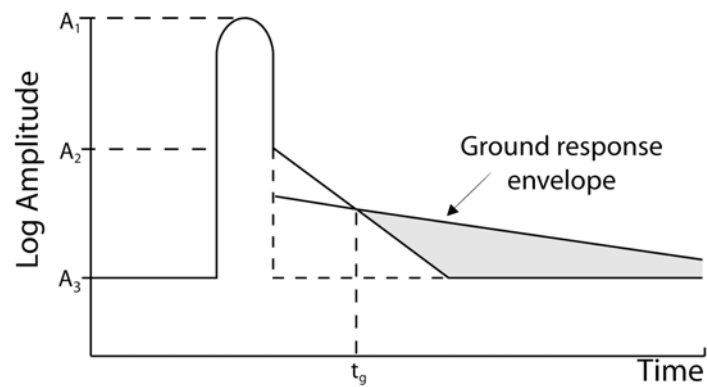


Figure: 5-22 Case where system "ring down" is faster than the ground response fall off but initial system residual is larger than ground response. Ground response becomes detectable after t_g .

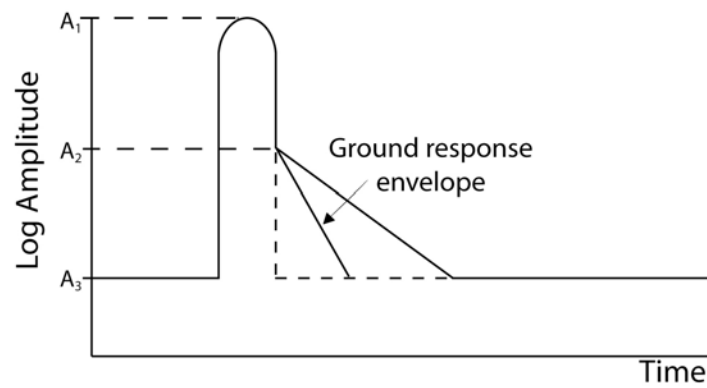


Figure: 5-23 Case where ground response is smaller than system residual response resulting in no detection of ground response.

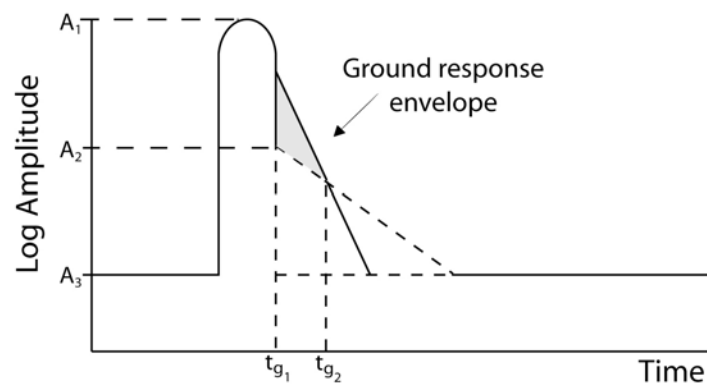


Figure: 5-24 Case where ground response initially exceeds system residual but ground response decays more quickly than system "ring down" rate leaving ground response detectable only between time t_{g1} and t_{g2} .

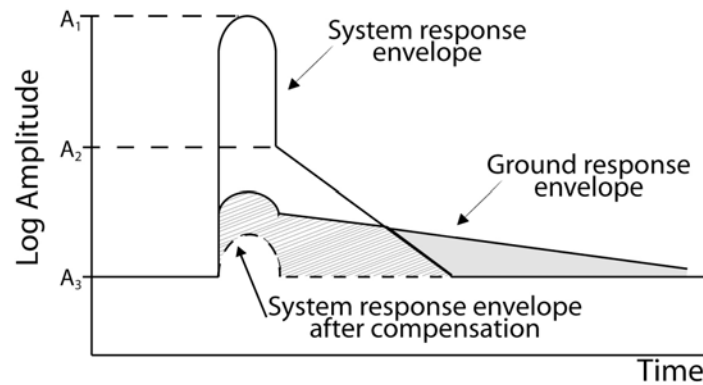


Figure: 5-25 In some cases the system response might be static and subtracted from the combined signal to make ground response visible at all times. This can apply to Figure 5-21 through Figure 5-24.

Unfortunately, the residual response is not easily determined and is not always stable. In particular, the residual response is often associated with the antenna system and its support structure. The “ring-down” or residual electrical currents in the structure are modified by the ground conditions which in turn makes the “ring-down” character variable with measurement location making removal difficult to impossible and a trial and error procedure at best.

The key parameters to characterize a system are A_2 which is the initial “ring-down” amplitude after the transmit pulse has terminated and B , the decay rate or “ring-down” rate. These are very dependent on system configuration and application needs. It is possible to have systems with an A_2 value which is -60 dB to -80 dB below A_1 and exhibit “ring-down” rates of -4 dB/ns.

5.9.2 DYNAMIC RANGE

The preceding has shown the general character of the GPR signal amplitude versus time. In the initial days of GPR, these data were then transferred on to a paper recording or recorded on to an analog tape recorder. These recording devices usually had limited dynamic range - typically much less than the 80 to 100 dB or more which the GPR data required for recording. Now most systems digitize the signal at some point along the path and record digital data. As a result, dynamic range of recording is less limited than it used to be.

Figure 5-26 shows typical signal levels that one may encounter in a system. The general character of the amplitude versus time response depicted in Figure 5-20 and Figure 5-21 through to Figure 5-25, is shown together with a binary dynamic range scale on the left typifying the digitization levels of a 16 bit A/D converter. In this particular example, we have chosen A_1 to be 50,000 mV and A_3 to be 10 μ V. Maximum and minimum recording of the receiver must be able to bracket A_1 and A_3 .

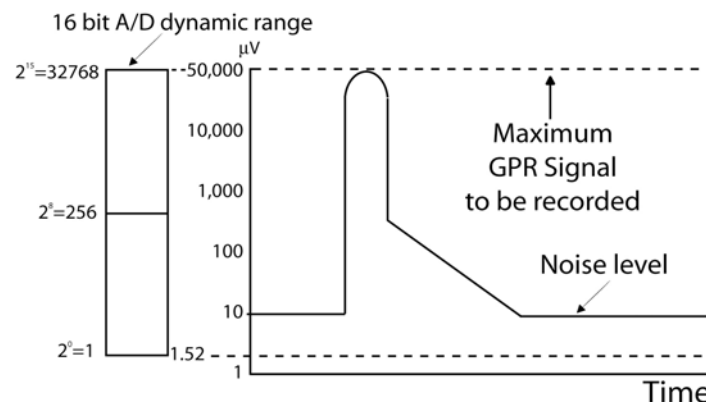


Figure: 5-26 The typical GPR amplitude envelope is plotted on the right against the recording levels of a 16 bit (bipolar) analog-to-digital converter that might be employed in a recording system.

In the configuration in Figure 5-26 a 16 bit bipolar A/D converter is assumed. This choice gives the smallest signal resolved as $1.5 \mu\text{V}$ if the maximum recording value of the A/D is $A_1 = 50,000 \mu\text{V}$. For this example, the noise level, A_3 , is greater than the least significant bit of the A/D converter.

For rigid system geometries where there is no variation in the position of the components, the value of A_1 can be controlled and the design objectives met. For bistatic antennas with arbitrary antenna geometries and orientations as well as possible changes in frequencies of the antennas, the value of A_1 can be highly variable and it is virtually impossible to guarantee that A_1 will always remain within the dynamic range of the recording system. As a result, it is common to see the peak signal during the transmit pulse limited (clipped) by the recording system.

This is not a major problem for many GPR applications as the information in the transmit pulse is not necessarily useful. Loss of signal during this time is common in time domain radars and is called transmitter blanking. In the situations where signals from shallow depths are critical, systematic attention must be given to the dynamic range of the recording system and the geometry of the antenna configuration to achieve signals which always remain within dynamic range.

In some instances, signal dynamic range can be decreased by applying a judicious amount of time varying gain to the radio frequency signal prior to recording and digitization. Figure 5-27 through to Figure 5-31 depict the basic concepts here.

For the signal shown in Figure 5-27, the dynamic range of the signal present is greater than the dynamic range of the recording device indicated.

By applying a judicious amount of amplification to the signal versus time, such as depicted in Figure 5-28, the dynamic range of the signal can be compressed. The time gain in Figure 5-28 attenuates the signal during the transmit pulse and amplifies the signal at an every increasing amount with time.

If the time gain is appropriately selected, the resulting signal will be compressed into the dynamic range of the recording system such as depicted in Figure 5-29. If the time gain is too large, the signals will reach the limit of the recording system and be clipped off and flat lined, such as shown in Figure 5-30.

On the other hand, if the time gain is not sufficient, the signal levels may be too small to be recorded by the recording system and there is no signal in some or all parts of the record as shown in Figure 5-31.

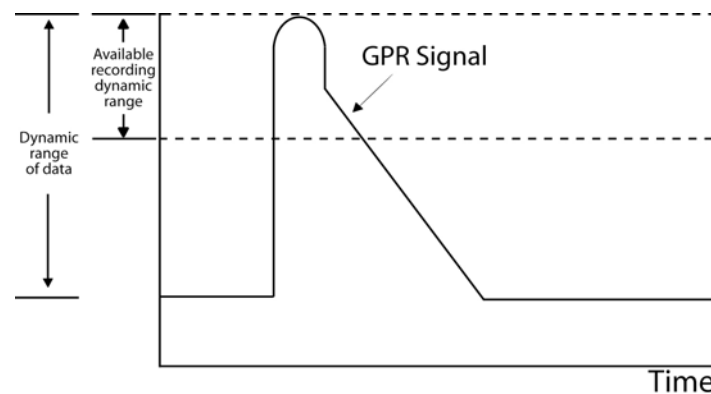


Figure: 5-27 Example where recording system dynamic range is smaller than that of the GPR signal.

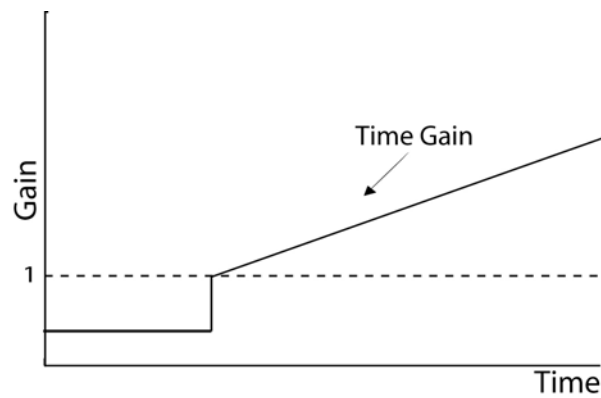


Figure: 5-28 Example of a time gain function that might be applied to the data in Figure 5-27 to compress dynamic range. The plot shows the amplification that would be applied to the GPR signal.

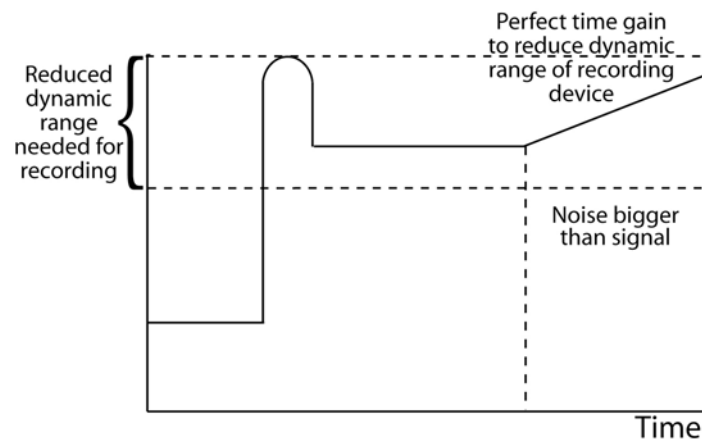


Figure: 5-29 If the time gain is selected very carefully, the resulting data can be compressed into the recording dynamic range. Note that this process may cause noise signals to appear as large or larger than real signals.

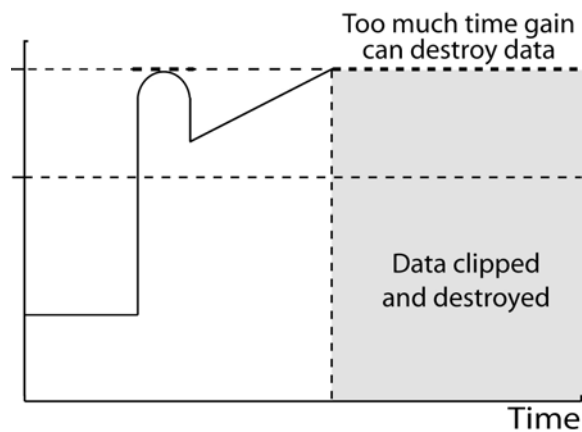


Figure: 5-30 If the time gain is too large, signals may be over amplified, exceed the recording dynamic range and limited or clipped. (Dotted line indicates where data exceed reading dynamic range).

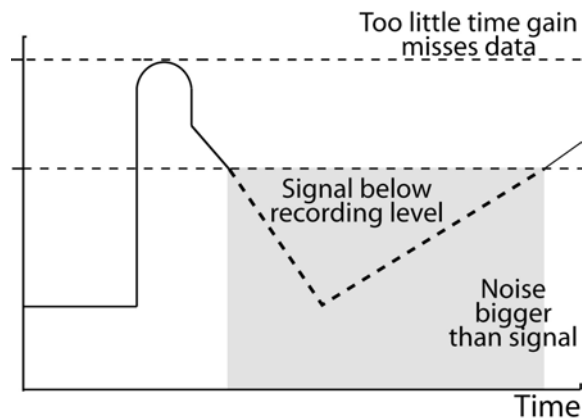


Figure: 5-31 If the time gain is too small, signals may not be recorded because they are below the recording threshold. The dotted line shows where data are too small for recording to detect.

In systems which have used time gain, the adjustment has often been left to the user. Unfortunately what often turned out to be a good time gain at one location was not appropriate at another location resulting in recording of no useful or distorted amplitude data.

In theory it might be possible to make a system which dynamically adjusted at every location to maximize the data in such a way to fit recording dynamic range. This is complicated and difficult to carry out although attempts have been made. While it looks simple, this kind of adjustment in the RF circuitry can introduce many artifacts and distortions which may severely degrade data quality.

A point to note for new GPR advocates is that some ETS (equivalent time sampling) GPRs have analog time gain which is applied to the analog sampled signal. This type of time gain does not address the dynamic range limits of the radio frequency electronics in the signal capture circuitry and is not of much benefit given modern A/D performances.

At present, modern general purpose systems do not use time gain in the radio frequency section of the receiver. Time gain is regularly applied after digitization and recording when displaying the data on screens or printing on paper. This dynamic range adjustment or time gain is reversible by the user and can be adapted interactively to meet user specific needs. Using post recording time gain is preferable to applying it in a irreversible manner before recording at present. Hardware time gain can be very useful and with electronic advances some variations of RF time gain will appear in general purpose systems.

5.9.3 SUMMARY

When attempting to understand the details of GPR system behavior, one needs to know the dynamic range of the recording system, the maximum signal likely attainable (A_1), the typical noise level (A_3), the after pulse initial “ring-down” amplitude (A_2) and the “ring-down” rate (B). When these parameters are known and understood, it becomes practical to understand ground responses and put them into the context of what is recorded. These basic parameters are key characteristics of a GPR system.

GPR records are frequently impacted by some or all of the amplitude artifacts and distortions described here. As technology matures and systems improve these artifacts are steadily being reduced. It is virtually impossible to eliminate some of the effects that are controlled by ground conditions and application constraints which are beyond the system users and designers

5.10 CENTRE FREQUENCY AND BANDWIDTH

Frequency and bandwidth go hand in hand in a GPR system. The operating frequency of a GPR system is usually given by indicating the centre frequency of its operating band. The associated factor is the bandwidth or the frequency range over which the radar has available power for use in sounding the ground. The bandwidth and the centre frequency of a radar system are determined by several components in the system, the primary ones being the antennas. A block diagram showing how the various system components determine the frequency of operation and bandwidth is presented in Figure 5-32.

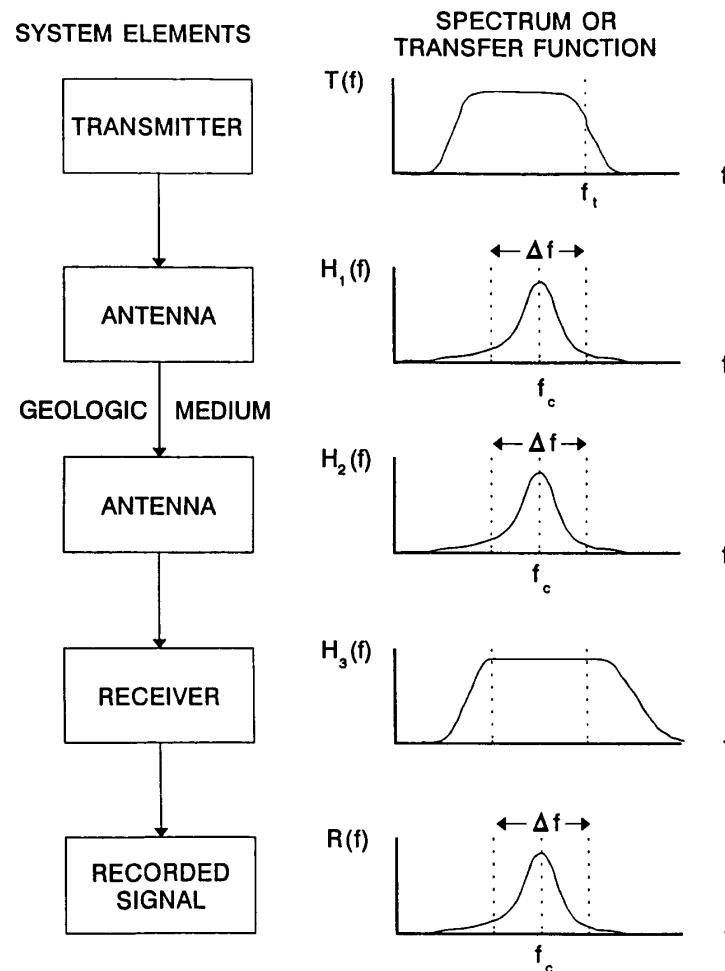


Figure: 5-32 Simplified signal flow through system elements depicting controlling factors in centre frequency and bandwidth.

The centre frequency of the radar system has a major impact on the depth of penetration of the radar system. The reason for this is that as the frequency decreases the signal attenuation in the medium decreases. In addition as the frequency of the radar system is lowered, the impact of clutter and the masking of desired signals by responses from smaller scale features is reduced.

Bandwidth is the other factor in the system. The wider the bandwidth the better the resolution of the radar. The concepts of bandwidth and pulse duration and spatial resolution are depicted in Figure 5-33.

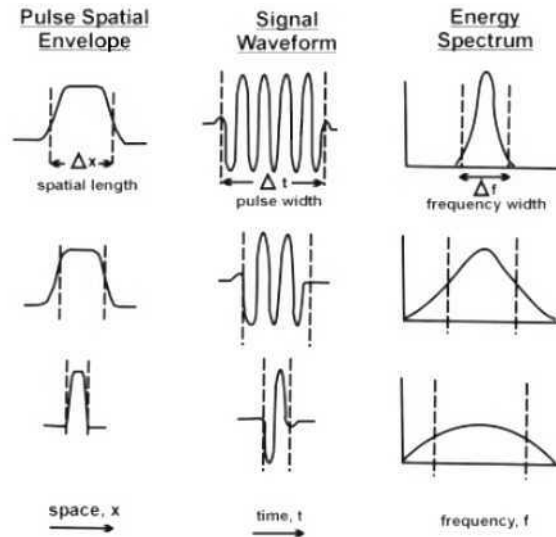


Figure: 5-33 Illustration of the relationship between spatial, temporal and spectral aspects of signal which control resolution.

For GPR systems designed for soil and rock, the objective is to achieve a bandwidth to centre frequency ratio of about 1. Some example calculations of resolution are shown for antennas of this type in Figure 5-34. Figure 5-35 shows the resolution versus system bandwidth for two geological setting, one a rock the other a wet soil. It is important to note that the resolution in the ground depends on the electrical properties of the ground. Figure 5-35 indicates this quite explicitly.

REFLECTOR RESOLUTION

Centre Frequency	Bandwidth (MHz)	Pulsewidth (ns)	Resolution (m)
200.0	200.0	5	0.25
100.0	100.0	10	0.50
50.0	50.0	20	1.00
25.0	25.0	40	2.00
12.5	12.5	80	4.00

Note: Resolution assumes a dielectric constant of 9

Figure: 5-34 Tabulation of spatial resolution versus antenna frequency.

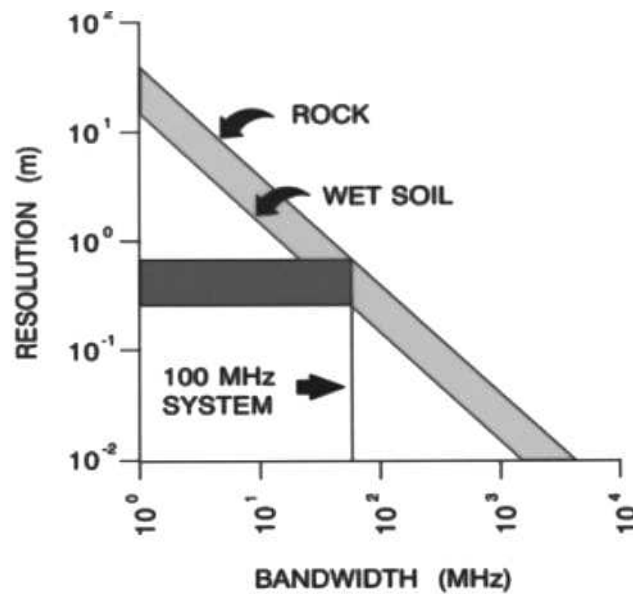


Figure: 5-35 Spatial resolution versus bandwidth illustrating how material velocity changes spatial resolution.

5.11 ANTENNAS

Antennas form the main part of a GPR system. Unlike antennas for communications needs and pulsed CW style air launch requirements, where the modulation of the radio frequency signal carries the information, GPR antennas must create and detect electromagnetic fields to extract the actual field characteristics. In other words, the measurement objective is the field amplitude in space and time, not the superimposed information.

In a GPR system, the transmit antenna must translate the excitation voltage into a predictable temporal and spatial distributed field. The receive antenna must detect the temporal variation of a vector component of the electromagnetic field created by the transmit antenna and the ground response.

The following are desired antenna characteristics.

- a. The exact source and detection locations must be definable.
- b. The transmitter and receiver responses must be time and space invariant.
- c. The vector character of the field linking the source voltage and received voltage must be quantifiable.

In practical terms, these requirements are difficult to achieve. The reason is that efficient field generation and detection requires the size of antennas to be such that field travel time across the antenna dimension be comparable to the temporal rate of change of the exciting voltage or field. In frequency domain terminology, the antenna dimension must be similar to the wavelength of the signals.

For efficient operation, finite size antennas must be used and they have the following characteristics.

- a. Field creation and detection occurs over a spatially (and temporally) distributed region. (In other words, source and detection points are imprecise).
- b. Field transit time or wavelength in GPR applications depends on the host environment and is not invariant. (In other words, antenna response cannot be perfectly invariant).

- c. A spatially distributed antenna means less precise vector characterization of the response since isolation of response to a single vector component becomes geometrically difficult.

The antennas that have been preferred for GPR have been short electric dipoles (or small magnetic dipoles). By making these antennas as small as possible without totally eliminating efficiency, a fair degree of faithfulness to desired predictable and invariant behavior can be achieved.

While other antennas have been used for GPR, such as log periodic or log spiral antennas, these antennas critically depend on their size to achieve a desired directivity or response character. While useful for communications applications, such antennas suffer from pulse dispersion (in space and time) and smeared (mixed) vector response, which render the specific GPR desired response much less quantifiable.

5.11.1 DIPOLE IMPULSE RESPONSE OR TRANSFER FUNCTION

The use of short electric dipole antennas yields relatively invariant radiated pulses and antenna directivity. Antennas are small provided

$$\frac{L}{v} \ll \Delta t \quad (5-27)$$

where Δt is the time duration for the fields or excitation voltage to change, L is the maximum spatial dimension of the antenna and v is the radiowave velocity in the host medium. (When the antenna is on the ground this is both a function of ground properties and antenna proximity to the ground). Another way of expressing this is

$$L \ll \lambda \quad (5-28)$$

where λ is the wavelength of sinusoidal signal in the host medium.

When antennas are small, the emitted field is roughly proportion to L^2 (Schmitt et al, 1966). There is a great incentive from a signal detection viewpoint to maximize antenna size.

In practical GPR design the required application bandwidth, B , is defined and the centre frequency is selected to be

$$f_c = B \quad (5-29)$$

And electronic excitation is optimized to create and detect signals in a bandwidth B centered at f_c . The dipole antenna length is selected such that

$$L < \frac{1}{4} \frac{c}{f_c} \quad (5-30)$$

With proper resistive loading, driving such an antenna with a bandwidth limited impulse will generate a clean emitted wavelet such as depicted in Figure 5-36. This is the antenna impulse response.

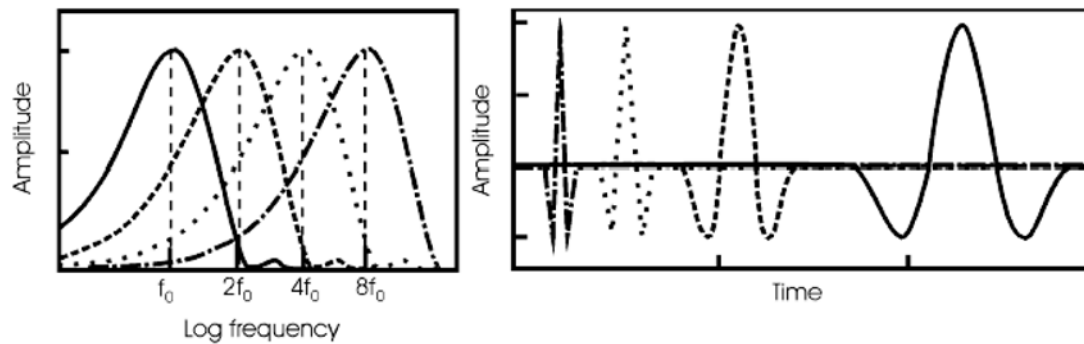


Figure: 5-36 A multiplicity of antennas with centre frequencies at binary multiples allow full coverage of a wide spectral range. The spectra and corresponding wavelet in time for 4 antennas with centre frequencies f_0 , $2f_0$, $4f_0$ and $8f_0$ are as displayed. The increase in time resolution associated with increase in bandwidth (i.e. $B=f_c$) is apparent.

The important point to note is that application resolution dictates bandwidth and hence maximum allowable antenna size (which limits efficiency). As a result one antenna size will not effectively satisfy all application needs. Deep geological sounding GPRs use long antennas which give greater efficiency but lower resolution. High resolution GPRs such as for concrete imaging use small antennas but have lower efficiency and give much less depth of penetration.

5.11.2 ANTENNA DIRECTIVITY

The directional characteristics of a short dipole antenna are controlled by the ground. Understanding antenna directivity helps greatly with understanding the source of GPR returns from within the ground. The analysis of this problem is complex but the basic characteristic can be fairly well explained.

Before continuing a great length, it must be stressed that GPR amplitude information has to date been used in a relative context. As a result, exact mathematical forms for fields and measurements have not been needed. As the technology advances, more demand for quantitative measurements are arising and further advances on quantifying responses which use some of the numerical solutions discussed in the section of GPR modeling will become more critical.

This current discussion addresses the far field radiation directivity for a short electrical dipole source in an overview fashion only. Background for this can be found in references Annan (1973), Annan et al (1975), Engatta (1983) and Smith (1999).

A short electrical dipole and the associated coordinate system are shown in Figure 5-37. When the dipole is in a uniform media, the relative electric field amplitude at a large distance is donut shaped as depicted in Figure 5-38. No energy is radiated from the ends of the antenna while energy is radiated uniformly in the plane perpendicular to the dipole axis. Figure 5-39 shows the cross sections through the donut commonly referred to as the TE and TM patterns.

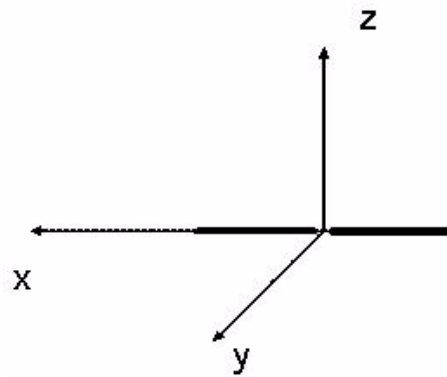


Figure: 5-37 Geometry and coordinate system for an electric dipole antenna. When placed on the ground, the X-Y plane would represent the ground surface.

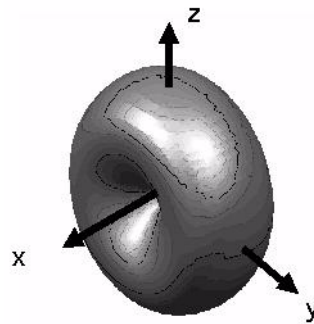


Figure: 5-38 3D presentation of pattern of a small electric dipole is donut-like in a uniform material. There is no radiation off the ends of the dipole.

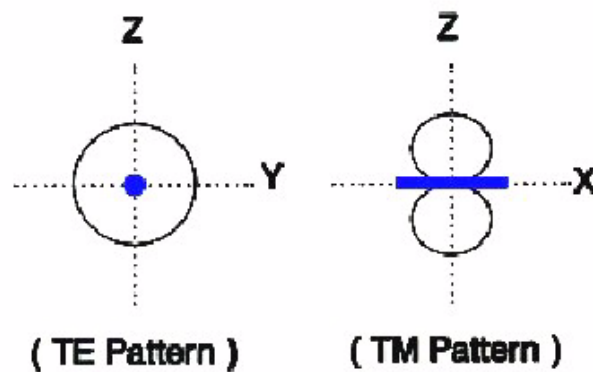


Figure: 5-39 Cross sections through the dipole pattern referred to as the TE (H plane) or TM (E plane) directivity patterns.

When the dipole antenna is placed on the ground surface, the pattern changes drastically as shown in Figure 5-40. The change in directivity is caused by the refractive focusing associated with the impedance change at the air-ground interface. Note that this pattern represents the far-field radiated component of the fields. Near the antennas the fields are not as sharply defined by peaks and nulls and there are secondary lateral and evanescent fields along the air-ground interface.

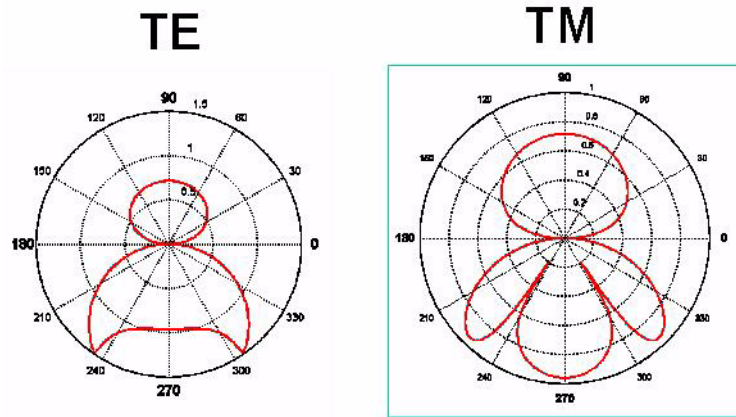


Figure: 5-40 When the dipole is on the ground surface, directivity is drastically altered and depends on ground permittivity. The TE and TM patterns shown here are for typical ground permittivity.

The peaks in the TE (H plane) pattern occur at the critical angle of the air-ground interface.

$$\theta_c = \sin^{-1}\left(\frac{v_g}{c}\right) = \sin^{-1}\left(\frac{1}{\sqrt{K_{tg}}}\right) \tag{5-31}$$

A subsurface null occurs in the TM (E plane) pattern in the critical angle direction.

The antenna directivity is obviously ground dependent. As the ground properties change, the antenna directivity will change. Figure 5-41 shows a sequence of patterns as K_g is carried from 3.2 to 80. As K_g increases, the pattern in the ground gets pointed more downward.

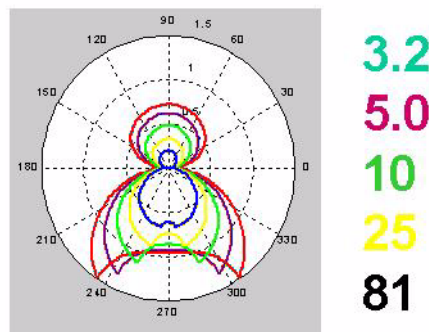


Figure: 5-41 When the ground permittivity changes, the patterns change. The TE pattern is shown for permittivities range from ice (low) to water (high).

Another practical consideration is the effect of antenna elevation off the ground surface. In real field situations, surface roughness and the need to transport antennas over the surface can limit close ground contact. Antenna elevation strongly affects antenna directivity as shown in Figure 5-42, the directivity is frequency dependent because the height effective is dependent on the relative distance in wavelengths above the surface. In the time domain frequency dependence translates into additional events and/or a dispersed radiated pulse.

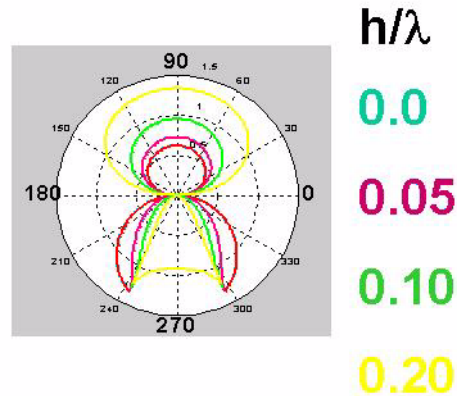


Figure: 5-42 Antenna elevation also impacts on directivity. The change in directivity is shown here as a function of height normalized against wavelength assumed pure sinusoidal excitation.

The reason that the signal into the ground at high angles (beyond the critical angle) is strongly attenuated is caused by the energy being of evanescent character in the air. The energy has to “jump the gap” between the antenna and the ground and the amplitude of the evanescent signal decreases exponential with normalized height.

In addition, signals above the ground are strengthened and the direct and reflected signals from the air-ground interface no longer cancel one another. See section 4.10 for wavefront character.

5.11.3 SHIELDING

What is antenna shielding? Figure 5-43 shows the conceptual idea of a shield. With GPR, the antenna is normally placed close to the air-ground interface. The shield is a “container” which encloses the antenna. The objective is to improve the antenna’s performance by placing the shield over it.

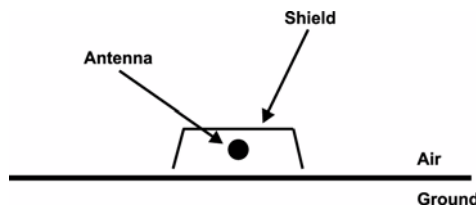


Figure: 5-43 Concept of a GPR antenna shield. The shield encloses the antenna to minimize coupling with signals in the air.

What is the purpose? Referring to Figure 5-44, signals can travel from a transmitter to a receiver along a number of paths. Shielding is used to achieve the following goals:

- maximize the energy on the path AA' to and from the subsurface target;
- minimize the direct transmitter to receiver energy on path B;
- minimize the energy which escapes into the air as on path CC';
- minimize external electromagnetic noise as indicated by signals D.

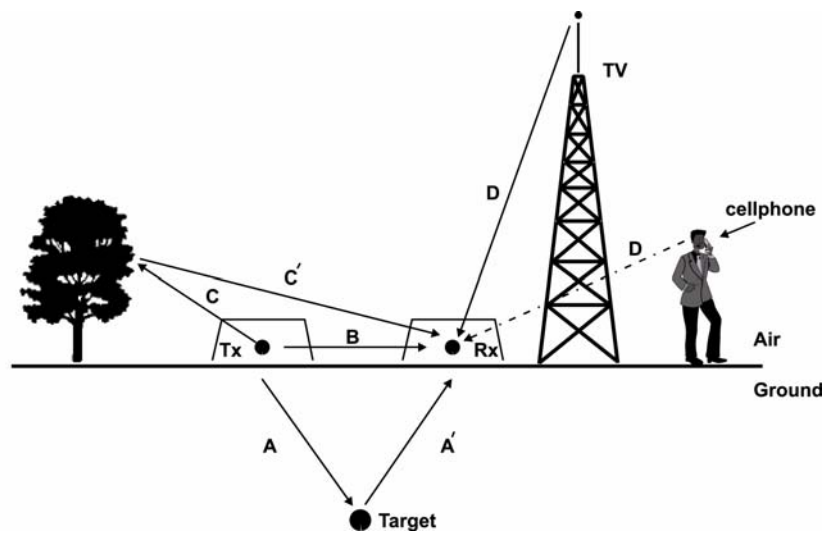


Figure: 5-44 A GPR system emits and detects radio wave signals. There are many possible signals and paths. The objective is to maximize the target response and minimize others.

Given these laudable benefits, what are the drawbacks? Antenna shielding requires a structure that has an electromagnetic response. If the structure is not designed properly or is damaged, its electromagnetic response can be large. In addition to the signals shown in Figure 5-44, energy goes from the transmitting antenna to both the transmitter shield and the receiving antenna shield and then to the receiving antenna as indicated in Figure 5-45. The shield generated signals can be large and reverberate for a long period of time.

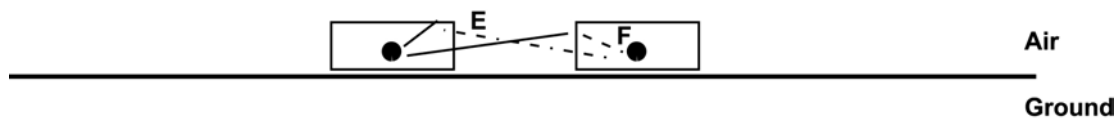


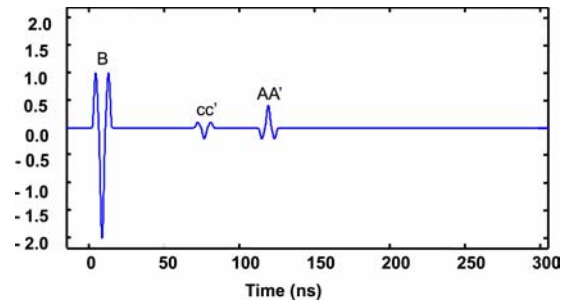
Figure: 5-45 Antenna shields must interact with radio waves to be effective. The shield can generate additional response which may be detrimental and interfere with the desired measurement unless extreme care is taken in the shield design.

Besides the electromagnetic response of the shield itself, an effective shield has to be larger than the antenna. This leads to considerable transducer size, weight and manufacturing costs penalties. In a nutshell, attempting to shield an antenna can create as many problems as it benefits.

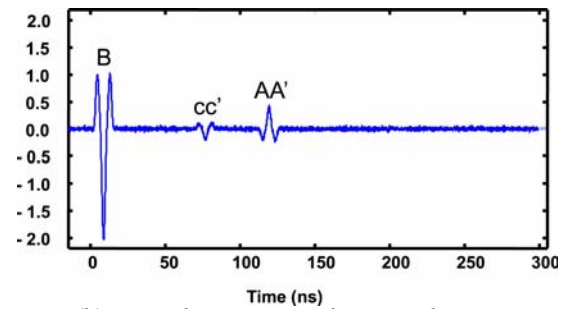
A series of radar traces are shown in Figure 5-46. (a) is the ideal response without external noise. (b) is the response observed when external noise is present. (c) shows the behavior which can occur if improper shielding is used. The reverberatory signal sunning down the trace for along period of time is the transient response of the shielding. (d) shows the result that a practical shield can achieve.

Shielded antennas can be readily constructed for higher frequency GPR systems, typically in the 100 MHz frequency range and above. The shields are about the same size as the antenna and use absorbing material to damp out the undesired signals.

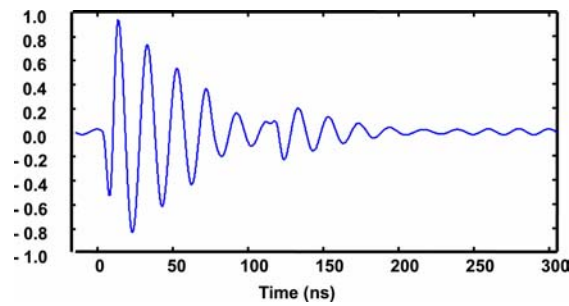
At lower frequencies, practical size and portability dictates minimal or no use of shielding.



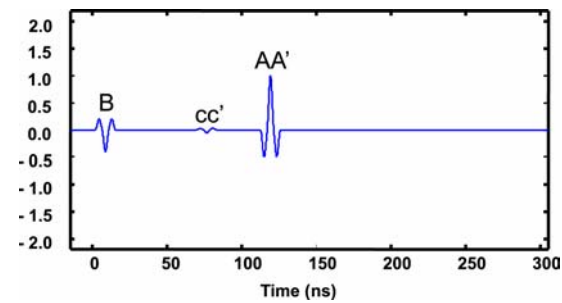
(a) Unshielded noise free response



(b) Typical response with external noise



(c) Transient response when shielding is improperly implemented



(d) Results that can be expected with a practical well implemented shield.

Figure: 5-46 Typical GPR traces for various shielding configurations.

Tips for GPR users are as follows.

- a. Shielding is never perfect no matter what some may claim.
- b. Question whether your application requires shielding. The highest fidelity and maximum depth of penetration at open sites may be obtained when shields are not used.
- c. Always look for GPR events attributable to spurious signals. Even with the most ideal shield, spurious signal leakage can and will occur.

6 MODELLING OF GPR RESPONSES

6.1 THE PURPOSE OF MODELLING

Modelling is critical to all geophysical methods. One can simulate the system behavior from excitation through to the response which would be observed or measured. Modelling or simulation enables quantitative predictions of responses leading to both a better fundamental understanding and a sound basis for interpretation.

GPR modelling is critical for the following reasons:

- understanding of physical behavior and quantifying response;
- providing performance requirements for design of measuring instruments;
- predicting response and sensitivity to parameter changes;
- optimizing survey design;
- understanding how to process data to extract information;
- enabling interpretation at a variety of levels of complexity; and
- facilitating mathematical inversion and quantification of interpretation uniqueness.

In summary, modelling underpins translation of geophysical observations into useful information (knowledge). GPR is no exception.

6.2 GPR MODELLING TYPES & DEFINITIONS

Modelling GPR responses has seen considerable evolution. Prior sections of these notes have been derived from fundamental physical principles that are a key aspect of modelling. Modelling the electromagnetic response of complex structures is not trivial. The basic modelling logic is depicted in Figure 6-1. Only with the vast improvement in computer power has it become possible to begin to address complex structures. It is therefore useful to put the history of GPR modelling into context.

Geophysical modelling, and GPR is no exception, has followed a traditional path. First, modelling of very simple structures is carried out. Usually solutions of an analytical nature are considered (such as the earlier sections of these notes). Systems are simplified so that a closed form mathematical formula can be derived. In the GPR realm, 1D models and simple analytical solutions were employed until the early 1990's.

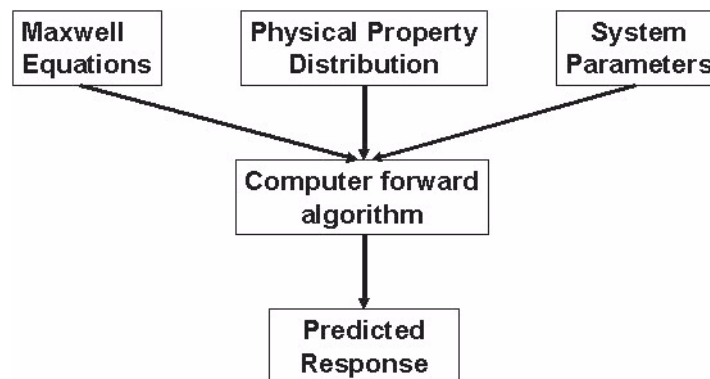


Figure: 6-1 This block diagram shows the general principles of the elements involved in forward modelling. One has to input the system characteristics combined with Maxwell's equations and physical properties to derive an output through a modeling algorithm based on these inputs.

As computer power permitted and software development allowed, movement to two-dimensional (2D) modelling occurred. In many instances the modelling has been 2D because 2D modelling allows much insight with minimal computing cost. As a result, 2D modelling simplifies the real world into structures that vary in two directions and are invariant in the third dimension (in geological terms called the strike direction of the structure). This has led to a variety of numerical solutions such as finite difference and ray tracing solutions. Integral equation solutions although possible, have not seen much usage.

Finally, full simulation modelling incorporates all three dimensions. Complex three-dimensional (3D) structures can only be modeled or simulated using numerical techniques. Techniques such as finite difference modelling (or finite element modelling) or integral equation modelling are the norm but implementations have only appeared since the mid 1990's and then only with use of powerful computer systems. 3D modelling can be extremely complex, requires addressing the full vector solution of the fields, and is intensive both in memory and CPU requirements.

As PC's become more powerful, more and more modelling of complex structures is occurring with less and less need for finesse to speed up algorithms and reduce dimensions. GPR is still a long way from fast reliable solutions for complex 3D structures readily accessible to the average user community.

6.3 ONE-DIMENSIONAL (1D) MODELLING

6.3.1 RADAR RANGE EQUATION (RRE)

The radar range equation (RRE) is the simplest form of model that has been used in GPR for some time. The purpose of the radar range equation approach has been to assess the ability of a radar to probe into a material and detect an object. It simplifies the 3D response using simplified parameterization. By estimating key system parameters, target parameters and material properties one can estimate depth of penetration and signal magnitude that can be expected.

The application of the RRE to GPR was first discussed by Annan & Davis (1977). This model has been used extensively for assessing the suitability of GPR and the possibility of it working in a particular situation. The major result of RRE is recognizing how strongly attenuation impacts GPR. This solution is by no means a complete answer to any problem but it certainly gives insight into sensitivity and signal levels. Mathematically, RRE expresses the received signal power which must be above the noise level to be detectable.

$$P_{RX} = \xi_{TX} \xi_{RX} G_{TX} G_{RX} g\sigma A \frac{e^{-4\alpha L}}{16\pi^2 L^4} > P_{NOISE} \quad (6-1)$$

Figure 6-2 shows a block diagram of the radar range equation with various terms explained. The RRE breaks the response down into a series of steps starting from the energy created in the electronic source and through to that which is detected at the receiving electronics. By following through these steps it is possible to estimate the magnitude of the return signal which is likely to be observed. These solutions can be set up as computer programs or in spreadsheets to facilitate sensitivity analysis.

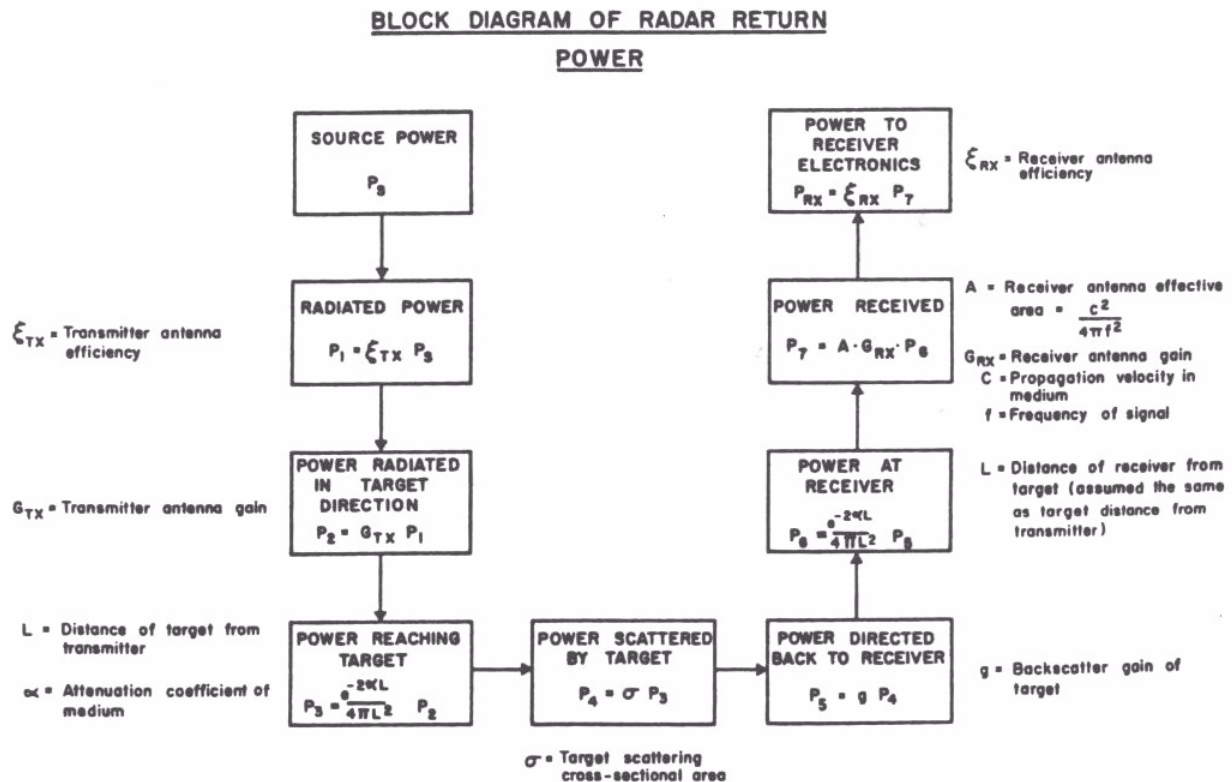


Figure: 6-2 The radar range equation (RRE) is used to provide a simplistic estimate of response by determining power losses throughout the various steps of the measurement process.

6.3.2 ONE-DIMENSIONAL (1D) LAYERED EARTH

The 1D layered earth model is a carry over from the petroleum seismic industry. Generation of synthetic seismograms for layered earth environments provides a way to start to understand the effect of multiple paths, reverberations, polarity changes and gradational interfaces.

1D GPR modelling is described by Annan & Chua (1992). The 1D model makes no claims to be quantitative about the amplitude of the response that would be observed with a GPR. The model provides a sense of the timing of events and the relative amplitude of the signals. Issues such as the polarity of an event and the change in amplitude at a gradational boundary are GPR topics which have been addressed (Annan et al (1992), Redman (1994)). Figure 6-3 demonstrates an example result of 1-D modelling. In this case a gradational boundary is being emulated to show the decrease in amplitude as an interface becomes gradational with respect to the dimension of the excitation pulse.

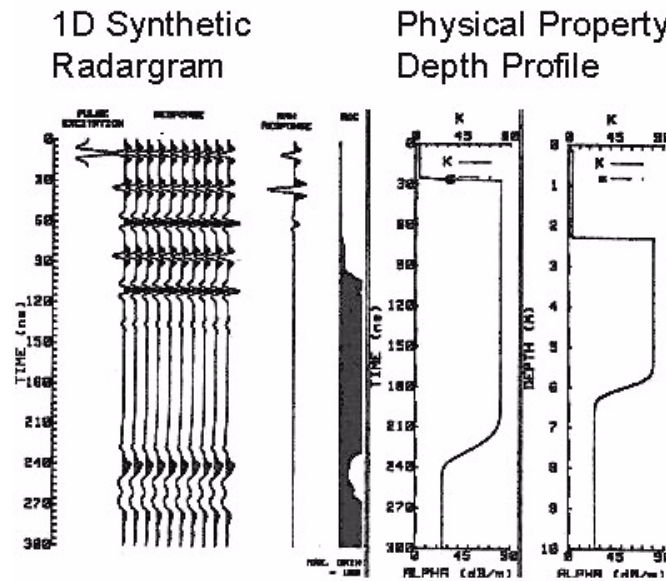


Figure: 6-3 One-dimensional GPR modeling involves defining the physical properties versus depth and then computing the response assuming no dimensionality to the source. This example on the right shows the physical model in terms of relative permittivity and attenuation and the resulting synthetic GPR response on the left.

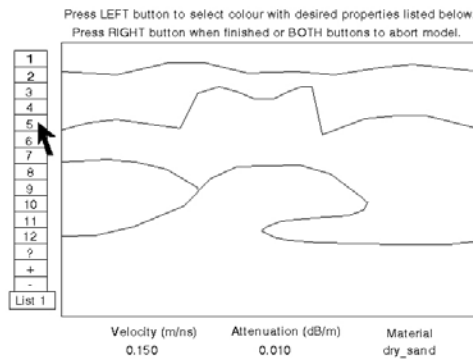
6.4 TWO-DIMENSIONAL (2D) MODELLING

6.4.1 RAY TRACING

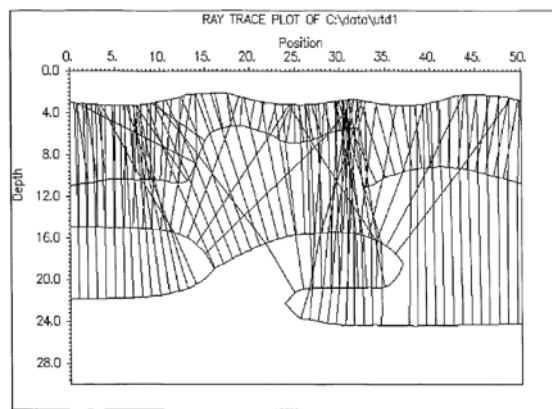
For GPR, one of the ways to carry out 2-D modelling is to use the technique of ray tracing. In a ray tracing model one assumes that the distances between objects is large and the pulse length duration is very short compared to the distances involved. The signals can be treated using geometrical optics approximations. Such GPR modelling concepts are again borrowed from the seismic field.

In a 2-D model, the responses can be broken down into electromagnetic field polarization where either the electric field (TE) or magnetic field (TM) is parallel to the 2D structure. The rays representing the electromagnetic fields are then traced through the model for the particular polarization type. The TE or TM separation reduces the vector complexity to a scalar problem. The rays are traced through the model and reflected and refracted at interfaces according to Snell's law and the Fernel reflection coefficients. Amplitude attenuation along the ray paths follows the ohmic dissipation exponential decrease.

Ray tracing modeling is for GPR described by Cai & McMechan (1995). The ray-tracing concept for an undulating interface is depicted in Figure 6-4 and the GPR response is shown in Figure 6-5. The model response can be computed for either TE or TM field polarization.



(a)



(b)

Figure: 6-4 Figure (a) shows the geometrical model for the ground structure. Figure (b) shows the various ray paths from the surface down to the individual reflecting horizons.

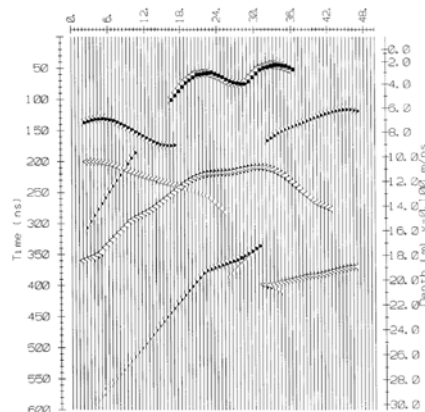


Figure: 6-5 This shows a synthetic response computed for a model shown in Figure 6-4. In this case, the specular reflections from the various horizons appear at the appropriate delay times accounted for by the various velocities in the section as well as the attenuation in the material.

This type of model can incorporate the far-field directivity of the GPR antenna. Examples of insights into the behavior of geologic structures in complex situations using such a model are given by Nobes & Annan (2000).

6.4.2 FK 2D MODELLING

2D modelling also lends itself to finite difference solutions. One of the fast ways of computing the grid response to an arbitrary 2D structure is to transform space and time into the temporal frequency and a spatial frequency (or wave number) domains. This transformation domain is called the FK domain, where F stands for frequency and K stands for spatial wave number and implies double fourier transformation.

The modelling involves taking each interface or target in the model and turning it into a reflectivity coefficient at each point in the 2D space. As with the ray tracing approach, the vector to scalar reduction by TE and TM separation can be employed. The FK domain approach enables the propagation signals using simple analytical calculations and manipulations. Once the propagation gets carried out in the FK domain, inverse fourier transform yields the space-time response.

While sounding complex, the calculations are fairly straightforward and the principles are extensively discussed in the seismic literature. Application of 2D FK solutions to GPR problems are described by Zeng et al (1995).

An example model is shown in Figure 6-6 and the resultant FK solution is shown in Figure 6-7. In general the FK modelling has speed benefits for complex structures and includes diffracted energy whereas ray tracing solutions deal only with specular reflection energy but do not address diffraction response. Ray tracing generally allows for physically larger problems because only the boundaries need to be considered.

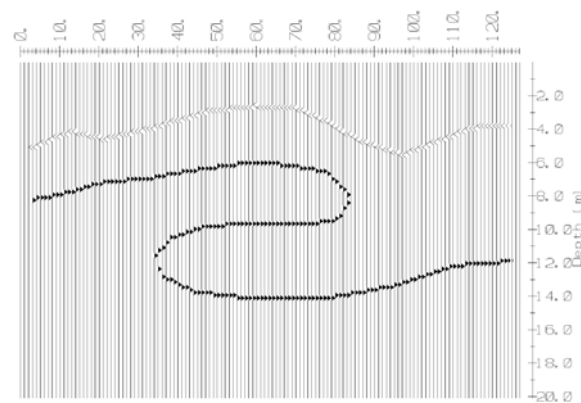


Figure: 6-6 When carrying out a two dimensional FK model, one places reflectivity at every point on a regular mesh. The model shown here is an example of reflectivity versus position.

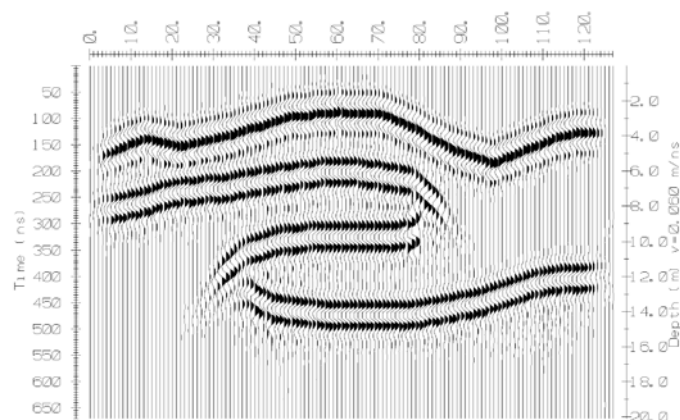


Figure: 6-7 This section shows the result of FK 2-D modeling output for the reflectivity model shown in Figure 6-6.

6.4.3 FULL FINITE DIFFERENCE (FD) SOLUTIONS

The first two 2D solutions discussed here are approximate solutions. Full 2D numerical simulation for either time (FDTD) or frequency (FDFD) domain is practical. TE and TM separation again allow reduction of the vector problem to a scalar calculation. Very little of 2D FD has occurred in the GPR field as the advent of 3-D modelling occurred at the same time as 2D modelling. Unlike the seismic and other geophysical modelling worlds where computer technology just could not handle 3D modelling for many years, demand for 3D GPR modelling began at the same time computer power allowed it to occur (see Giannopoulos (1997)).

The importance of 2D FD modelling is that it can be fit into a moderate size computer and is a scalar calculation rather than a vector solution. The vector solution can be built up by adding the two types of responses which are implicitly vector fields but have no mixing.

6.4.4 2½ D SOLUTIONS

In some situations, including the localized 3D nature of the source of the electromagnetic fields is desirable for ground models which are two-dimensional. 2½ D modelling exploits the 2D solution by splitting the excitation in TE and TM components, solving the 2D problem and combining the results at the end. As with simpler 2D, little GPR work in this area has occurred. 2½ D is more common in traditional EM (Hohmann 1987). A good GPR example is the work of Lampe and Holliger (2000).

6.5 THREE-DIMENSIONAL (3D) MODELLING

6.5.1 3D RAY TRACING

3D ray tracing solutions have a long history in seismic (Kline and Kay (1965), Cerveny and Ravindra (1971)) and electromagnetics (Luneburg (1964), Borne and Wolf (1980)). In these cases, the signals propagate large distances through the material compared to the wavelength and the ray optics approximation is quite suitable in many instances.

For GPR, 3D ray tracing solutions have seen limited use and development. There are two reasons for this. First, GPR signals are strongly attenuated limiting the conditions where the geometric optics assumptions are fully applicable. Secondly, by the time the demand for 3D modelling started to occur, computer power had reached the level where it was possible to consider full numerical solutions and hence the use of approximate solutions, such as ray tracing which becomes complex in 3D, were perceived to have little benefit.

6.5.2 3D FINITE DIFFERENCE MODELLING

The majority of 3D GPR modelling uses numerical finite difference style techniques. Depending on the particular application, the solution may be set up as finite element or finite difference but the general implication is that one is solving the full vector field at a mesh of points in 3D space.

The initial 3D modelling for GPR was reported by Roberts & Daniels (1996). 3D modelling for EM induction was also becoming available Alumbaugh and Newman (1994). This modelling required use of a Cray super computer to generate results. Similar modelling results are reported by Bergmann et al (1996), Wang & Trip (1996), Carcione (1996) and Holliger & Bergmann (2000).

It is beyond the scope of this brief discussion to get into the details of numerical simulation. Referring to the above papers is the best way to learn about 3D GPR modelling. There are a number of different techniques which are used to approach these problems and considerable skill and modelling experience is required to confidently enter this area of GPR at present. One must solve the vector field equation for the field components with full variation of the material properties.

One can solve for the fields for particular sinusoidal excitation frequency. This approach was the most common method to start with as commonly returned to as FDFD (finite difference frequency domain) modelling.

Using a frequency domain solution, the time domain solution is obtained by modelling at a number of different frequencies and then Fourier transforming the frequency response into the time domain to obtain the transient response.

More common now is the FDTD (finite difference time domain) solution. The approach here is to by-pass the frequency domain and solve the full transverse vector wave equation in the time domain. These results require both spatial and temporal finite differencing or numerical discretization. To date, however, the complexity of the responses and the length of time required to compute them has limited widespread use. As computer power increases and computer codes become more efficient, more and more utilization of the numerical solutions is occurring.

The key reason why full 3D numerical solutions are needed is that they provide the basis for inverting or extracting quantitative information about the subsurface in an automatic fashion.

Staggered Grid Concept

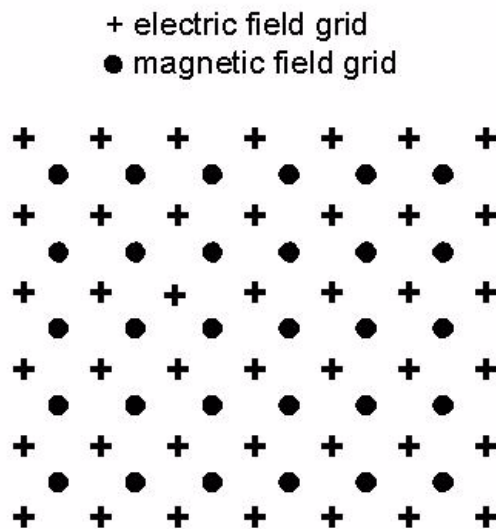
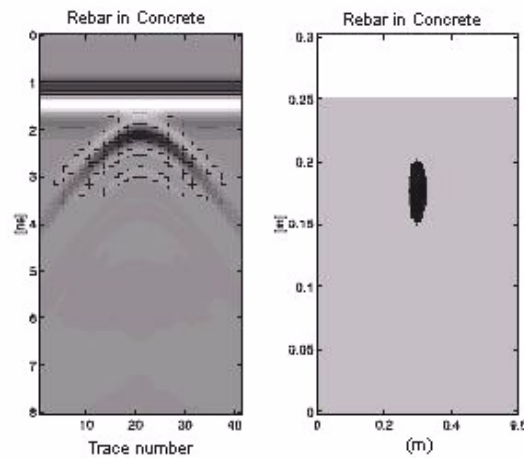


Figure: 6-8 This grid pattern shows the concept of the staggered grid for electromagnetic modeling. The electric and magnetic fields are computed independently at grid points which are off set from one another. The magnetic fields at points around an electric field point are used to update the electric field. Similarly the electric field points around an individual magnetic observation point are used to update a magnetic field.

The general approach to 3D modelling is to establish a grid. If a single vector field (i.e. electric or magnetic) is used then a second order spatial difference equation is required. More commonly, a staggered grid, where both the electric and magnetic field are computed alternately in time using first order derivatives rather than second derivatives as proposed by Yee (1965), has become the standard in electromagnetic modelling.

The example grid shown in Figure 6-8 shows a staggered grid. The electric field is computed on one set of mesh nodes while the magnetic field is computed at another set of mesh nodes which are offset.

Once these solutions are computed they can be displayed as fields versus time such as the 3D wavefront shown in Figure 6-9. These examples were drawn from the paper by Giannopoulos (1997).



:Simulated GPR scan by GPRMAX2D (left) and image representation of the geometry of the model (right). Note that the vertical scale is exaggerated.

Figure: 6-9 An example of using a finite difference time domain (FDTD) computational algorithm based on a staggered grid to compute the response of a reinforcing bar buried in concrete.

Other topics which are addressed in FDTD models are the inclusion of dispersive electric properties (Bergmann et al (1999), Young and Nelson (2001)). In all numerical models, the edges or boundaries of the model space can create artificial events. Delving into the modelling field requires learning about devising absorbing boundary conditions (Holtzman and Kastner (2001), Oguz, Levent (2001)).

6.5.3 INTEGRAL EQUATION – EQUIVALENT SOURCE SCATTERING

The equivalent source method is an elegant and physically intuitive means of formulating EM responses (Hohmann (1987), Annan (1974)). Instead of numerically solving for all the fields, the approach was the known response and formulates the response for localized targets which can greatly reduce the size of the numerical calculation.

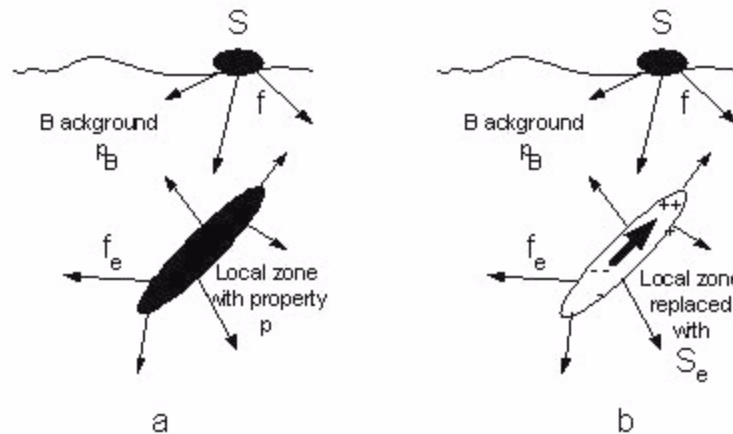


Figure: 6-10 The conceptual idea of an embedded localized inhomogeneity (a) being transformed into an equivalent signal source (b) in a known background.

Details of this methodology and beyond this presentation. The concept is explained in scalar form here. Referring to Figure 6-10, a localized target with differing properties is present in a media of a known response which can be characterized by the green's function

$$\mathbf{g} = (\mathbf{r}, \mathbf{r}', \mathbf{t}, \mathbf{t}') \quad (6-2)$$

If a source is present and described in space and time as $s(\mathbf{r}, \mathbf{t})$, the fields created, $f(\mathbf{x}, \mathbf{t})$, are mathematically expressed as the convolution

$$\mathbf{f}(\mathbf{r}, \mathbf{t}) = \iiint \mathbf{g}(\mathbf{r}, \mathbf{r}', \mathbf{t}, \mathbf{t}') s(\mathbf{r}', \mathbf{t}') d^3r' dt' \quad (6-3)$$

By describing the target as a difference in physical properties $\Delta p = (p - p_B)$ incorporated in the background response green's function, the excitation field $f(\mathbf{r}, \mathbf{t})$ will cause an apparent source signal

$$\mathbf{s}_e(\mathbf{r}, \mathbf{t}) = \Delta p f_{\text{TOTAL}}(\mathbf{r}, \mathbf{t}) = \Delta p (f(\mathbf{r}, \mathbf{t}) + f_e(\mathbf{r}, \mathbf{t})) \quad (6-4)$$

This new equivalent source generates the response

$$f_e(\mathbf{r}, \mathbf{t}) = \iiint \mathbf{g}(\mathbf{r}, \mathbf{r}', \mathbf{t}, \mathbf{t}') \mathbf{s}_e(\mathbf{r}', \mathbf{t}') d^3r' dt' \quad (6-5)$$

with the source signal satisfying an integral equation of the form

$$\mathbf{s}_e(\mathbf{r}, \mathbf{t}) = \Delta p f(\mathbf{r}, \mathbf{t}) + \Delta p \iiint \mathbf{g}(\mathbf{r}, \mathbf{r}', \mathbf{t}, \mathbf{t}') \mathbf{s}_e(\mathbf{r}', \mathbf{t}') d^3r' dt' \quad (6-6)$$

when the material contrast Δp is small, the approximation is used.

$$\mathbf{s}_e(\mathbf{r}, \mathbf{t}) \approx \Delta p f(\mathbf{r}, \mathbf{t}) \quad (6-7)$$

This is called the Born approximation and enables fast calculation of responses.

Because this solution has a form which can be computed in direct manner where approximated, the inversion procedures currently common in GPR (and most EM) use this modelling approach as the basis for structuring inversion schemes. For this reason, more detail is provided here than on other modelling.

6.6 INVERSION

Inversion is the mathematical technique used to describe the extraction of physically quantifiable parameters out of a set of observed data. In concept, a measurement system obtains data at a number of spatial points which contain encompass a number of different frequencies or different time delays (i.e. band limited transfer function or impulse response). This information is indicative of targets or structures buried in the ground. The goal is to infer the spatial distribution of the material properties which give rise to the observed response.

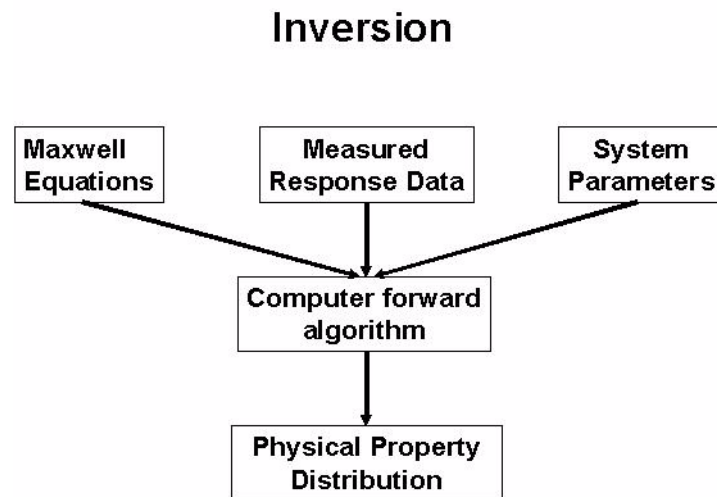


Figure: 6-11 Inversion of GPR data requires forming the opposite steps as discussed for Ford modelling. Given the model, the algorithm and the observation of ground response, one reverses the modelling steps to extract the physical property description.

The forward modelling described provides the tools whereby the responses can be predicted if a known distribution of physical properties is given. Inversion is the reverse of this process. The concepts are shown figuratively in Figure 6-11. Given the observed fields these observations must be transformed back into a spatial distribution of physical properties which are hopefully unique and dependable. The subject of inversion is well known in the geophysical community and excellent discussions of the topics can be found in Tarantola (1987) and Oldenburg et al (1993).

The first successful extraction of physical properties from GPR is described by van der Kruk (2001). In this work the vector fields at the surface as a function of time are processed to extract changes in permittivity and conductivity in the subsurface. The solution is formulated using the Born approximation integral equation solution. This work provides an excellent basis for understanding the future evolution of inversions of GPR responses into quantifiable material properties.

To date, the approach in GPR has been to estimate or image reflectivity versus spatial location in the subsurface. An introductory discussion is provided by Annan (1997). Techniques of migration and synthetic aperture are applied as opposed to full inversion. The reflectivity imaging concepts are well developed in the seismic field. An insightful discussion on this is given by Bleistein and Gray (2001). Discussion of the GPR aspects and the handling of some aspects of the vector character are discussed by Green et al (2002), Moran (2000).

7 SURVEY DESIGN

Proper design of GPR surveys is critical to success. Setting expectations and optimizing data acquisition to meet expectations requires planning. This chapter builds on excerpts of the paper Annan & Cosway (1992) on the subject of survey design.

7.1 EVALUATING GPR SUITABILITY

Prediction of whether GPR will "work" for the problem at hand is not clear cut. In general it is easier to rule out situations where radar is totally unsuitable than to state with confidence that radar will be successful. Again, this is not a unique feature of the GPR method but is a fact of life with all geophysical methods. GPR tends to have more mystery because people have not normally had as much experience with it as with some other methods.

There are some basic tools which assist the GPR user in the decision making process. The two most important are the radar range equation and numerical simulation techniques. Some examples are described by Annan and Chua (1988).

The radar range equation (RRE for short) does a basic allocation of available power against all the loss mechanisms to yield a "yes/no" answer on whether a target will return sufficient power to be detectable. The RRE has to simplify the problem at hand; therefore, the results are good guides, not absolute predictors of success or failure. The basic steps of the radar range equation are depicted in Figure 7-1. Example results of an automated program to carry out these calculations are shown in Figure 7-2. Nomograms for specific systems and targets can also be generated such as shown in Figure 7-2.

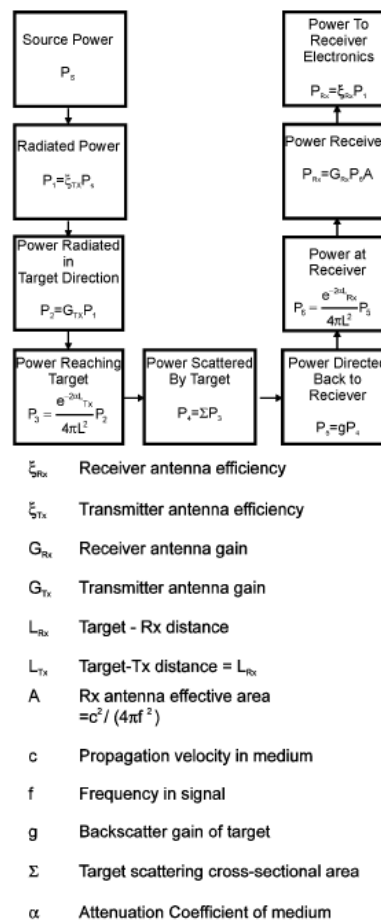


Figure: 7-1 Block Diagram of radar range equation.

System Performance Factors

System Q (dB)	133.98	Tx voltage (V)	1000.00
Tx to antenna effcy (dB)	-20.00	Rx noise (uV)	200.00
Transmitter antenna gain (dB)	3.00		
Antenna to receiver effcy (dB)	-20.00		
Receiver antenna gain (dB)	-1.45		
Net system Q (dB)	98.53		

Propagation Factors

Spreading losses (dB)	-74.02
Attenuation Losses (dB)	-4.00

Target Factors

	<i>POINTS</i>	<i>ROUGH</i>	<i>SPEC</i>	<i>SPEC THIN</i>
Target backscatter gain (dB)	-5.37	8.60	19.85	-38.72
Net Performance	15.14	29.11	40.36	-18.21
Target amplitude (uV)	1143	5709	20853	25
Stacks	1	1	1	66
Windows (ns)	667			

RADAR RANGE PAPER COEFFTS**Model Parameters**

	<i>POINT</i>	<i>ROUGH</i>	<i>SPEC</i>	<i>PEC THIN</i>	
Centre Freq. (MHz)	100.00	B1-8.54	1.56	0.62	-6.47
Target range (m)	20.00	B20.00	1.00	2.00	2.00
Attenuation (dB/m)	0.10	B34.00	-1.00	0.00	0.00
Target diameter (m)	0.50				

Host K	25.00	Target Reflection (dB)	-11.14
Target K	8.00	*Thin layer reflection (dB)	-69.71
Layer Thickness (m)	0.00	*Thin layer beta (dB)	-58.57
Conductivity Attenuation		*Diameter/wavelength (dB)	-1.58
5.00 mS/m	1.69 dB/M	Wavelength (m)	0.60

* If these values exceed -10 dB then, the assumption and approximations used to derive these formulas are invalid.

Figure: 7-2 Example of a radar range calculation.

Numerical simulation techniques (NST for short) are now becoming well developed for GPR. Simple programs for 2D earth structures are commercially available and are instructive to use. More complex 2- and 3-dimensional modelling programs are not available for general use but are available at research institutions.

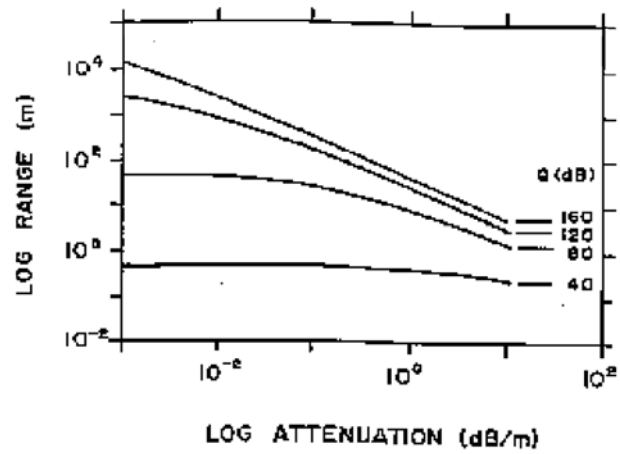


Figure: 7-3 Radar range equation nomogram example.]

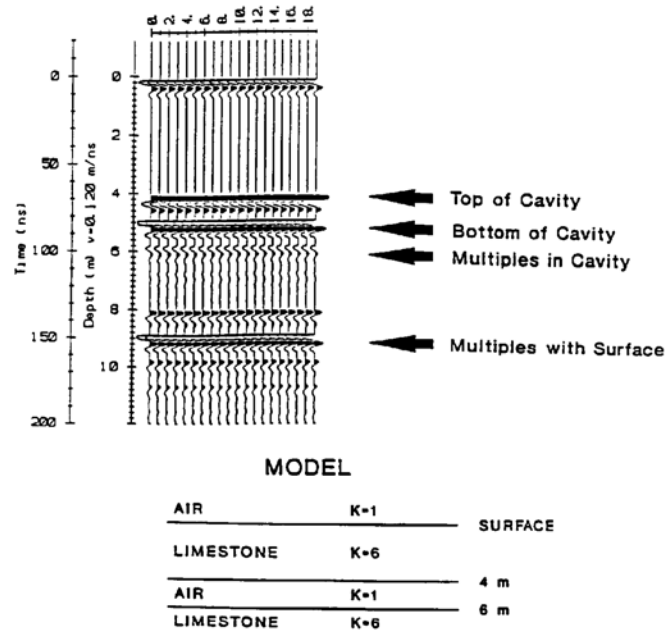


Figure: 7-4 Illustration of a synthetic radargram to predict a GPR response.

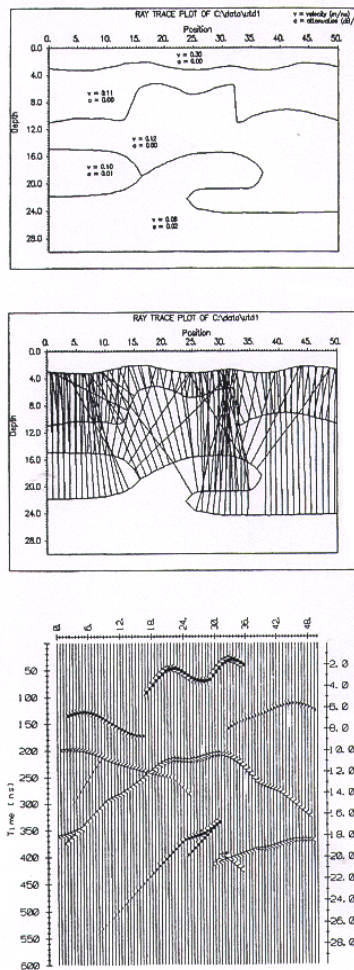


Figure: 7-5 Modeling such as this 2 dimensional ray trace stimulation helps users utility of GPR .

Answering the question "Will GPR work???" is neither easy nor exact. Addressing the following three questions will certainly help in anticipating the answer.

Question 1: Is the target within the detection range of the radar irrespective of any unusual target characteristics?



Figure: 7-6 What is the target depth?

Discussion of Question 1

The way to answer this question is to calculate or measure the host attenuation coefficient. Using the radar range equation and the system performance factor (example in Figure 7-2), compute the maximum range that a reflector of the anticipated target type can be detected. If the target is at a depth greater than this range, radar will not be effective. A conservative rule-of-thumb is to state that radar will be ineffective if the actual target depth is greater than 50% of the maximum range.

Commercial radar systems can typically afford to have a maximum of 60 dB attenuation associated with conduction losses. A rough guide to penetration depth is

$$D = \frac{35}{\sigma} \quad (7-1)$$

where α is attenuation in dB/m and σ is conductivity in mS/m. These equations are not universal but are applicable when attenuation is moderate to high $\alpha > 0.1$ dB/m or $\sigma > 1$ mS/m which is typical of most geologic settings.

Question 2: Will the target generate a response detectable above the background clutter? In other words, does the target have sufficient contrast in electrical properties and is it physically large enough to reflect or scatter a detectable amount of energy?



Figure: 7-7 What is the target geometry?

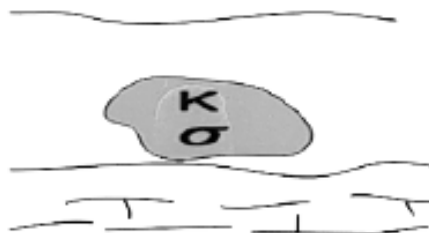


Figure: 7-8 What are the target electrical properties?



Figure: 7-9 What is the host material?

Discussion of Question 2

Power reflectivity is estimated using the expression

$$P_r = \left[\frac{\sqrt{K_{\text{Host}}} - \sqrt{K_{\text{Target}}}}{\sqrt{K_{\text{Host}}} + \sqrt{K_{\text{Target}}}} \right]^2 \quad (7-2)$$

Two conservative rules-of-thumb for predicting success are as follows. First, the electrical properties of the target should be such that the power reflectivity be at least 0.01. (Note that a metal target is equivalent to $K_{\text{Target}} \rightarrow \infty$.) The size of the target also is a factor in the amount of energy scattered. While specific shape is also important, the size effect dominates and can be best seen from the scattering cross section of a sphere versus wavelength shown in Figure 7-10. For targets small with respect to the wavelength, scattering cross section depends on wavelength. For targets larger than the wavelength, the cross section stabilizes to a constant.

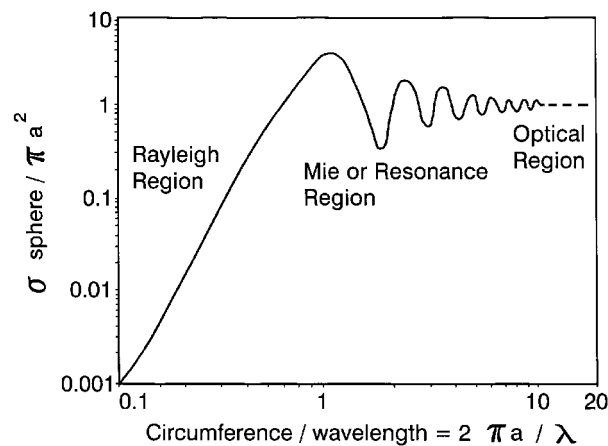


Figure: 7-10 Variation of the scattering cross section of a spherical target as a function of dimension normalized against wavelength (diagram from Skolnik(1970)). While specific to a sphere, similar behaviour is displayed by any object of finite dimension. The response increases until the object is on the same order of size as the wavelength. For GPR to penetrate through a heterogeneous material, it highly advantageous that the GPR wavelength be large compared to the scale of heterogeneity.

Question 3: Can you confirm that other obvious conditions will not preclude use of GPR?



Figure: 7-11 What is the survey environment like?

Discussion of Question 3

One example would be a radio transmitter located at the site. Another example would be a tunnel lined with metal mesh to prevent loose rock from falling. In the first case external signals may saturate the sensitive receiver electronics. In the later, all the radar signal would be reflected at the tunnel wall and none would penetrate into the tunnel wall.

If the answers to all the above questions are "yes", there is a good chance GPR will work. The above conditions are posed in a conservative manner and intended to err on the pessimistic side. More detailed analyses can employ RRE and NST techniques. In general it is almost impossible to obtain reliable estimates of all of the parameters involved in RRE and NST; these procedures are most effectively used as part of a sensitivity analysis. The conclusions drawn will be fuzzy but informed.

As with all predictions nothing beats a real field trial. If practical, a field evaluation stage should be an integral component in survey design optimization. Unfortunately, financial constraints usually are a real and limiting factor.

7.2 REFLECTION SURVEY DESIGN

The most common mode of GPR surveying is common-offset, single-fold reflection profiling as depicted in Figure 7-12. In such a reflection survey, a system with a fixed antenna geometry is transported along a survey line to map reflections versus position.

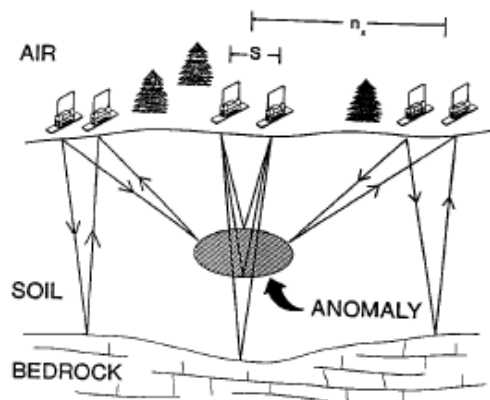


Figure: 7-12 Schematic illustration of common-offset single-fold profiling.

There are seven parameters to define for a common-offset, single-fold GPR reflection survey. These are the frequency, the time window, the time sampling interval, the station spacing, the antenna spacing, the line location and spacing, and the antenna orientation.

7.2.1 SELECTING OPERATING FREQUENCY

Selection of the optimal operating frequency for a radar survey is not simple. There is a trade off between spatial resolution, depth of penetration and system portability. As a rule, it is better to trade off resolution for penetration. There is no use in having great resolution if the target cannot be detected!! The following is a brief summary of more extensive discussions of this subject given by Annan & Cosway (1994).

There are three main issues which control frequency selection, namely,

- i. Spatial resolution desired,
- ii. clutter limitations, and
- iii. exploration depth.

Each of these issues yields a constraint on frequency. A brief description of each topic is presented and the frequency constraint given without detailed derivation.

Resolution of two events requires that the radar pulse envelope time duration be shorter than twice the separation delay time between two features to be resolved. Assuming a centre frequency to bandwidth ratio of 1, the constraint on the centre frequency, f_c , takes the form

$$f_c^R > \frac{75}{\Delta z \sqrt{K}} \text{MH z} \quad (7-3)$$

where Δz is the spatial separation to be resolved in metres and K is the dielectric constant or relative permittivity. In other words, spatial resolution places a lower bound on the centre frequency. (and required bandwidth).

Clutter in GPR systems refers to the radar signals returned from material heterogeneity in soils and rock. The radar response of small scale features (i.e., fine scale bedding, cracks and joints, laminations), increases rapidly as radar frequency increases as evident in Figure 7-10. The data example in Figure 7-13 clearly show how clutter increases with increasing frequency). If the radar frequency becomes too high, one can often reach the point where one "can't see the forest for the trees"!! In order to "see" to depth into the ground, the amount of energy scattered by clutter should be minimized. To achieve this, the signal wavelength should be much longer (we use a factor of 10) than the typical heterogeneity or clutter dimension, ΔL , in the host environment. The clutter centre frequency constraint takes the form

$$f_c^C < \frac{30}{\Delta L \sqrt{K}} \text{MH z} \quad (7-4)$$

Note that this constraint also implies that the target sought must be considerably larger than the clutter dimension. If this is not true, then identifying the target response becomes the problem of looking for the "needle in the haystack".

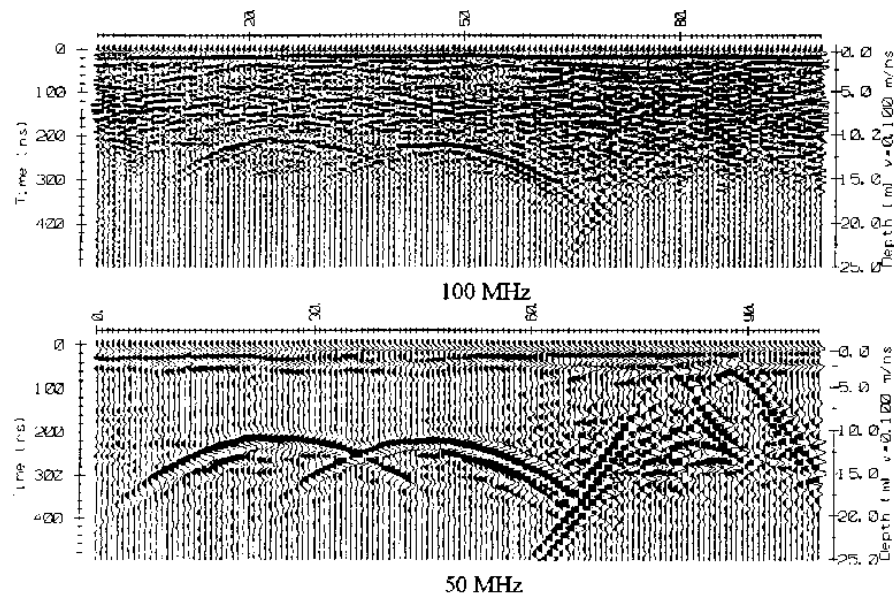


Figure: 7-13 The above data sets clearly illustrate the clutter frequency concept. These data were acquired over two tunnels in an area of gneissic bedrock. The rock texture had a spatial scale of 30 cm. At 100 MHz the clutter is clearly visible. At 50 MHz much of the clutter from the rock texture is suppressed.

The third frequency, referred to as the exploration depth frequency, requires that the target cross section occupy a major fraction of the radar beam in order that sufficient energy be returned for detection. Furthermore, the target dimension should be as close in size as possible to a Fresnel zone in order that the returned signal arrive coherently. Derivation of a simple guide to encompass these trade offs without resorting to a full radar range analysis is not simple but a basic constraint on the centre frequency is that

$$f_c^D < \frac{v\beta\sqrt{K-1}}{D} \quad (7-5)$$

where β is the ratio of radar beam footprint to target size ratio and D is depth in metres. An assumption of $\beta = 4$ is reasonable for GPR applications and one obtains

$$f_c^D < \frac{1200\sqrt{K-1}}{D} \text{ MHz} \quad (7-6)$$

as a centre frequency constraint.

As a general rule, the three frequencies should be computed and, if the survey problem has been properly posed, one should find that

$$f_c^R < f_c < \min(f_c^D, f_c^C) \quad (7-7)$$

If the resolution frequency is greater than the depth or the clutter frequency, the desired spatial resolution is incompatible with the clutter dimension or depth of exploration.

A quick guide to frequency selection is to use Table 7-1 which is based on the assumption that the spatial resolution required is about 25% of the target depth.

Table: 7-1 Antenna centre frequency as a function of exploration depth.

Depth (m)	Center Frequency (MHz)
0.5	1000
1.0	500
2.0	200
7.0	100
10.0	50
30.0	25
50.0	10

The above are values based on practical experience. Since every problem requires careful thought, the above values should only be used as a quick guide and not a replacement for thoughtful survey planning.

7.2.2 ESTIMATING THE TIME WINDOW

The way to estimate the time window required is to use the expression

$$W = 1.3 \frac{2 \times \text{Depth}}{\text{Velocity}} \quad (7-8)$$

where the maximum depth and minimum velocity likely to be encountered in the survey area are used. The above expression increases the estimated time by 30% to allow for uncertainties in velocity and depth variations.

If no information is available on the electrical properties. Table 7-2 provides a quick guide.

Table: 7-2 Time Windows

Depth (m)	Rock	Wet Soil	Dry Soil
0.5	12	24	10
1	25	50	20
2	50	100	40
5	120	250	100
10	250	500	200
20	500	1000	400
50	1250	2500	1000
100	2500	5000	2000

7.2.3 SELECTING TEMPORAL SAMPLING INTERVAL

One of the parameters utilized in designing radar data acquisition is the time interval between points on a recorded waveform. The sampling interval is controlled by the Nyquist sampling concept and should be at most half the period of the highest frequency signal in the record. For most ground penetrating radar antenna systems, the bandwidth to centre frequency ratio is typically about one. What this means is that the pulse radiated contains energy from 0.5 times the centre frequency to 1.5 times the centre frequency. As a result the maximum frequency is around 1.5 times the nominal centre frequency of the antenna being utilized.

Based on the assumption that the maximum frequency is 1.5 times the nominal antenna centre frequency, the data should be sampled at a rate twice this frequency. For good survey design it is better that one uses a safety margin of two. As a result the sampling rate should be approximately six times the centre frequency of the antenna being utilized. Based on this analysis Table 7-3 summarizes suitable sampling intervals versus operating frequency when one assumes a centre frequency to bandwidth ratio of 2

Table: 7-3

Antenna Center Frequency (MHz)	Maximum Sampling Interval (ns)
10	16.70
20	8.30
50	3.30
100	1.67
200	0.83
500	0.33
1000	0.17

The function relationship is

$$t = \frac{1000}{6f_c} \quad (7-9)$$

where f_c is the centre frequency in MHz and t is time in ns.

In some instances it may be possible to increase the sampling interval slightly beyond what is quoted but this should only be done when data volume and speed of acquisition are at a premium over integrity of the data. In any event the sampling interval should never be more than 2 times that quoted here.

7.2.4 SELECTING STATION SPACING (SPATIAL SAMPLING INTERVAL)

The selection of spacing between discrete radar measurements (see Figure 7-7) is closely linked to the centre operating frequency of the antennas and to the dielectric properties of the subsurface materials involved. In order to assure the ground response is not spatially aliased, the Nyquist sampling intervals should not be exceeded. The Nyquist sampling interval is one quarter of the wavelength in the host material and expressed as

$$\Delta x = \frac{c}{4f\sqrt{K}} = \frac{75}{f\sqrt{K}} \text{ (in m)} \quad (7-10)$$

where f is the antenna centre frequency (in MHz) and K is the relative permittivity of the host. If the station spacing is greater than the Nyquist sampling interval, the data will not adequately define steeply dipping reflectors or diffraction tails. In areas of flat lying reflectors, this criteria can be compromised.

The spatial interval of measurement is clearly illustrated by the example sections shown in Figure 7-14 and Figure 7-15. The 50 MHz data in Figure 7-14 were collected with a station spacing of 3m which is considerably larger than the computed Nyquist interval of 0.5 to 0.77. The data in Figure 7-9 clearly define the strong relatively flat lying reflectors. The steeply dipping events are aliased and appear as 'hash' on the section. The same section sampled at a 0.5m station interval shown in Figure 7-15 clearly defines the steeply dipping features.

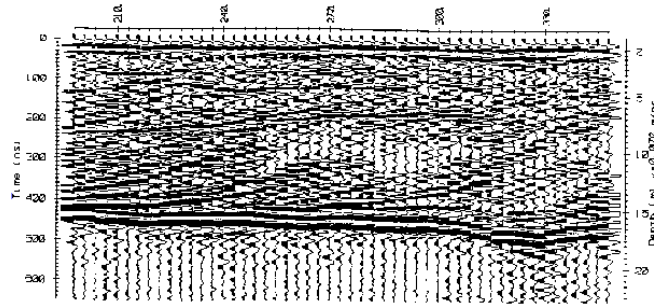


Figure: 7-14 GPR reflection section from a deltatic environment obtained using 50 MHz antennas and a 3m station spacing.

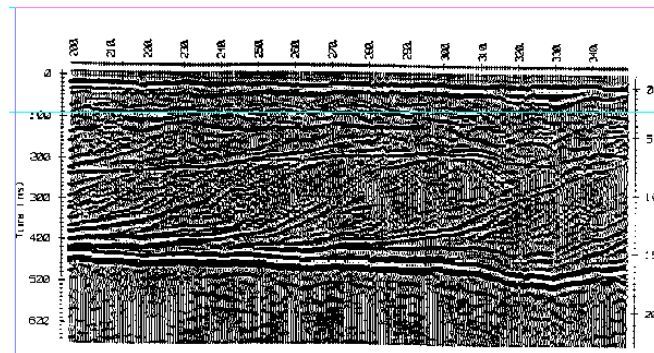


Figure: 7-15 Same section as Figure 7-9 but station interval reduced to Nyquist sampling interval of 0.5 m.

There are practical trade-offs to be made in selection of station interval. From a practical viewpoint, data volume and survey time are reduced by increasing the station interval. From a data interpretation standpoint, adhering to the Nyquist sampling interval is very important. There is also nothing to be gained by spatial oversampling. The sampling interval is extremely important as this example indicates and should be carefully weighed in the survey design process.

The visual aspect of data to the human eye is also an important factor. Data which are adequately simple may appear slightly blocky. Suitable interpolation in the data display program can remedy this effect.

7.2.5 SELECTING ANTENNA SEPARATION

Most GPR systems employ separate antennas for transmitting and receiving (commonly referred to as bistatic operation) although the antennas may be housed in a single module with no means of varying the antenna separation. The ability to vary the antenna spacing can be a powerful aid in optimizing the system for specific types of target detection.

To maximize target coupling, antennas should be spaced such that the refraction focussing peak in the transmitter and receiver antenna patterns point to the common depth to be investigated. Since the antenna pattern peaks at the critical angle of the air-earth interface as illustrated in Figure 7-16, (Annan, 1973, Annan et al, 1975 Smith, 1984). An estimate of optimum antenna separation is given by the expression

$$S = \frac{2 \text{ Depth}}{\sqrt{K - 1}} \quad (7-11)$$

Increasing the antenna separation also increases the reflectivity of flat lying planar targets which can sometimes be advantageous.

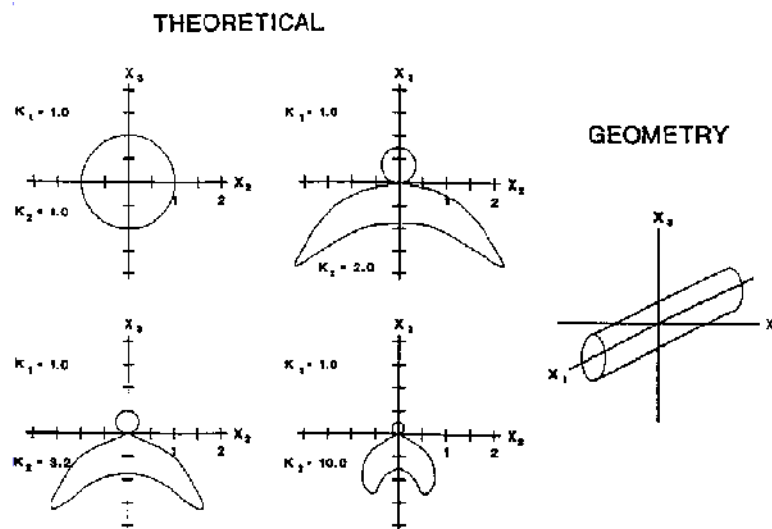


Figure: 7-16 Variation in antenna pattern as relative permittivity of the ground changes. (Upper medium is air).

A very practical reason for increasing antenna separation is receiver dynamic range. The direct transmitter to receiver signal can be very large if the antenna separation is small. While electronic circuits may handle the overload safely, there is distortion and recovery time which make detection of shallow events impossible (transmit pulse blanking is the term commonly used). As minimum separation of a half-wavelength at the centre frequency is recommended.

A factor which should be considered when working in lossy ground is the effect of path length increase created by separating antennas. The path length is

$$L = (S^2 + 4\text{Depth}^2)^{\frac{1}{2}} \quad (7-12)$$

In lossy ground, return signals are attenuated by a factor

$$e^{-\alpha L} \quad (7-13)$$

One should not make S so large that L becomes a great deal larger than 2 x Depth in high loss conditions.

If little is known about the survey area, a safe rule-of-thumb is set S equal to 20% of the target depth. In practice, a small antenna spacing is often used because operational logistics usually demand simplicity of operation. Depth resolution of targets decreases as antenna separation increases although this factor is small until S approaches the target depth.

7.2.6 SURVEY GRID AND COORDINATE SYSTEM

An important aspect of survey design is establishment of a survey grid and coordinate system. The use of a standardized coordinate system for position recording is very important; the best data in the world are useless if no one knows where they came from.

Generally, survey lines are established which run perpendicular to the trend of the features under investigation in order to reduce the number of survey lines. Line spacing is dictated by the degree of target variation in the trend direction. If isolated small targets are sought, the line spacing should be less than the radar footprint illustrated in Figure 7-17.

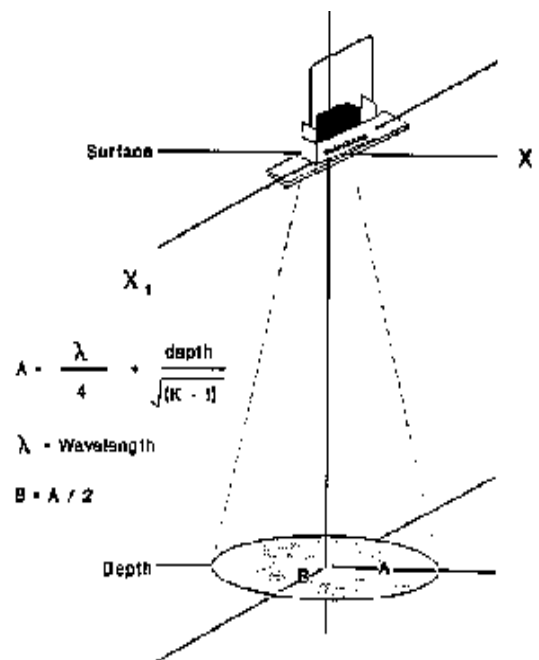


Figure: 7-17 Simplified GPR footprint concept where shaded zone depicts area illuminated at depth. (Annan and Cosway, 1992).

The selection of survey line location and orientation should be made such as to maximize target detection. All survey lines should be oriented perpendicular to the strike of the target if the target has a preferred strike direction. In attempting to cover an area to map a feature such as bedrock depth, the survey lines should be oriented perpendicular to the bedrock relief and line spacing should be selected to adequately sample along-strike variations without aliasing. In situations where strike is known and the structure 2-dimensional, a very large spacing between lines can be employed. If there is no two dimensionality to the structure, then line spacing must be the same as the station spacing to assure that the ground response is not aliased. Needless to say, when Δx is a fraction of a meter, a tremendous amount of data have to be collected to fully define a 3-dimensional structure.

7.2.7 SELECTING ANTENNA ORIENTATION

The last factor and seldom discussed factor to be considered is the antenna orientation. In general, the antennas used for GPR are dipolar and radiate with a preferred polarity. The antennas are normally oriented so that the electric field is polarized parallel to the long axis or strike direction of the target. There is no optimal orientation for an equi-dimensional target. In some instances, it may be advisable to collect two data sets with orthogonal antenna orientations in order to extract target information based on coupling angle. If the antenna system is one which attempts to use a circularly polarized signal, the antenna orientation becomes irrelevant. Since most commercial systems employ polarized antennas, orientation can be important. The various arrangements of antenna deployment are illustrated in Figure 7-18. The most commonly used is the one designated 'PR-BD'.

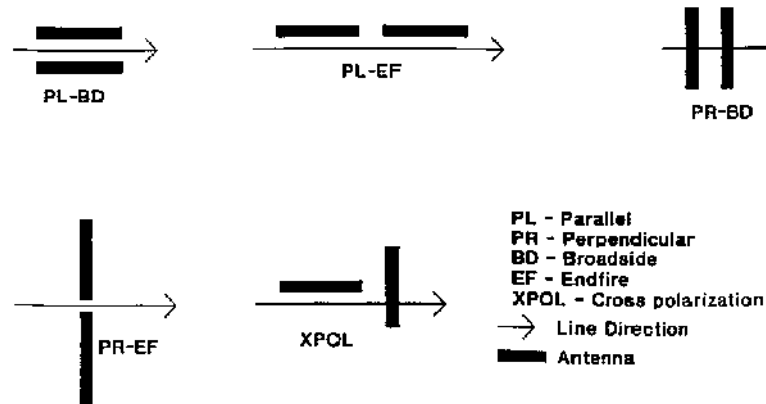


Figure: 7-18 Illustration of the various modes for antenna deployment. (E field assumed aligned along the antenna axis)

Antenna orientation affects the subsurface footprint size. As the simplified beam pattern (see Figure 7-17) indicates, the simple dipole antenna has a broader footprint in the "broad side" direction than in the "endfire direction". The field example shown in Figure 7-19 graphically illustrates the difference in pattern widths. For this reason, the 'PR-BD' survey configuration tends to give a radar section which is more of a 2D slice through the subsurface and is not subject to a large amount of "side swipe" clutter from objects off line.

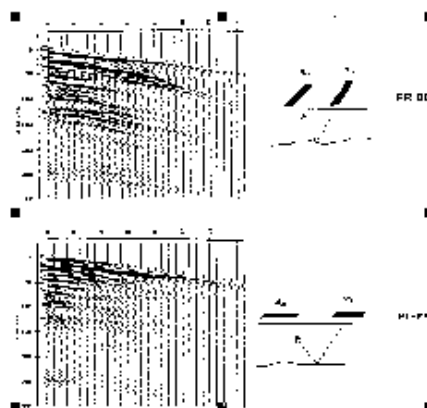


Figure: 7-19 CMP sounding data acquired with 2 modes of antenna polarization.

For surveys where interpretation of data in a quantitative manner is important, this result is beneficial. In search and detect surveys, a broader search swath obtained by the 'PL-PD' and 'PL-EF' may be more desirable.

7.3 CMP/WARR VELOCITY SOUNDING DESIGN

The CMP (common mid-point) and WARR (wide angle reflection and refraction) sounding modes of operation are the electromagnetic equivalent to seismic refraction and wide angle reflection. CMP/WARR soundings are used to obtain an estimate of the radar signal velocity versus depth in the ground by varying the antenna spacing at a fixed location and measuring the change of the two-way travel time to the reflections as illustrated in Figure 7-20 and Figure 7-21.

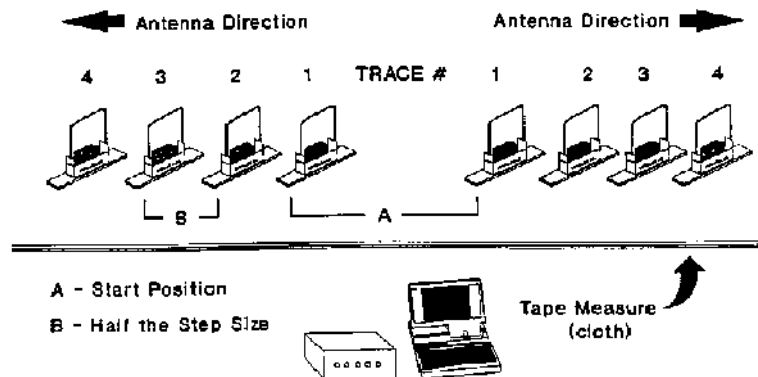


Figure: 7-20 Procedure for conducting a CMP velocity sounding.

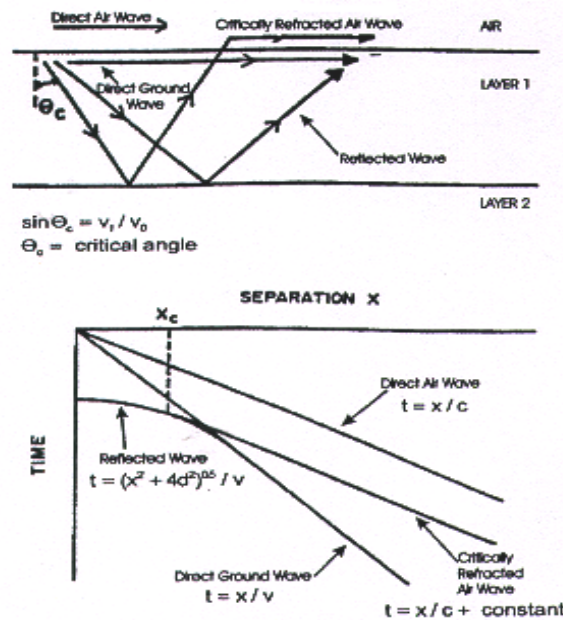


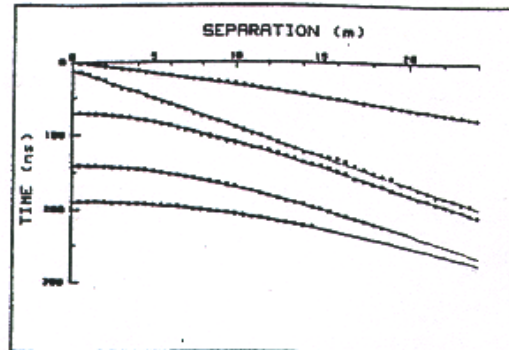
Figure: 7-21 Illustration of CMP sounding ray paths and idealized event arrival-time versus antenna separation and display.

In the CMP sounding, both the antennas are moved apart about a fixed location. In a WARR sounding, one antenna is held fixed while the other is moved away. In early GPR systems utilizing metallic cables, the WARR approach of sounding was preferred because cable handling was a major concern in obtaining data free of system artifacts. With modern systems such as those employing fibre optics cables, the CMP approach is the standard mode of operation since the reflected signal is more likely to come from a fixed spatial location rather than moving about on the surface of a reflector as occurs with a WARR sounding.

Optimal CMP/WARR soundings are obtained when the electric fields of the antennas are parallel and the antennas are moved apart along a line which is perpendicular to the electric field polarization (the 'PR-BD' configuration in Figure 7-18). This configuration gives the widest angular coverage of a subsurface reflector. In addition, close coupling of the antennas to the ground should be maintained in order to maximize reflection energy detectable at angles beyond the critical angle of the air-earth interface.

The procedure for a CMP/WARR sounding is simple. A reflector is normally identified from a reflection section. A point on the ground surface is selected which is over the reflector. Antennas are then positioned over the target point with minimal separation. The initial spacing is usually nx , the Nyquist station interval selected for reflection profiling. Data are then acquired at antenna separations which increase as integer multiples of nx . If the CMP mode is used, both antennas are moved out from the centre point in steps of $nx/2$. If WARR mode is used, one antenna is moved out in step intervals of nx . The maximum separation in a CMP/WARR sounding is usually 1 to 2 times the reflector depth. If the ground attenuation is high, the signals may die out before the maximum separation is reached.

The reflection arrival times should have a hyperbolic dependence (to first order) on antenna separation. Example data sets are shown in Figure 7-19 for both the PR-BD and PL-EF antenna configurations. Analysis of the move out hyperbola of time versus separation permits estimation of propagation velocity and target depth. The basic interpretation procedure is "T2 - X2" analysis commonly used in early seismic reflection interpretations. In simple terms, a plot of travel time squared versus antenna separation squared yields a straight line relationship whose slope gives a velocity estimate and whose time intercept yields a depth estimate (see Figure 7-22). Computerized schemes of varying degrees of complexity are now commonly used to do this type of analysis such as the velocity stack shown in Figure 7-23.



Event	Intercept	Velocity	K	Depth
Airwave	+0.00	.305	1.000	
Groundwave	+12.46	.130	6.357	
Reflector 1	+72.23	.122	6.067	4.399
Reflector 2	+141.41	.107	7.914	7.540
Reflector 3	+189.49	.120	6.239	11.300

Event	Layer Velocity	K	Thickness
Layer 1	.122	6.07	4.4
Layer 2	.0906	11	3.14
Layer 3	.16	3.52	3.84

Figure: 7-22 T2-X2 analysis of CMP/WARR sounding.

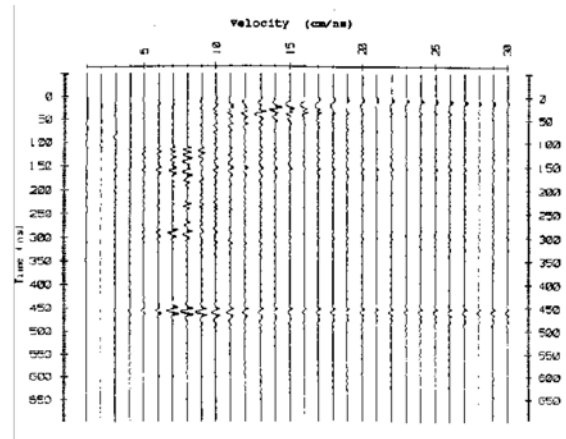


Figure: 7-23 Example of moveout velocity stacking of a PR-BD data set.

CMP/WARR soundings provide a measure of signal attenuation in the ground although to date the estimation is more qualitative than quantitative. In addition, at sites with a large amount of surface clutter, CMP/WARR soundings can aid in separating above and below ground reflections.

While not discussed in detail here, one can also conduct multifold GPR reflection surveys. By measuring reflection data at a multiplicity of offsets along a line, CMP data is available at each station and a full velocity section can be derived. These type of data are very important when large velocity variations occur and migration processing is to be used to reconstruct more representative depth sections from GPR data. Papers by Fisher et al (1992 a & b) and Grieves (1998) illustrate these concepts.

7.4 3D SURVEY DESIGN

Refer to the Annan et al. paper, **Maximizing 3D GPR Image Resolution: A Simple Approach**, 1997.

7.5 BOREHOLE SURVEY DESIGN

Refer to the Annan et al. paper, **Cross Hole GPR for Engineering and Environmental Applications**, 1997.

8 DATA PROCESSING

Ground penetrating radar (GPR) is now used extensively for a variety of applications in many differing fields. The ubiquitous access to inexpensive computer facilities means that more and more computer processing of GPR data occurs. The objective here is to provide a brief overview of GPR data processing. The very broad nature of the topic makes it impossible to provide a complete discussion. The focus, will be to indicate the steps which should be followed in data processing and to stress the need for the processor (the person not the computer) to remember that there must be a cost benefit at the end of the day.

Processors (the people not the computers) can exploit many of the developments of seismic data analysis which have evolved to a very high level. Numerous commercial software packages are available which allow almost any imaginable data manipulation. For anyone contemplating use of seismic processing on GPR data, the excellent text by Yilmaz (1987) should be considered essential reading. While all seismic processing can not be applied to GPR data, the vast majority can be used directly as evidenced by Fisher et al (1992a), Maijala (1992), and Rees & Glover (1992).

GPR data are most often treated as a scalar quantity while the electromagnetic fields which are the basis of the method are vector quantities. Extensive use of GPR where the vector nature of the field has been exploited are few but growing. For processors with a seismic background, GPR data are more analogous to shear wave than compressional wave data.

The processing flow for GPR data is depicted in Figure 8-1. The initial stage of operations is the acquisition of data and this is normally accompanied by real-time display. In many applications the real-time display is used for on-site interpretation and may indeed be the end point for the radar survey. Frequently data are now recorded and are available for post-acquisition processing and re-display. The highlighted zone in Figure 8-1 is the topic of this paper. The areas of data processing have been grouped under the headings: data editing, basic processing, advanced processing, and visualization/interpretation processing. Processing is usually an iterative activity. A data set will flow through the processing loop several times with the data changes visually monitored by the processor (i.e. the person). Straight through batch processing may be applied on large data sets after iterative testing on selected data samples.

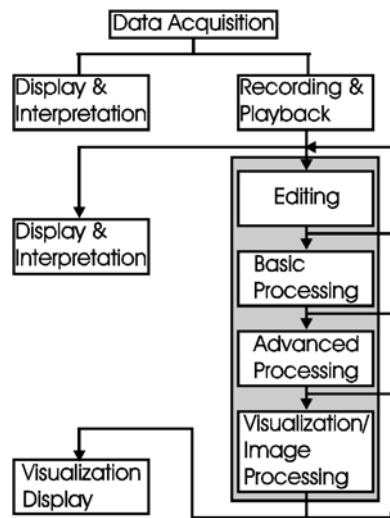


Figure: 8-1 A general overview of GPR data flow.

The data processing subdivisions indicated are meant to reflect that the data manipulation becomes more and more processor (i.e. the person) dependent and hence more subjective because a particular end result is sought. The following discussion is biased toward single fold, common offset, reflection profiling data processing owing to the fact that the majority of GPR data is of this type.

The issue of data display, hard copy and visualization while somewhat beyond the scope of data processing is an inherent factor in data processing. Raw information, which is normally an amplitude versus time signal with several decades of dynamic range, must be manipulated for the display devices which have about one decade of dynamic range. Since so many formats such as color mapping, grey scale mapping and line graphs are available, it is difficult to totally divorce processing from presentation considerations.

8.1 DATA EDITING

Once data are recorded, the first step in processing is data editing. Field acquisition is seldom so routine that no errors, omissions or data redundancy occur. Data editing encompasses issues such as data re-organization, data file merging, data header or background information updates, repositioning and inclusion of elevation information with the data.

While this may sound like a trivial exercise, it is often the most time consuming one for a production survey. Large volumes of information have to be systematically maintained so that further processing can be done without having to constantly account for idiosyncrasies of acquisition. In many instances background information on acquisition is used in the processing stages. For instance, the centre frequency of the acquisition system antennas is a very important factor in processing. The temporal and spatial sampling interval are also important in most advanced processing steps. Data recorded on equal spatial and temporal time intervals are virtually mandatory for most of the advanced processing methods. As a result, data editing is essential before further processing in many situations.

Figure 8-2 illustrates some of the many activities involved with data editing. The upper portion of the figure shows a typical file header which contains initial survey information including the number of traces in the file, the start and end position, the frequency of acquisition, as well as the processing history. The lower section shows a final raw data plot. In this case polarity, statics and topography corrections have been applied, three files have been merged and all this information is annotated properly for future reference. A basic time gain has been applied to make the display.

```

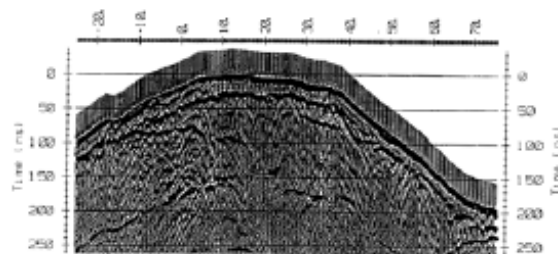
Barrrow 1
Rathcroghan Mound Radar Survey. Co Roscommon.
Base line from -37' at +.25M station interval.
20/05/93
NUMBER OF TRACES = 499
NUMBER OF PTS/TRC = 375
TIMESGRO AT POINT = 47
TOTAL TIME WINDOW = 500
STARTING POSITION = -37.000000
FINAL POSITION = 87.500000
STEP SIZE USED = 0.250000
POSITION UNITS = metres
NOMINAL FREQUENCY = 50.000000
ANTENNA SEPARATION = 1.000000
PULSER VOLTAGE (V) = 400
NUMBER OF STACKS = 128
SURVEY MODE = Reflection
ELEVATION DATA ENTERED : MAX = 9.192000 MIN = 0.916750
SIGNAL SATURATION CORRECTION APPLIED
THIS FILE A MERGING OF \2 AND c:\gmaud\maeve4.
POLARITY FLIPPED FROM POSITION -37.000000 TO -0.500000
POLARITY FLIPPED FROM POSITION -37.000000 TO -0.500000
POLARITY FLIPPED FROM POSITION -37.000000 TO -0.500000
SOURCE DATA FILE = c:\gmaud\maeve2
FIRST BREAK POINT CORRECTED. THRESHOLD = -10000
FIRST BREAK POINT CORRECTED. THRESHOLD = 5000

PROCESSING SELECTED:
Trace Stacking : 1
Points Stacking : 5
Trace Differencing: N
Gain Type : SEC
Velocity : 0.100 m/ns
Attenuatn: 2.000 dB/m
Amount : 500 Maximum
Selection : Time = all
Trace = 50 to 450

PLOT LAYOUT PARAMETERS:
Trace Spacing : 0.013"
Trace Width : 0.050"
Trace position : 1.000" to 3.500"
Left/Right Margin : 0.000" / 0.000"
Border Size : 0.500"
Page Length/Width : 10.000" / 7.500"
Printer Name : HP LaserJet II 300dpi

```

(a)



(b)

Figure: 8-2 a) Example of data processing documentation, b) example data set from an archaeological investigation whose history is described in 7.2. The data were assembled from three data sets and have had tomography, polarity and static correction applied. An SEC time gain is applied in the plotting.

To date, multifold GPR data acquisition is not done extensively. If it becomes more common, this step of processing is the one where re-organization and sorting of multifold coverage data would be handled. The steps are essentially the same as with multifold seismic data (Fisher et al, 1992a).

8.2 BASIC PROCESSING

Basic data processing addresses some of the fundamental manipulations applied to data to make a more acceptable product for initial interpretation and data evaluation. In most instances this type of processing is already applied in real-time to generate the real-time display. The advantage of post survey processing is that the basic processing can be done more systematically and non-causal operators to remove or enhance certain features can be applied.

8.2.1 DEWOW

The initial basic processing step is usually temporal filtering to remove very low frequency components from the data. This step is frequently referred to as 'de-wowing' the data. Very low frequency components of the data are associated with either inductive phenomena or possible instrumentation dynamic range limitations. This process has historically been done using analog filters in hardware but with the advent of true digital acquisition this has also become a data processing issue (Gerlitz et al, 1993).

8.2.2 TIME GAIN

The next step of basic processing is usually to select a time gain for the data set. Time gain has historically been very subjective and also very much display device dependent.

Radar signals are very rapidly attenuated as they propagate into the ground. Signals from great depth are very small and display of this information at the same time as signals from a shallower depths is difficult. When the amplitude of display is optimal for shallow depth signals, events from greater depths may be invisible or indiscernible. Equalizing amplitudes by applying some sort of time dependent gain function compensates for the rapid fall off in radar signals from deeper depths. This is referred to as "time gain".

Figure 8-3 indicates the general nature of the amplitude of radar signals versus time. On the left there is a idealized earth which has horizons at equal depth intervals which all have the same reflectivity. On the right is an idealized depiction of the amplitude of the returns from each horizon as a function of time.

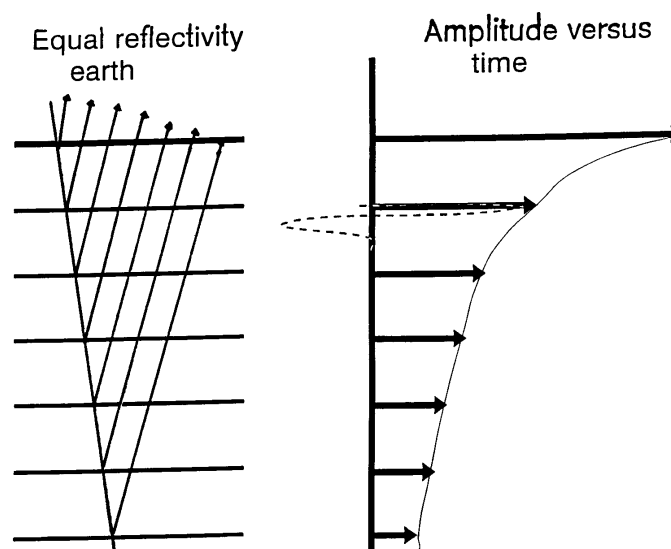


Figure: 8-3 Layered earth model of equal reflectivity horizons and impulse response with envelope of reflection amplitude depicted.

A major problem with GPR data is that the attenuation in the ground can be highly variable. One can have a low attenuation environment where exploration depths of 10's of meters can be readily achieved. In other situations attenuation can be quite high and depths of only 1 to 2 meters can be penetrated. The behavior of the radar record versus time is depicted in Figure 8-4 for the low and high attenuation extremes.

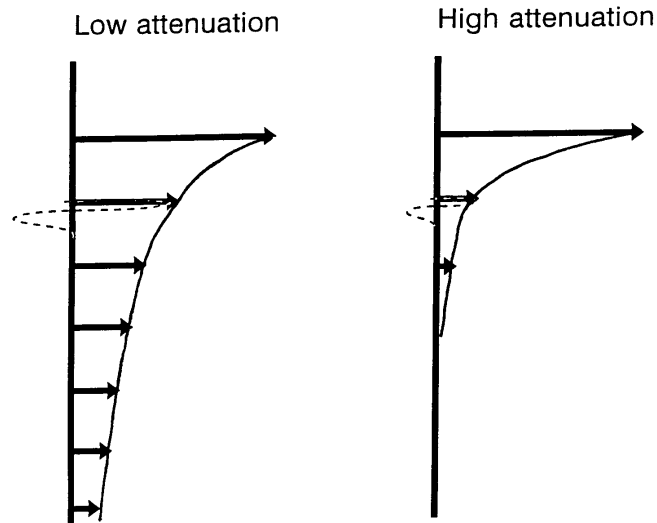


Figure: 8-4 Equal reflectivity layered earth response in lower and higher attenuation media.

A simplified way of viewing the amplitude of the signals versus time is shown in Figure 8-5. A spherical wave spreading into the ground will fall off inversely as the distance of the waveform into the ground and will also die out exponential depending on the conductivity losses in the material. Assuming a constant velocity earth it is possible to transform depth into time and hence derive an amplitude of the signal versus time for the spherical wave reflecting from the simplified equal amplitude reflection layered earth.

AMPLITUDE VERSUS DEPTH

$$A(d) = A_0 \exp(-2ad) / 2d$$

AMPLITUDE VERSUS TIME

$$A(t) = A_0 \exp(-avt) / (vt)$$

a = attenuation
v = velocity

d = depth
t = time

Figure: 8-5 Concept of translation amplitude fall of versus depth to fall off versus time.

The concept of time varying gain is simple. One applies a gain to the data which increases in time after the transmit pulse. The rise of the gain function is tailored to accommodate the drop off and signal amplitude versus time. The concept is depicted in Figure 8-6.

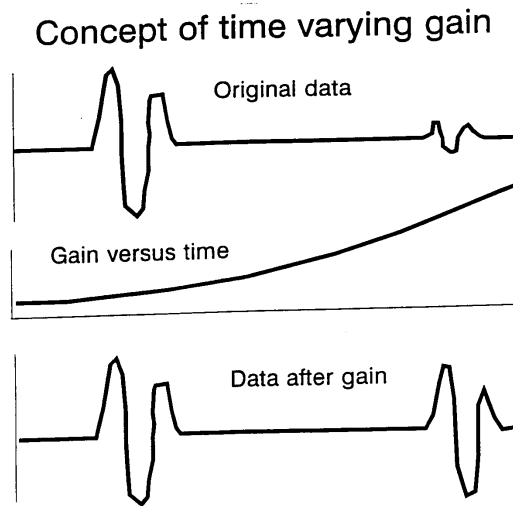


Figure: 8-6 Concept of time varying gain where signal amplification varies with time.

In order to put the variation in amplitude versus time into perspective, the average amplitude on a radar section was computed. The amplitude versus time is shown in Figure 8-7. It can be seen that the signal drops several orders of magnitude from time zero out to a time of about 300 or 400 ns at which point the signals drop back down to the noise level. An indication of the noise levels can be estimated from the data before time zero on the plot. In this case the noise level is about 10 to 15 microvolts.

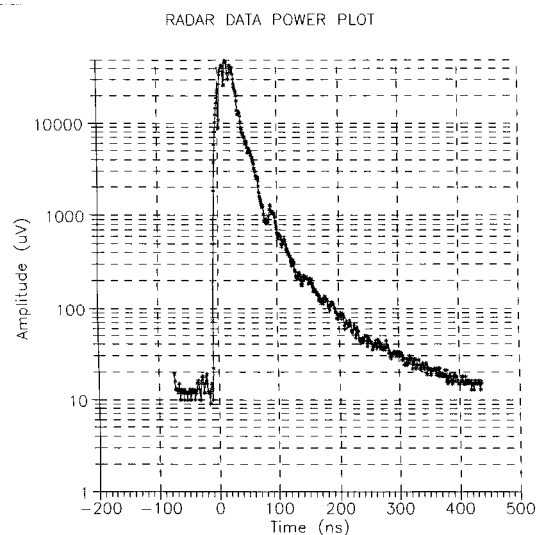


Figure: 8-7 Composition display of radar signal versus delay time for a radar section.

Systematic ways of selecting gain are available. Generally the first step in selecting gain is to examine the amplitude versus time fall-off of the data. This can be done trace by trace or on a section basis. Generally, working on a section is the most useful way of approaching the problem but again there are degrees of variability in this. Figure 8-8 7.8 shows an average amplitude versus time plot for high pass (dewow) filtered but otherwise raw data set shown in Figure 8-2. The key point to note is that the radar signal amplitude falls off with time in a fairly systematic fashion. If one wants to display these data on a display device with a dynamic range of 20 dB (i.e., a factor of 10 between the smallest and largest signal) then the 60 dB dynamic range of the real signal has to be compressed into a dynamic range of 20 dB of the display device. Figure 8-9 shows the average signal amplitude versus time after the time gain used for

the plot in Figure 8-2 has been applied.

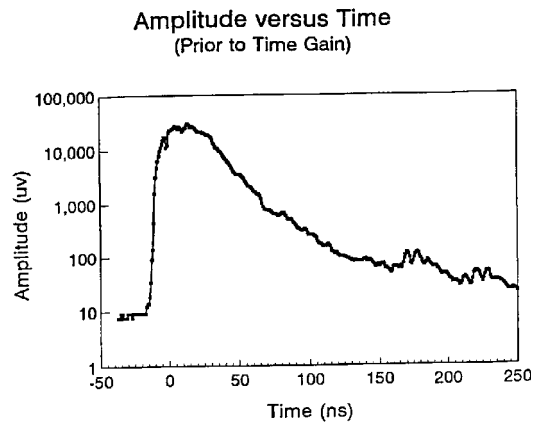


Figure: 8-8 The average amplitude of the radar signal versus time for the data set presented in Figure 8-3 prior to time gain.

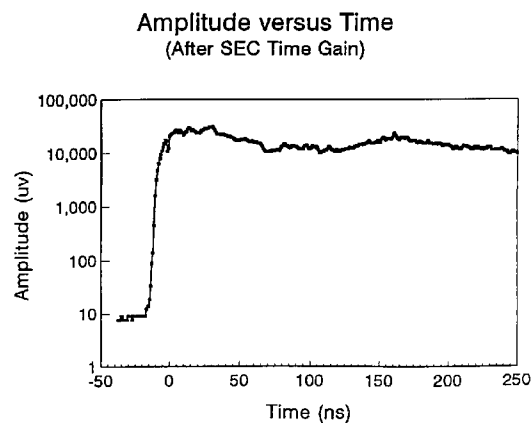


Figure: 8-9 The average signal amplitude of the radar signal versus time for the data set presented in Figure 8-2b after the application of an SEC time gain.

There are a variety of ways of applying gain to radar data. The issue is whether or not one wants to maintain some sort of amplitude fidelity or whether one only wants to display all of the signals in the data. For stratigraphic horizon continuity sometimes showing all the information irrespective of amplitude fidelity is important. In this case a continuously adaptive gain such as AGC (automatic gain control) is used. With AGC gain, each data trace is processed such that the average signal is computed over a time window and then the data point at the centre of the window is amplified (or attenuated) by the ratio of the desired output value to the average signal amplitude.

Physical phenomenon based systematic gains, such as spherical and exponential compensation (SEC) gain, attempt to emulate the variation of signal amplitude as it propagates in the ground. The data displayed in Figure 8-2 have had an SEC gain applied and comparing Figure 8-8 and Figure 8-9 shows the degree to which the time gain has compressed the signal dynamic range.

Examples of SEC and AGC gain on a short set of radar traces are shown in Figure 8-10 and Figure 8-11. These are practical gain implementations which limit the maximum amount of gain that can be applied.

A variety of other gains can be applied. Gain should be selected based on some a priori physical model, not at the user whim. The objective should be to modify the data while retaining its full utility without introducing artifacts.

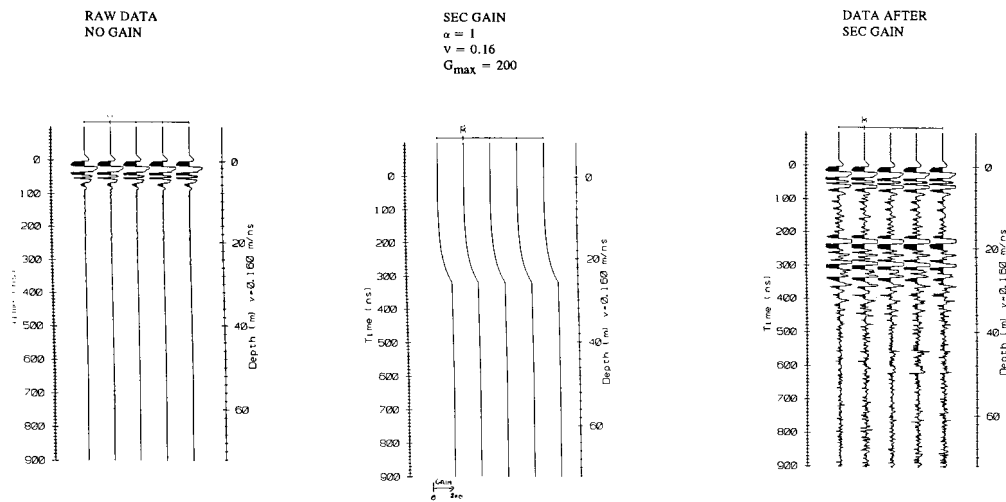


Figure: 8-10 Illustration of raw data traces, the spherical and exponential compensation (SEC) gain versus time and the resulting gained traces.

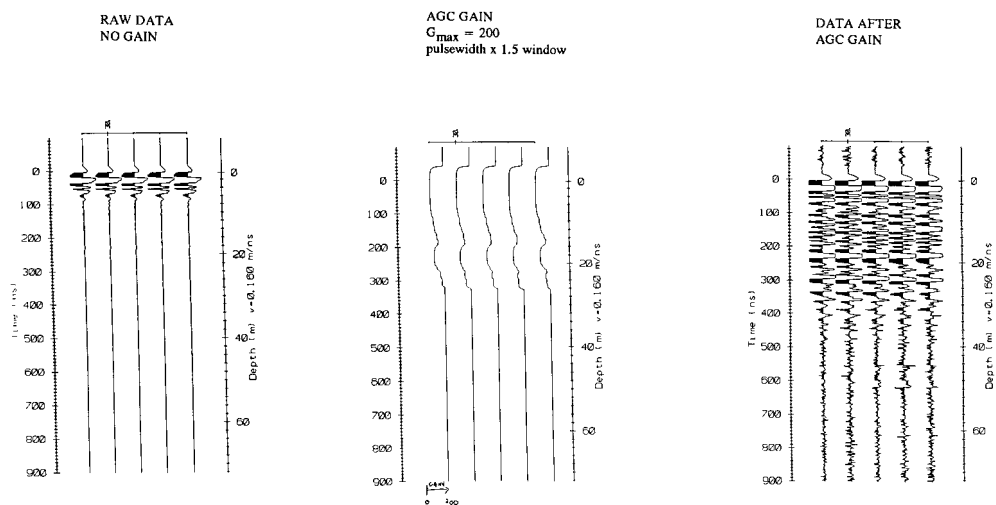


Figure: 8-11 Illustration of raw data traces, the automatic gain compensation (AGC) gain versus time and the resulting gained traces.

8.2.3 TEMPORAL AND SPATIAL FILTERING

Temporal and spatial filtering are often the next stage of basic processing. Filtering can be applied before or after time gain as long as the effect of the gain is understood since time gain is a non-linear process. Temporal filtering means filtering along the time axis of the data set. A whole host of different types of temporal filtering may be applied from bandpass filtering using fast Fourier transforms (FFT) through to various types of linear and non-linear time domain convolution filter operators. Figure 8-12 shows the amplitude spectra for the data set shown in Figure 8-2 before and after an SEC gain function has been applied. Note the change in spectra induced by the time gain which is a non-linear operator. In both cases the average amplitude spectrum for the whole section has been generated. From the spectra it can be seen that the majority of the energy is limited to a finite bandwidth and appropriate use of band limiting filtering may improve signal-to-noise without significantly altering the data. A low pass filter with an 50 MHz corner using an FFT approach generates the section shown in Figure 8-13a while Figure 8-13b shows the result of a 80 to 120 MHz bandpass filter.

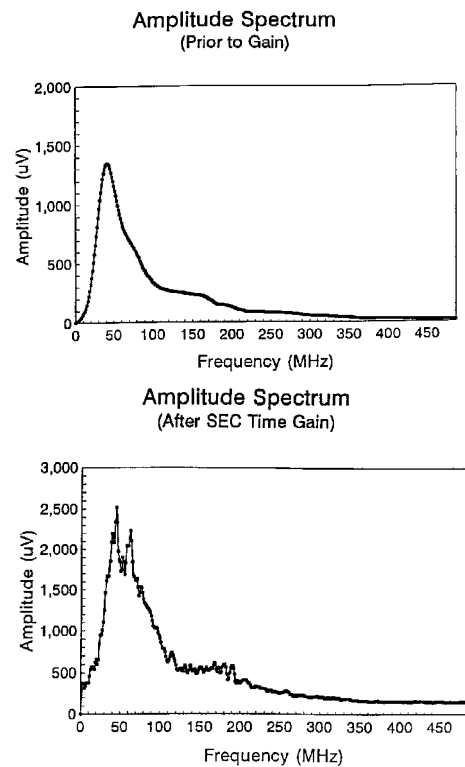


Figure: 8-12 a) Average time amplitude spectrum shown in Figure 8-3 prior to time gain. b) Average amplitude spectrum for data shown in Figure 8-3 after application of an SEC time gain.

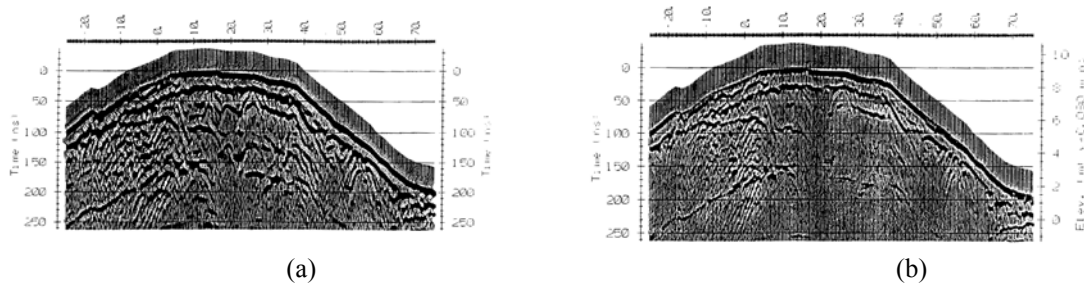
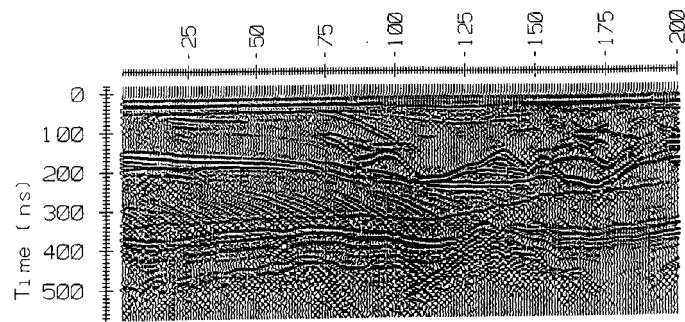
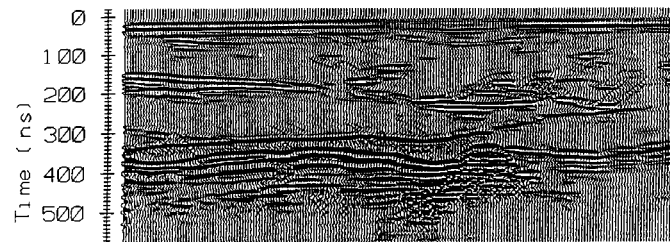


Figure: 8-13 a) Data set shown in Figure 8-2b after low pass zero phase FFT filter with a cosine taper between 50 MHz and 100 MHz. b) Data set shown in Figure 8-3 after 80 to 120 MHz bandpass zero phase FFT filter.

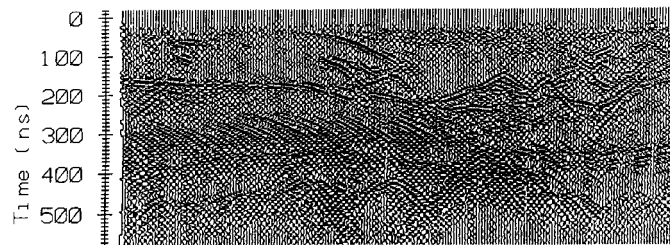
Similar filtering operations can be applied in the spatial domain. The 3 radar sections shown in Figure 8-14 present the original radar section plus an example of high pass and low pass spatial filtering. The high pass spatial filter retains dipping events and suppresses flat lying events. The low pass filter has the opposite effect in that it enhances flat lying events and suppresses dipping responses.



(a)



(b)



(c)

Figure: 8-14 a) Example of time gained data in fluvial sand environment. b) Illustration of spatial low pass filtering as applied to data shown in a. Note enhancement of flat lying reflectors. c) Illustration of high pass filter applied to data shown in b. Note enhancement of dipping events and diffraction details.

Median and alpha mean trim filters offer powerful data "clean-up" filters for noise spikes. These filters can be applied in both the time or space domain. These filters may be applied before and after time gain but are usually most useful if applied before time gain and any type of data adaptive filtering. An example of spike removal from a data set using a 3-point temporal filter followed by trace spatial median filter is illustrated by the before and after sections in Figure 8-15.

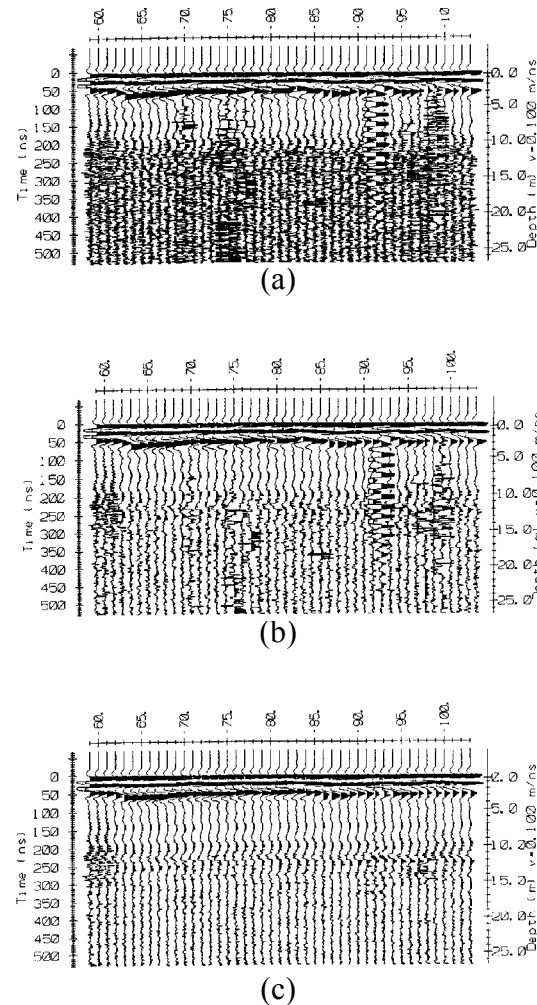


Figure: 8-15 a) An original data set with a large amount of spurious localized noise events. b) The data shown in a) after a 3-point temporal median filter. c) The data set shown in Figure 8-15b after a 3-point spatial median filter.

8.2.4 DISCUSSION

The examples cited in this discussion are by no means exhaustive and a wide variety of simple data manipulations are available to enhance basic aspects of GPR data. As evident from the preceding, the order in which these processes are applied can also be varied producing different results because of the non-linear nature of some steps. As indicated earlier, the bias in this discussion is to single fold reflection data.

Basic data processing should leave the data sets reasonably intact. In other words, the processing should not be such that it radically distorts the information from that which was collected. Again the degree of distortion is subjective and obviously excessive bandpass filtering can drastically alter a data set as evidenced by the spatial high and low pass filtering shown in Figure 8-14. Normally minor changes to the overall data set occur if simple basic processing steps are applied intelligently.

8.3 ADVANCED DATA PROCESSING

Advanced data processing addresses the types of processing which require a certain amount of operator bias to be applied and which will result in data which are significantly different from the raw information which were input to the processing. Such processes include well-known seismic processing operations such as trace attribute analysis, FK

filtering, selective muting, normal move out correction, dip filtering, deconvolution, and velocity semblance analysis as well as more GPR specific operations such as background removal, multiple frequency antenna mixing and polarization mixing (Tillard & Dubois, 1992).

8.3.1 ATTRIBUTES

Dealing with all these topics is impossible in the space available in this paper but two examples will be provided. One topic of interest is the use trace attribute analysis common in seismic processing (White, 1991). In this case a time series is decomposed using Hilbert transform and minimum phase assumptions into a real and imaginary time series from which the envelope and the frequency can be estimated at every point along the trace. Figure 8-16 shows the envelope of the data set originally shown in Figure 8-2a. Figure 8-17 shows the instantaneous frequency computed for the same data set.

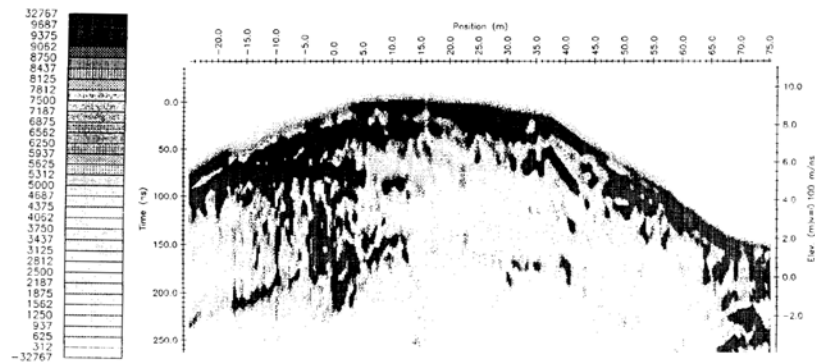


Figure: 8-16 The amplitude envelope for data shown in Figure 8-2b. The envelope more accurately reflects the GPR resolution.

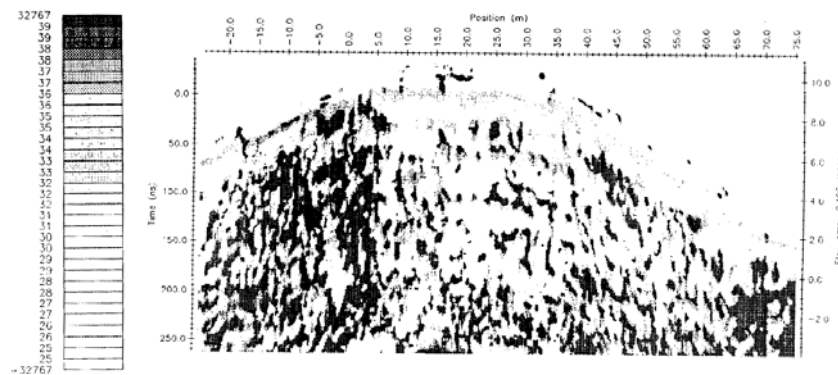


Figure: 8-17 The instantaneous frequency for the data shown in Figure 8-2b. The instantaneous frequency tends to reflect the spatial scale of the radar targets.

The benefit of the envelope display is that it reflects the resolution of the data. One tends to get a false sense of resolution because of the oscillatory nature of the radar pulse. In fact the bandwidth or envelope of the pulse is what determines resolution not the time between zero crossings (which reflects the dominant frequency in the data). For this reason the envelope is extremely useful for generating more simple presentations which are representative of the data spatial resolution.

The instantaneous frequency can be a good indicator of certain types of features which selectively respond to the spectrum of the incident signal. An example of this is a thin layer in a stratigraphic sequence. If the layer is close to the thickness where the pulse spectrum is at the tuning frequency of the layer then an enhancement in the response of

that particular frequency will occur. Instantaneous frequency gives a rough feel for the texture on spatial scale of the GPR signal scattering sources.

8.3.2 DECONVOLUTION

Examples of deconvolution and other types of filtering are given by Todoeschuck (1990) and Turner (1992). It is important to note that deconvolution ("decon") of GPR data is not straight forward and has seldom yielded a great deal of benefit. Part of the reason for this is that the radar pulse is often as short and compressed as can be achieved for the given bandwidth and signal-to-noise conditions. Another important factor is that some of the more standard deconvolution procedures have underlying assumptions required for wavelet estimation such as minimum phase and stationarity which are not always appropriate for GPR data. The rapid decrease in GPR signal amplitude means that decon artifacts may mask weaker deeper events if time gain is not applied before decon and the non-linear nature of time gain may substantially alter wavelet character if gain is applied before decon. As a result decon can be both difficult to apply systematically and exhibit little enhancement in resolution. Instances where deconvolution has proven beneficial occurred when extraneous reverberation or possibly system reverberation have been involved. Deconvolution can then provide substantial pulse compression benefits.

8.3.3 BACKGROUND SUBTRACTION

One of the most common operations specifically applied to GPR data is the use of background removal. Most often this takes the form of a high pass filter or an average trace removal. More sophisticated approaches which yield similar results are orthogonal trace decomposition (Friere & Ulrych, 1988).

Average trace removal is a form of spatial filtering. In some situations where transmitter reverberation and time synchronous system artifacts appear it is very effective in allowing subtle weaker signals which are lost to become visible in a processed section. Figure 8-18 illustrates this concept with before and after sections where average trace removal has been applied. In this case, the target is shallow and the ground response is masked by the transmit pulse.

This type of processing is often necessary, but should not be used routinely. If data always exhibit the need for this processing serious equipment flaws are present in acquisition.

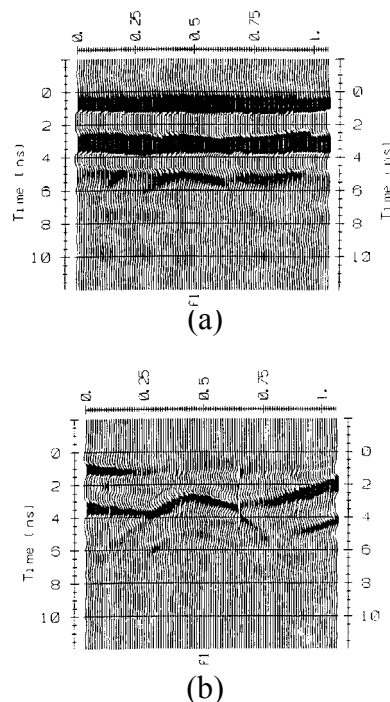


Figure: 8-18 a) Example of initial data set over a buried pipe. b) Data set shown in a) after the average trace for the whole section has been subtracted. The hyperbolic response is clearly visible as are the gently sloping edges of the excavation.

8.3.4 VELOCITY ANALYSIS FROM CMP

Another radar data processing is to analyze velocity sounding data to extract velocity versus depth functions. This can be done by picking events and using T-2 - X-2 analysis or a variety of other methods. Figure 8-19 shows how a CMP data set has been stacked using a move out correction where the constant velocity can be applied. The resultant stacked data shows the velocities which the data add up most coherently.

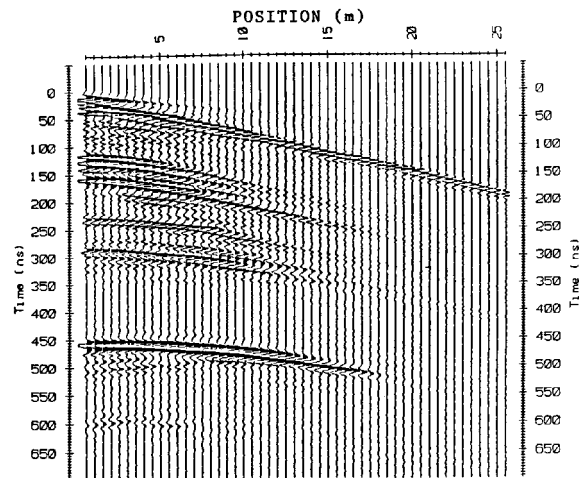


Figure: 8-19 CMP Data.

Much more sophisticated versions of this algorithm are available in many of the seismic processing packages. Quite often they are referred to as semblance analysis routines. Example results are given in Figure 8-20.

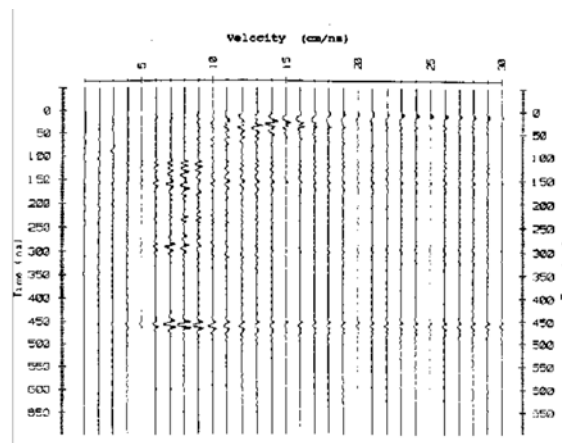


Figure: 8-20 Velocity versus depth.

8.3.5 DISCUSSION

The important feature of advanced processing is that it focuses on making weaker signals visible, enhances specific components of the data for an interpretation requirement, or derives quantitative information such as velocity and attenuation versus depth from the data. The advanced processing methods also have the potential of introducing artifacts in areas where there are no responses in the ground giving rise to specious interpretations. Considerable user insight is required when this type of processing is applied so that undue emphasis is not placed on artifacts induced in the response by the processing.

8.4 VISUAL/INTERPRETATION PROCESSING

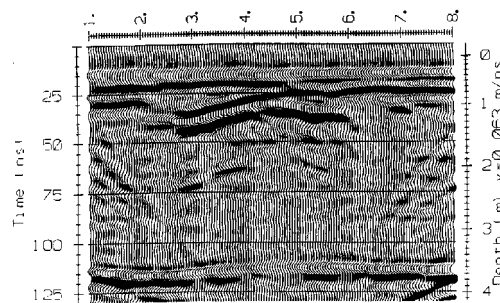
Processing in this context is usually conducted when a good deal of information about a site is available and a need for the processing has been defined which achieves a final objective. Processing in this class will often result in data which are totally changed from the original data set. Furthermore the type of processing is usually subjective in the sense that there is some a priori bias in the processor's mind as to what end product is desired.

processing in this class includes topics such as migration using various types of algorithm, event picking, subjective gain enhancement and amplitude analysis. All of these require completion of the previously mentioned processing steps and availability of corollary control information.

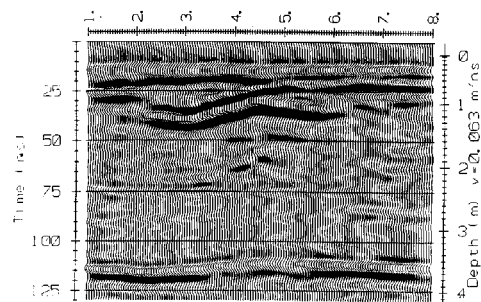
8.4.1 MIGRATION

For example, migration is extremely useful and reconstructs the radar image in a form which is probably a better representation of the ground (Fisher et al, 1992b) Unfortunately migration requires a good knowledge of the velocity structure in the ground and a processor who is aware of the artifacts that migration introduces into the section. As a result it is dangerous in the hands of a novice but powerful in the hands of a processor who has acquired the ability to use it effectively and recognizes the limitations. Migration is often an interactive process as background velocity is adjusted to optimize the migrated result.

Figure 8-21 shows an example of data from a site before and after migration (Brewster, 1993). In this case the migration has been used to remove defractions from vertical sheet pile walls at the edge of the site. These metal sheets were driven down into the soil to act as a containment barrier. The reflections and scattering from these metal walls are visible across most of the cell and tend to mask some of the other features in the data set. Migration very conveniently removes the diffractions by placing these events back in the correct spatial location. While an enhancement is quite visible in the data, it is not easy to assess what distortion, if any, have been generated.



(a)



(b)

Figure: 8-21 a) Example of GPR data from a contaminated DNAPL spill. Note the dipping events which slope down from each end of the section associated with scattering from sheet pile containment walls driven into the ground. b) Data in a) after F-K migration. Note that the wall events have been migrated out of this section. The strong reflection between 2 and 6 m position at times of 25 to 40 ns is the return from a DNAPL pool.

The key to success in the migration process rests in having a good knowledge of the velocity section and quite often with single fold GPR data this information is not available. Migration is then very much at the discretion of the processor rather than controlled by the site conditions. Iterative migration by varying velocity structure to make the most acceptable (to the processor) result is common.

8.4.2 EVENT PICKING

Another way of manipulating data is to pick events and display the reduced event data set. This is a very useful thing because it simplifies the data set and pulls out only those features which are deemed important. The important point to note is the very subjective and application dependent nature of the processing. Figure 8-22 shows the result of picking both amplitudes and arrival time data from a 2D grid of which Figure 8-21 shows one section to create a target depth versus position plot over an area. This information was subsequently used to estimate the volume of a DNAPL contaminant in the ground.

Pool 1 Topography, at 36 hours

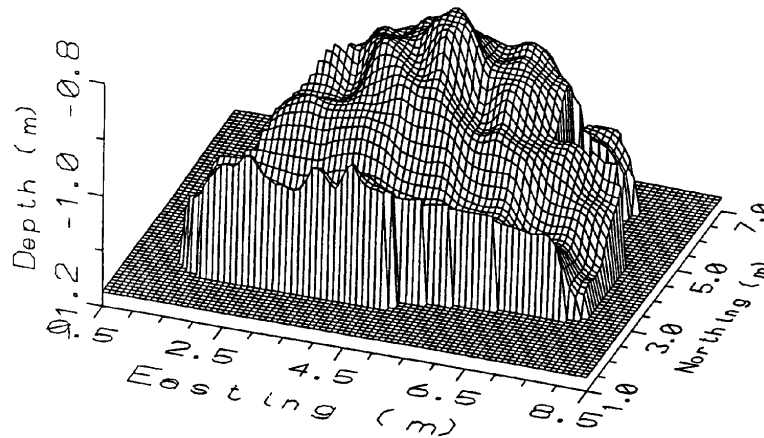


Figure: 8-22 Depth to top of the DNAPL pool shown in Figure 7-21 based on an event picking grid of survey lines. Figure 7-21 shows the radar cross section of 5 east.

Visual/interpretation processing are most useful when one wants to move to 3D visualization of data versus space and time. For example, Figure 8-23 from Brewster (1993) shows a 3D view of DNAPL contamination pools for which data shown in Figure 8-21 and Figure 8-22 were prior stages of processing. While raw data can be displayed this way, most often the essential information is enhanced and the rest of the information suppressed. Frequently the end product is the most easy to present to non-technical users. This is perhaps the most dangerous area of data processing in that the visualization may over simplify the problem and give a false impression of real conditions.

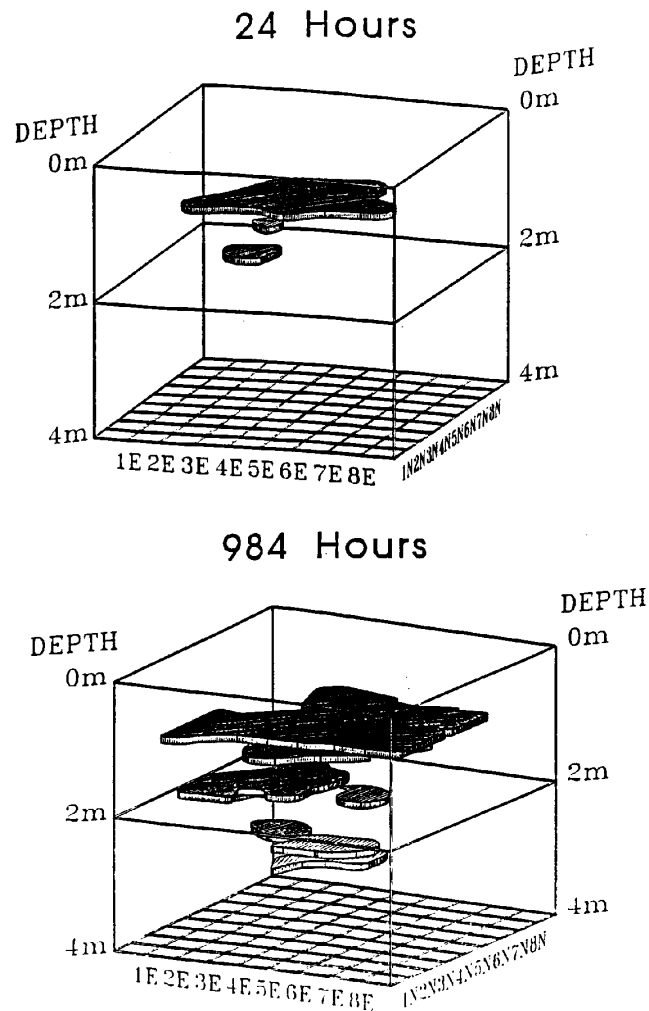


Figure: 8-23 Simplified time and 3D spatial visualization of DNAPL pools based on procedures as illustrated by Figures 7-21 and 7-22.

8.4.3 VOLUME VISUALIZATION

Affordable access to 3D visualization tools and the rapid advance in computer technology are opening these tools to everyday GPR analysis. The degree of preprocessing needed to make these displays effective varies and encompasses all of the topics discussed here and more. The power of collecting reflection survey data in a tight grid and dumping it into 3D display software is enormous. Trends and subtle hard to correlate events become very visible when displays are animated.

In general, these displays lose their impact when printed in hard copy form. To indicate the types of display available a number of examples are given in Figure 8-24; this includes chair cuts, slices and variable capacity.

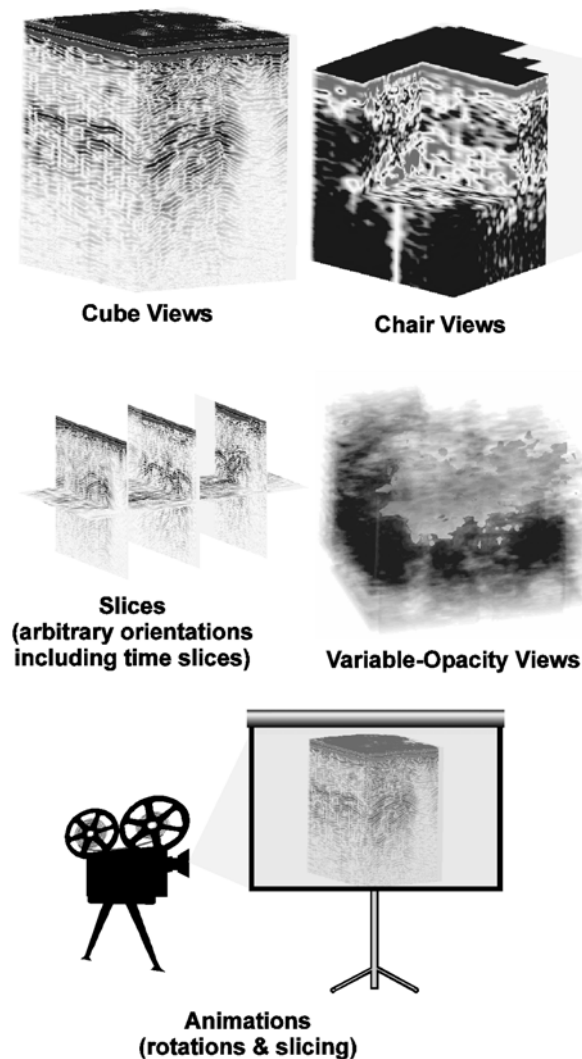


Figure: 8-24

8.5 DISCUSSION

The preceding has provided a brief overview of the steps of data processing which are entailed in GPR analysis. As has been previously stated, the amount of processing can vary from none through to quite sophisticated analysis and manipulation.

As some of the simple processing steps presented here have vividly illustrated, processing can markedly alter the appearance of a data set. As a result it is very important that a processing trail be maintained for audit purposes. Since survey results in engineering and environmental projects may be used as evidence in legal proceedings, it is imperative that the means of creating a processed data set be reproducible. Figure 8-2a illustrates how the historical genesis of a processed data set is maintained in a commercial software package.

All of the processing methods discussed and display methods illustrated can be carried out on readily available personal computers with relatively low cost commercial software. Anyone who wishes to process GPR data can do so with a modest capital outlay.

Perhaps the most important fact that should be kept in mind is that there must be an end objective. For any GPR survey, a value of some sort is always attached to the survey objective. (Otherwise why do it in the first place??) How-

ever this value is defined, one must remember that processing entails time, resources and money. While people do not always recognize it, the biggest single cost is the human time entailed in data manipulation, data organization and thought. Usually this requires a reasonably well trained person whose time is not inexpensive. While computer costs must be considered, man power costs frequently exceed equipment costs.

Figure 8-25 shows a simplified chart of the above concepts. The vertical axis shows a value or a financial cost implication. The horizontal axis shows a measure of time elapsed during processing. As the degree of processing increases, the amount of time and hence costs increase.

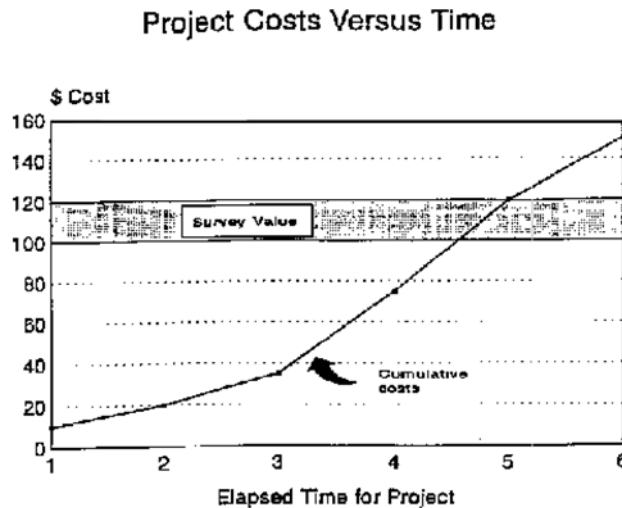


Figure: 8-25 Illustration of how the value of GPR survey is fixed while costs climb as time passes as will ensure if iterative and uncontrolled data processing occur.

It is important that this type of analysis be carried out before one does extensive GPR processing. By taking the survey value and dividing it by cost, one obtains a benefit-to-cost ratio and processing should not be carried on beyond the point where the benefit-to-cost ratio is one as indicated in Figure 8-26.

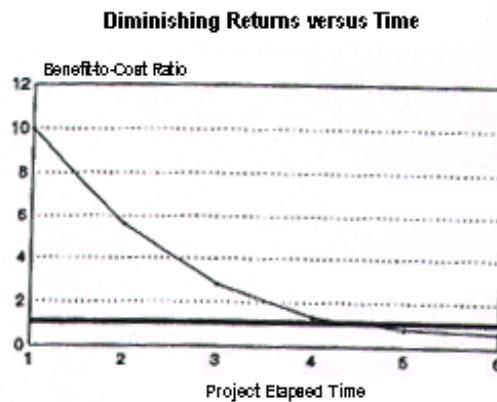


Figure: 8-26 As time and processing increase, the benefit-to-cost ratio decreases. When the ratio approaches unity, the benefit of further processing and analysis becomes dubious.

Unlike some applications of geophysical methods such as petroleum or mineral exploration where quite large financial rewards exist at the end of the successful project, there are smaller and quite often much more poorly defined rewards at the end of engineering and environmental geophysics projects. Since this is the area where GPR finds its use most often, the benefit-to-cost ratio is one which has to be kept in mind and frequently approaches unity early in the data processing scheme.

While research institutions and government agencies with unconstrained man-power and resource availability can carry out much more advanced processing, many commercial applications often have benefit-to-cost ratios such that the processing is terminated at the field acquisition step. In other words, no processing is done!!

8.6 FINAL WORDS

The preceding has been an attempt to provide an overview of the current state-of-practice of ground penetrating radar data processing. While less than an exhaustive treatise, the important points that should be noted are the following:

- a) GPR data processing is within the financial and technical reach of anyone who wishes to process data, not just the few who have extensive high power computing facilities and software development resources.
- b) Many of the vast array of reflection seismic processing techniques can be used directly on GPR data.
- c) GPR data are not totally identical to seismic data and there are GPR specific processing techniques.
- d) An audit trail should be an integral part of any data processing program.
- e) Data processing has to have a cost benefit and, for many GPR projects, processing is cost limited rather than technology or methodology limited.

The processing of GPR data is still truly in its infancy. The flood gates are opening to GPR world wide and there is an explosive growth in GPR awareness. These factors will feed a growth in GPR processing because more and better GPR results will be obtained, advances in processing and presentation will occur, processing costs will decrease and a higher value will be placed on GPR results. The cost benefits of processing will become easier to establish and hence processing will be more readily justifiable and more frequently used.

9 INTERPRETATION, CONCEPTS & PITFALLS

Interpretation is very application dependent and can be very subjective (in that it depends greatly on the individual doing the interpretation). The following are the critical aspects of data interpretation.

1. Have a clear understanding of the survey objective.
2. Develop a conceptual model of the geological setting or application structure.
3. Organize the data into systematic sets which are easily correlated with site maps.
4. Establish an estimate of velocity and attenuation (or depth of exploration achieved).
5. Develop a scenario for the radar response expected based on the initial conceptual model (i.e. a slowly varying continuous event for a major geologic horizon, a spatially limited diffraction hyperbola for a pipe). Use modelling tools if they are available. If possible process data to enhance the type of response expected.
6. Decide if the GPR data are consistent with the model.
7. Correlate radar data with geologic control and ground truth such as drilling, excavation, coring or construction drawings.
8. Create visualizations of the GPR results suitable to the application.
9. Carry out drilling or follow up control work based on GPR inferences.
10. Review data after additional control becomes available and, if necessary, return to step 2 and re-think.

The following are small vignettes addressing specific problems.

9.1 Gradational Interfaces

Many GPR problems require detection of the response of interfaces which are not sharp and clean cut. Natural interfaces are often blurred by the natural depositional sequence involved in the creation of the stratigraphy. Many man-made interfaces can also be indistinct as construction practice may lead to mixing of materials.

The water table example is a classic example of a gradational boundary. The water table has one of the largest property contrasts in nature yet invariably it may not yield a strong radar response, particularly at higher frequencies.

The gradational nature of the water table interface is depicted in Figure 9-1. Water is distributed in a gradational fashion in the pore space due to capillary suction.

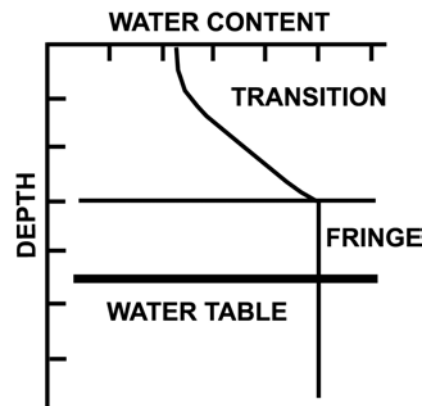


Figure 9-1: Schematic illustration of how water content varies with depth. The change from residual water content to saturation is note sharp but gradual. Transition width depends on soil texture.

Figure 9-2 depicts a simple model of a gradational boundary and a sharp boundary. The transition in the gradational case spans a width of 0.5 meters which is typical of the transition width in the Camp Borden sands in the example section presented in Figure 9-5. The synthetic GPR responses for a 100 MHz radar system are shown in Figure 9-3.

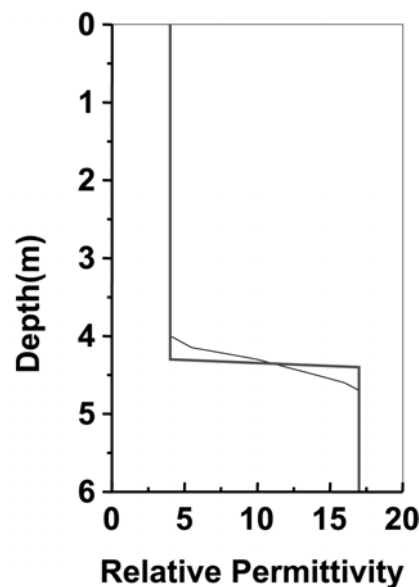


Figure 9-2: Two model profiles of permittivity versus depth - one abrupt and one with graded permittivity over a 0.5 width.

From the simple modelling results, it is apparent that introducing a gradational transition substantially reduces the water table reflection amplitude. It also smears the reflection out with lower frequency content; the gradational boundary acts as a low pass filter on the GPR pulse.

The synthetic data are also plotted in cross section form in Figure 9-4. The contrast between the sharp boundary and the gradational boundary response is very apparent. The blurred response of the gradational interface is quite similar to that observed in the radar sections shown in Figure 9-5.

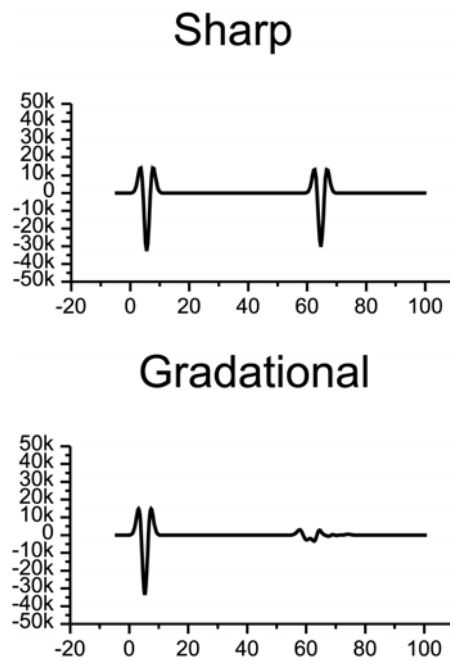


Figure 9-3: Results of synthetic radar calculation for two cases shown in Figure 9-2.

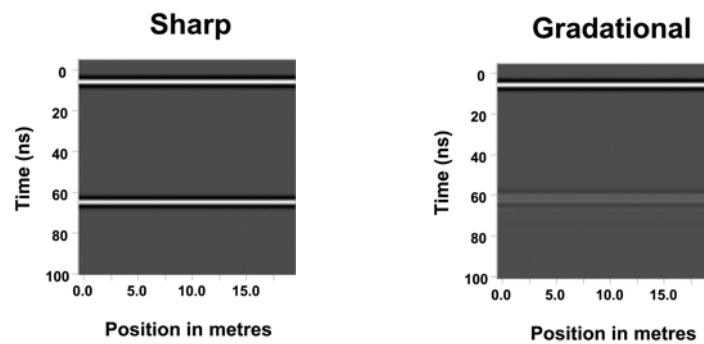


Figure 9-4: Gray scale displays of the sharp and gradational responses on a comparable scale to the GPR sections in Figure 9-5. The gradational response has reflections width similar to the water table reflection.

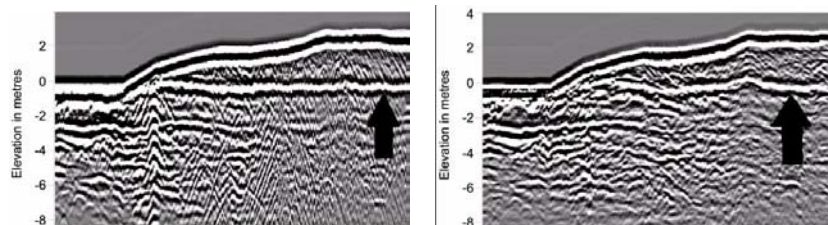


Figure 9-5: The figure on the left shows a 100 MHz pulseEKKO 100 section of water table test line collected in step mode at 20 cm station intervals. Antennas axes were aligned perpendicular to the survey line. The figure on the right is the same as the left only this shows antennas were axes oriented parallel to line direction and antennas moved continuously resulting in less accurate spatial positioning. Rubber banding was used to covert data to equal spatial positioning prior to plotting.

In summary, many interfaces are not as sharp and clean as the ideal case. GPR responses will tend to be weaker and more blurred than the ideal. These are important concepts for GPR users to keep in mind.

9.2 Velocity Determination Using Hyperbolic Fitting

The full utility of GPR data requires knowledge of how fast the signals travel in the material under investigation. Several techniques have been used such as CMP (common mid-point), WARR (wide angle reflection and refraction), known-depth-target, hyperbolic fitting to a local target and diffraction tail matching.

All of these techniques require GPR measurements along a traverse where the geometry is varying in controlled fashion. In other words, the distance to a target varies in such that estimations of velocity can be extracted.

For pipe and cable location of rebar and conduit location, line-like features are localized targets if the GPR system traverses perpendicular to the feature alignment. To estimate velocity, the path length to the object must vary. Figure 9-7 illustrate this using a linear pipe or cable as an example. In order to extract velocity information, the radar system must be moved perpendicular to the axis of the pipe or cable. The long-axis direction is commonly called the “strike direction” or “strike” for short. If a GPR traverses perpendicular to the strike, the distance varies from the radar system to the pipe in a systematic fashion. Traversing parallel to the pipe strike yields no change in the distance of the pipe and hence, a flat non-changing event on the GPR record. Figure 9-8 shows these two extremes using real data from a clay drainage pipe in a farm field.

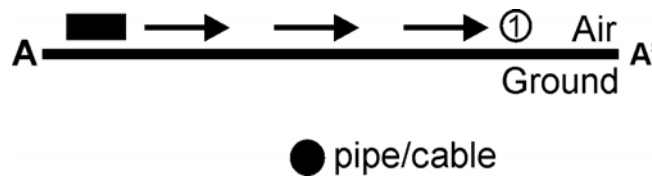


Figure 9-6: Cross section through area with GPR traverse perpendicular to pipe or cable strike direction.

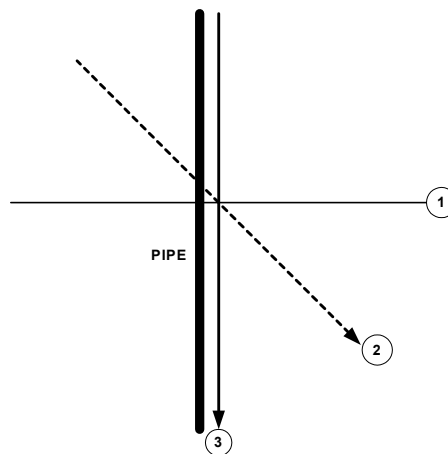


Figure 9-7: Plan view looking down or ground from above. Traverse 1 is perpendicular to strike and is optimal for velocity determination. Traverse 2 is at an oblique angle and 3 is parallel to the pipe strike axis. Data from traverses 2 and 3 are not suitable for determining velocity.

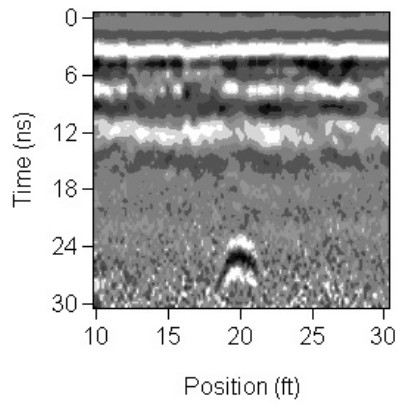


Figure 9-8: GPR data over clay drainage pipe perpendicular to pipe direction (line 1 in Figure 9-7)

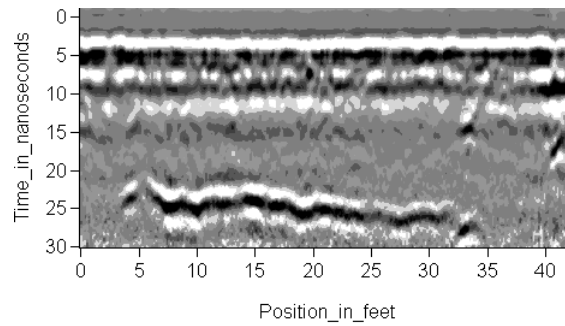
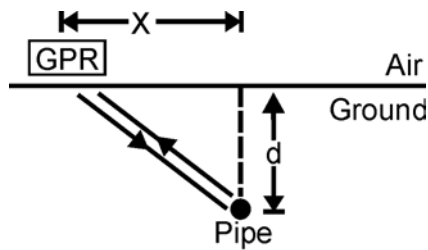


Figure 9-9: GPR data over a clay drainage pipe parallel to pipe direction (line 3 in Figure 9-7).



GPR Travel Time

$$T = \frac{2(x^2 + d^2)^{1/2}}{v}$$

or

$$T = \left(\frac{4x^2}{v^2} + T_0^2 \right)^{1/2}$$

where

$$T_0 = \frac{2d}{v}$$

Figure 9-10: Relationship between GPR position (x), object depth (d) and travel time (T). T_0 is travel time when GPR is directly over the object.

GPR cross-sections display signal amplitude versus position (normally on the horizontal axis denoted as x) and time (which is normally the vertical axis denoted as T). A local target has a travel time versus position as depicted in Figure 9-10. The mathematical form is a hyperbolic shape (inverted U on a GPR section) relating spatial position (x) to travel time (T). Figure 9-11 shows the response in a GPR cross-section as the target depth is varied. Figure 9-12 illustrates the behavior as the velocity is changed.

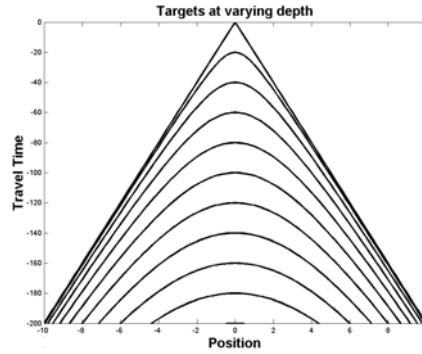


Figure 9-11: Schematic variations in GPR response when object depths varied for constant velocity.

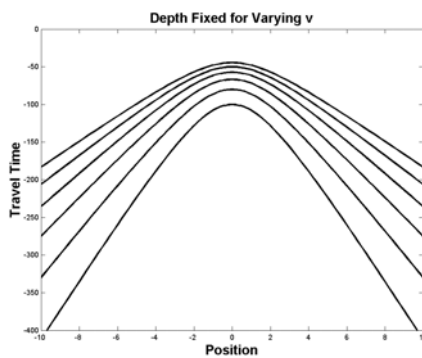


Figure 9-12: Schematic variations in GPR response when velocity is varied for a fixed object depth.

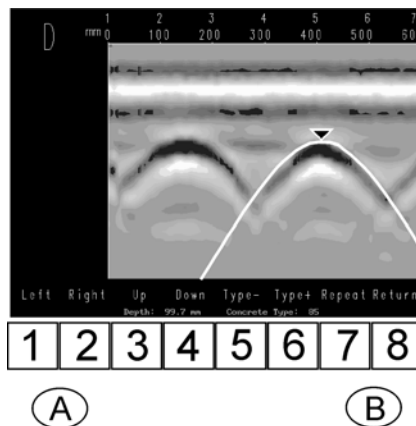


Figure 9-13: Example of shape fitting to a target response on the screen in the field. This feature is standard on Noggin Smart Systems and Conquest.

A handy interpretation aid is to visually fit a model hyperbolic shape to the GPR data as illustrated in Figure 9-13. Placing the top of the model (triangle point) over the apex (top of inverted U) in the data section selects T_0 . Adjusting the model shape to match the data yields an estimate of the velocity, v . Combining v and T_0 yields an estimate of the depth to the top of the target.

This tool is routinely employed in many of Sensors & Software Inc.'s Smart Systems. Users must be cautious since the velocity estimate can be erroneous if the traverse is not perpendicular to a linear feature strike. Good field practice entails several traverses over an object. Only use the hyperbolic fitting on the traverse that gives the most steep slope to the arms of the inverted U. This approach assures getting the most correct velocity. A traverse not perpendicular to a strike will always yield a velocity higher than the true velocity object depths will appear deeper than reality.

9.3 Polarity

The polarity of a GPR signal can be very helpful in interpretation of data. In this section, we will provide some basic insight into polarity, what causes it and how you recognize it in data.

The first thing is to define what we mean by polarity. A GPR signal normally reduces to a wavelet in time which has three half cycles such as shown in Figure 9-14. This up-down-up or down-up-down nature of the signal is common and is the result of the radiation characteristics of a small dipole antenna. The relative amplitude of the half cycles are 1, -2, 1 or -1, +2 or -1. The resultant signal has no DC or average value.

The user must develop a systematic convention for antenna deployment in order that the sign convention is consistent for a given survey application. There is no particular standard for what is defined as positive and negative. Normally at Sensors & Software Inc. we define the polarity of the signal based on the sign of the voltage of the first half cycle. A positive voltage in the first half cycle means a positive pulse while a negative voltage during the first half cycle means a negative pulse or polarity.

Sometimes it is easier to describe a positive wavelet according to Sensors & Software Inc.'s sign convention as a signal that looks like an "M". A negative polarity wavelet would be one that looks like a "W". These concepts are depicted in Figure 9-14.

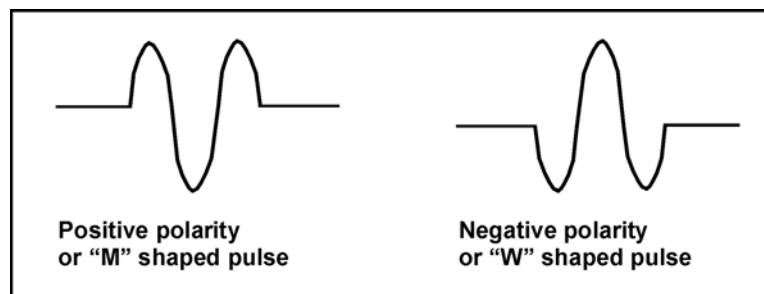


Figure 9-14: The typical GPR wavelet is an "M" or "W" shaped pulse as depicted here.

When a GPR measurement is made, there are signals which travel directly from the transmitter to the receiver as well as reflections coming from the subsurface. Figure 9-15 depicts the basic concepts of a simple measurement showing the direct air wave, the direct ground wave and a subsurface reflection. In this case we use a positive transmit pulse (having an "M" shaped wavelet). The direct airwave will have a positive "M" shaped wavelet whereas the direct ground wave will have a negative or "W" shaped wavelet. The polarity of the reflection from the subsurface horizon, however, can either be positive or negative ("W" or "M" shaped).

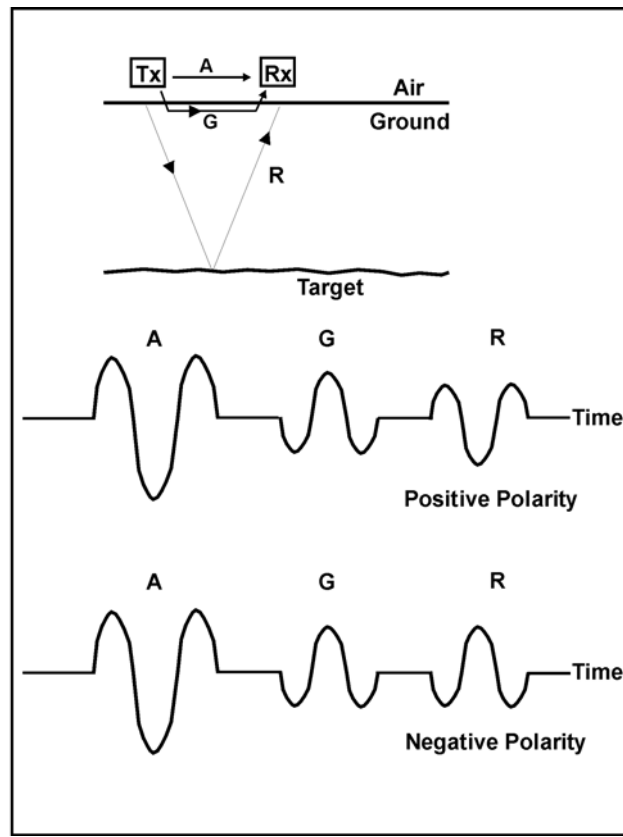


Figure 9-15: When GPR measurements are made, the transmitter and receiver are placed on the material to be probed. The minimal number of events which will normally be observed are 3 which are the direct wave A, the direct ground wave G, and a reflected signal R. Two idealized radar traces are shown here which show the polarity of the various wavelets associated with the arrivals. Two traces are shown because the reflected signal could have either a positive or a negative polarity.

The polarity of the reflected signal is dictated by the nature of the change in the electrical properties which cause the reflection. Figure 9-16 depicts the details of reflection from a target interface. Reflection is caused by a change in the electromagnetic impedance. A higher impedance target yields a positive reflection coefficient whereas a lower impedance target yields a negative reflection coefficient. In GPR, metal is a very low impedance (essentially 0) material and will always give rise to a negative reflection wavelet. On the other hand, a void in soil or rock represents a high impedance material and will give rise to a positive reflection wavelet.

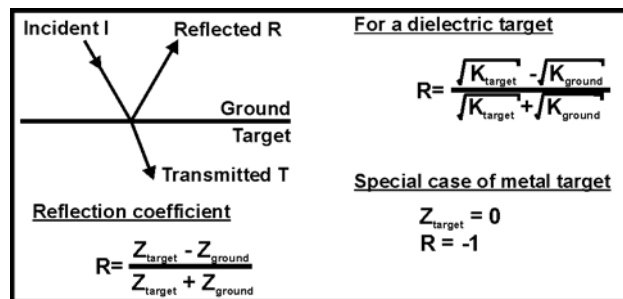


Figure 9-16: When a signal is incident on an interface, the reflected signal is dictated by the change in impedance on the interface.

An example data set is shown in Figure 9-17. These GPR measurements were made on a concrete structure which contained metal rebar and an air filled duct. The polarity of the signs of the wavelets from the reflections are clearly in accord with the above discussion. In the particular sections shown here, positive signals are shown as black, negative signals are shown as white and background level signal (which are zero amplitude) are shown as gray.

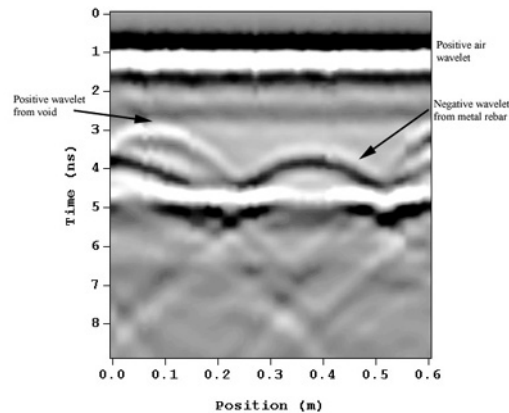


Figure 9-17: An example of GPR data from concrete data. Positive wavelets are black-white-black bands, negative wavelets are white-black-white bands and the background gray represent zero signal level. In this case the radar profile passed over a metal reinforcing bar and an air filled non-metallic conduit in the concrete.

9.4 Airwave Events

'Airwaves' is the name given to events on GPR records which are associated with energy that leaks into the air and gets reflected back into the GPR receiver. The source of these airwave reflections can be any above ground objects such as telephone poles, overhead wires, walls, vehicles, etc. (see Figure 9-18).

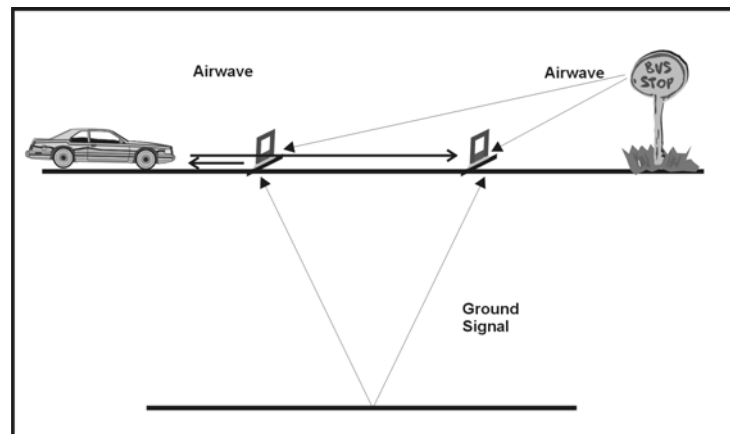


Figure 9-18: Radar energy that leaks into the air can reflect from surface objects in the GPR survey area. These 'airwave' reflections can look like subsurface targets in the GPR record.

GPR users tend to think that all GPR responses come from within the ground. It is very natural to think that GPR systems only look downwards and implicitly believe any event on a record must be from the subsurface. In fact, because the ground absorbs energy so rapidly whereas air does not, airwave events will often appear on GPR records.

Airborne signals cause problems in two different ways:

- the airwave response may mask weaker subsurface signals and make them difficult or impossible to see or interpret,
- airwaves may be falsely interpreted as a buried object when in fact the object is above the ground.

The GPR data set shown in Figure 9-19 is an example of how a false interpretation could occur. This particular data set was acquired along a road profile. The objective of the survey was to see whether there were karst (void) features underneath the roadway which could pose hazards to vehicular traffic. Several hyperbolic responses typifying the presence of localized features were apparent on the record.

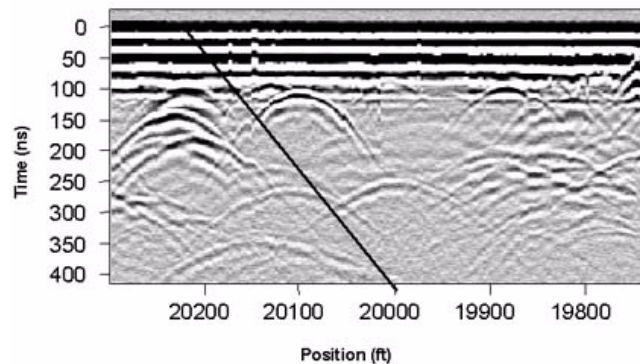


Figure 9-19: Airwave reflections from trees in the GPR survey area. All the reflectors below 100 ns in the data are caused by surface objects.

To the uninitiated, these ‘hyperbolic’ features can easily be misconstrued as coming from localized cavities beneath the roadway. An experienced GPR operator should routinely question the source of all signals particularly when the amplitude versus time response indicates that signals in the ground are decaying at a very rapid rate. The amplitude of the hyperbolic responses in Figure 9-19 are anomalously large given the attenuation in non-anomalous areas of the data.

A second reason that these features can be identified as airwave events is the slope of hyperbolic tails. These events have an airwave slope which indicates that the source of the signal is in the air.

Indicators of airwaves are:

- use your eyes to look for potential sources of airwave in your survey areas;
- when profiling, always run some profile lines towards or away from a surface object to evaluate whether or not the object is scattering energy. The response from the object will show up on the GPR record as a straight line event which slopes at the airwave velocity (see Figure 9-20, Figure 9-21 and Figure 9-22 lines B – B¹ and C – C¹);
- check diffraction tails of hyperbolic events for slopes close to the airwave speed; and
- check the frequency content of events as airwave energy often has higher frequency content than subsurface responses.

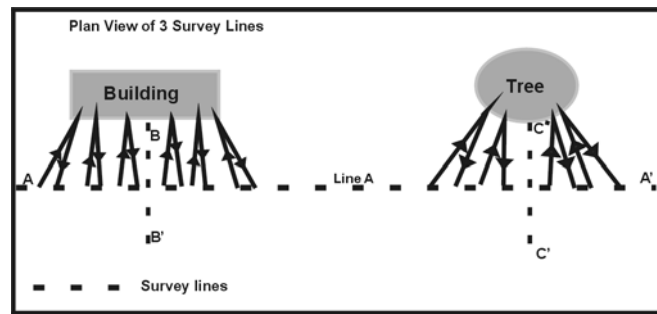


Figure 9-20: A figure showing the orientation of 3 GPR survey lines (A, B and C) in an area where a building and a tree are present. The figure also shows how during data acquisition of Line A, radar energy leaks out into the air; reflections from the buildings and the tree and returns to the receiver. Although not depicted the same leakage occurs on Lines A, B and C are shown in Figure 9-21.

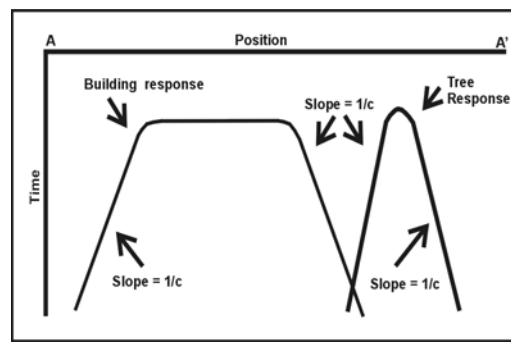


Figure 9-21: Airwave responses from Line A in Figure 9-20. As the GPR survey line is run from A to A' it approaches and passes the building and then approaches and passes the tree. The sloped responses occur as the distance to a surface object decreases as it is approached or increases as it is passed. When the GPR is run parallel to a long linear surface object like a building, the airwave response is a flat event. When the GPR is run beside a point target like a tree the airwave response is the classic hyperbolic shape.

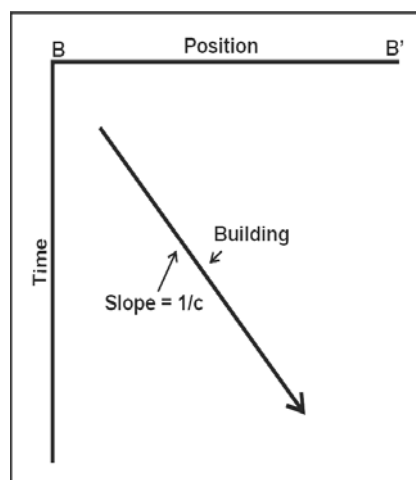


Figure 9-22: Airwave response from Line B in Figure 9-20. As the GPR survey line is run from B to B' the building gradually gets further away. Consequently, the building creates a straight reflector starting early in time at position B and later in time at B'. The slope of this is $1/c$ where c is the speed of light.

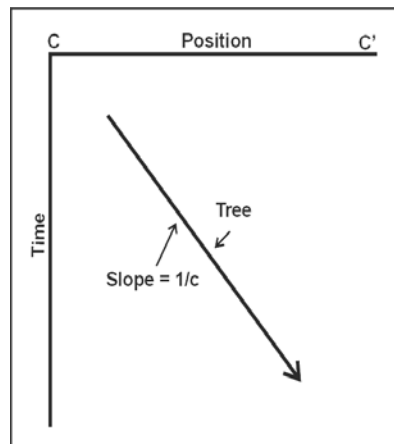


Figure 9-23: Airwave response from Line c in Figure 9-20. As the GPR survey line is run from C to C' the tree gradually gets further away. Consequently, the tree creates a straight reflector starting early in time at position C and later in time at C' . The slope of this line is $1/c$ where c is the speed of light.

Removing or eliminating air launched energy is difficult. Sometimes it can be minimized by optimizing antenna and/or survey line orientation. Airwave tends to get launched as vertically polarized fields off the ends of the dipolar GPR antennas traditionally used. Vertical features such as pipes, poles and trees make good targets. Changing the antenna orientation is only practical in some types of surveys and not all situations.

Digital processing may filter out the airwave features. For survey lines with airwave targets are at or beyond the end of the line, the airwave event will have a fixed slope (Figure 9-22 and Figure 9-23) allowing digital dip filters to remove the airwave energy and leave all the rest of the data intact.

In other situations the difference in frequency content between ground events and airwave events can be used to advantage. Low pass temporal filtering can suppress airwaves and enhance ground responses.

In some situations GPR just cannot be used because the airwave events dominate. This is a fact of life and must be accepted as one of the limitations of GPR.

Avoid the fallacy that shielded antennas will eliminate airwaves. Shielding of GPR antennas is never fully effective. Shielding can reduce airwave events (by a factor of two to even ten) but it never fully eliminates their presence. “Shielded” antenna data should always be treated as suspect when it comes to airwaves.

9.5 X Marks the Spot

For many years GPR records with rather unique X character have cropped up. Figure 9-24 shows 2 examples of such records.

These examples show several partial X's. This characteristic X is caused by GPR measurements made in close proximity to a long length of wire such as fence or cable.

The concepts underlying the cause of the response are depicted in Figure 9-25. When a GPR system is placed near a long metal wire, some of the energy couples from the transmitter onto the wire. The energy then travels along the wire in both direction until it reaches the end of the wire and then bounces back.

As one moves the radar system along beside the wire, the point at which the energy jumps on to the cable or wire moves the reflection from the ends of the wire move in time on the GPR record.

Figure 9-25 explains how the geometrical changes the delay times for the signals traveling along the wire. Generally the signals propagate along the wire at a speed very similar to that of the soil or rock in the area if the wire is on or near the ground. If the wire is elevated in the air then signals will travel at the speed of light (0.3m/ns).

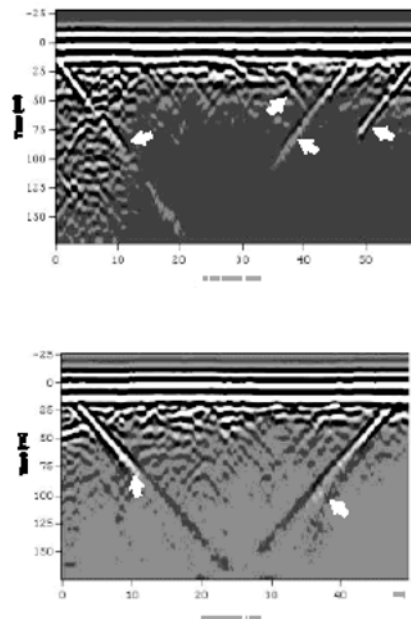


Figure 9-24: Two examples of X events which travel along a wire near a transmitter-receiver GPR configuration. The strong steeply dipping events show a partial X character. Signal attenuation is sufficiently high that the arms of the X don't cross in these examples.

This unique response can be seen when a metallic measuring tape is placed along the survey line and the radar system is moved along beside the tape. Quite often people will use fabric or plastic tape measures which should not show this effect. Unfortunately, some manufacturers embed thin metallic strength strands into fabric tapes. GPR users should examine measuring tapes closely to avoid this potential problem. The examples in Figure 9-24 show X events caused by 50 m tape measure with a hidden metal strength strand.

If you see this type of GPR response be aware of the mechanism that causes it and make sure that the tape measure that you are using is not the source of the problem. If this is not a factor then look around you for a buried wire or cable or a broken down fence which may be the source of the problem. Keeping antennas as far as possible from the cable or wires will minimize impact.

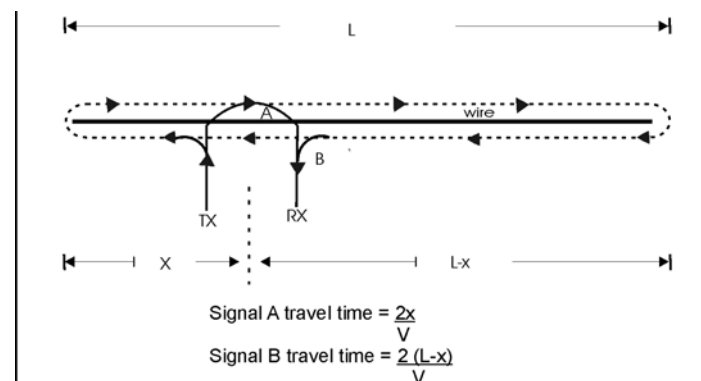


Figure 9-25: Events on a GPR record are caused by signals which couple into a nearby wire or cable. Signal A travels from the transmitter along the wire to the left end, reflects and travels back to the receiver. Signal B travels from the transmitter along the wire to the right, reflects from the end, and travels back to the receiver.

9.6 Plastic Water Pipe Diameter Determination

GPR users often ask whether GPR can determine the diameter of a pipe which has been detected. In many situations, the pipe diameter is smaller than the GPR resolution length. As a result, estimating diameter is difficult.

Specific applications occur where the pipe diameter can be determined even where the diameter is small compared to the resolution length. Water filled plastic pipes are a prime example.

The GPR response of a non-metallic pipe is dictated by the material filling the pipe, not the pipe composition. For water filled non-metallic pipes, the water controls the GPR response. Water has a very slow GPR velocity causing the signal transmitted through the pipe to be refracted diagonally across the pipe. The concept is shown in Figure 9-26.

The slow velocity means that the travel time for the signals across the pipe is quite long. Reflection from the opposite side of the pipe will be substantially delayed.

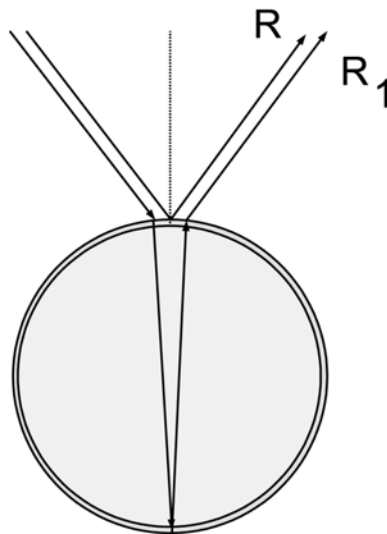


Figure 9-26: A water filled pipe represents a unique GPR target. The low velocity causes the transmitted energy to be refracted diagonally across the pipe.

Many GPR records show detection of the top and the bottom of a water filled plastic pipe. The difference in travel time between the top and the bottom responses provides a way to estimate the pipe diameter.

The rays representing the reflections from the top and the bottom of the pipe are depicted in Figure 9-27. The reflection from the top and the bottom are locked in time with respect to one another by a fixed delay time.

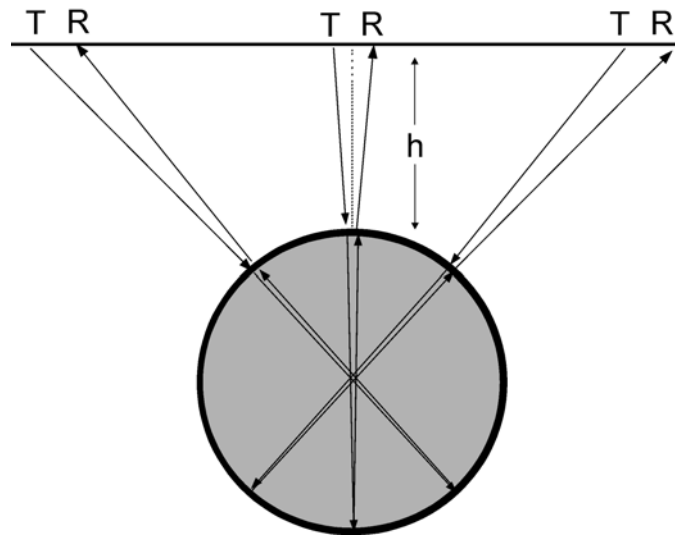


Figure 9-27: When one traverses a pipe, the GPR signal is reflected from the normal point on the pipe's circumference. Transmitted energy traverses diagonally to the opposite wall of the pipe and is reflected. Rays always pass through the pipe center as sketched.

The GPR response will be as depicted in Figure 9-28. The top and bottom of the pipe yield identical hyperbolas offset in time. Where water is very fresh, multiple echoes of the signal traveling back and forth in the pipe may be detected as shown in Figure 9-28.

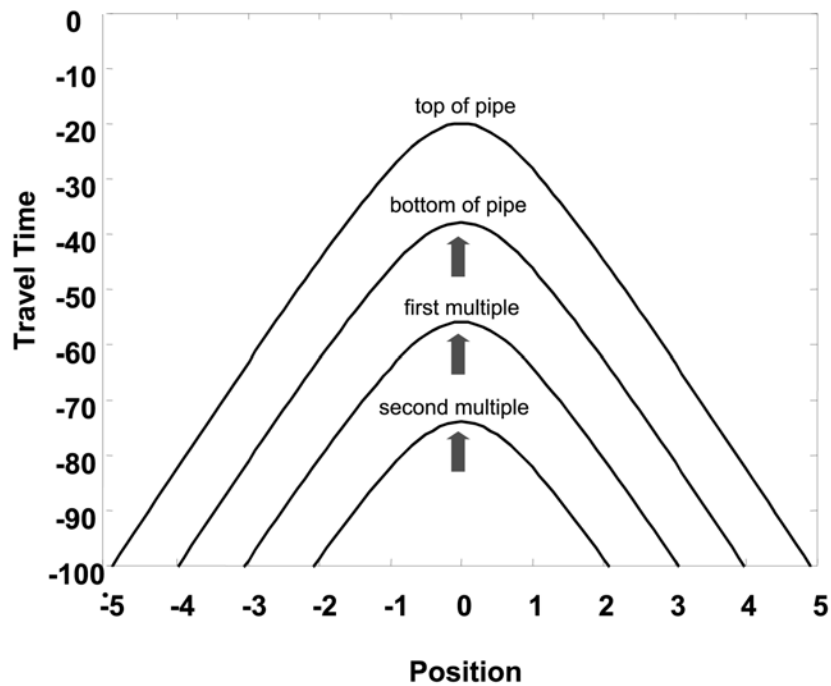


Figure 9-28: Travel time for multiple reflections in a water filled pipe. The top hyperbola represents the reflection from the top of the pipe whereas the three other hyperbolas occur at a fixed delay time (30 cm diameter, 0.5 m deep).

The unique feature of the response is that the top and bottom response track one another with a fixed time delay between them. This time delay is determined as

$$T_n = \left(\frac{4x^2}{v^2} + T_0^2 \right)^{1/2} + n\Delta t$$

$$T_0 = \frac{2h}{v}$$

where h is depth to the top of the pipe, v is velocity in the ground, x is offset of GPR from pipe axis, Δt is the time for signal to do a two way transit through the pipe and n is the number of two way transits.

$$\Delta t = \frac{2d}{v_w} \quad \text{and} \quad d = \frac{v_w \Delta t}{2}$$

where d is pipe diameter and v_w is water velocity (0.033 m/ns or 0.11 ft/ns).

An example GPR response traversing perpendicular to a 6" diameter water filled pipe is shown in Figure 9-29. Looking closely one can see a hint of a third hyperbola representing a second pass (first multiple) through the pipe.

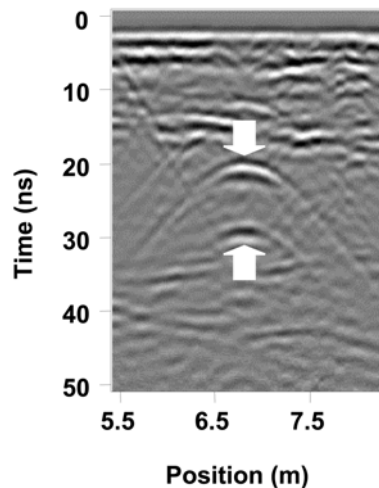


Figure 9-29: GPR response over a 6 inch plastic water main. the hyperbolic response from the top of the pipe is followed by a second response from the bottom of the pipe. The delay time of about 8.2 ns is the delay time for a 6 inch water pipe.

Figure 9-30 shows a profile along the axis of a pipe where the top and the bottom reflection track each other. The apparent depth variations are caused by the fact the profile does not track perfectly along over the pipe but wanders off to the side and back.

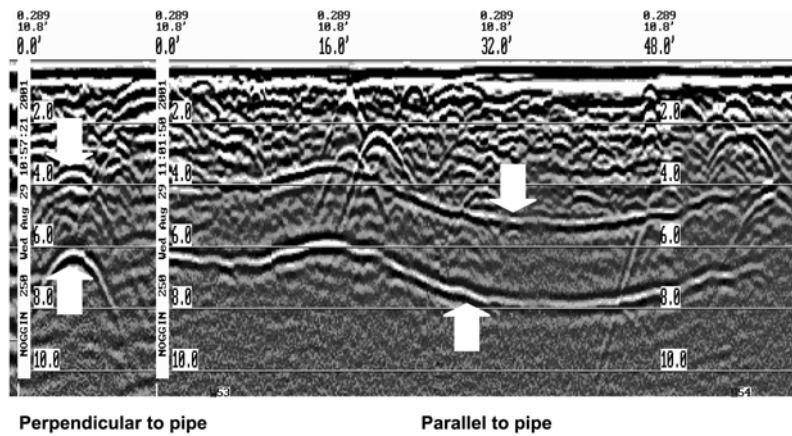


Figure 9-30: This Noggin SmartCart record shows a traverse perpendicular to a pipe followed by a traverse along the pipe. The top and bottom reflection of the pipe are clearly visible.

The following table provides a summary of travel time versus pipe diameter. A quick estimate of diameter is obtained by measuring delay time between the events on the GPR record.

Diameter (cm)	Diameter (in)	Δt (ns)
5	2	2.7
10	4	5.4
15	6	8.1
30	12	16.2
50	20	27

9.7 Antenna Shielding

What is antenna shielding? Figure 9-31 shows the conceptual idea of a shield. With GPR, the antenna is normally placed close to the air-ground interface. The shield is a “container” which encloses the antenna. The objective is to improve the antenna’s performance by placing the shield over it.

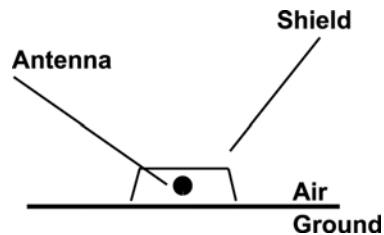


Figure 9-31: Concept of a GPR antenna shield. The shield encloses the antenna to minimize coupling with signals in the air.

What is the purpose? Referring to Figure 9-32, signals can travel from a transmitter to a receiver along a number of paths. Shielding is used to achieve the following goals:

- maximize the energy on the path AA' to and from the subsurface target
- minimize the direct transmitter to receiver energy on path B
- minimize the energy which escapes into the air as on path CC'
- minimize external electromagnetic noise as indicated by signals D

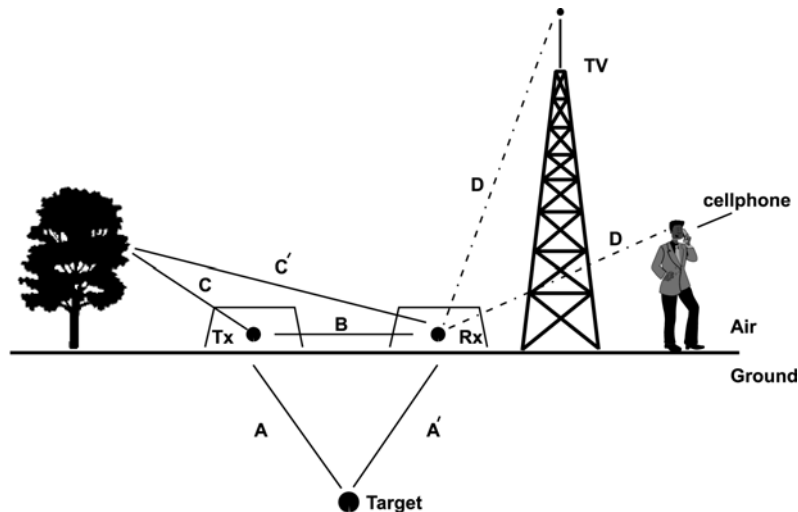


Figure 9-32: A GPR system emits and detects radio wave signals. There are many possible signals and paths. The objective is to maximize the target response and minimize others.

Given these laudable benefits, what are the drawbacks? Antenna shielding requires a structure that has an electromagnetic response. If the structure is not designed properly or is damaged, its electromagnetic response can be large. In addition to the signals shown in Figure 9-32, energy goes from the transmitting antenna to both the transmitter shield and the receiving antenna shield and then to the receiving antenna as indicated in Figure 9-33. The shield generated signals can be large and reverberate for a long period of time.

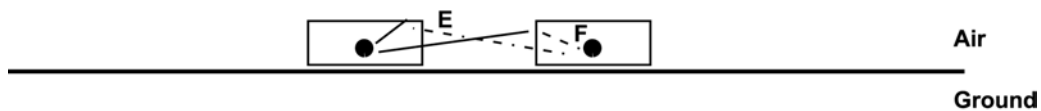
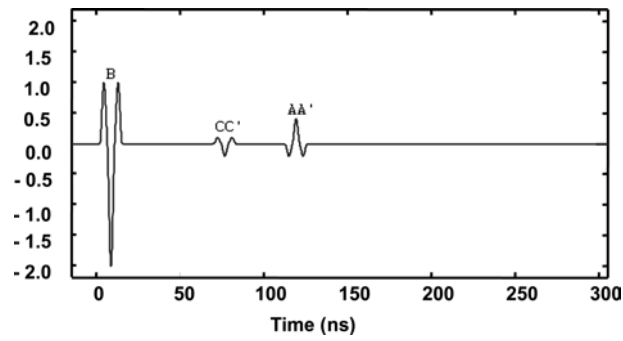


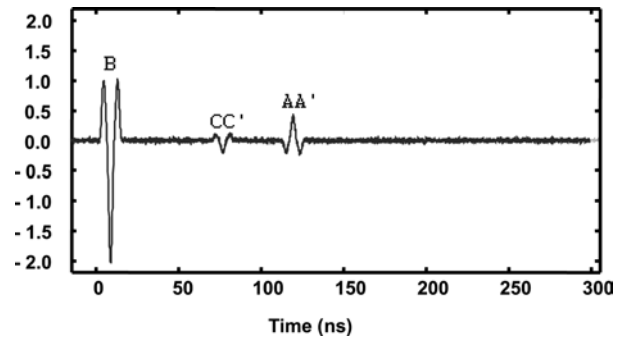
Figure 9-33: Antenna shields must interact with radio waves to be effective. The shield can generate responses which may be detrimental and interfere with the desired measurement unless extreme care is taken in the shield design.

Besides the electromagnetic response of the shield itself, an effective shield has to be larger than the antenna. This leads to considerable transducer size, weight and manufacturing cost penalties. In a nutshell, there is no free lunch and attempting to shield an antenna can create as many problems as benefits.

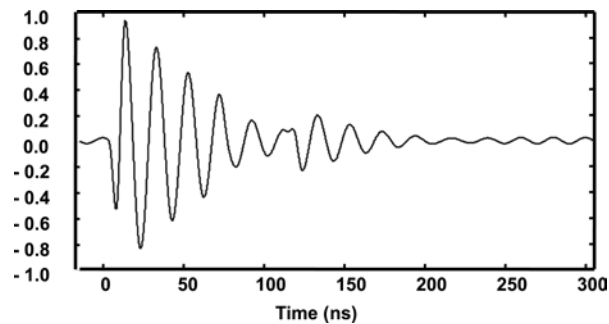
A series of radar traces are shown in Figure 9-34. (a) is the ideal response without external noise sources. (b) shows the response observed when external noise is present. (c) shows the behavior which can occur if improper shielding is used. The reverberatory signal running down the trace for a long period of time is the transient response of the shielding. (d) shows the result that a practical shield can achieve.



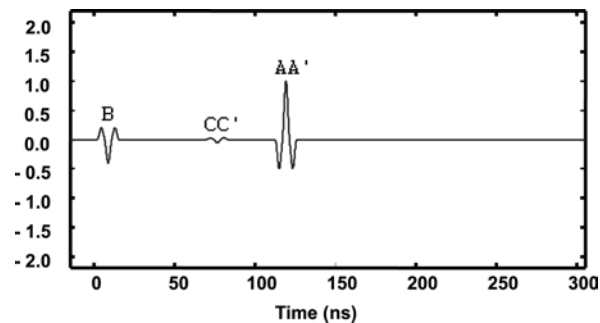
(a) Unshielded noise free response.



(b) Typical response with external noise.



(c) Transient response when shielding is improperly implemented.



(d) Results that can be expected with a practical well implemented shield.

Figure 9-34:

Shielded antennas can be readily constructed for higher frequency GPR systems, typically in the 100 MHz frequency range and above. The shields are about the same size as the antenna and use absorbing material to damp out the undesired signals.

At lower frequencies, practical size and portability dictates minimal or no use of shielding.

Tips for GPR users are as follows:

- a) Shielding is never perfect no matter what some may claim.
- b) Question whether your application requires shielding. the highest fidelity and maximum depth of penetration at open sites may be obtained when shields are not used.
- c) Always look for GPR events attributable to spurious signals. Even with the most ideal shield, spurious signal leakage can and will occur.

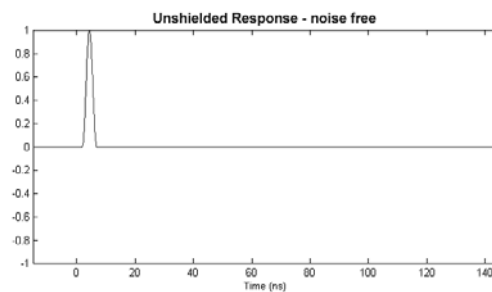
9.8 Ringing on Radar Records

Ringling is a term generally used in the GPR community for signals which reverberate in a regular fashion. Such responses are created when a GPR signal interacts with an object in such a way that the signal repeatedly bounces around within an object or between two or more objects.

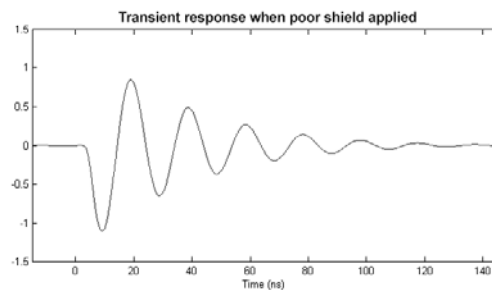
The most common acoustic analogy is a bell. When a bell is tapped with a hammer, it will ring for a considerable amount of time. The elastic energy causes the bell to deform in a rhythmic fashion as it propagates around the bell. The sound, which has a fixed tone determined by the bell size and composition, then slowly dies out.

Reverberation or ringing represents a resonant condition in the system. The general concept is shown in Figure 9-35 which illustrates the transient response of an object.

In Figure 9-35, the upper trace (a) shows the input signal which is an impulse and the lower trace (b) shows an oscillating signal which lasts for a considerable period of time.



(a)

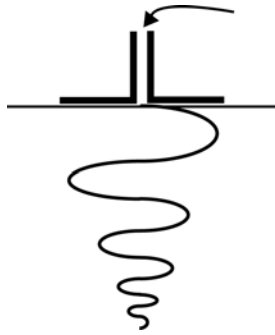


(b)

Figure 9-35: Example of a reverberating response. (a) The input excitation shown as an impulse. (b) The target behavior oscillates and decays slowly with time.

Sources of ringing in GPR measurements are many. Some common ones are:

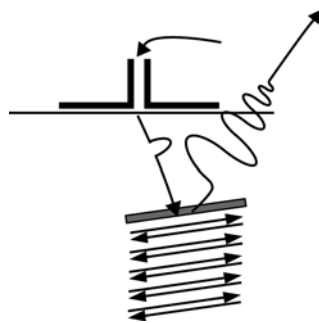
- an undamped dipole antenna (Figure 9-36(a))
- inappropriately constructed antenna shielding (Figure 9-36(b))
- a metal object in close proximity of the antennas (Figure 9-36(c))
- a strong target near the antenna or ground interface (Figure 9-36(d))



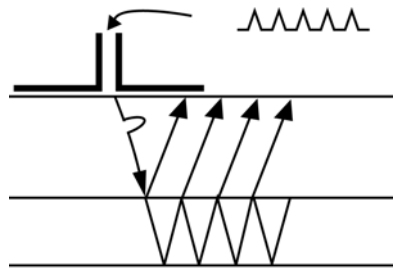
(a) Undamped electric dipole antenna will support electrical current which travels back and forth repeatedly generating signal.



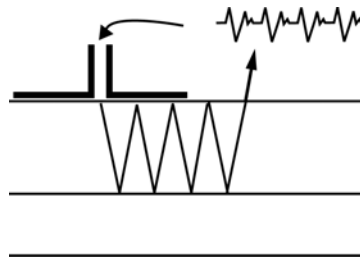
(b) Currents generated on antenna shield bounce back and forth emitting signal.



(c) Current bouncing back and forth on metal object of similar size to antennas. See Figure 9-37 (a), (c) and (d).



(d) Partially transparent layer on structure which contains signal which can bounce back and forth. See Figure 9-37(e).



(e) Strong reflector generates signals which bounce back and forth between the object and the antenna (and/or shield, and/or ground surface). See Figure 9-37(b).

Figure 9-36:

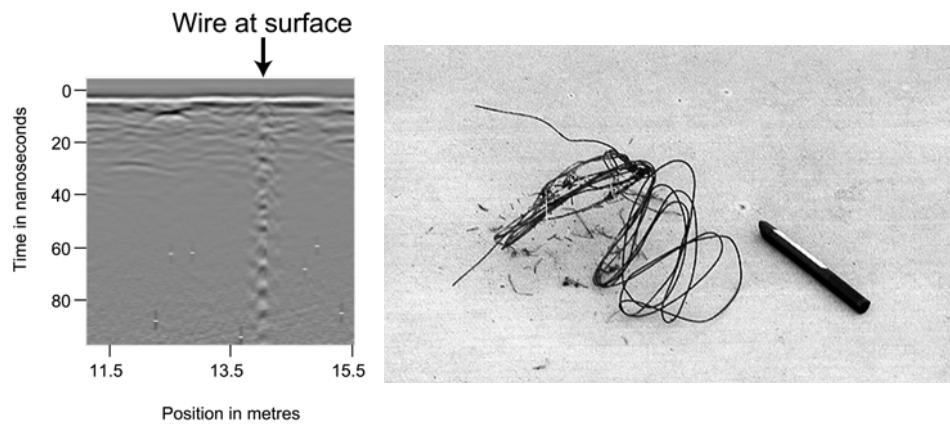
The fundamental period or repetition rate for the oscillation is a characteristic feature of ringing/reverberation. The repetition rate is directly related to a spatial dimension of the object(s) causing the reverberation. The reverberation period,

$$t = \frac{L}{v}$$

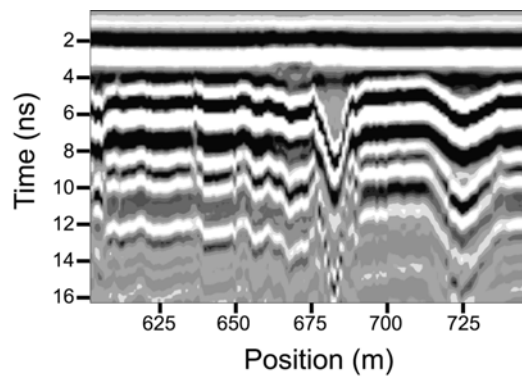
is a function of an object dimension, L , and also the velocity, v , in the object surrounding material. It is possible to have a multiplicity of different dimensions yielding a multiplicity of periods causing a more complicated signal. Generally one period will be dominant.

GPR reverberation is very selective because the excitation signal, object geometry and material properties must be in accord to get a resonant response. Generally, the ground severely dampens out reverberation because it absorbs energy, but it is quite common to see examples in GPR records. Figure 9-37 shows example of real survey data which help provide insight as to what should be expected. The individual example captions indicate the source of the ringing.

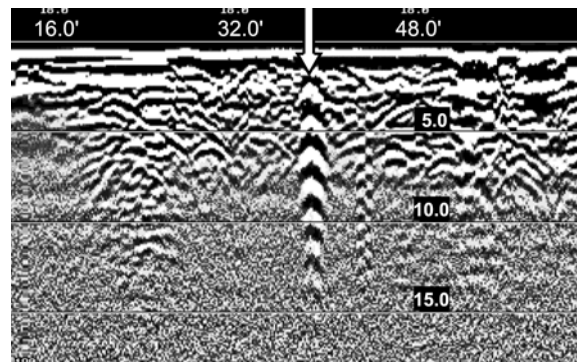
In addition to these examples in Figure 9-37, an example is presented in Section 9.7 Antenna Shielding.



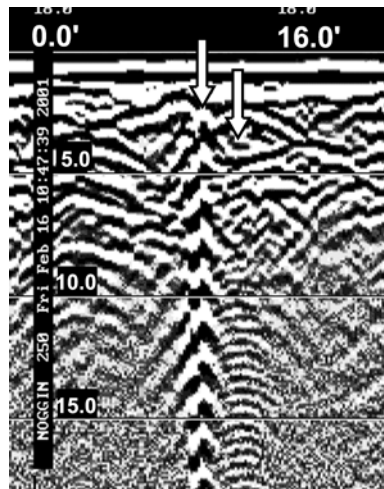
(a) A recent 250 MHz survey exhibited a ringing event. A scrap piece of wire (above right) was found in grass)



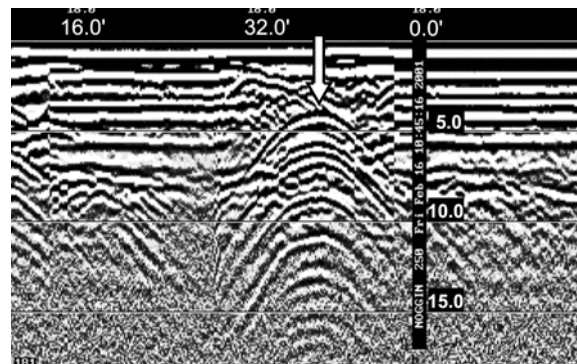
(b) Example of multiple reflections on an ice road. The GPR signal bounces up and down several times because the ice-water boundary is a very strong reflector and ice is transparent.



(c) A large buried metal object generates a low frequency (compared to GPR pulse) reverberating signal.



(d) Two metal objects side by side with low and high frequency ringing.



(e) A target creates multiple equi-spaced responses that extend over a long time interval.

Figure 9-37:

9.9 GPR Time Zero & Depth Estimates

Interpretation of depths from Ground Penetrating Radar requires data knowledge of zero time in a GPR recording. While this sounds like a trivial matter, precise location of zero time requires clear terminology and an understanding of instrument operation.

Most important is the recognition that we are measuring signals that travel at the speed of light. We have to account for the finite time that signals take when traveling through our measurement apparatus.

First, two definitions:

T_0 = time zero - the time when the GPR transmitter initiates signal emission via the GPR transmitting antenna.

R_0 = first break - the time when the GPR receiving antenna detects the on-set of the signal traveling directly from the transmitter.

These two quantities are very important in GPR because R_0 is normally detectable on GPR records whereas T_0 is not recorded. The event determining R_0 normally travels on the direct path from the transmitter to receiver antenna at the speed of light.

$$R_0 = T_0 + \frac{S}{c}$$

S - antenna separation
c - speed of light (0.3 m/ns)

The key concepts are illustrated in the block diagram in Figure 9-38 and the sketch of a received signal in Figure 9-39.

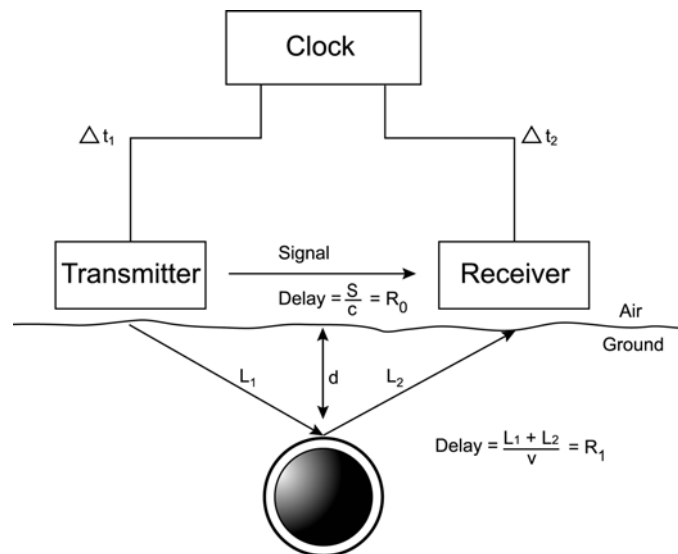


Figure 9-38: Simplified GPR system and measurement configuration illustrating signal time delays.

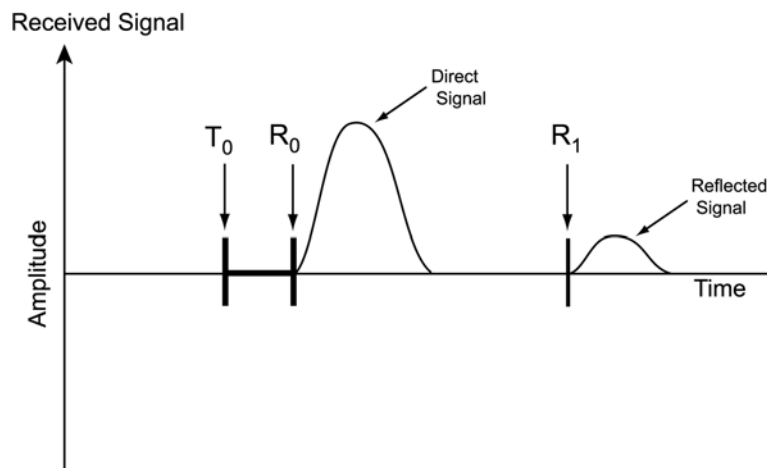


Figure 9-39: Illustration of a GPR received signal displayed as amplitude versus time.

While we may have a very precise clock, the cabling and electronic devices in the transmitter and receiver have associated time delays, Δt_1 and Δt_2 , which can be large. Unless every cable and circuit component time delay is measured, knowing when the transmitter emits and the receiver records is not possible. In normal GPR practice, calibrating cables and circuit delays is not cost effective. The procedure is to measure R_0 and infer T_0 by knowing S .

When determining depth, the measurable times are R_0 and R_1 . Quite often depth, d , is estimated by the simple calculation

$$d = \frac{(R_1 - R_0)v}{2} \quad (9-1)$$

while the correct solution is actually

$$d = \frac{1}{2} \left(v^2 (R_1 - (R_0 - S/c))^2 - S^2 \right)^{1/2} \quad (9-2)$$

which reduces to the first expression $S=0$ (the transmitter and receiver are spatially coincident). In the equation, v is the propagation velocity in the ground.

When using GPR systems where antenna separation can be varied, operators should always record the value of S . For fixed antenna geometries, accommodations for S can be designed into the instrument data recording stream. It is always important to keep track of the value of S in reports.

For deep geological sounding, $S \ll d$ and the approximate solution expressed in Equation 9-1 is perfectly satisfactory for determining depth.

For non-destructive testing and buried utility applications, having $S \approx d$ is common and the exact solution in Equation 9-2 must be used.

9.10 GPR Antenna Elevation

GPR users invariably ask “Why can’t we lift the GPR off the ground?”, or “How close to the ground must the GPR be?”

The simplest answer is that the best GPR data are normally obtained when the GPR antennas are closely coupled to the ground.

So, the question arises: “Why does anyone ever want to raise the antennas off the ground?” The prime reason is that some applications lend themselves to transporting the GPR system on a vehicle. In this case, the system can be moved rapidly over the ground and large areas can be covered efficiently. Unfortunately, to move quickly over most ground the antennas have to be raised so that the sensors do not get damaged when traversing a rough surface.

A compromise, based on an understanding of the trade-offs, must be reached. Lifting antennas above the ground has operational benefits but is detrimental for many reasons which are outlined below.

What happens when the antennas are raised off the surface?

1. In many instances, antennas and electronics are designed to match the low impedance ground and don't always work as well when deployed in air.
2. When antennas are elevated, more energy goes into the air and less into the ground. The antenna pattern variation with height is depicted in Figure 9-40 and Figure 9-41.

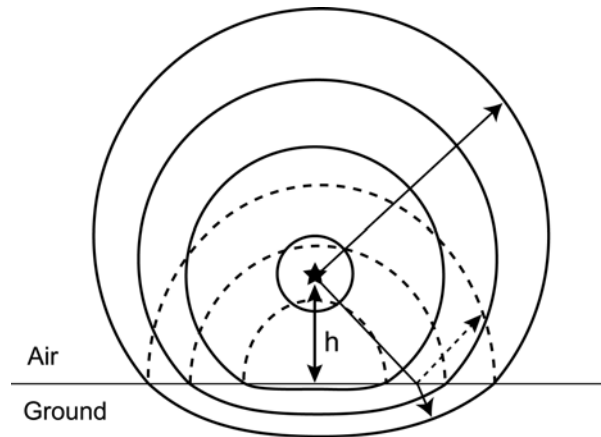


Figure 9-40: Illustration of antenna geometry over the ground. The critical parameter is the distance between the antenna element and the ground surface, h .

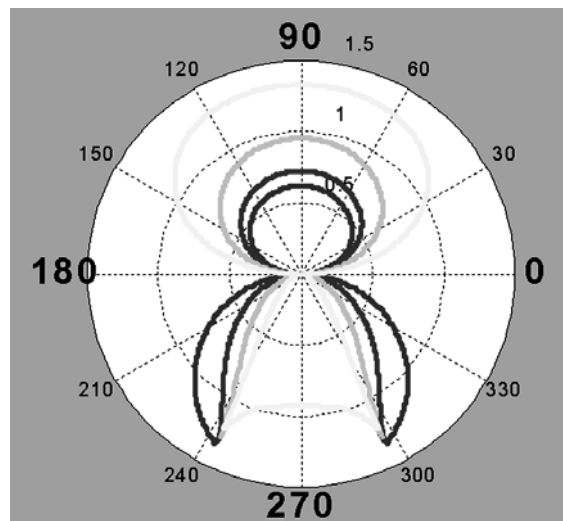


Figure 9-41: Illustration of how antenna directivity changes with the normalized height of the antenna above the ground surface.

3. When mapping small objects, the response of small targets is substantially reduced as the systems are elevated above the surface, as shown in Figure 9-42.

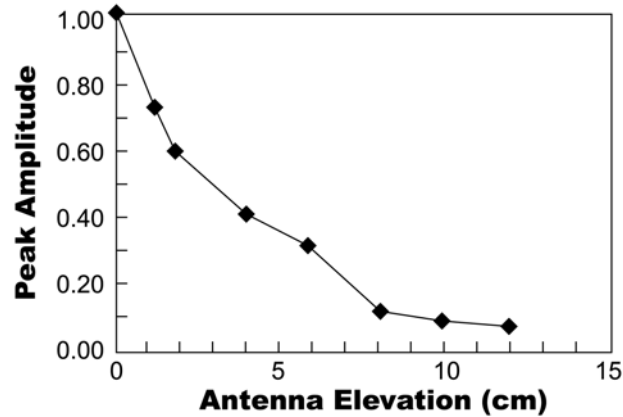


Figure 9-42: Amplitude at the peak of a response decreases with elevation 10 cm diameter target with a 1000 MHz GPR system, showing a substantially reduced sensitivity to a target for a GPR measurement.

4. When mapping small targets, the spatial resolution of the measurement is substantially degraded with elevation of the GPR transducers.
5. When antennas are elevated more energy goes into the air and the measured results are more prone to contamination by air wave events. This is depicted in Figure 9-43.

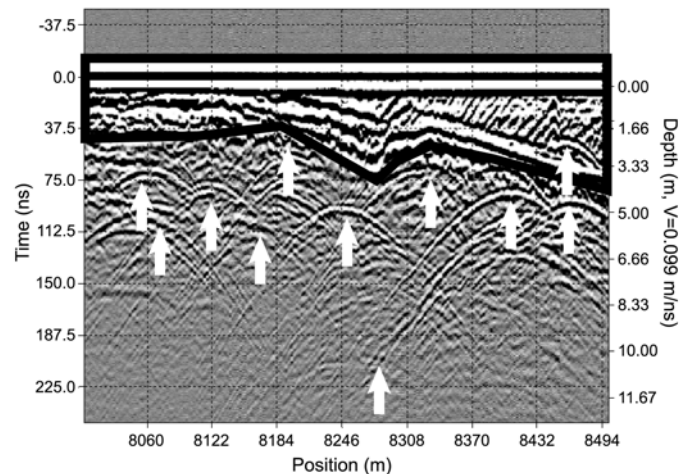


Figure 9-43: The data shown here were acquired with the GPR antennas elevated about one third of a wavelength above the ground surface. The scattering from trees in the surrounding area (indicated by arrows) are quite visible on the record. Response from subsurface geology is within the area indicated by the thick line.

6. The GPR loses sensitivity for detecting steeply dipping targets such as geological horizons, which can have substantial dip.

While there are many good reasons for keeping GPR antennas on the ground, some applications can tolerate antennas being lifted.

If the application has most of the following features then operating with antennas elevated off the surface may be perfectly satisfactory.

- a) The targets being sought are large and relatively flat lying.
- b) The survey area has few surface obstructions and has a flat surface.
- c) The measurement environment has low loss conditions (so good penetration is achieved).
- d) The targets are relatively shallow.

As a guide, good ground coupling occurs if the antennas are kept within 0.1 center frequency wavelengths of the surface, where the wavelength is in the material being probed.

In summary, conventional GPR gives best results when the transducers are kept close to the ground. Be sure to carefully assess your application before operating with the antennas elevated off the surface as the results may not be as good as you had anticipated.

9.11 Determining Layer Thickness & Velocity from CMP Data

In many GPR applications, CMP data acquisition is used to estimate the velocity in the subsurface. The most common method of analyzing CMP data is to use the classic “ $t^2 - x^2$ ” method of extracting velocities and depths.

With modern computers, it is much more common for CMP data to be analyzed using a semblance approach which gives a measure of coherence of GPR signal move-out versus antenna separation. Peaks in the semblance function indicate the move-out velocity and arrival time for distinct reflections from the subsurface.

Translation of the semblance analysis data into true velocities and depths is sometimes required. The procedure for this is commonly known in petroleum seismic reflection. The equations involved are normally referred to as the Dix equation. This analysis was carried out by Dix (1956) and is a mainstay for determining interval velocities in the layered structures.

9.11.1 Analysis Procedure

The basic concept of the layered earth giving rise to a number of reflections is depicted in Figure 9-44. The earth is assumed to be made of layers of arbitrary thickness and velocity.

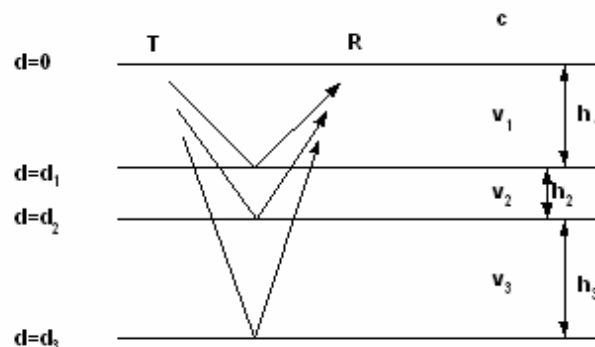


Figure 9-44: In a simple layered earth environment, the variables are the layered thickness and the velocity of each layer. These parameters need to be estimated from the GPR data.

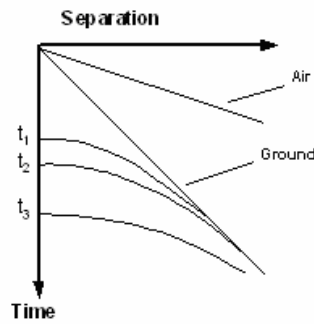


Figure 9-45: The layered sequence in Figure 9-44 would generate a CMP GPR section as shown above. The direct air and ground waves are indicated as well as the hyperbolic reflection events from horizons 1, 2 and 3, which have intercept times of t_1 , t_2 and t_3 .

When a CMP measurement is carried out in such a structure, one sees the idealized events arriving as depicted in Figure 9-45. Each of the horizons gives rise to a reflection event which closely follow hyperbolic move-out in the antenna separation travel time space. Mathematically, the shape differs slightly from a hyperbola but petroleum seismic analysis in numerous text shows that this deviation is so small as to be inconsequential until extremely large antenna separations occur.

The result is that an event from a flat lying horizon can be expressed mathematically as

$$t_n^2(x) = t_n^2 + \frac{x^2}{w^2} \tag{9-3}$$

where t_n is the velocity with zero antenna separation and $t_n(x)$ is the travel time for a finite antenna separation x . The value w is known as the move-out or “RMS” velocity.

w is a weighted mixture of all the velocities in the section above the horizon giving rise to the reflection. As a result, it is not a true material velocity but rather a weighted sum.

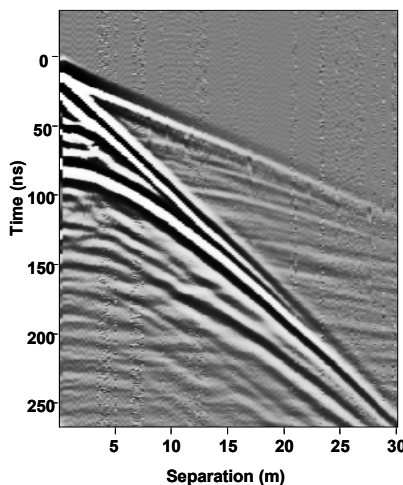


Figure 9-46: This is an example from a CMP from an area where there is a strong water table reflection at a travel time of 70 ns. The section above the water table has sands with varying water content well below saturation.

An example CMP record is shown in Figure 9-46. This illustrates the raw radar traces with events occurring at varying times down the trace. Examining the record, it is clear that many of the events move-out in a hyperbolic shape with time as antenna separation is increased. With modern computer analysis, a process called semblance analysis is normally applied to CMP data which yields a measure called $S(w,t)$. The semblance measure S is such that it will yield a peak when there is an event in the GPR data which has a move-out velocity w .

Various forms of indicator can be used. Some of the common ones applied are

$$S_1(w, t) = \left| \sum_j r_j \left(t + \frac{u_j}{w} \right) \right| \quad (9-4)$$

$$S_2(w, t) = \frac{\left| \sum_j r_j \left(t + \frac{u_j}{w} \right) \right|}{\left| \sum_j \left| r_j \left(t + \frac{u_j}{w} \right) \right| \right|} \quad (9-5)$$

$$S_3(w, t) = \frac{\sum_j r_j \left(t + \frac{u_j}{w} \right)}{\sqrt{\left(\sum_j r_j^2 \left(t + \frac{u_j}{w} \right) \right)}} \quad (9-6)$$

where

$$u_j = \left(t^2 + \frac{x_j^2}{w^2} \right)^{1/2} \quad (9-7)$$

The r_j in the above equations is the radar trace for antenna separation x_j . The goal is to get a function S which peaks sharply whenever there is a coherent event that moves out in a hyperbolic form in time-offset space.

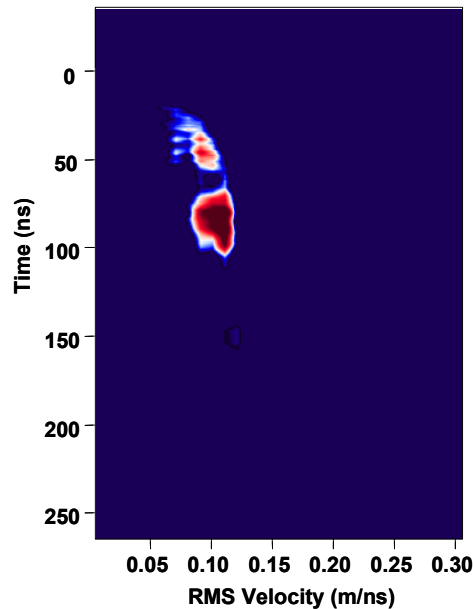


Figure 9-47: This cross section is the semblance analysis for the data shown in Figure 9-46. Peaks occur at travel times of 40 ns, 50 ns and 70 ns. RMS velocities are picked to be 0.95, 0.98 and 0.105(m/ns).

The normal analysis process is to generate a contour map of S as a function of w and t . An example of this is shown in Figure 9-47. Data are interpreted by selecting the peaks in this function. The peaks identify particular reflecting horizons. From the peaks in S one creates a table of values which are the zero offset time and RMS velocity for the domain t reflecting horizons. One normally tabulates this as indicated in Table 1. The values t_n and w_n indicate the intercept time and the RMS or move-out velocity for the horizon.

Table: 9-1 The Dix analysis for the layered sequence in Figure 9-47.

Dix Analysis for GPR Data						
Horizon Number	Intercept Time (ns)	Stacking Velocity (m/ns)	Interval Thickness (m)	Dix Depth (m)	Interval Velocity (m/ns)	
0	0	0.000		0.00		
1	40	0.095	1.90	1.90	0.095	
2	50	0.098	0.55	2.45	0.109	
3	80	0.105	1.74	4.18	0.116	

Note: If the intercept and velocity data are not consistent, a negative interval velocity can occur and is indicated by computation error #NUM!!!

Note: GPR velocities lower than 0.03 and higher than 0.3 are not realizable and indicate poor input information.

9.11.2 Intercept Time & RMS Velocity Conversion to Depth & Interval Velocity

For many applications it is satisfactory to estimate the depth of horizon by just using the simple equation

$$d_n = \frac{t_n w_n}{2} \quad (9-8)$$

This gives a quick number which is quite often all that is required.

In some instances, however, obtaining a more correct velocity and depth model is desirable. This is the problem which Dix addressed for reflection seismic many years ago. The approach can be viewed as peeling the onion layer by layer; starting from the top, t_n and w_n are used to extract depth and velocity working down through the section.

The mathematical details can be found in many text. One good reference is Grant & West (1965) (pages 143-145).

To a very good approximation, the true velocity in layer n can be expressed in terms of the RMS velocity and intercept times as

$$v_n^2 = \left(\frac{t_n w_n^2 - t_{n-1} w_{n-1}^2}{t_n - t_{n-1}} \right)^{1/2} \quad (9-9)$$

Once the velocity in layer n is known, one can determine the thickness of the layer. Mathematically this is expressed as

$$h_n = \frac{1}{2} v_n (t_n - t_{n-1}) \quad (9-10)$$

Finally, the depth of each layer or horizon can be expressed as

$$d_n = \sum_{i=\phi}^n h_n \quad (9-11)$$

Such calculations are very quickly implemented in spreadsheet analysis and can be integrated into normal data analysis.

The layer velocity derived in this manner is called the “interval velocity”. This means this is the velocity in the interval between depth n-1 and depth n. For some applications knowing the velocity in a particular layer enables estimation of other parameters such as porosity, water content, density, etc. Again, extraction of this information requires some prior knowledge of the geology.

For the data shown in Figure 9-46 and the semblance result in Figure 9-47, intercept times and RMS velocity for two events have been tabulated. The resulting spreadsheet calculations are shown in Table 9-1.

In general, these calculations are easily carried out but there is considerable sensitivity to errors as larger depths are

explored. One can see from the nature of the velocity function that slight errors can cause gross variations in interval velocities. Handling these errors is the trick of stabilizing the solution and requires constraints which are often based on understanding the physical setting from where the data are acquired with GPR velocities less than 0.033 m/ns are highly unlikely and greater than 0.3 m/ns impossible. Care should be exercised when using the Dix analysis outputs.

9.11.3 Direct Air Wave & Ground Wave

Unlike seismic applications, GPR quite often has two other events on the CMP record which are strong signals, namely, the direct air wave and the direct ground wave. Both these waves run parallel to the air-ground interface and arrive with zero offset times of zero. When carrying out semblance analysis $S(w,t)$ will often show maxima at $(v_1,0)$ and $(c,0)$ where c is the speed of light. Sometimes the semblance processing will mute these events out.

This information is not used in the Dix analysis, but the direct ground wave event which yields at maximum at $(v_1,0)$ can corroborate the velocity determined for the first layer of the stack.

Often a thin veneer of higher velocity material may be present near surface and the reflection from this horizon merges with the direct ground wave such that it is not resolvable in the $t^2 - x^2$ analysis. In this case, the velocity value obtained for the direct ground wave may be more representative at very shallow depths than that which is derived from the first reflection interval velocity which is averaging a thicker zone.

9.11.4 Summary

The preceding has been a quick overview of transforming CMP data into velocity versus depth. The Dix style analysis and seismic is directly applicable to GPR as these above results show.

Using this type of analysis the interpreter should be cautious about over interpreting interval velocities and thicknesses as errors can arise in unpeeling the layered earth stack.

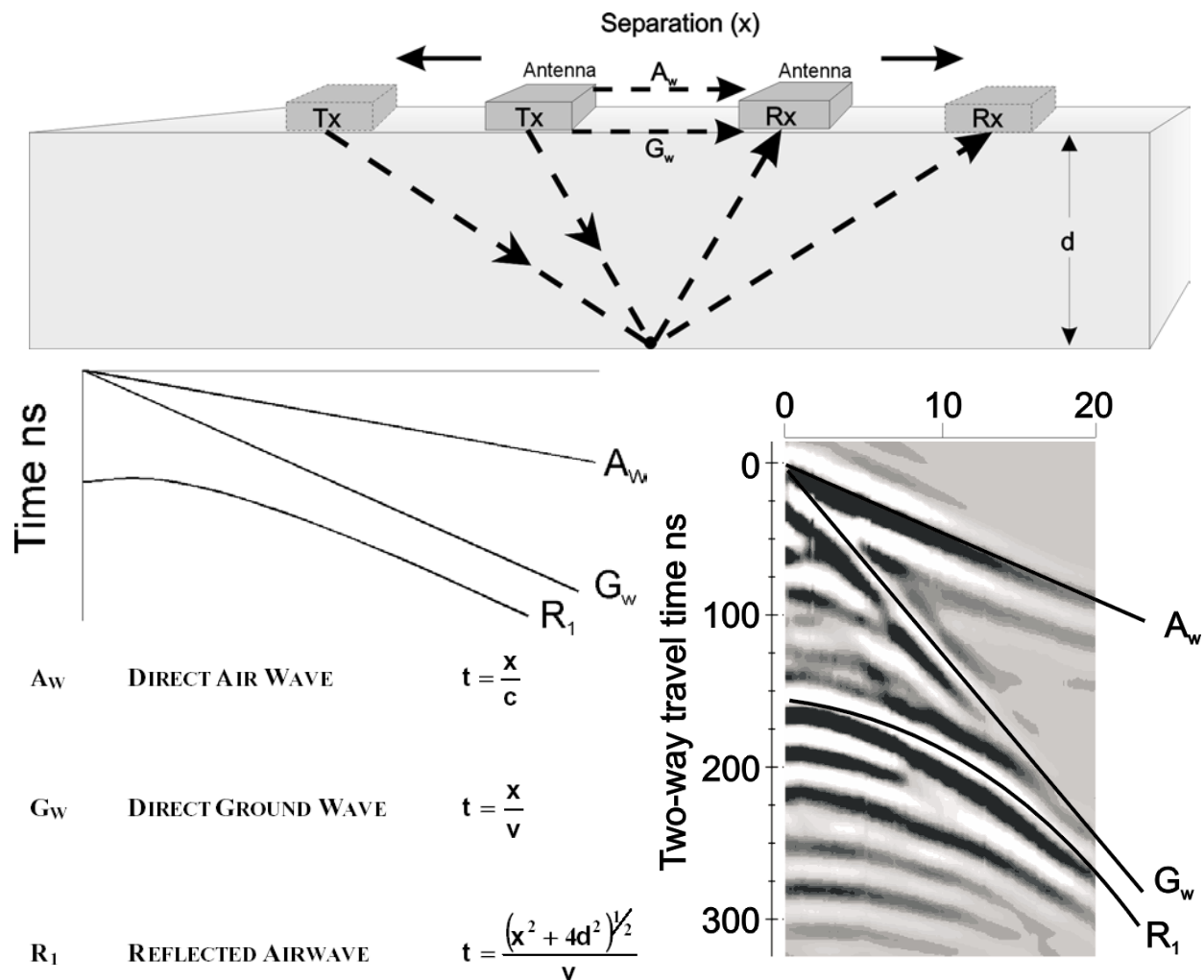
9.12 CMP Analysis

VELOCITY MEASUREMENT

Ground penetrating radar (GPR) measures the time for signals to transmit to and from a target. The target depth or distance is determined by multiplying travel time by velocity in the host material, which is frequently unknown. Common mid-point (CMP) soundings are used to measure velocity and hence translate regular GPR time observations into reliable depth estimates.

The below illustration show how a CMP measurement is made and the principles of how radar signal arrivals are used to estimate velocity. Signals can follow a variety of paths from the transmitter (Tx) to the receiver (Rx). In a CMP sounding the antenna geometry is varied in a controlled fashion so that signal arrival times follow predictable mathematical forms enabling velocity estimation.

In the below example, the arrival time of A_w with distance confirms the speed of light, c , to be 0.3 m/ns while G_w and R_1 indicate ground velocity, v , is 0.1 m/ns.



10 CASE STUDIES

10.1 MINING & QUARRYING

ANISOTROPY IN COAL

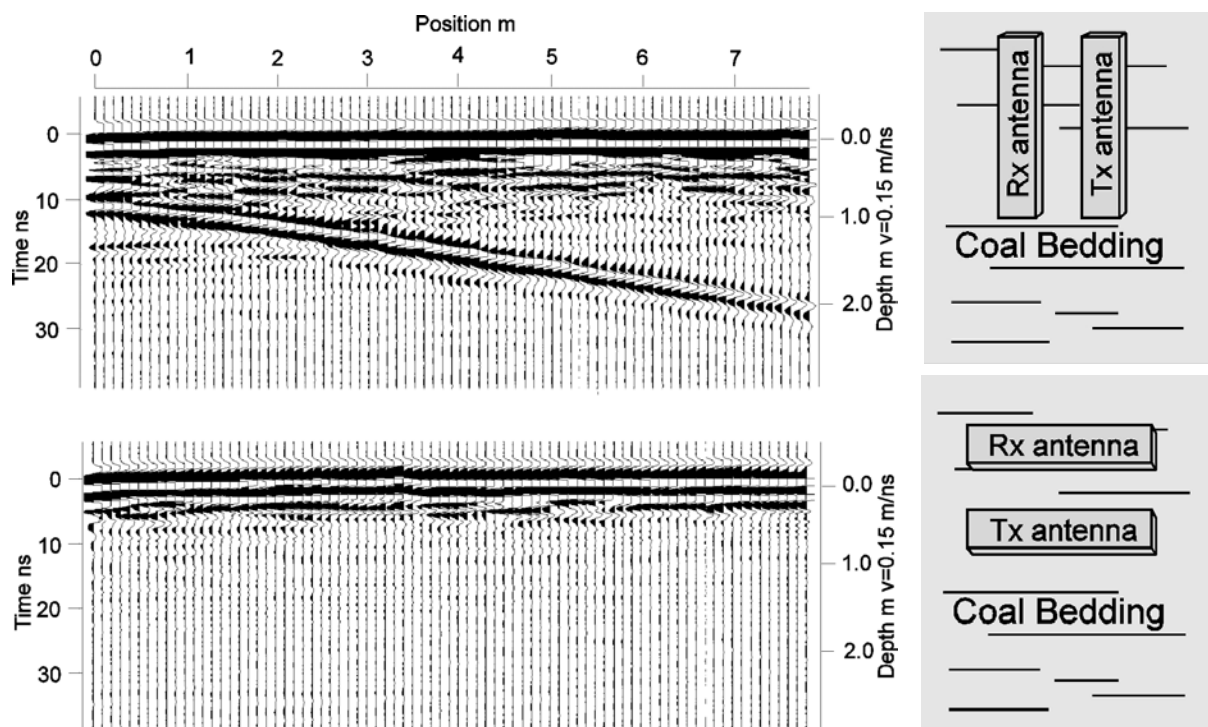
Interest in the use of ground penetrating radar (GPR) for coal mining is widespread. Coal is frequently transparent to radio wave signals and GPR enables mine engineers to quickly and easily locate and avoid potential problems, such as pockets of methane gas, preventing accidents. GPR is also used to map unstable roof conditions.

While coal can be extremely transparent to GPR signals, it is important to realize that coal often has a grain much like wood, and only produces results when surveys are conducted "against the grain". This study demonstrates the extreme effects of antenna orientation on GPR measurements in coal.

The two data sets below were acquired using a pulseEKKO GPR system with 450 MHz antennas, with two antenna orientations. The first data set was collected with the antennas running perpendicular to the coal seam (against the coal grain). This approach proves successful as the data show a strong return from an adjacent entry. The second survey was conducted with the antennas parallel to the coal seam. With this antenna orientation GPR does not detect the entry or define any features in the coal.

These highly varied results from using different antenna orientations are a valuable lesson in effective use of GPR in coal mining applications. This study demonstrates the effectiveness of GPR for coal mapping and indicates how to prevent time loss and undesirable results due to using the improper survey procedure.

Data compliments of United States Bureau of Mining, Pittsburgh, USA Fracture Mapping



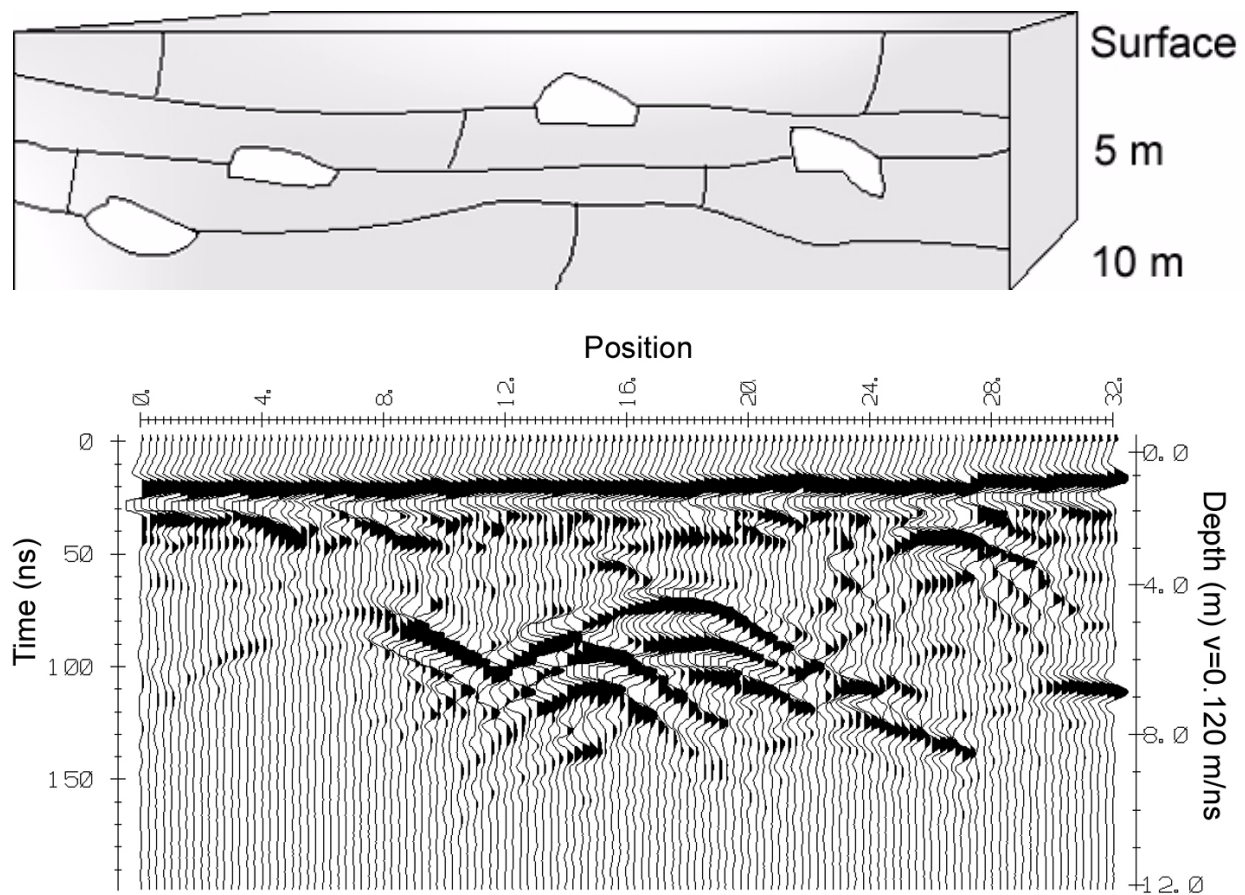
LIMESTONE CAVITIES

Ground penetrating radar (GPR) is frequently used to detect cavities in rock for construction planning. Limestones are transparent to GPR signals and the karstic cavities (filled with air or water) common in limestone give strong radar return signals.

At a building site in Italy, located on cavity prone limestone, the geotechnical planning necessitated locating cavity formations before building construction could begin. The data below were acquired using a pulseEKKO GPR system with 100 MHz antennas. The data clearly indicates open cavities one to two meters in diameter located throughout the limestone to a maximum detection range of eight meters.

Following the survey, excavation work confirmed the radar interpretations. This information enabled the site engineer to adapt construction accordingly, avoiding mishaps due to building on weakened limestone.

Data compliments of IGS, Italy.



GRANITE QUARRY MAPPING

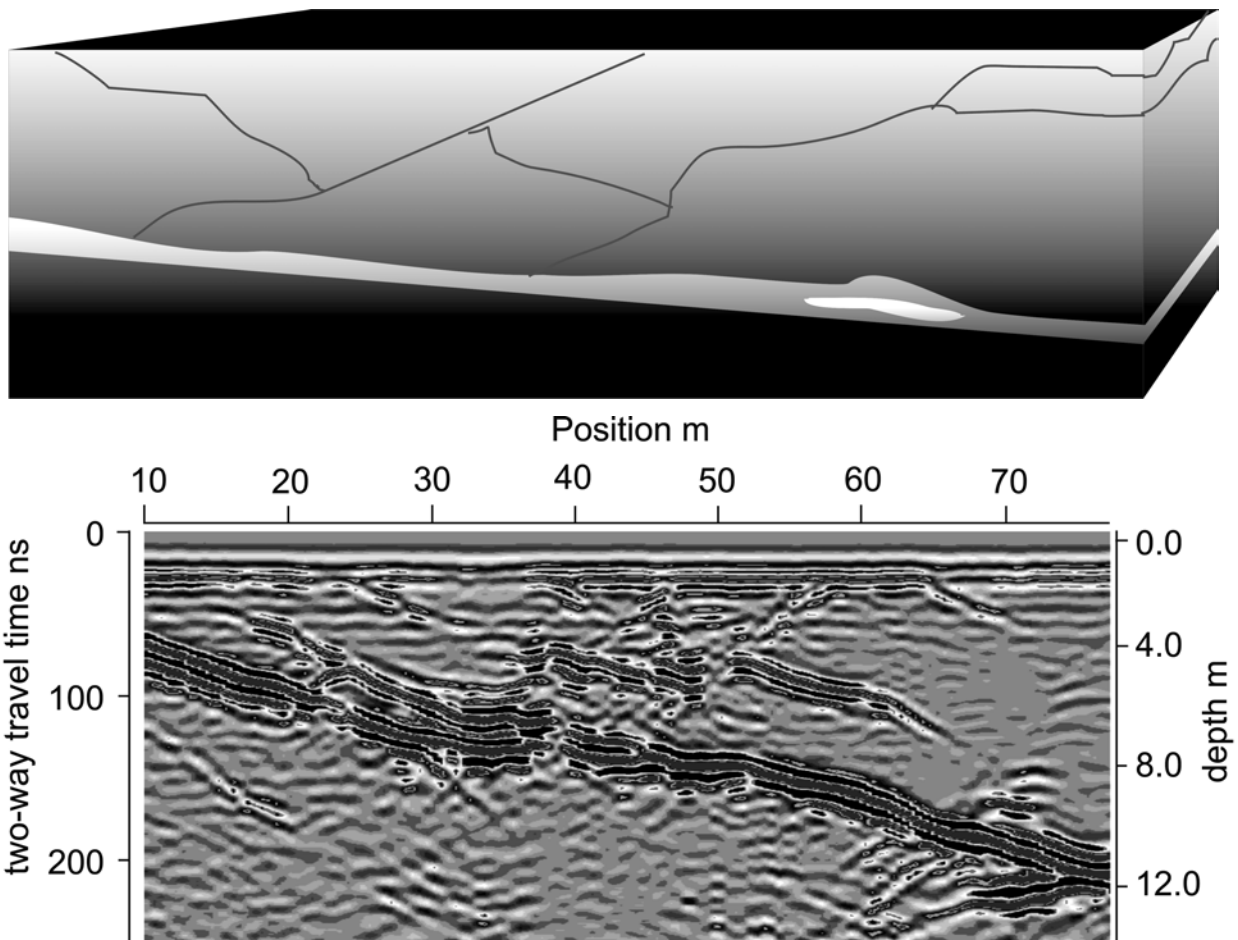
Efficient rock quarry operations require extensive knowledge of the rock conditions within a site.

Granite quarry sites are frequently mapped using ground penetrating radar (GPR) systems. GPR detects bedding planes, fractures and variations in rock type which help rock mechanic engineers plan and expedite extraction.

A pulseEKKO GPR system with 100 MHz antennas was used in this case to quickly and efficiently obtain data. The data set shown below clearly identifies a major fracture in the rock to a depth over 12 meters. Minor cross jointing is also visible in this section. These data were acquired in winter when the surface was covered by two meters of snow.

Following the survey the granite was successfully extracted using information from the GPR data collected. The data clearly identified optimal locations to mine, making granite block extraction more dependable and predictable.

Data compliments of multiVIEW Geoservices Inc.



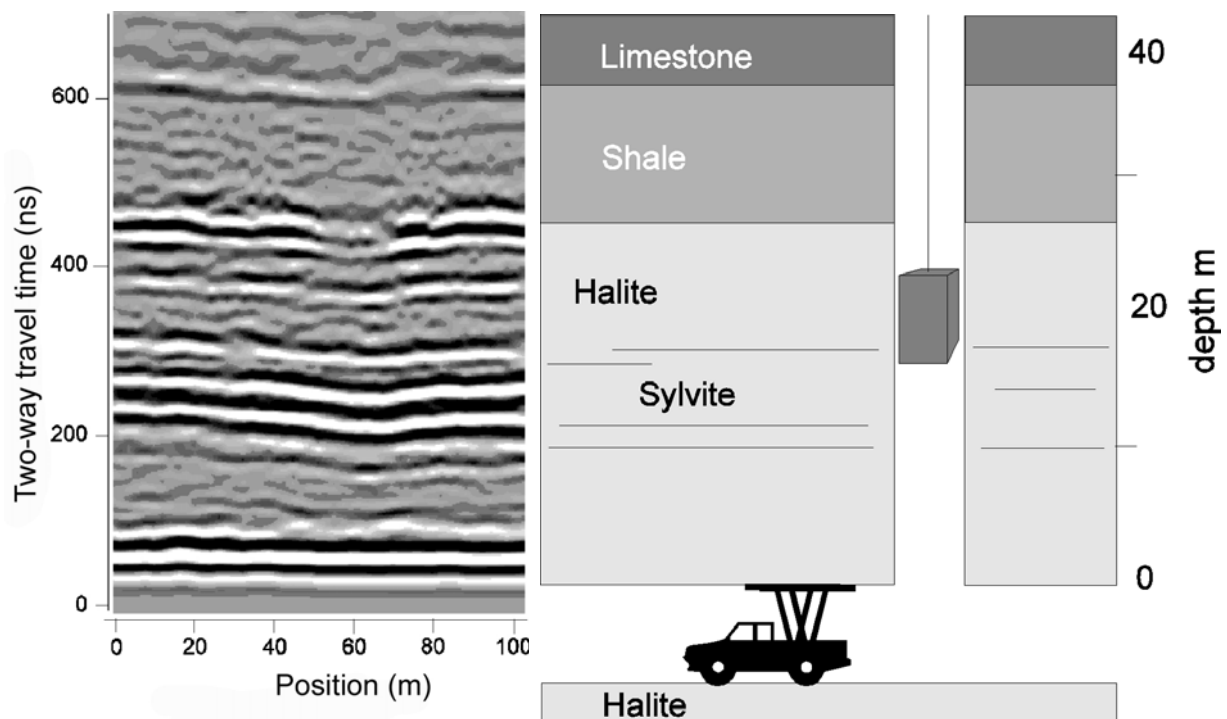
POTASH MINE SAFETY

Ground penetrating radar (GPR) is a powerful tool for mapping mine geology. GPR can define geology in all directions around underground structures and help assess rock mass stability. The study demonstrates the efficiency of GPR for this application.

In potash mines in Saskatchewan, Canada, mining engineers regularly need to measure the thickness of salt over the mine entries and whether or not water is present in the salt formations. If major geological deformations occur, mining is not viable. A pulseEKKO GPR system with 100 MHz antennas was used by the crew to survey the mine roof using a mechanical arm to hold the antennas on the back. The data show that the geology in this section of the mine is fairly flat-lying, indicating the area is stable for mining activity.

GPR saves development time and ensures that mining areas are safe and viable.

Data compliments of Potash Corporation of Saskatchewan, Canada

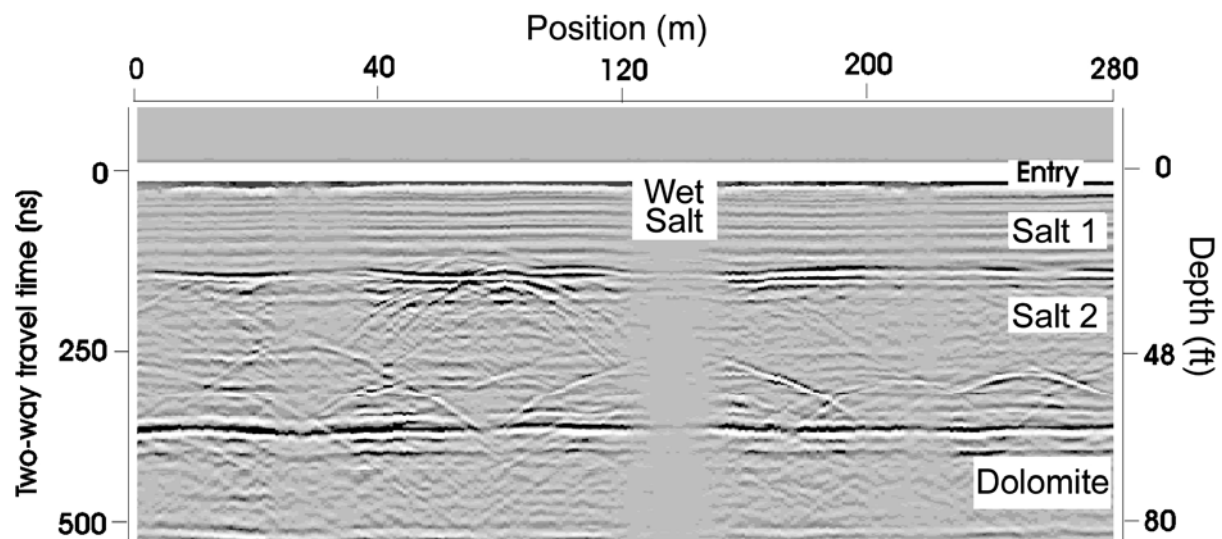


SALT MINE GEOLOGY

Salt mines are usually located where geologic strata are flat lying or gently sloping. Mining operations are often not viable if major geological deformations occur so mine production engineers require rapid methods to map the geological structure ahead of mining.

Ground penetrating radar (GPR) systems have been used for this purpose in salt and potash mines globally. The below data are from a mine located in southwestern Ontario, Canada. Salt is mined at a depth of 1760 feet below ground. Normal practice involves removing 48 feet (18 m) of salt below the mining level.

The section shown was acquired in less than 15 minutes and the ground conditions could be monitored by mine personnel throughout the surveying operation. The data were collected using a pulseEKKO 100 system with 100 MHz antennas.



100 MHz pulseEKKO radar survey data along an entry floor in a salt mine in Southwestern Ontario, Canada. The boundary of interest is the contact between the salt and a water bearing dolomite at a depth of 62 feet (19 m). The continuity of reflectors within the formation indicate that the area will be suitable for mining.

10.2 GEOTECHNICAL & ENVIRONMENTAL

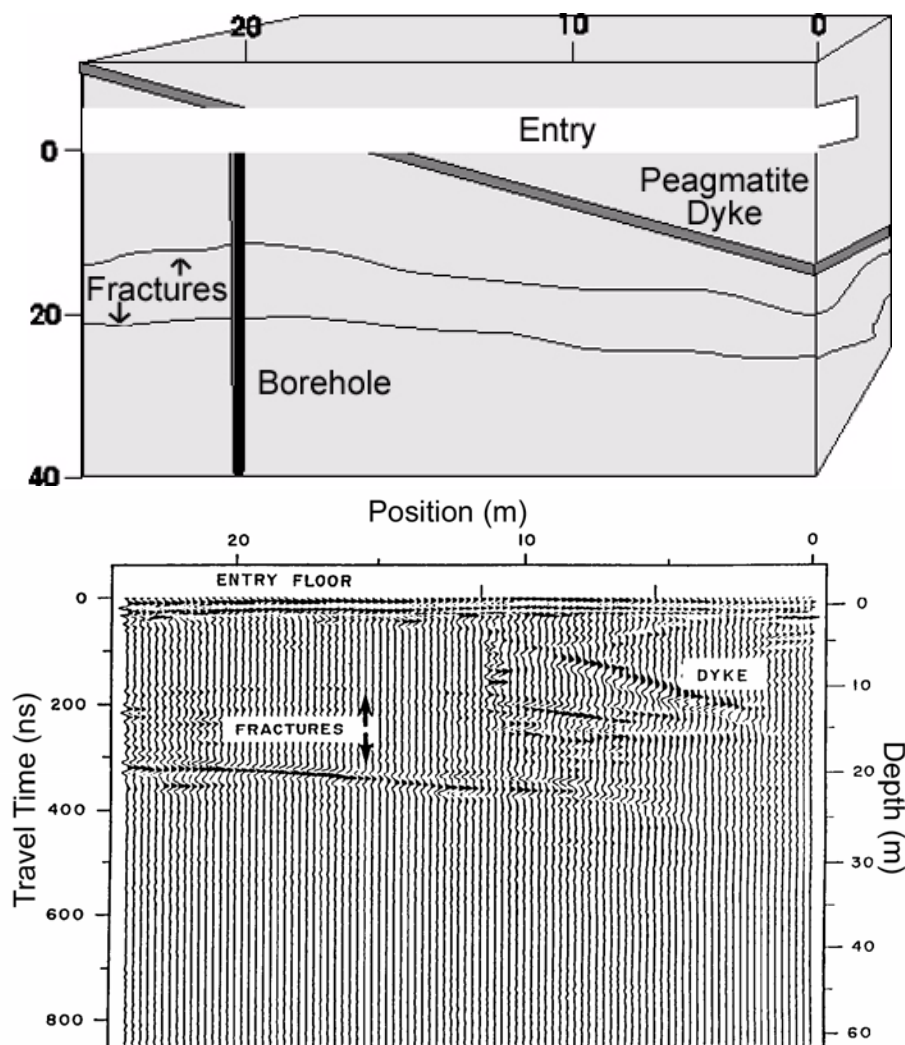
FRACTURE MAPPING

Ground penetrating radar (GPR) is regularly used to survey potential underground nuclear waste storage sites. Government and nuclear agencies worldwide seek to determine the feasibility of storing hazardous nuclear bi-products in bedrock.

This study was conducted at an underground research laboratory operated by Atomic Energy of Canada. The survey was aimed at identifying suitable locations for storing the nuclear waste at this site, without fear of extensive leaching through fractures should a leak occur.

The below data were obtained using a pulseEKKO GPR system with a 50 MHz antenna along a 25 meter survey line in an underground entry.

Following the GPR survey, it was determined that the site was not viable for nuclear waste storage. The GPR survey located water bearing fractures in the granite, making the site unsuitable as leaching could occur.



MINE SHAFT DETECTION

Ground penetrating radar (GPR) is often used to determine whether or not shallow mining activity has taken place.

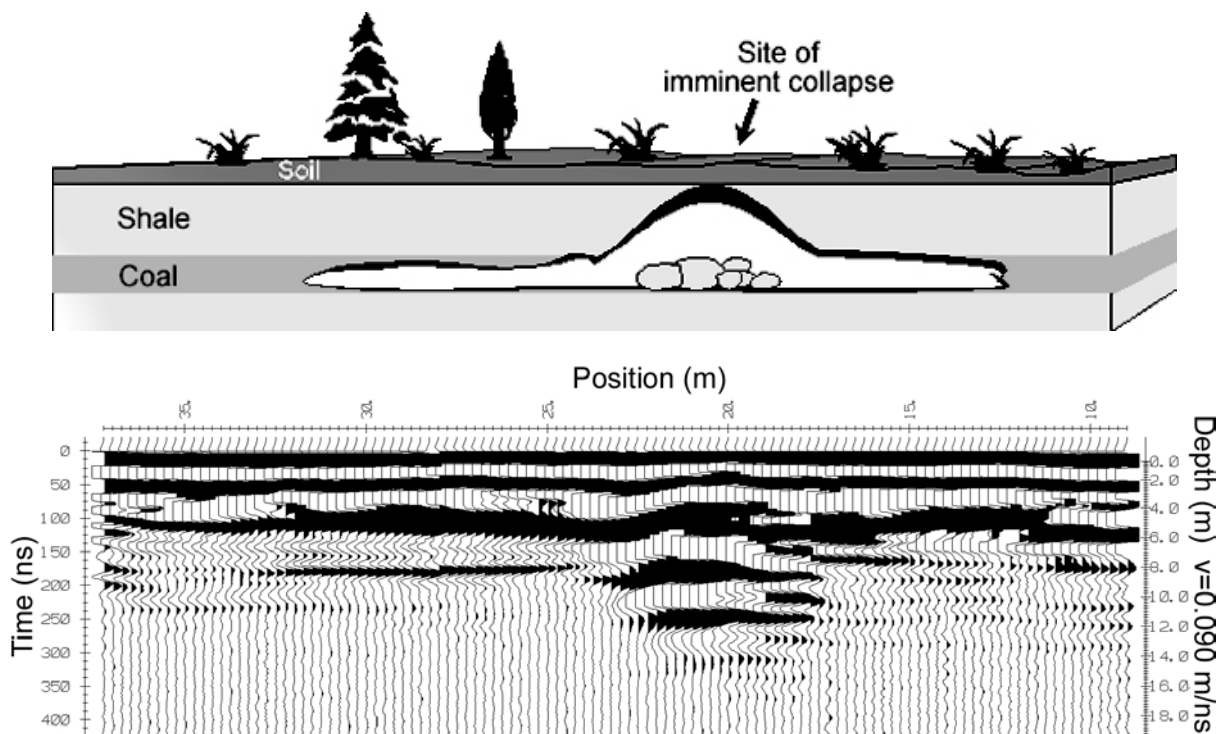
This study was conducted near Nottingham, England, in a three acre parcel of land with a known coal seam located subsurface. The objective was to determine if any mining activity had occurred in the coal seam.

A pulseEKKO GPR system was used with a 50 MHz antenna to survey this area. The system quickly and easily collected the below section.

Although surface topography and mining records show no indication that the coal has been worked, the data indicates otherwise. The major disturbance at 21 meters is generated by an old shaft leading down to the coal seam.

The subsurface disturbance determined by the GPR survey defines hazardous ground below the entry, and localizes the site of imminent collapse.

Data compliments of Structure Testing Services (UK) Ltd.



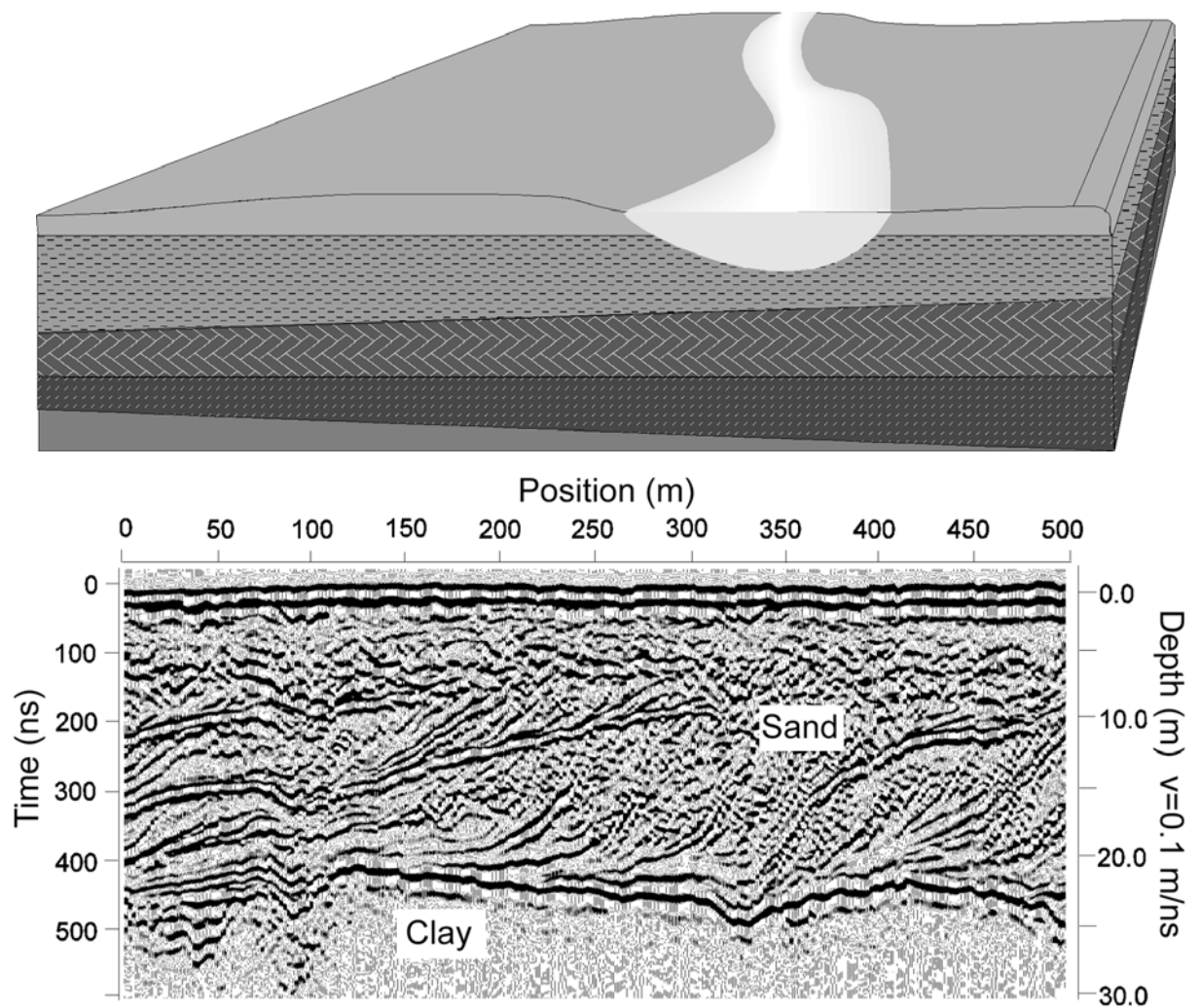
GEOLOGICAL STRATIGRAPHY

A major application of ground penetrating radar (GPR) is mapping geologic depositional history. This new advancement enables geologists to relate current stratigraphy formation to that of older deposits. This study was conducted to determine the effectiveness of GPR in defining depositional history.

A pulseEKKO GPR system with 50 MHz antennas was used to quickly and accurately survey the William River Delta on the southern shores of Lake Athabaska, Saskatchewan, Canada. The data clearly detect and display numerous depositional layers, erosional unconformities, and cross bedding.

This important application of GPR provides valuable insight to geologists studying groundwater flow, contaminant transport, as well as petroleum engineers dealing with similar geologic conditions in reservoir rocks at greater depths.

Data compliments of University of Calgary, Department of Geography.



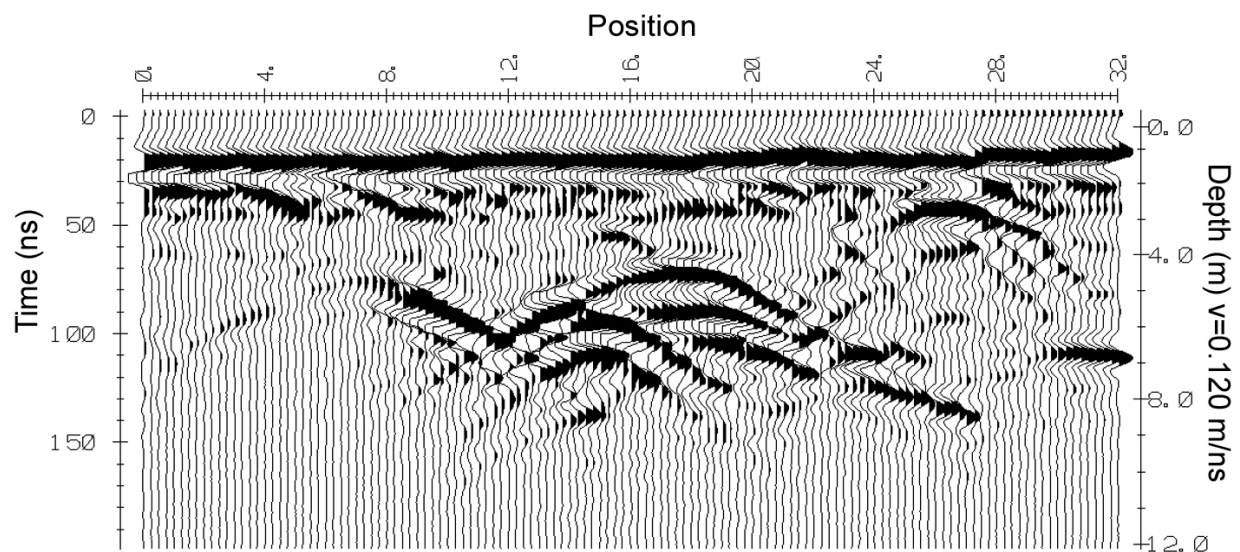
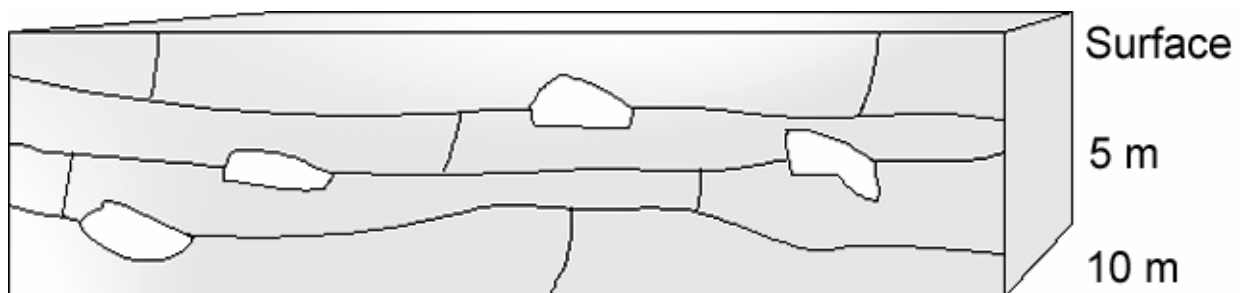
LIMESTONE CAVITIES

Ground penetrating radar (GPR) is frequently used to detect cavities in rock for construction planning. Limestones are transparent to GPR signals and the karstic cavities (filled with air or water) common in limestone give strong radar return signals.

At a building site in Italy, located on cavity prone limestone, the geotechnical planning necessitated locating cavity formations before building construction could begin. The data below were acquired using a pulseEKKO GPR system with 100 MHz antennas. The data clearly indicates open cavities one to two meters in diameter located throughout the limestone to a maximum detection range of eight meters.

Following the survey, excavation work confirmed the radar interpretations. This information enabled the site engineer to adapt construction accordingly, avoiding mishaps due to building on weakened limestone.

Data compliments of IGS, Italy.

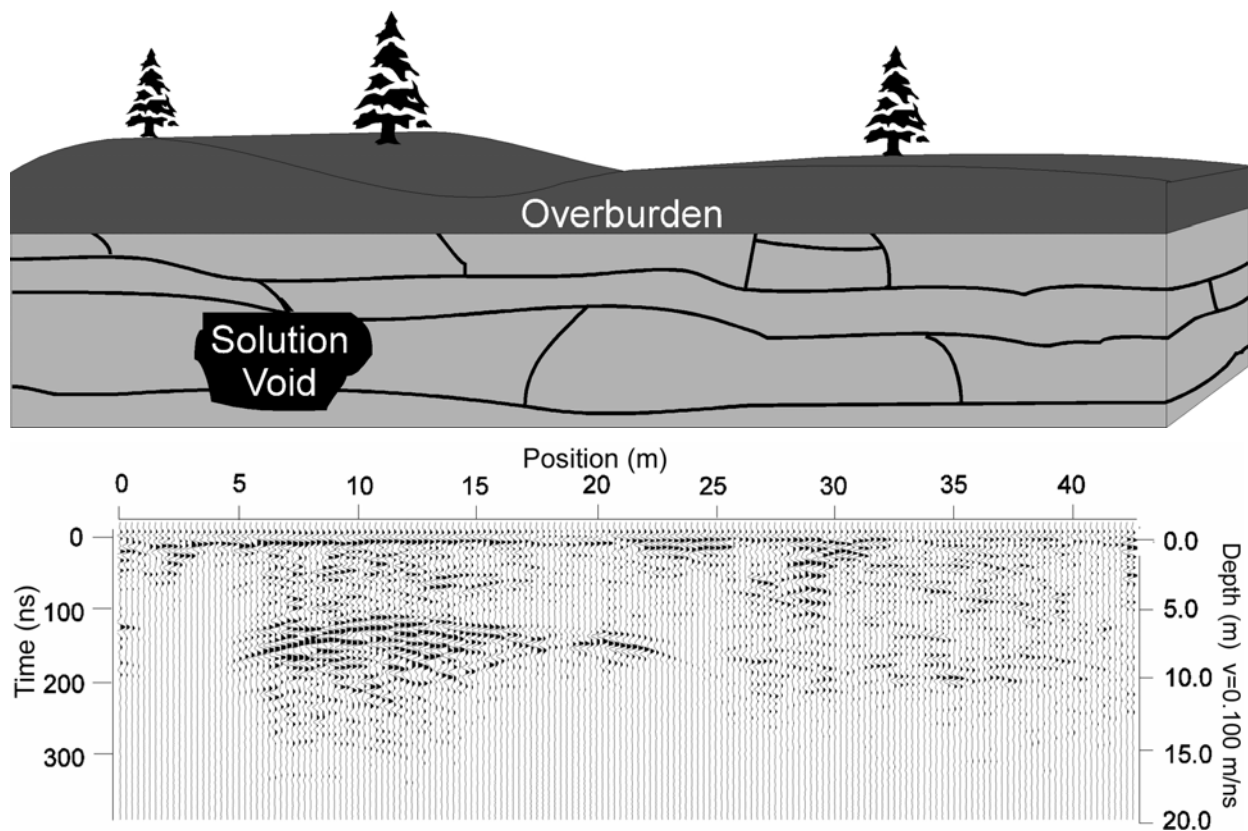


GEOLOGIC HAZARDS

Sink hole development can be hazardous particularly in residential areas. Sink holes commonly form in areas underlain by limestone containing cavities; such limestone is called karstic limestone. The cavities form when groundwater flow dissolves and washes away parts of the limestone and can grow until they reach the surface causing sink holes.

Ground penetrating radar (GPR) provides a quick and easy means of imaging karst features. GPR data often aid in construction and rehabilitation of roads and buildings by providing advanced warning of hazardous situations.

This GPR survey was conducted in a residential area where a surface collapse had recently occurred. One resident was concerned that his home was in danger, and wanted to know if a collapse was imminent near his house. A pulseEKKO GPR system with 100 MHz antennas was used to quickly and accurately map subsurface conditions. The survey indicated that there was no problem near the house but located a cavity about five meters below the surface in the backyard.



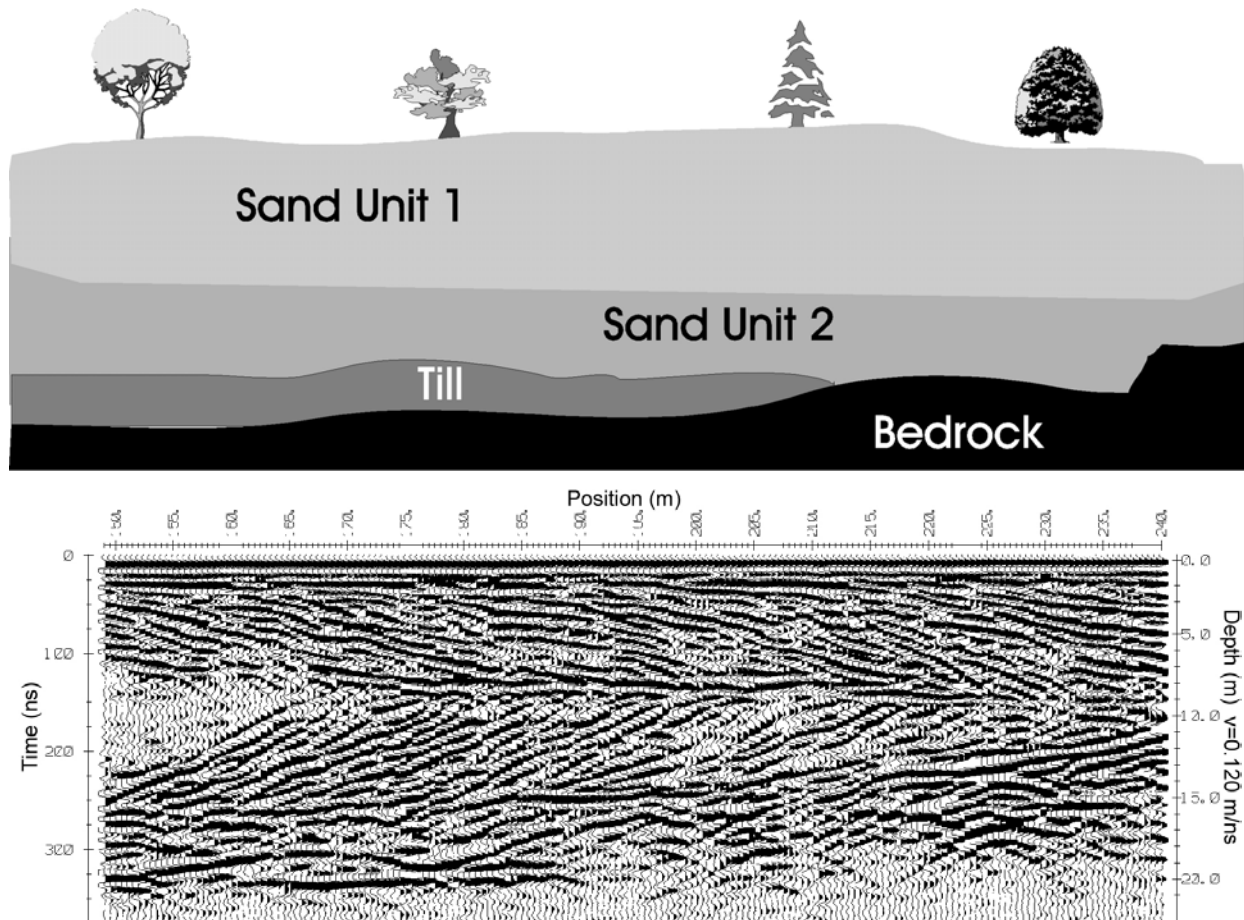
OVERBURDEN STRATIGRAPHY

Ground penetrating radar (GPR) systems are used worldwide to delineate soil stratigraphy and determine depth to bedrock for engineering purposes. Applications include road, rail and pipeline design as well as engineering planning for expansion of dam sites and buildings.

This study was conducted in an area of glacial outwash sand and gravel deposits near Marathon, Ontario, Canada. The survey objective was to determine the overburden stratigraphy at the site of a pulp and paper mill slated for expansion. A pulseEKKO GPR system with 100 MHz antennas was used. The system was operated in winter weather conditions by a two person crew.

The information obtained from the GPR survey facilitated locating and construction designs for the pulp and paper mill waste water storage area.

Data compliments of multiVIEW Geoservices Inc.



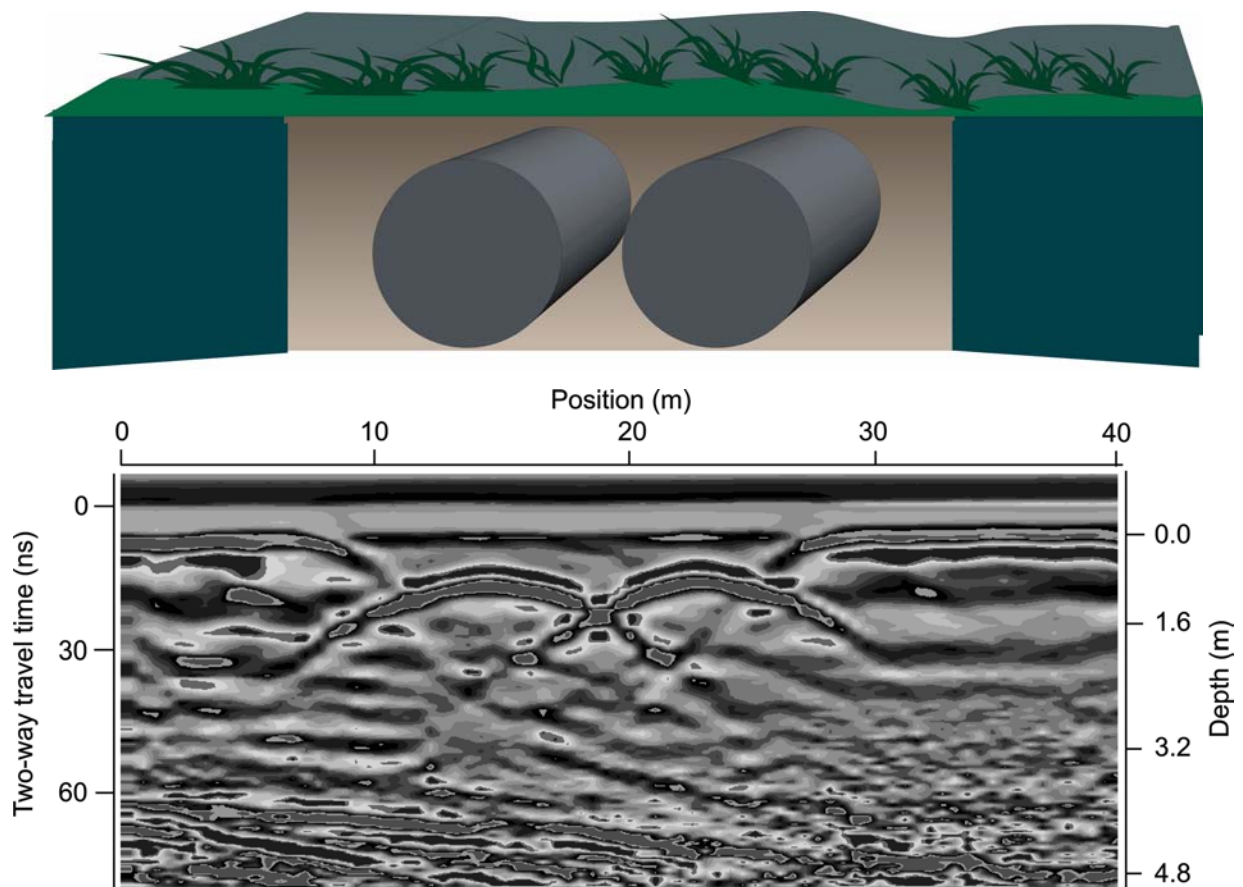
DETECTION OF BURIED TANKS

Ground penetrating radar (GPR) systems are often used to find buried tanks. Environmental concerns and avoiding construction surprises necessitate locating USTs (underground storage tanks) before engineering site work commences.

A GPR system was used here to find the exact position of tanks, without disturbing the soil above. GPR provides a safe, quick and non-destructive means to find buried materials without putting crews at risk of contamination.

The data were collected using a pulseEKKO system with 200 MHz antennas.

Data compliments of A-Cubed Inc.



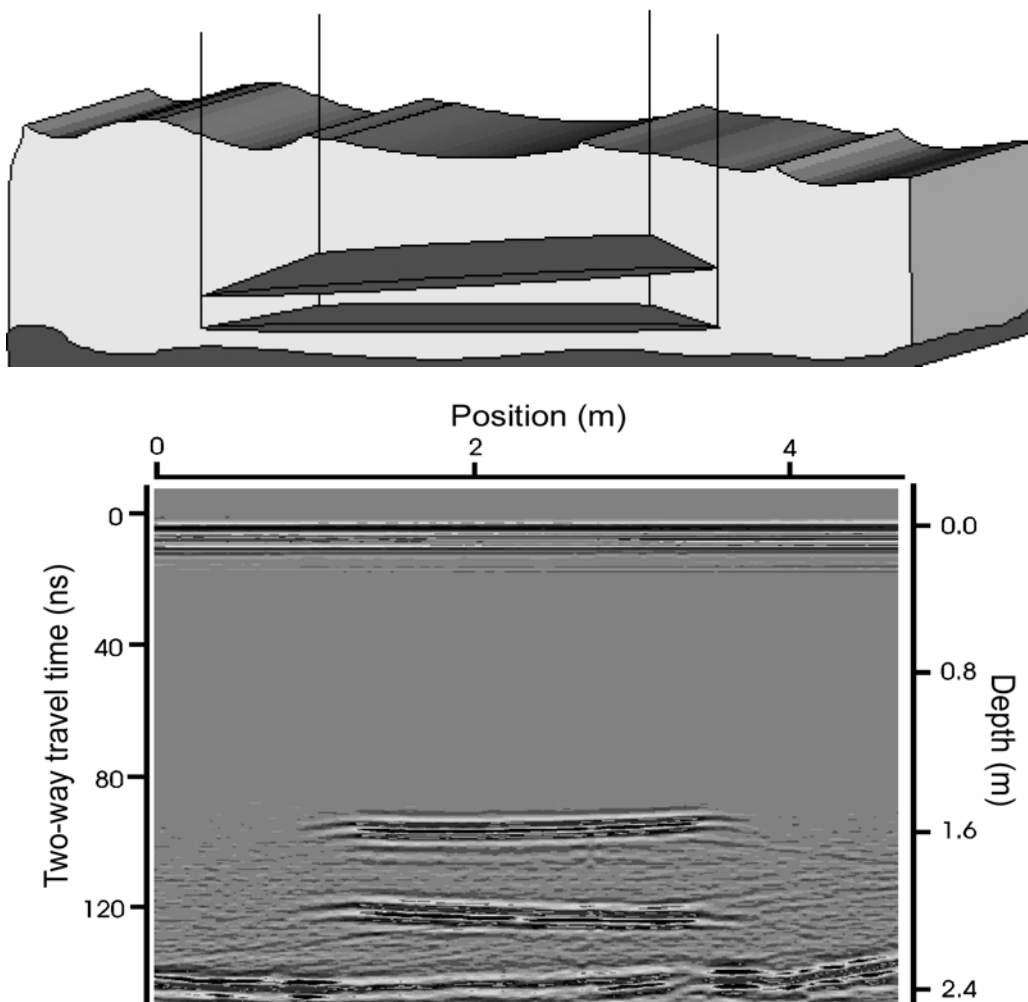
UNDERWATER MAPPING

Ground penetrating radar (GPR) technology can easily penetrate freshwater and map objects below the surface. This new application of GPR technology can reduce the use of conventional underwater mapping methods, which are inefficient in shallow water.

This experiment was conducted at Cornell university to test the efficiency of GPR in mapping objects underwater. A pulseEKKO 1000 GPR system with 450 MHz antennas was used to locate two small plates suspended at 150 and 190 cm below the water surface. The plates were suspended from a raft at different angles, and the survey was performed on the raft. The GPR system successfully and accurately located the 6 mm thick plates, and also located the river bottom at the correct depth.

The success of this experiment proves that GPR is not only a viable means of mapping underwater objects, but is also faster and more reliable than conventional methods for shallow freshwater lakes and rivers. This new underwater capability expands the applications of GPR to include pipeline locating, police investigations, environmental investigations, and treasure mapping.

Data compliments of Cornell University, Department of Agriculture & Biological Engineering, USA



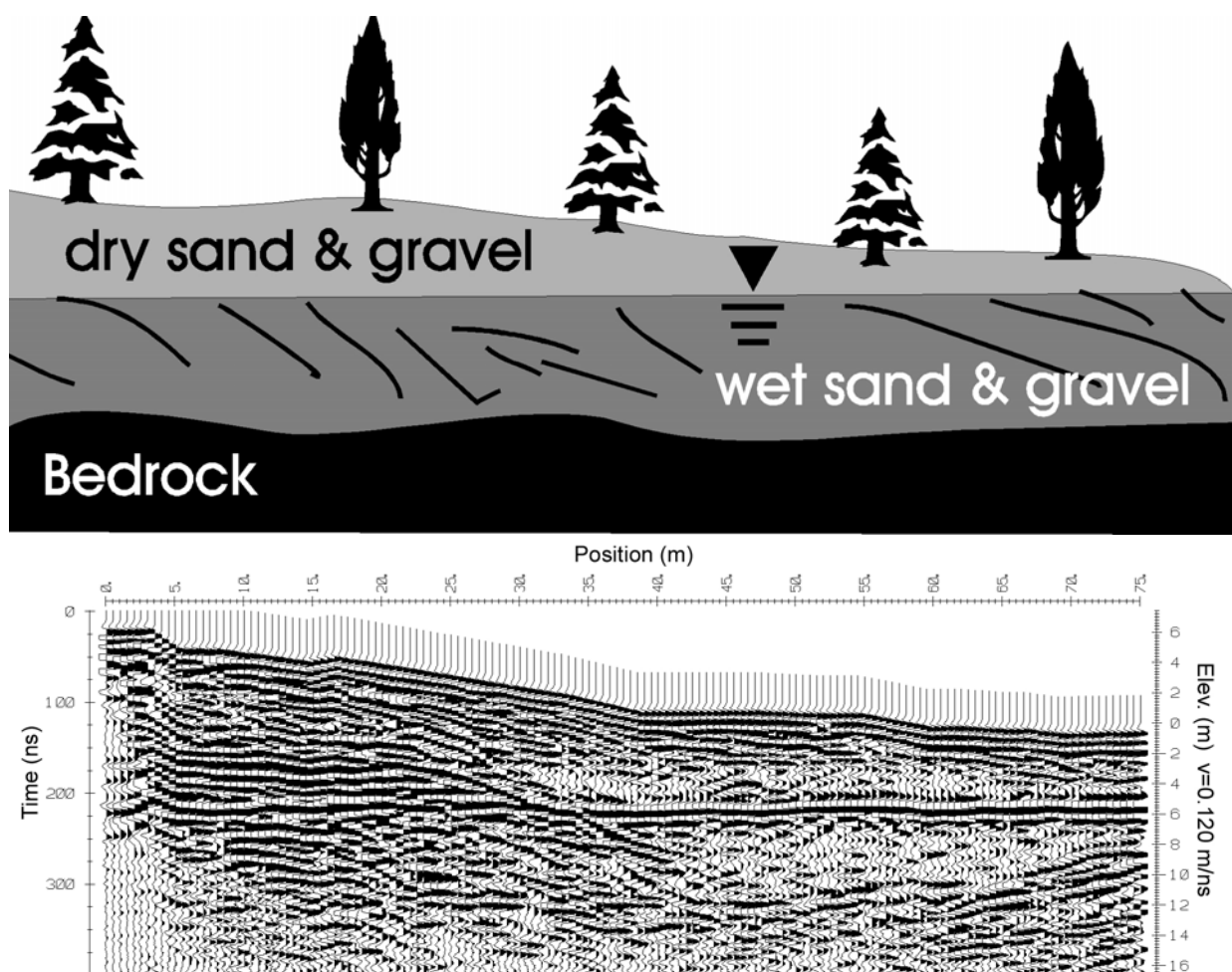
WATER TABLE MAPPING

Ground penetrating radar (GPR) can efficiently map groundwater conditions and benefits for groundwater and contaminant hydrogeology studies.

This survey was conducted near Lake Superior in Ontario, Canada, when planning an expansion of a pulp and paper mill. A pulseEKKO GPR system was used with 100 MHz antennas to accurately map the groundwater conditions and the depth to bedrock.

The information obtained from the survey allowed the engineers to select optimal sites for the waste water lagoons minimizing the risk of toxic chemicals leaking into surrounding groundwater.

Data compliments of multiVIEW Geoservices Inc.



100 MHz radar data mapping water table and bedrock is glacial sand and gravel deposits.

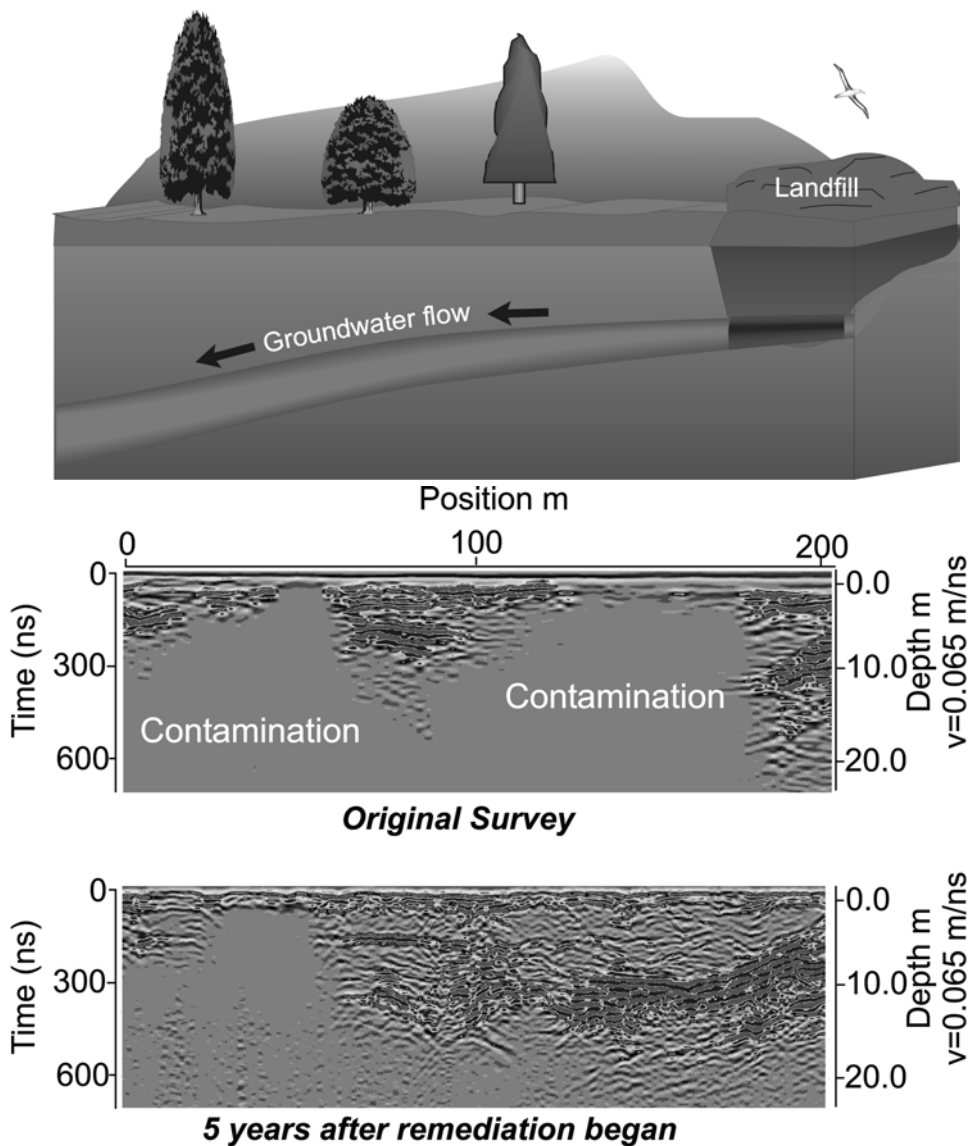
CONTAMINATED GROUNDWATER

Ground penetrating radar (GPR) provides a powerful means of monitoring the remediation of contaminated groundwater caused by salts or leachates, hydrocarbons or other organic materials.

This pulseEKKO GPR survey was conducted near a municipal landfill site in Ontario, Canada. Contaminants leaching from the landfill are transported by groundwater flow to a nearby stream. Knowing the lateral extent and depth of contamination ensures optimal installation of monitoring and remediation wells.

A pulseEKKO GPR system using 50 MHz antennas determined the extent of contamination, which is indicated by the absence of signals on the first data set above.

Repeated at time intervals, GPR surveys allow the impact of remediation measures to be monitored. As shown in the lower data set, this site remediation was quite successful. After five years some areas initially opaque to GPR signals have become transparent.



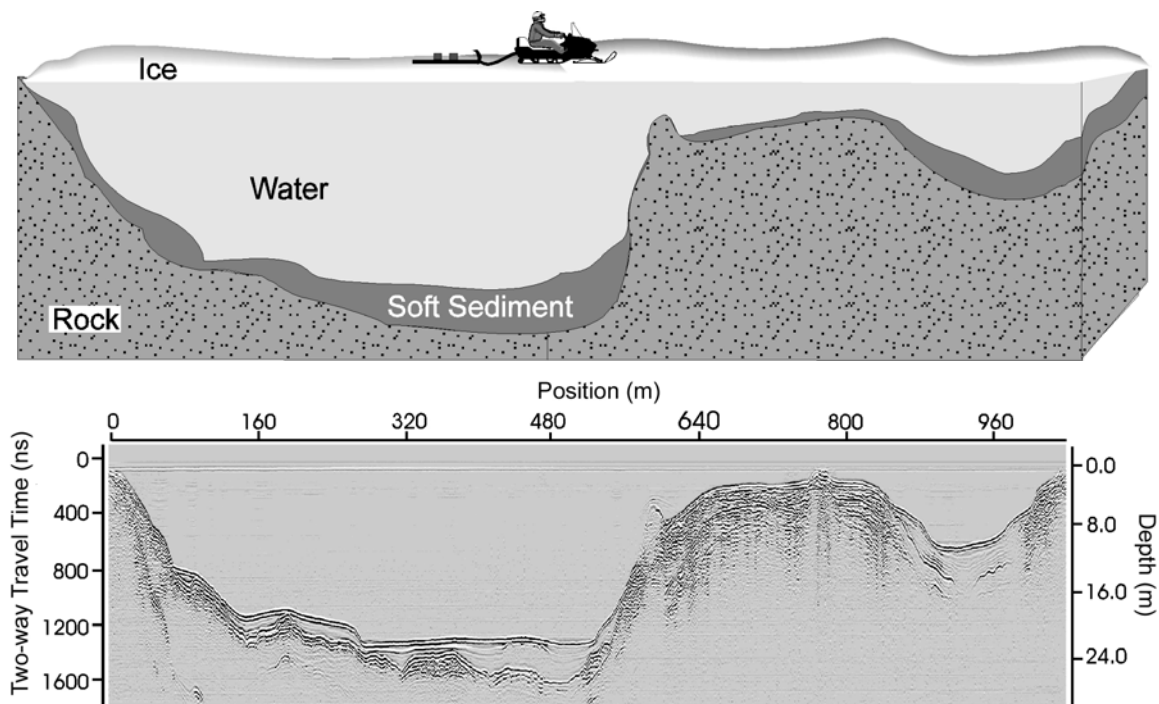
BATHYMETRY & SUB-BOTTOM PROFILING

Ground penetrating radar (GPR) is frequently used for mapping water depth and sub-bottom stratigraphy in freshwater lakes and rivers. Surveys are usually conducted from boats or rafts. In areas where open water freezes, surveys can be carried out through the ice.

This study was performed on a lake in Northern Saskatchewan in conjunction with site surveys for uranium mine development. The measurements were made using a pulseEKKO GPR system with 50 MHz antennas. The pulseEKKO GPR system was mounted on a sled and towed by a skidoo which facilitated rapid reconnaissance work.

The above section shows the soft sediment to rock boundary. This information was used to locate optimal areas to deposit mine tailings.

Data compliments of Cigar Lake Mining Corporation & Golder Associates Ltd., Canada



THE NOGGIN GOES SWIMMING

A Noggin 250 recently undertook a waterborne survey. Although the mode of operation is not what we normally recommend for our Noggin products, the results were quite impressive. Noggin systems are designed to be very water resistant but they are not truly designed for submersion.

At a site in Oregon, Brian Herridge of 3Dgeophysics.com and Scott Mills from GeoDesign of Portland, Oregon, were confident GPR could image bottom stratigraphy in the Umqua River.

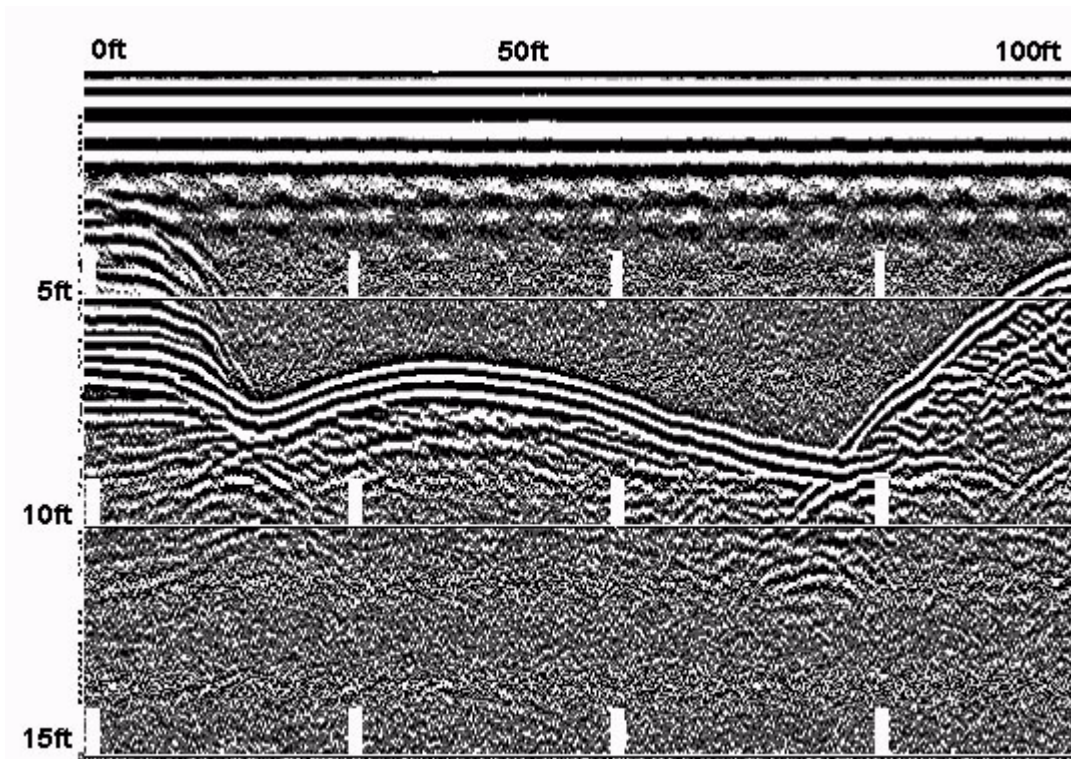
Information about the bottom stratigraphy was necessary as part of a geotechnical design project to be undertaken by Brown and Caldwell and GeoDesign. Using GPR provided a more environmentally friendly and lower cost solution than drilling.



The Noggin was placed directly in the water and towed around using a small paddle boat (see picture below). Several lines about 100 feet in length were surveyed with quite spectacular results. An example profile is shown below.

These raw Noggin PCX images show water depth and subsurface stratigraphy to a depth of about 9 feet (3 metres). These results are typical of what can be obtained in freshwater conditions; water is transparent to GPR systems when the total dissolved solids (TDS) are low. As well, the slow speed of radio waves in water gives superb depth resolution.

There are many geotechnical problems which call for imaging water depth and sub-bottom stratigraphy in shallow lakes and rivers. Normally we would recommend putting the Noggin into a small floating boat made of fibreglass, plastic, wood or rubber. The Noggin can sound right through the bottom of the boat structure and see through the water into the sub-bottom. This makes for a very efficient way of carrying out shallow water surveys. Noggins can be used in this way in any number of applications. The Noggin is so simple to deploy, you only need to let your imagination define a potential application and then try it out.



Warning: Noggins will not see through sea (salt) water. The energy from the system is rapidly absorbed and very little penetration will be achieved. Only use Noggins in freshwater with low TDS counts. Contact our professional staff if you have any questions about Noggins and their use in water.

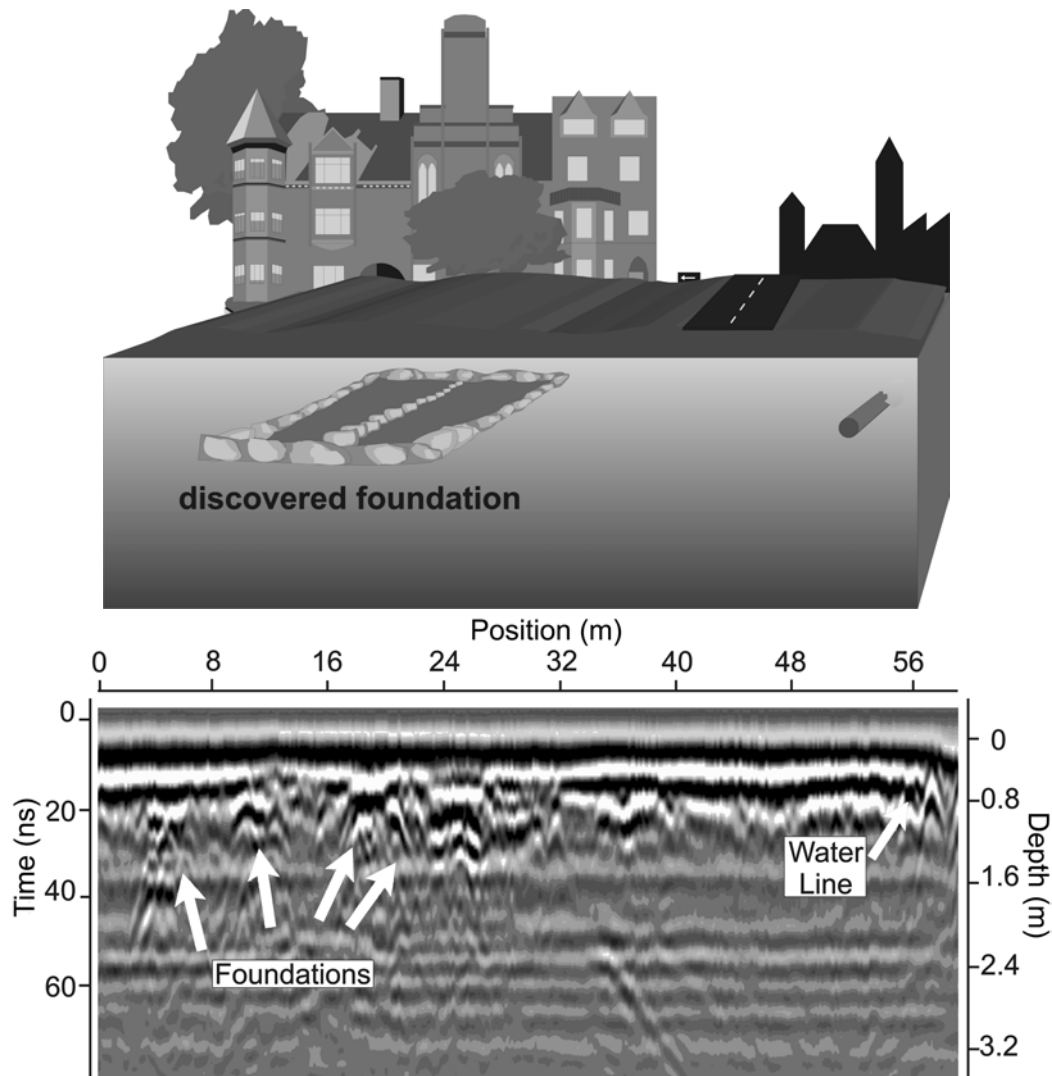
10.3 FORENSIC & ARCHEOLOGY

OLD CATHEDRAL FOUNDATIONS

Archeologists use ground penetrating radar (GPR) to map dig sites because radar anomalies accurately pinpoint hotspots to be investigated. Area surveys provide a powerful means of detecting the extent and shape of buried structures.

This GPR study was conducted in Denmark, where an old cathedral foundation was known to exist underneath the modern city. Parts of the cathedral had been discovered when waterlines were installed, though the extent and location of the foundation remained unknown. A pulseEKKO GPR system with 200 MHz antennas was used to efficiently map the extent and location of the foundation. The data collected clearly show the foundations and also locate the waterline.

The resulting survey information facilitated future city planning to avoid disrupting the historical structure.



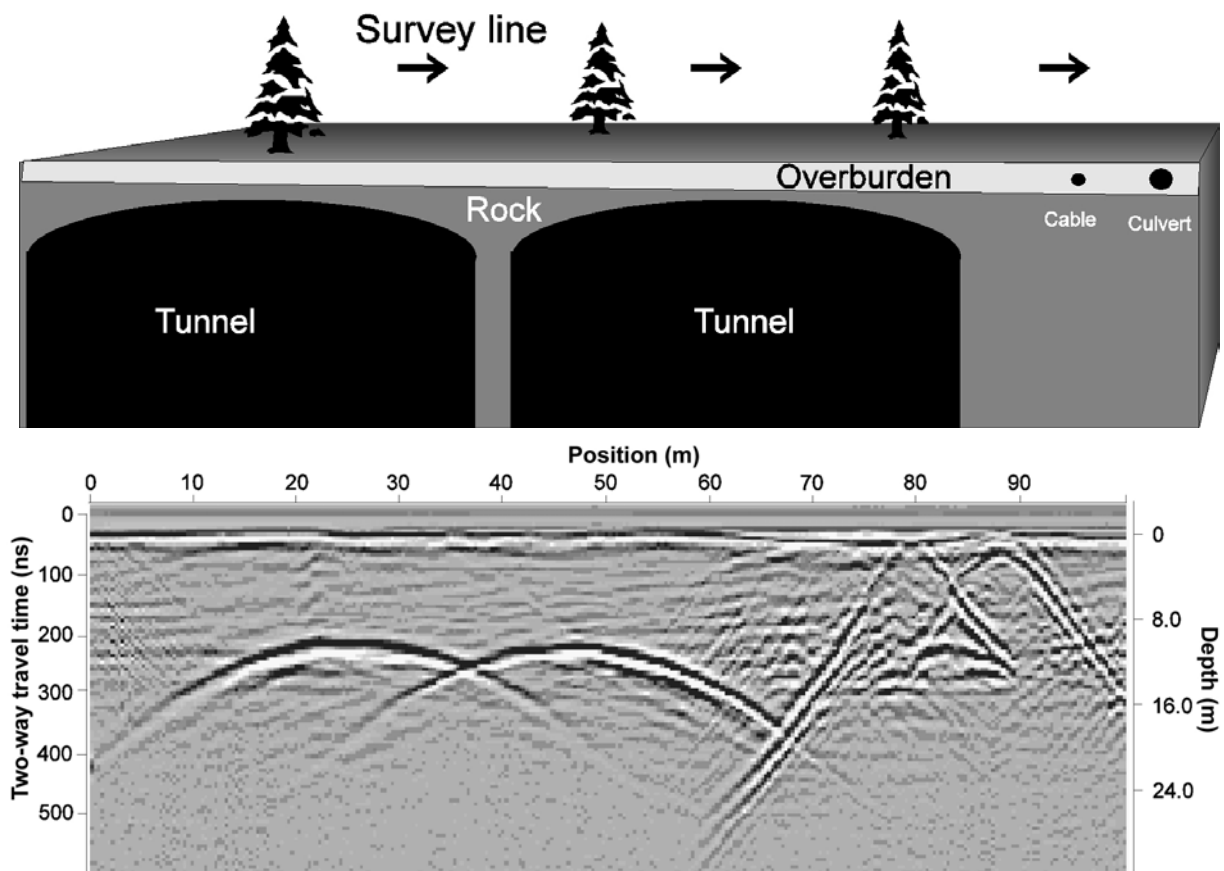
SUBSURFACE STRUCTURE MAPPING

Ground penetrating radar (GPR) provides a powerful means of mapping subsurface structures. Where many existing maps are old and inaccurate, GPR can provide a precise account of utilities, tunnels, pipes and cables, as well as surrounding features. This is important information to have for future planning and development.

The below 50 MHz pulseEKKO results from Sweden accurately locate the tunnels cut in bedrock at 11 meters below surface. A cable and a culvert at one meter depth are also detected. The GPR information indicates minor fracturing in the surrounding bedrock, which is invaluable information for detecting potentially hazardous situations.

The efficiency of GPR subsurface structure mapping is a significant advancement for city planners, civil engineers and developers. It not only informs of existing structures underground, but also warns of potentially hazardous situations enabling proper precautions to be taken before any unwanted situations arise.

Data compliments of TS Geokonsult (Sweden).



Ground penetrating radar clearly locates the two tunnels shown in the diagram, represented by the two arches on the left side of the data set. The two shallower features on the right side are generated by a cable and culvert approximately 1 m deep.

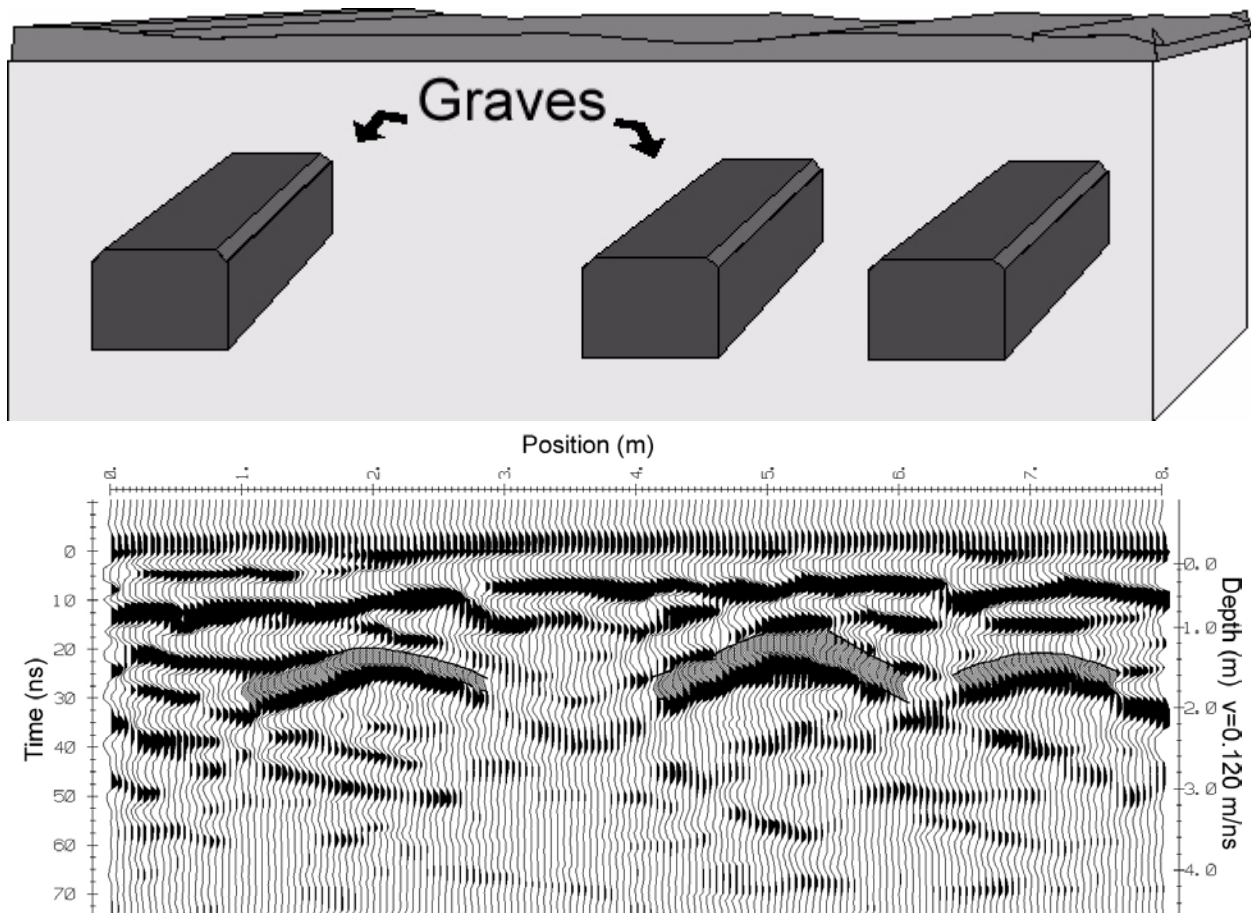
GRAVE LOCATION

Location of unmarked graves in cemeteries is an unusual but regular application of ground penetrating radar. Where there are no markers or indications of grave locations development, construction projects can be quickly brought to a halt until the history of the site is evaluated.

Ground penetrating radar (GPR) systems respond to buried objects as well as disturbed soil, providing a powerful method to define unmarked grave locations. Other applications include forensic investigations and archaeological site evaluations.

In this case a pulseEKKO GPR system was used with a 200 MHz antenna. The data were acquired by students at the University of Calgary. The portable nature of the pulseEKKO system made data acquisition quick and easy. The soil at the site was silty sand.

Data compliments of University of Calgary, Department of Geography, Canada



THE LOST SQUADRON

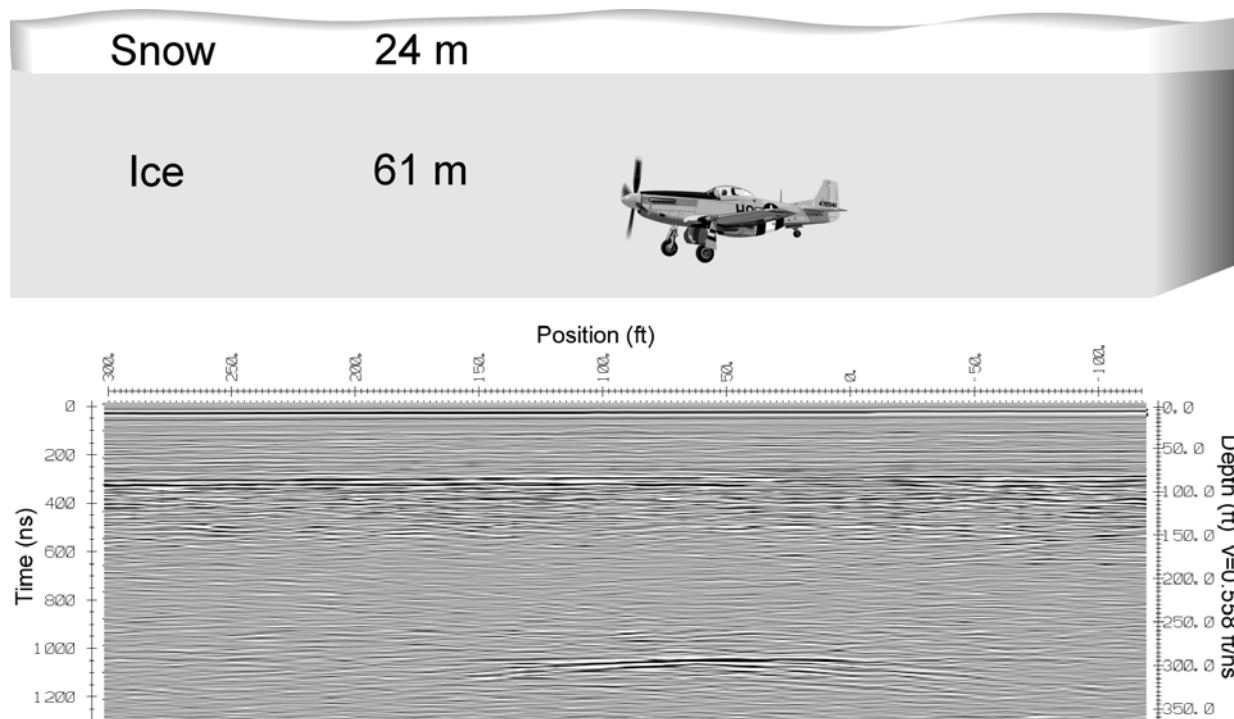
Ground penetrating radar (GPR) is commonly used in glaciology, as ice is easily penetrated by GPR signals.

GPR enabled the recovery of The Lost squadron in Greenland. A squadron of aircraft were forced to land in Greenland during WWII, although the exact location remained a mystery. The Lost squadron, consisting of six P-38F Lightning fighting bombers and 2 B-17E "Flying Fortresses" were last seen on the Greenland ice in July 1942.

A one-man survey crew used a pulseEKKO system to map out the exact location of the squadron in May 1992, 50 years after the squadron's disappearance. The pulseEKKO system was excellent for use in this case because of the lightweight, modular design enabling one person to use it easily.

Following the GPR survey, the site was excavated and a nearly complete aircraft has been successfully recovered.

Data compliments of Greenland Expedition Society



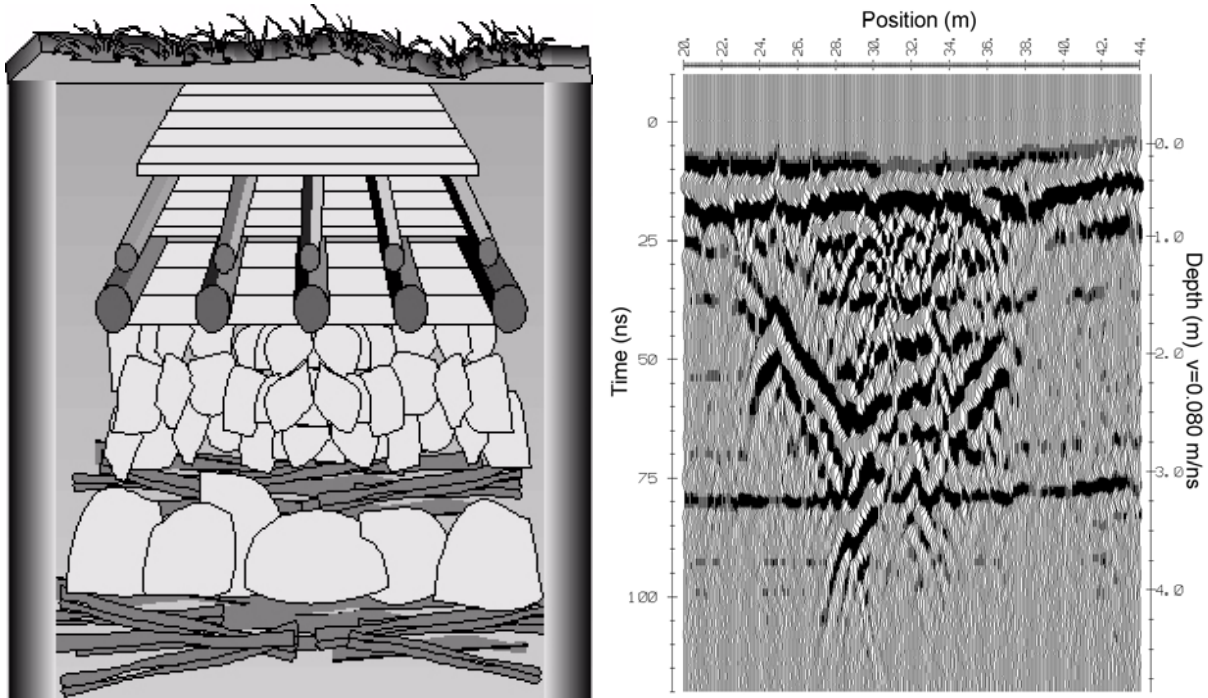
BURIED VIKING ROADS

Ground penetrating radar (GPR) is in use worldwide to map objects for archeological digs. GPR systems determine the best locations to dig and map the layout of obliterated roads and buildings.

This study was conducted in Denmark, beside the Alling River et sjellbro. A pulseEKKO GPR system successfully located and mapped an ancient Viking road which sunk into a peat bog. In 1952 a stone carving was discovered in the meadow nearby, which marked the crossing of the ancient road system. Parts of the road were excavated from 1952-57 and in 1980.

The construction of the road consists of four structures. The two lower portions are comprised of small rocks and twigs indicating the road was built in the early iron age. The two upper sections are wooden structures, one being constructed in the late iron age, around 756 AD, and the other in the Viking age at about 1000 AD.

The GPR system was used to efficiently locate the ancient road system, without disturbing the structure.



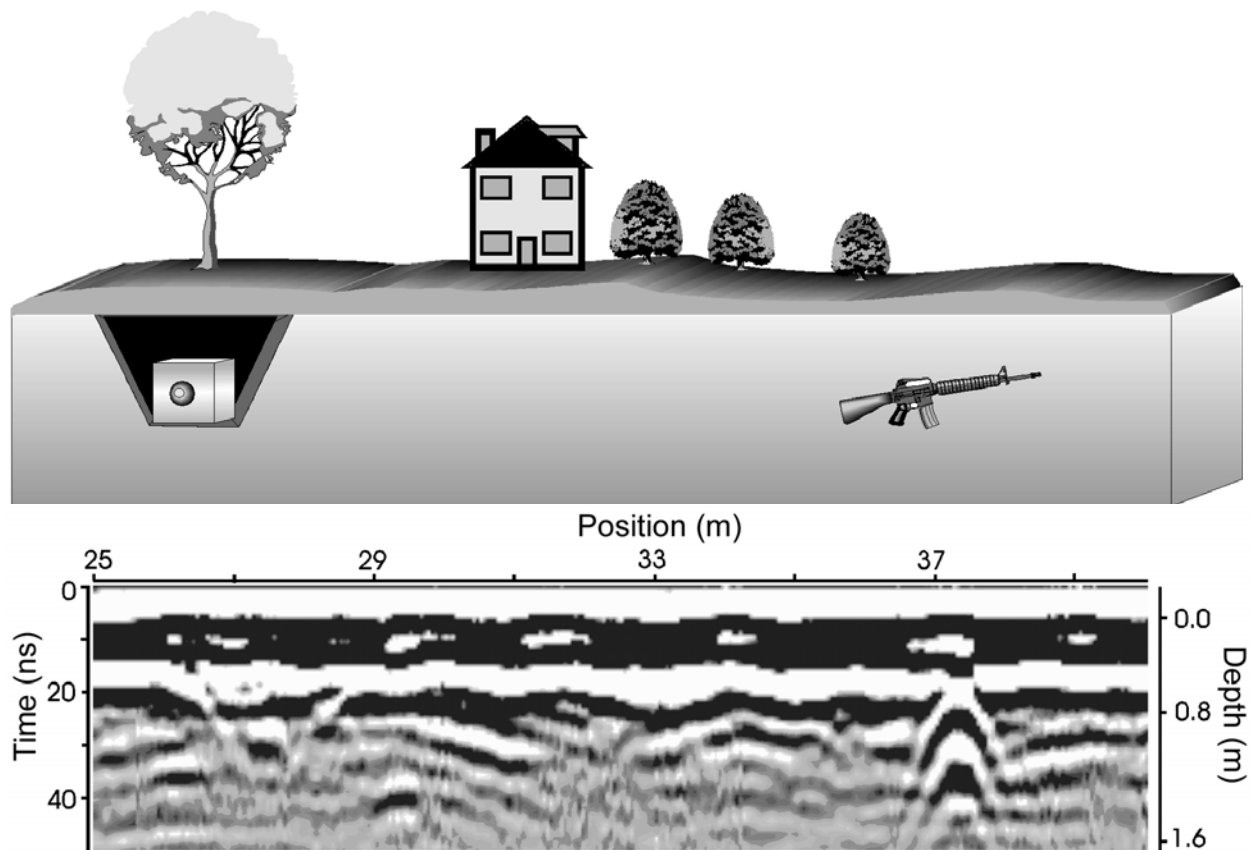
FORENSIC INVESTIGATIONS

Ground penetrating radar (GPR) is frequently used by police for forensic investigations. The ability to quickly locate soil disturbances, voids, and trenching, as well as both metallic and nonmetallic objects makes GPR a valuable tool for use in forensic studies.

In this case, the police had a search warrant and were on a seizure mission for evidence in a racketeering sting operation. A GPR survey was used to find money, firearms, and narcotics said to be buried at a private premises. One person surveyed the front and back yard, the garage as well as some forest area behind the property, using a pulseEKKO 100 system equipped with an odometer wheel and 200 MHz antennas. The data were displayed on a computer screen in real-time, enabling the police crew to immediately excavate and tag the significant finds as evidence.

The profile above collected in the front yard of the home shows trenching on the left side as well as a buried metallic object on the right. The pulseEKKO survey allowed police to quickly collect evidence to strengthen their case.

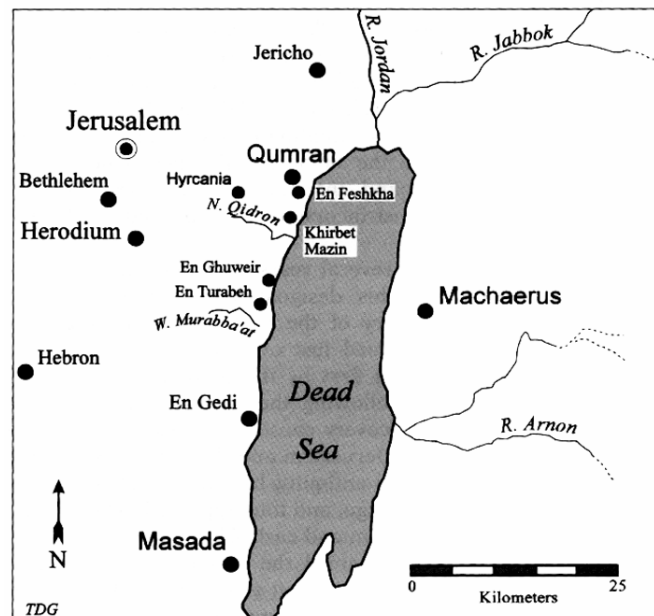
Data compliments of multiVIEW Geoservices, Canada



IN SEARCH OF CAVES AND GRAVES IN ISRAEL

Harry M. Jol has a Ph.D. from the University of Calgary where he wrote his thesis on Ground Penetrating Radar. He also has a M.Sc and a B.Sc from Simon Fraser University in British Columbia. His interests include geomorphology and GPR, particularly in coastal, deltaic, aeolian and geoarchaeological settings. Dr. Jol is currently a tenured Associate Professor in the Department of Geography and Anthropology at the University of Wisconsin-Eau Claire. The following is written by Dr. Harry Jol.

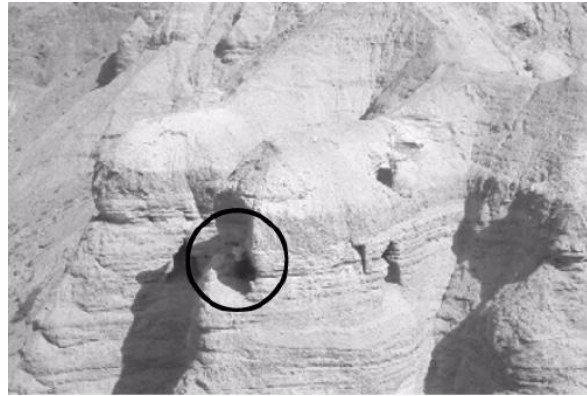
The Dead Sea Scrolls, which were accidentally discovered in a cave by a Bedouin boy in 1947, are one of the greatest manuscript discoveries of the twentieth century. The Scrolls reveal the history of the Second Temple period - a time of important developments in monotheistic religions.



The Qumran and surrounding region (from Golb, 1995).

Since 1947 the Qumran region, on the north-western shores of the Dead Sea, Israel, has been subject to countless probes. GPR has been used at the site on several occasions in the past with R. Eisenman being the only one to publish any GPR interpretations.

Encouraged by these earlier results, a multi-site expedition used GPR during the summer of 2001. The expedition was initiated with the hope of better understanding the Qumran site.



Cave 4, the site of one of the Dead Sea Scrolls discoveries. Circled is the entrance to the cave.

The GPR portion of the project had two major objectives: 1) to identify if there were more caves in the marl cliffs that contained artefacts associated with Qumran; 2) to determine the positions of previously unknown or unmarked graves in the cemetery east of Qumran.

The site was culturally important and needed to be treated with sensitivity and care. Geophysical methods, such as GPR, provided just the right approach - non-invasive and non-destructive.

Portable and digital, Sensors & Software's Noggin^{plus} 500 system and the pulseEKKO 100 GPR system were used to collect data. The Noggin SmartCart system was ideal for rapid data collection over the graveyard area while the low frequency pulseEKKO system was used in the search for caves. The application of radar stratigraphy analysis on the collected data aided in identifying the geometry of possible buried archaeological features.

The Qumran site has a thin, electrically resistive fan deposit with a more conductive marl unit below. The site conditions reduced GPR penetration to approximately 1 to 2 m but allowed enough penetration to map disturbances and voids in the near subsurface.

The first objective, to identify if there were more caves along the marl cliffs, was achieved by running pulseEKKO 100 GPR surveys along the cliff tops and along the cliff faces. Individuals with antennae were lowered with ropes along the cliff faces and surveys were conducted along predetermined lines. Two sites were chosen for excavation based on GPR images that showed hyperbolic features between 0.5 and 1.0 m depth.

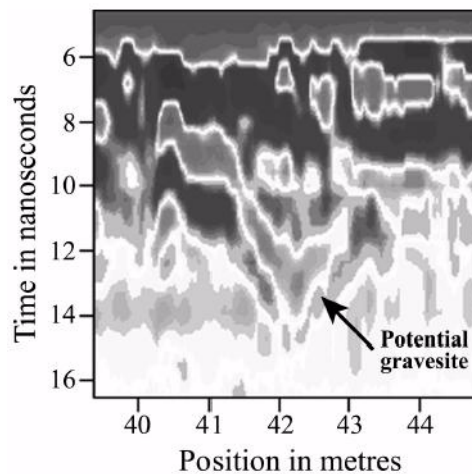


A grave with surface expressions (stones piled up in oval pattern) just east of Qumran Archaeological site.

Once excavated, the first site showed a localized patch of pebbles at a depth of 0.5 m that had interfingered with the marl deposits. The second site resulted in the recovery of archaeological artefacts from the floor of a cave that had collapsed.



GPR profile showing a “hyperbolic” pattern along the cliff face. As the site was excavated, artefacts were located from an interpreted collapsed cave. The horizontal line is at approximately 0.5 m depth.



GPR profile showing a “V” shaped reflection pattern that is interpreted as a potential gravesite. There is no surficial expression of the site being a grave. Total depth is approximately 1.5 m.

The second objective was to locate potential travesties at the Qumran cemetery where burial stones had been removed due to vandalism, construction projects, or use in other burials. Since no complete map of the Qumran cemetery had been constructed, GPR was utilized to map the subsurface with the hope of identifying unmarked burial sites.

Initially, an experiment was conducted on known grave sites so that GPR reflection patterns could be identified. Two patterns emerged as burial signatures - a hyperbolic feature and/or a “V” shape.

An extensive GPR survey was conducted along the outer edges of the exposed cemetery as well as empty patches of ground within the exposed cemetery. Interpretation of the GPR profiles, as they were collected, located over 100 potential graves that did not show surficial expressions.

GPR proved to be an effective method for locating and mapping potential caves and graves at the Qumran site without disturbing the historically important surroundings. Based on the results and discoveries of this initial study, further GPR surveys will be conducted at the site during the summer of 2002.

Support for the Multi-site Expedition to Qumran was provided by the John and Carol Merrill Foundation, Frankel Fund, Biblical Archaeology Society, University of Wisconsin-Eau Claire and Sensors & Software Inc.

10.4 BURIED UTILITIES

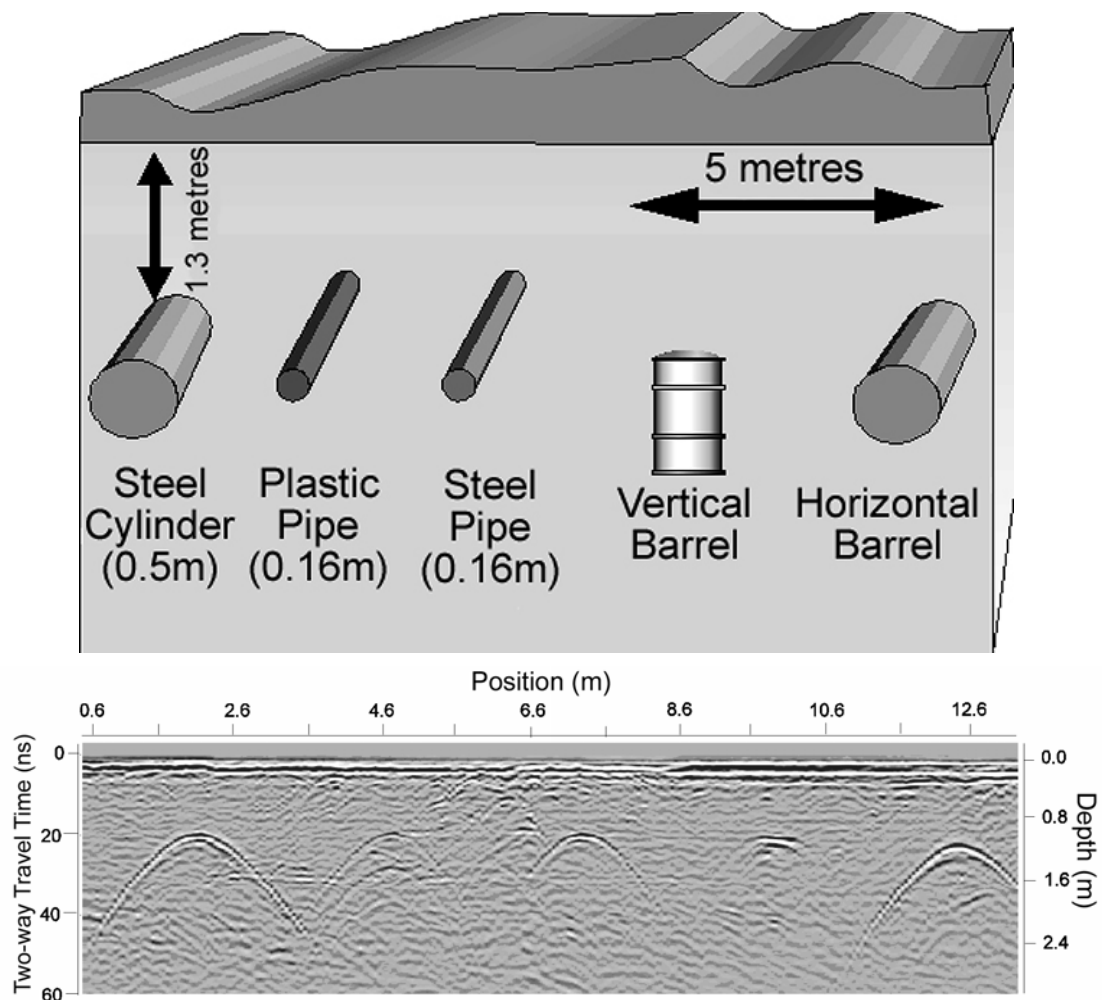
PIPES & BARRELS

The below data section demonstrates the use of ground penetrating radar (GPR) for pipe and barrel location. The pulseEKKO GPR systems clearly locate both metallic and nonmetallic objects. The data also displays the ability of pulseEKKO GPR systems to locate small objects, such as the pipes.

The hyperbolic shape (inverted U) of the GPR response is diagnostic of localized targets. The top of the hyperbola indicates feature location. The shape of the tails gives a measure of velocity and depth.

The example data shown here were acquired using a pulseEKKO 1000 system with 450 MHz antennas. The data were recorded using 16 stacks at 0.1 meter step intervals. Note the difference in response for the two barrel orientations indicate that GPR can distinguish geometry.

Data compliments of University of Waterloo, Canada

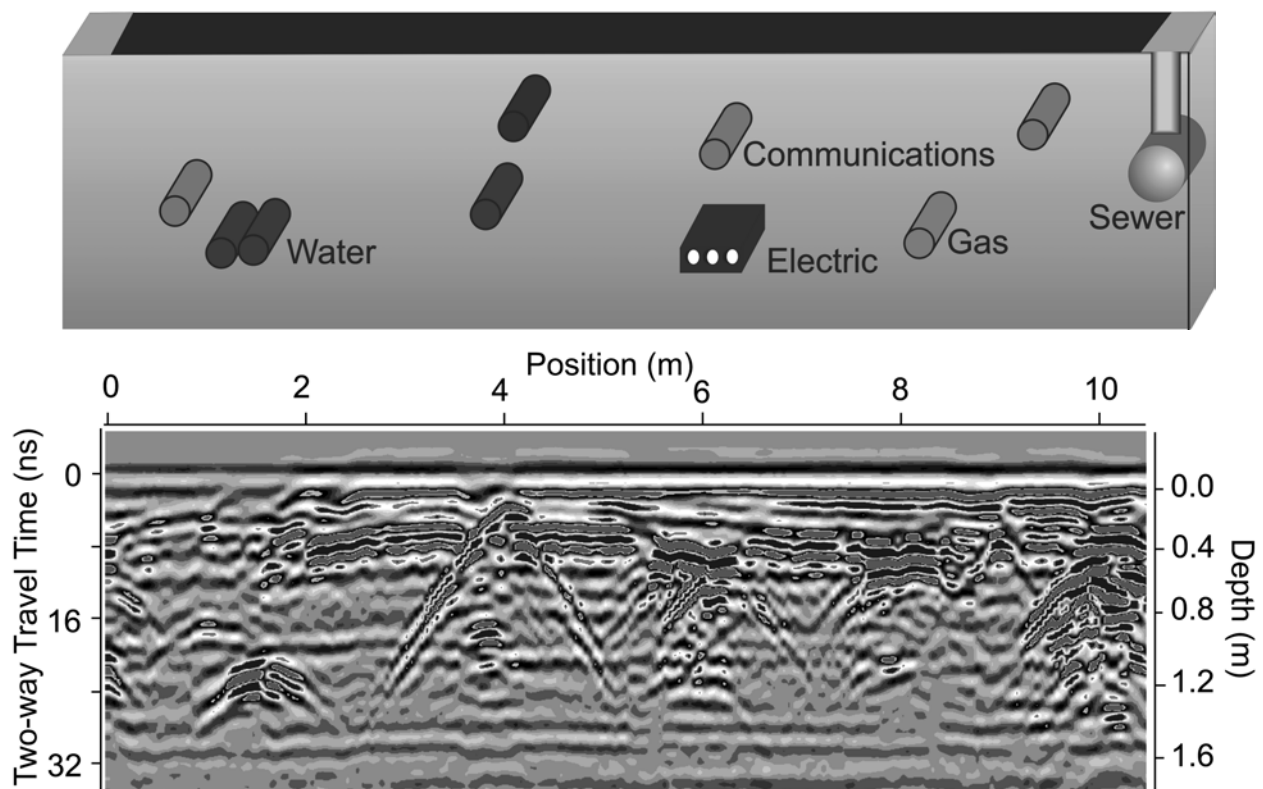


UTILITY DETECTION

The accurate location of buried utilities is imperative for contractors. Hitting a high voltage power line or water main can be dangerous, disruptive to citizens, as well as expensive.

Ground penetrating radar (GPR) systems are used globally to locate metallic and nonmetallic utilities underground. GPR's high resolution capabilities allow detection of closely spaced utilities which is often the case under roadways in urban areas.

The below data were collected using a pulseEKKO GPR system with 450 MHz antenna on a major road in Kuala Lumpur, Malaysia. The contractor needed to know where he could safely dig without hitting a utility while installing fiber optic communication cables. The survey was carried out in a few minutes, and locations of the utilities were marked on the pavement as the survey was being conducted. The fiber optic cable contractor quickly and safely trenched between sites of buried utilities.



TRACKING A STORM SEWER

At a recent Underground Focus Utility Workshop, we had the opportunity to see utility locating in action. The seminars were held at Dekalb College in Covington, Georgia near Atlanta. The objectives of the workshop were to expose utility locators to new technologies and practices in the industry and to provide hands-on experience with the various techniques.



Figure 1: Location of storm drain intake.



Figure 2: Location of GPR lines.

After construction of the Dekalb College site, no as-builts were provided by the contractor. As a result, no records of the underground utility pipes and cables were available. The technologies showcased at the seminar helped locate some of the buried utilities.

Ground penetrating radar (GPR) proved to be very effective at the site. One interesting exercise involved locating a storm water drainpipe under the circular driveway outside the lecture hall. While the intake could be seen at the curb,

the location of the storm drainpipe was unknown. Figure 1 shows the circular driveway with the drain intake at the edge of the curb.

Several GPR traverses around the intake located a large pipe. A series of GPR transects were then carried out to track the alignment of the pipe. Three transects perpendicular to the pipe are indicated on the photo in Figure 2. The GPR response on the three transects are shown as Lines 1, 2 and 3. The drainpipe was expected to continue down grade to the right in the photo in Figure 1 and 2. Instead, the pipe ran in the opposite direction.

To address the drainage/slope issue, we then profiled along a transect (Line 4) which joined the pipe location determined from Lines 1, 2 and 3. This data provided a continuous profile along the axis of the pipe. The depth of the pipe along the traverse is seen readily on Line 4 in Figure 3 and 4.

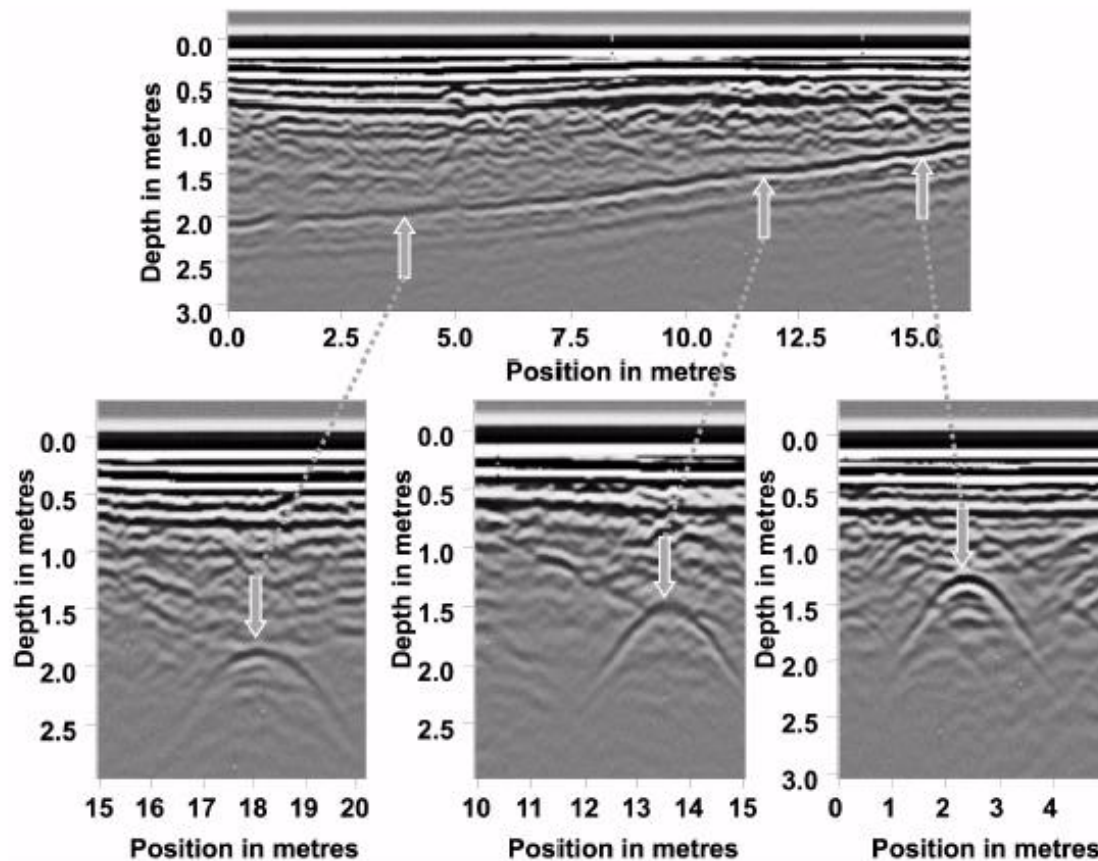


Figure 3: GPR survey lines over the storm sewer. Lines 1, 2 and 3 run perpendicular to the path of the sewer pipe. These lines show the pipe at different depths, indicating that it is sloping. Line 4 runs parallel, along the length of the pipe, confirming the slope.

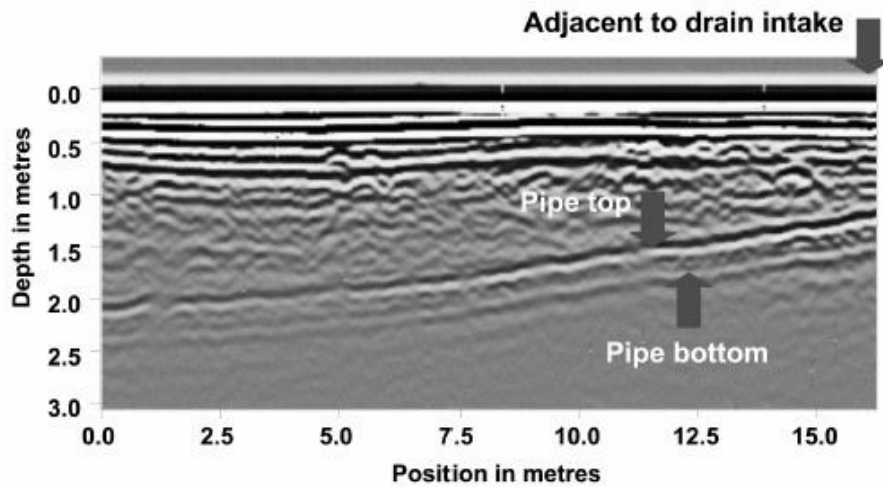


Figure 4: The GPR response from the storm sewer shows the reflections from the top and bottom of the pipe. Assuming the pipe is air-filled, the pipe diameter was estimated at 36 inches.

From the transect in Figure 4, it was apparent that the depth of the pipe increased from right to left by about 3 ft (1 m). In addition, it was possible to see the reflections from the top and the bottom of the pipe. The storm drain appeared to be a concrete pipe with no apparent metallic structure associated with it. Using the depth of the top and bottom of the pipe and assuming the pipe was air filled (there had been no rain for an extended period of time) it was possible to estimate the pipe diameter at about 36 inches (90 mm).

This example illustrates the power of using GPR. The exercise of locating the pipe, marking the alignment and tracking the depth as well as estimating its diameter took about 10 minutes.

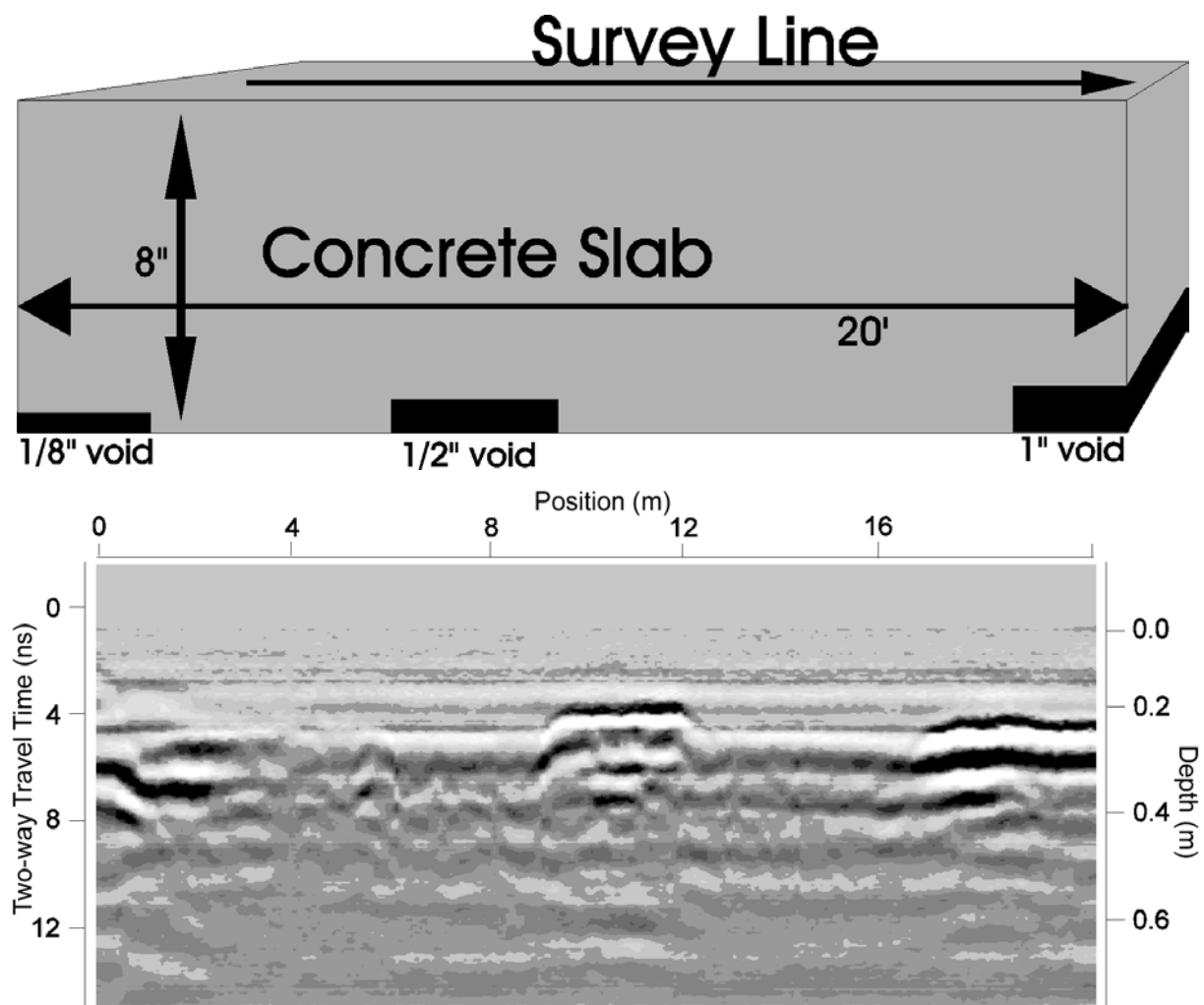
10.5 STRUCTURE ASSESSMENT (NDT)

VOIDS BENEATH CONCRETE

Retaining wall, road and sewer collapses are commonly caused by soil erosion beneath or behind concrete structures. Ground penetrating radar (GPR) can detect these unsupported void areas when they are in their infancy and help to eradicate hazardous collapses.

This experiment was conducted in College Station, Texas to test GPR for mapping voids beneath concrete. The Texas Transportation Institute test site consists of an eight inch concrete slab with small voids from 1/8" to 1". A pulseEKKO 1000 GPR system with 900 MHz antennas accurately located all the voids quickly and easily, as clearly displayed in the data set below.

The success of this experiment not only confirms that GPR is an accurate means of void detection, but shows that GPR can locate very small features, meaning that they can be detected and fixed before reaching a hazardous condition.



Strong reflectors are induced by relatively small air filled gaps under concrete.

RAILROAD BED MAPPING

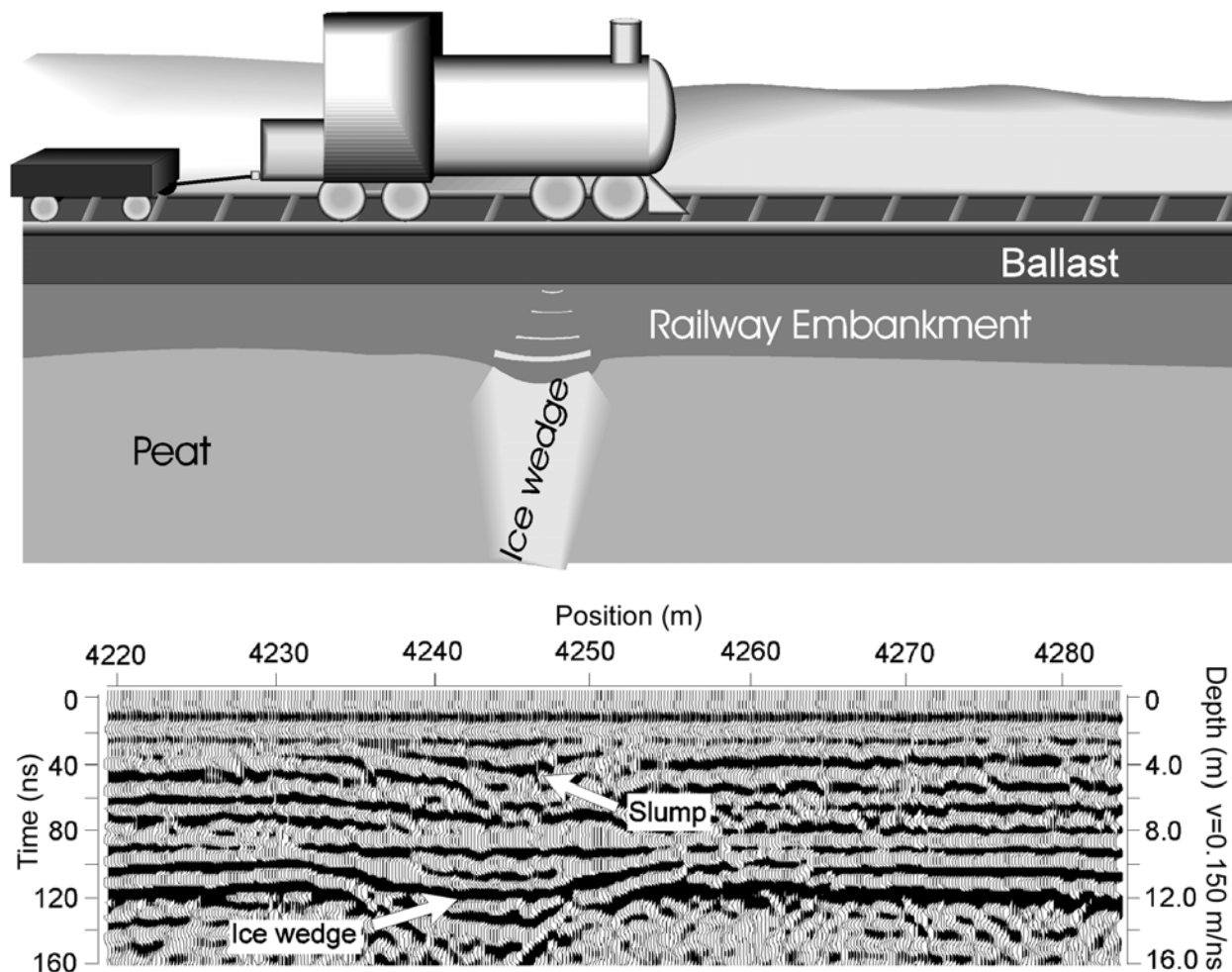
Safe and rapid rail service requires continuous maintenance of tracks and rail beds. Ground penetrating radar (GPR) provides a quick and easy method of investigating subsurface conditions. The efficiency and speed of GPR surveys permit remediation to start before conditions become hazardous.

Large sections of the trans-Siberian railway are constructed on a berm overlying permafrost terrain known to contain ice wedges and lenses. If ground ice melts, rails can subside and possibly causing train derailment. A rail-mounted pulseEKKO 100 GPR system with integrated wheel odometer attachment allowed for a quick and easy survey.

The survey determined the exact location of the ice wedge at 4243 meters along the survey line. The data also clearly show the slumping due to the subsurface conditions and locates the ballast, railway embankment and peat layers.

The information obtained in this survey proved invaluable to the engineers as the location of the ice wedges was determined before melting occurred. The situation was rectified before any damage was done to the railway equipment or any passengers were put in danger.

Data compliments of multiVIEW Geoservices Inc.



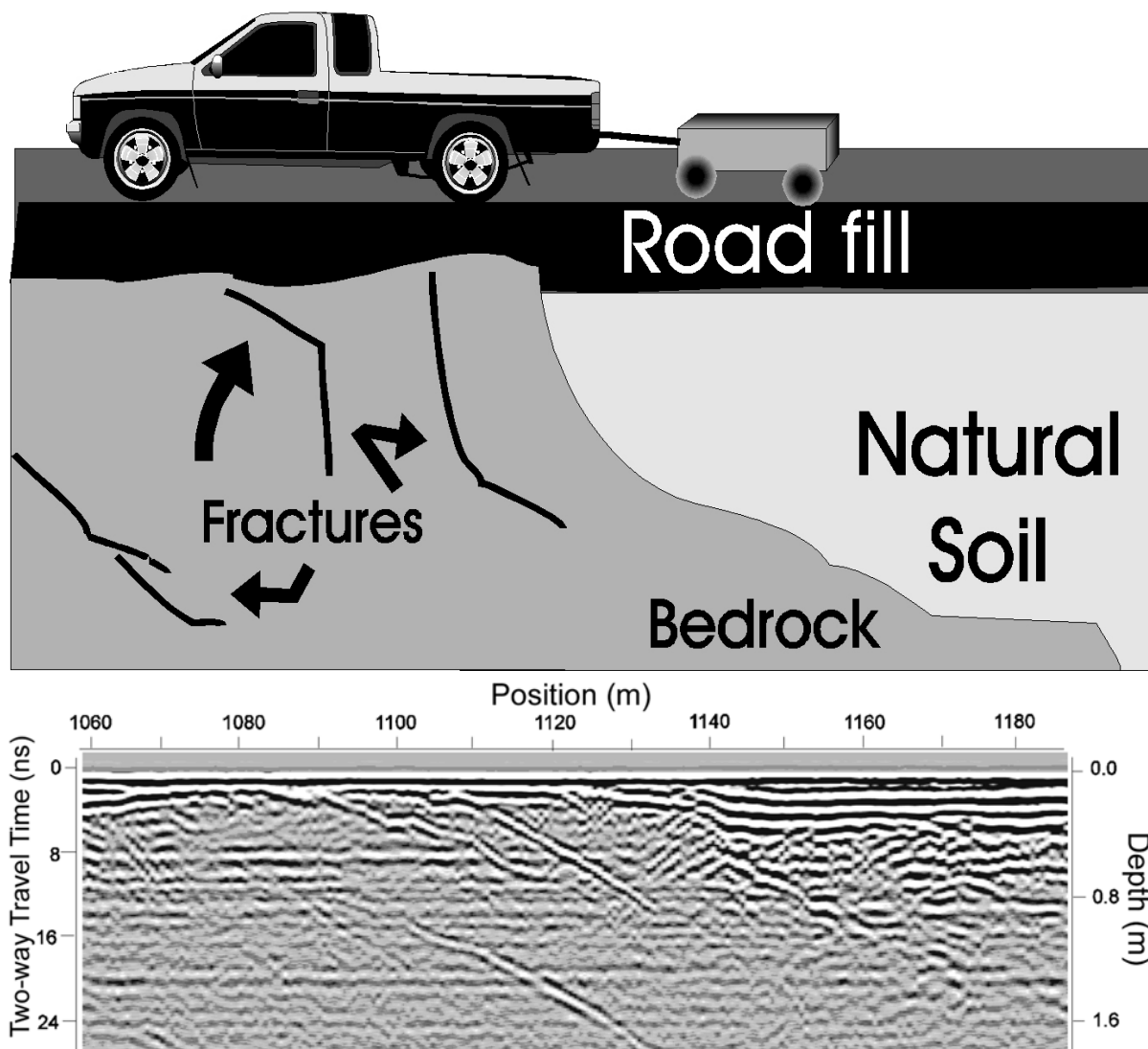
ROAD BEDS

Ground penetrating radar (GPR) is effective in defining potential problem areas on roadways. Data can be collected quickly with vehicle mounted systems, and can accurately define subsurface conditions.

This study was conducted in Sweden to evaluate the cause of pavement failure. The pulseEKKO 1000 system was used with a 900 MHz antenna to look through the roadbed and pavement to the bedrock below. The GPR data clearly indicate cracks developing in the pavement which correlate with differential subgrade settlement. In this case, shallow bedrock is more stable than adjacent fill.

The information obtained from the GPR survey allowed for timely maintenance and repair of the roadway.

Data compliments of TS Geokonsult, Sweden

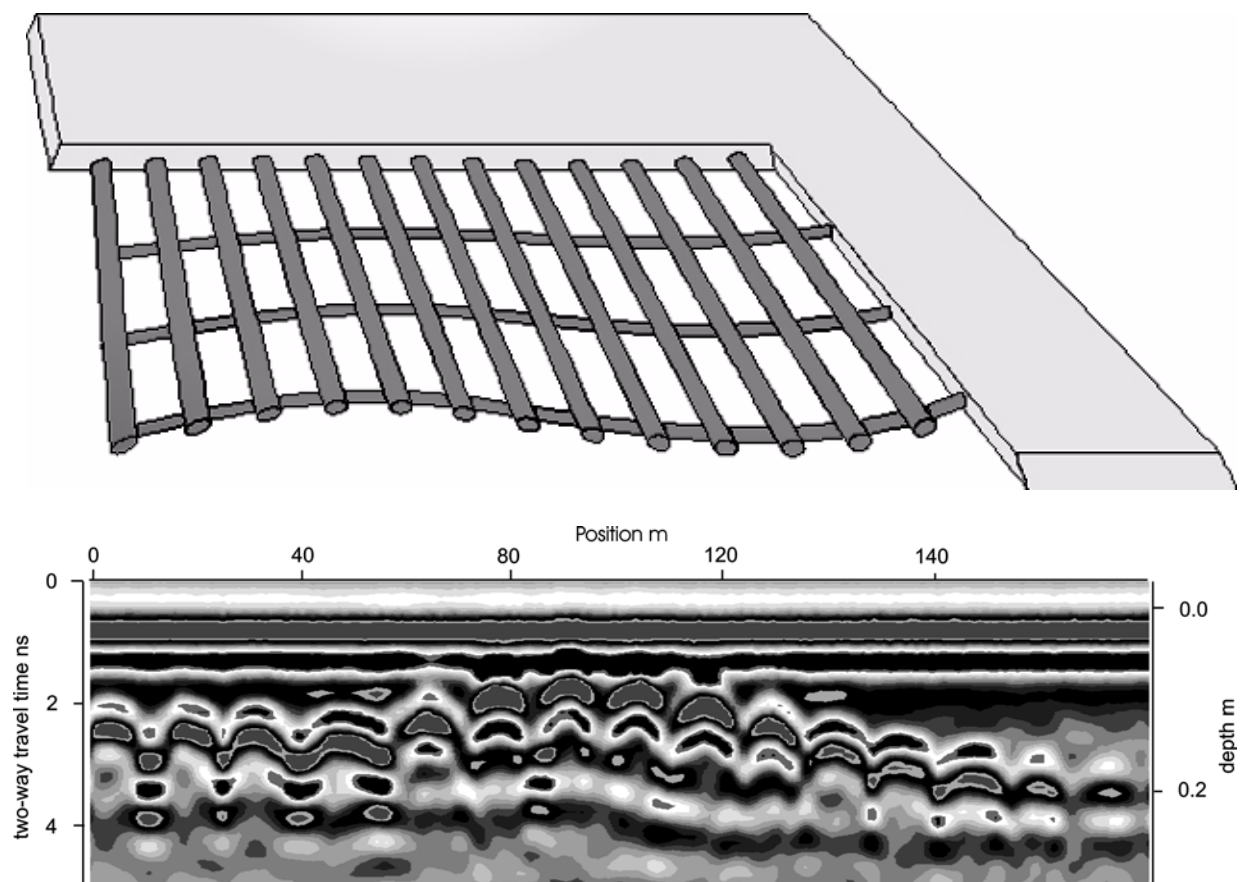


REBAR MAPPING

Ground penetrating radar (GPR) is an invaluable tool for construction planning as well as road, pavement, and building maintenance and repair. The accuracy of GPR systems in the detection of rebar position and condition is important in determining the stability of the structures. This study demonstrates the effectiveness of GPR for mapping rebar.

This survey was conducted on the floor of a one story slab on grade building using a pulseEKKO 1000 system with 1200 MHz antennas. The data collected clearly show the rebar to a depth of eight to 15 centimeters, and show the reinforcement curving up due to improper emplacement during construction.

The bottom of the concrete is weakly visible and is most readily detected when the rebar is closest to the surface.

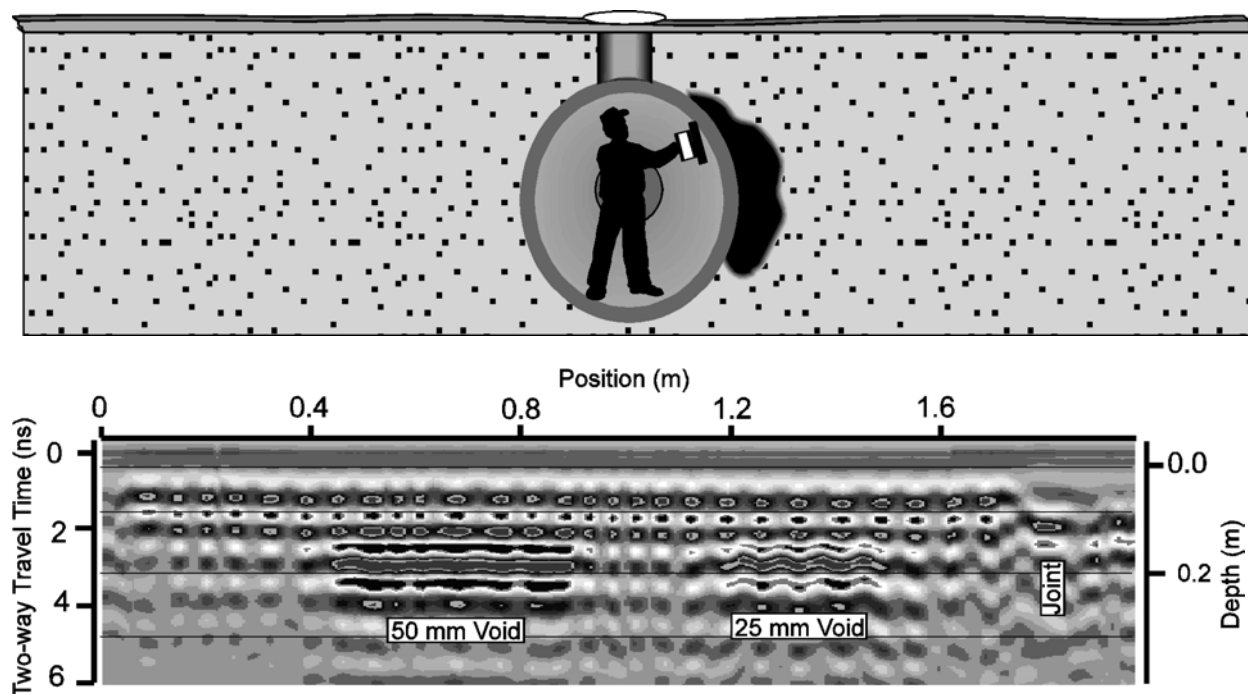


VOIDS BEHIND PIPES

Ground penetrating radar (GPR) is in use around the world for locating voids behind nonmetallic pipes and tunnels because it can both find voids and estimate the size of the voids, even through reinforced pipe. Early detection of voids is crucial to protect the structural integrity of the pipe and prevent extensive damage. The loss of material flowing through the pipe is expensive and can pose an environmental threat.

This pulseEKKO survey was conducted in a one meter diameter reinforced concrete pipe to demonstrate the use of GPR for void definition. A pulseEKKO 1000 GPR system with 1200 MHz antennas was used to define the pipe wall as well as the surrounding areas. In this case the pipe walls consisted of 100 mm thick concrete with a double layer of 10 mm diameter rebar placed 50 mm apart. 50 mm and 25 mm thick pieces of 300 mm polystyrene squares were placed outside the pipe to simulate voids.

The pulseEKKO data above clearly locate both the 50 mm and 25 mm thick polystyrene pieces and differentiates between the thickness of each piece. The dots on the data between the travel time of 1.6 and 2.2 indicate the rebar present within the concrete pipe.



GPR MAPS FOUNDATION STRUCTURE

GPR can be used to map subsurface conditions with minimal impact on surrounding activity. The current survey objectives were to assess construction practices and to locate utilities in a hotel ballroom prior to renovation.

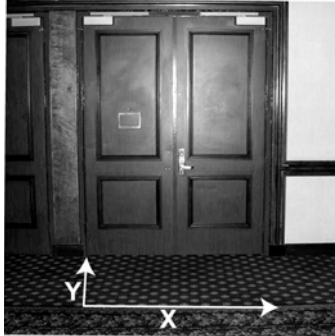


Figure 1: Photo of the doorway to the ballroom. Note the carpet on the floor is laid over concrete slab-on-grade.

To investigate, a Noggin 1000 Smart Handle system was deployed. The lines were laid out through a doorway to obtain “through-the-wall” data. The floor area was carpeted and underlying the carpet was concrete slab-on-grade.



Figure 2: The Noggin 1000 SmartHandle System configuration.

A photo of the doorway is shown above in Figure 1. This shows the position of the doors, the carpet over the floor and the survey line layout.

The Smart Handle system configuration is shown in Figure 2.

The grid acquisition mode for the Smart System enabled acquisition of data to image the subsurface in plan map form.

A GPR cross section is shown in Figure 3. Note how this section through the doorway reveals the rebar as well as an embedded utility. A trench associated with construction of footings is also visible beneath the concrete intervals. The resulting data were processed using the EKKO Mapper software to generate the plan map shown in Figure 4, which slices through the subsurface between depths of 0 inches and 12 inches.

The depth slice clearly shows the rebar pattern and utilities location in the subsurface. Based on this, plans for renovation can be made with a better understanding of the prior construction practice.

The above example clearly illustrates the power and the non-intrusive nature of GPR for building retrofit planning.

The data were acquired in 15 minutes while the ballroom was in use with no impact on daily activities. The initial plan map was created within a few minutes after data acquisition.

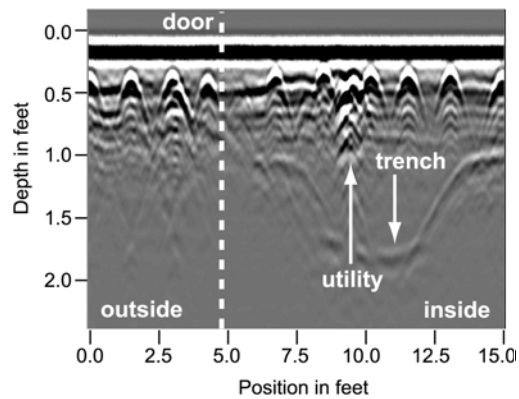


Figure 3: A sample GPR cross section through the middle of the ballroom doorway. Note the rebar, the utility lines and the trench beneath the concrete.

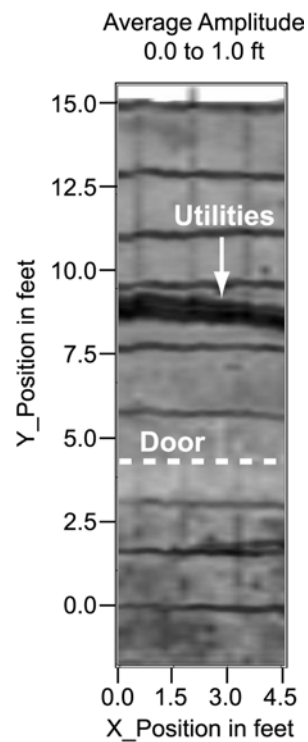


Figure 4: GPR depth slice map between 1 and 12 inches, showing the plan layout of the conduit and reinforcing construction elements.

CONQUEST GIVES THE CONCRETE PICTURE!

Conquest is specifically designed for non-destructive concrete inspection. Based on the Noggin 1000, Conquest is an integrated GPR system which allows the user to gather data, process it and evaluate the results in the field. Downloading the information to a computer or laptop is an available (but not required) feature.



Figure 1: Conquest on the test sidewalk

There is increasing demand for mapping features within concrete before cutting or drilling occurs. Conquest can locate conduit, rebar, and post-tension (PT) cables embedded in the concrete, as well as voids located beneath it. The repair costs of cutting a conduit or PT cable can be high, not to mention the losses due to downtime.

The following example illustrates data collected from a 1200 x 1200 mm concrete test sidewalk located at Dofasco in Hamilton, Ontario (Figure 1). Buried in this sidewalk were rebar and conduits of different sizes and composition (Figures 2 & 3). A plastic grid was overlain on the sidewalk and data were collected along the lines marked on the grid.



Figure 2: Items buried in the sidewalk

The scan was taken several months after the concrete had properly cured. Wet or freshly poured concrete is not favourable for GPR measurements, due to the presence of free ions and water, which absorb the radar signal. Once the concrete has cured, the ions become “locked” into the concrete structure, allowing increased penetration of the radar waves.

After processing the raw data, Conquest generates plan maps at a series of depths in the concrete. The rebar and conduits are shown in the depth slice in Figure 4. One inch diameter conduits are seen at the bottom of the figure; two of them are buried directly underneath rebar. The larger diagonal conduits are more visible in the deeper slice shown in Figure 5.

By analyzing different depth slices, Conquest can help the user locate the position and depth of any embedded features. Drilling and cutting can then be carried out in the areas defined by the image that are clear of rebar and conduits.

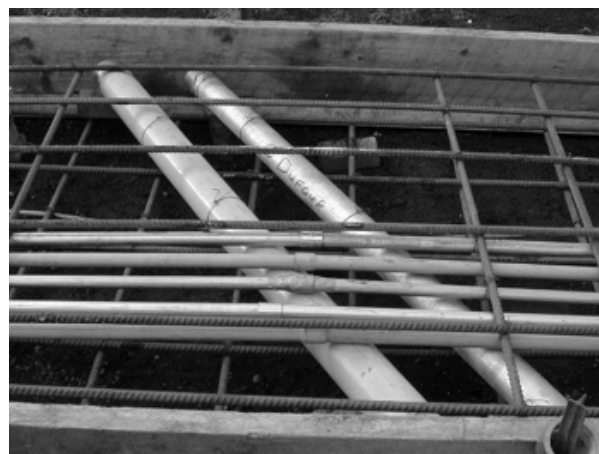


Figure 3: Close-up of the scanned area. There are 5 conduits running from left to right all 1” diameter. From top to bottom, the conduit materials are: galvanized steel, PVC, electro-metallic tubing (EMT), galvanized steel and PVC.

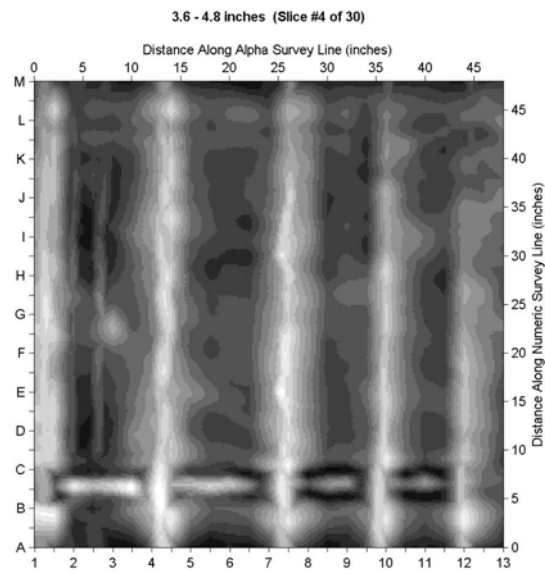


Figure 4: Depth slice between 4.8" - 6.0".

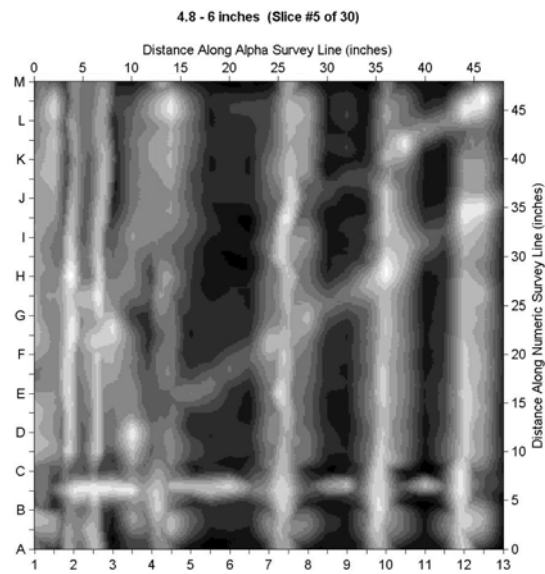


Figure 5: Depth slice between 6.0" - 7.2" The diagonal conduit on the left is 4" PVC, while the one on the right is 3" galvanized steel.

IMAGING OF A CONCRETE SLAB-ON-GRADE

Many problems such as assessing whether reinforcing is present or if conduits are embedded in the concrete require examination of slab-on-grade concrete structures. Related problems include estimating slab thickness, detecting voids beneath the concrete, and locating utility pipes, cables or tanks under the slab.



Figure 1: Photo of the test slab with axes indicated. A Noggin 1000 SmartCart maps the area.

The slab example presented here comes from the UK premises of Geomatrix Earth Sciences. A site photo is shown in Figure 1. The 3.5 x 4.5 m slab thickness varies from about 140 to 180 mm (6 to 7 in) thick and has a steel mesh embedded in it. The site has been examined any times with GPR but was only carefully studied recently. In November 2000 an accurately positioned GPR survey was carried out using a Noggin 1000 SmartCart system. Data was acquired at 10 cm line spacings with 1 cm station intervals in both directions over the slab.

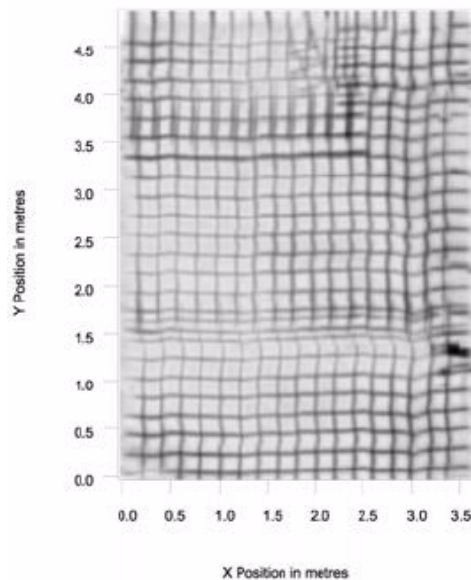


Figure 2: Depth slice centered at 100 mm (4 in) depth showing lapped sheets of reinforcing mesh. The mesh depth varies; out of slice features appear as weaker responses. By looking at several depth slices, depth variation becomes more apparent.

Figure 2 shows a 100 mm (4 in) thick depth slice centered at a 100 mm (4 in) depth. The image shows several overlapping sheets of mesh are used to reinforce the concrete. The bright spot at coordinate (X = 3.5, Y = 1.4) is a void under the slab.

Figure 3 shows a similar slice centered at a depth of 500 mm (20 in) below the surface. In this slice a 150 mm *6 in diameter plastic drainpipe is clearly visible.

The site flooded in the spring of 2001. This resulted in an increase in the water table levels in the local area as well as flooding over the slab and into the buildings. Subsequent to the flood, the site was resurveyed in early June 2001 to determine if there had been any erosion of fill from under the slab. Figure 4 shows a depth slice of the fill material at a depth of about 300 mm. The distinct oblong feature was not observed previously.

The anomalous feature was drilled and was found to be caused by the presence of water saturated silt underlying the concrete slab. Other areas of “normal” response were underlain by coarse gravel fill.

The slab surveys have taken very little time - typically about 1.5 to 2 hours to survey once - and about 1 hour to process the data. The unique feature is that all equipment and processing is standard commercial product - not research-only technology.

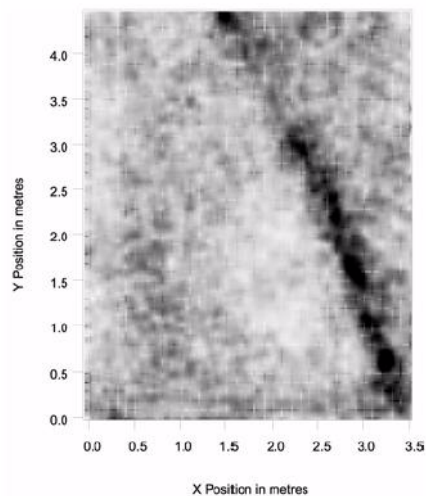


Figure 3: Depth slice centered at 500 mm (20 in) which detects a 150 mm (6 in) diameter plastic drainpipe.

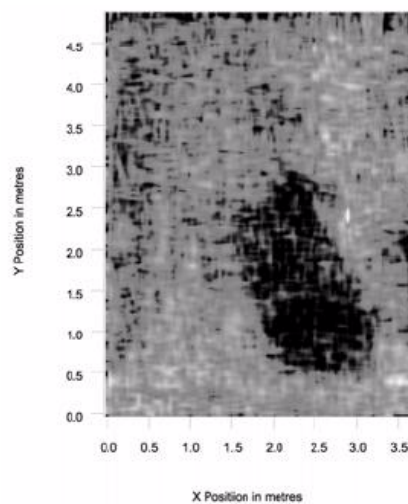


Figure 4: Depth slice at 300 mm (12 in) which shows the area after the site was flooded. An anomalous oblong area exhibits a lack of signal.

NOGGIN LOCATES SINKHOLE

Sinkholes are a problem in many geographic areas. Quite often we will see headlines reporting that a major structure is suddenly sinking into the ground because a sinkhole is forming. The present subject of Noggin Notes describes the mapping of a developing sinkhole in Florida.

The interesting case history is from a recent project of BCI Engineers and Scientists Inc. based in Lakeland, Florida. BCI regularly conduct geotechnical investigations around residential and commercial structures. The current investigation was carried out in October 2000 when BCI was contracted to investigate a depression in the ground surface near a house.

BCI use a broad range of geotechnical tools for their customers. GPR is a standard part of their investigation arsenal. The current work was carried out using a Noggin SmartCart with 250 MHz and 500 MHz transducers. The GPR survey consisted of 26 transects across the residential property; several transects ran directly across the shallow depression in the lawn. Figures 1 and 2 display some examples of these measurements. These images show the classic GPR response of a sinkhole.

Both traverse images show a number of shallow point-like reflector responses (the inverted V's on the record). These responses are from utilities and irrigation pipes buried in the lawn.

The most widespread feature is the fairly continuous horizon indicated as B in the figures. This horizon is a sand-to-clay boundary located at about 4 to 6 ft below the surface.

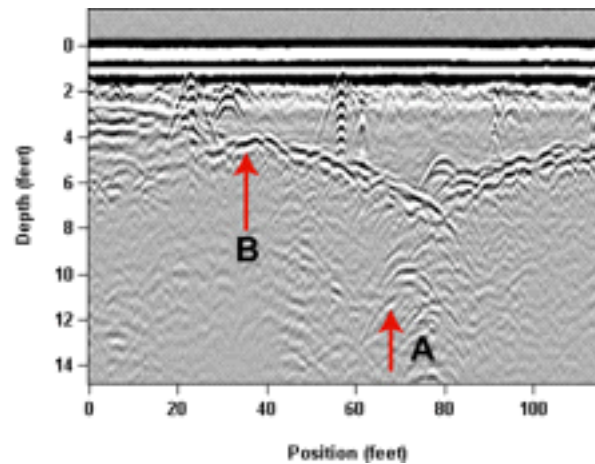


Figure 1: Example of a GPR traverse over a sinkhole: This image shows the depression of the sand/clay interface (B) with strong localized (inverted U's) responses (A) beneath the deepest point. Near surface utilities and irrigation pipes are visible as shallow inverted U's in the top 2ft.

The sand/clay boundary is ubiquitous and normally at a fairly constant depth. In the area where the depression was noted, the sand/clay boundary is pulled down and its response fades out in some locations. This depression of the sand/clay interface into a funnel shape (if viewed in 3-D) is a strong indicator of subsidence at depth. Here the boundary drops about 2 ft. deeper in the depressed area.

A second indicator of sinkhole development is the series of reflections at deeper depths that form beneath the depression in the sand/clay boundary. Such responses are usually localized in nature and indicate cavities which are generated from active reworking of the underlying soil. Example features are labelled A in Figure 1 and 2.

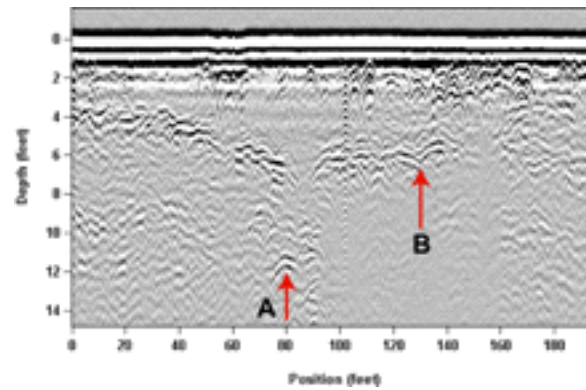


Figure 2: A second example of traversing over a sinkhole. Note the absence of the sand/clay boundary reflection A at position 85ft. where deeper localized targets A are indicated. The subsidence blurs out the sand/clay interface which causes the GPR reflection to fade.

The absence of a reflection from the sand/clay boundary is another indicator of sinkhole development. Lack of reflection occurs in the area of most severe subsidence because the soil mixing in an area of active reworking creates an indistinct interface.

This use of the Noggin SmartCart System demonstrates a very cost effective means of evaluating subsurface conditions. The results are extremely graphic, the analysis can be made in the field, and the information readily interpreted by anyone with a little bit of experience using GPR in sinkhole terrain.

We thank all the folks at BCI for providing us with this very educational example.

ON TRACK WITH NOGGIN^{PLUS} 250 SMARTCART

Reconstruction of older city areas often results in the burial of historic features. Foundations, roads and rail lines are often covered over by new construction. Our latest Noggin case study comes from Atlanta, Georgia.

An archaeologist survey in 1994 discovered sections of buried rail tracks in a downtown Atlanta area (see map in Figure 1) where Kelly Street had been disrupted by the construction of the I-20 freeway. The tracks are believed to be trolley tracks constructed in 1899 by the Atlanta Railway Company for electric trains linking downtown Atlanta to Grant Park which is now recognized as a Georgia historic district.

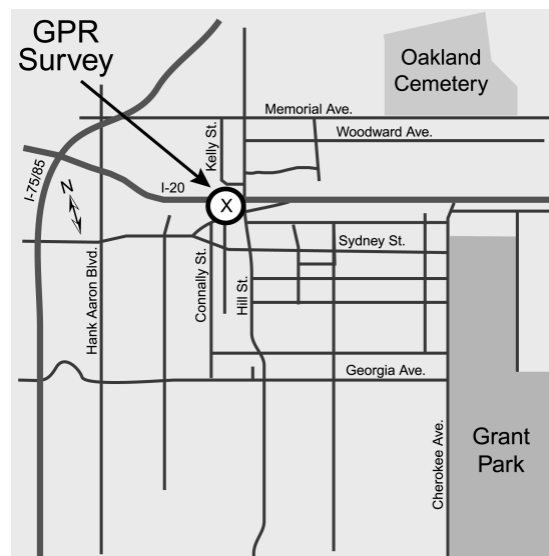


Figure 1: The GPR survey was carried out on a part of a relocated road that had been put over trolley tracks laid down in the late 1800's.

The Kelly Street Trolley Tracks are now being considered for inclusion in the National Register of Historic Places. The Georgia Department of Transportation (DOT) and area planners needed to relocate the buried tracks and map out their extent. Selected excavation of parts of the area is being considered to evaluate the methods and materials used in the early trolley line construction.

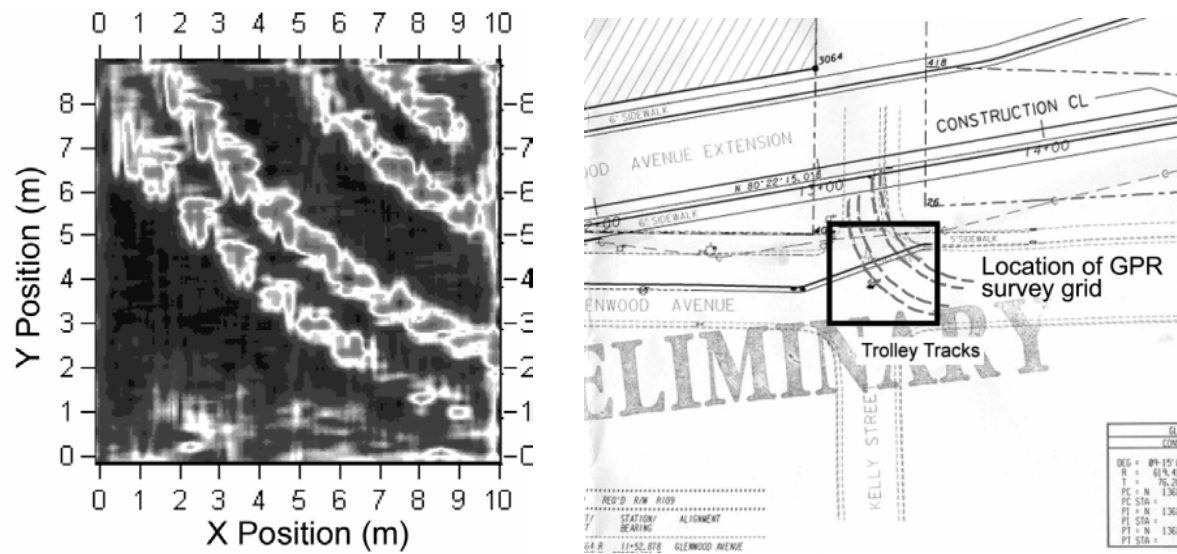


Figure 2: The survey grid of 10m by 10m (right) clearly shows the trolley tracks when plotted using EKKO_Mapper software (left)

Before any excavation could be contemplated, a means to locate the buried tracks was required. While in the area, a Sensors & Software Inc. staff member tested the usage of GPR for this site evaluation with a quick Noggin SmartCart survey. An exploratory 10m x 10m grid was established in the area where the lines were previously seen. A Noggin-*plus* 250 reconnaissance survey was conducted with 0.5 m line spacing.

The resulting data were then processed to quickly create a map on site using EKKO_Mapper. The results are shown in Figure 2. A depth slice centered at 0.25 m below surface clearly indicated two sets of trolley tracks curving around the corner on the previous Kelly Street alignment. A tighter survey line spacing and higher GPR frequency are recommended for future surveys to improve spatial resolution.

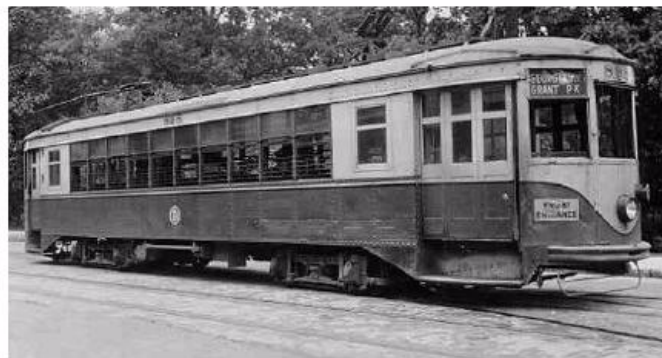


Figure 3: An Atlanta trolley car typical of the early 1900's.

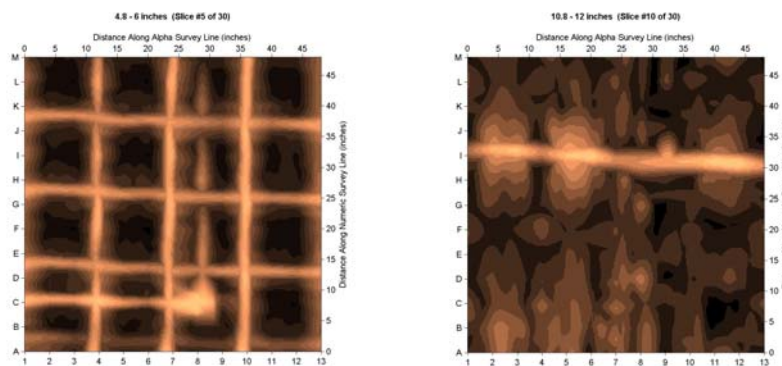
Archaeologists, urban planners and construction engineers are converts to the power of Noggin SmartCart systems with integrated GPS positioning and fast mapping output with EKKO_Mapper. The resulting subsurface imaging solution cannot be matched.

ON-SITE PROCESSING & 3-D IMAGING

New transitions are occurring with concrete inspection as demonstrated by the Sensors & Software Inc.'s Conquest. Users measure data following a prescribed menu to image an area. The data are immediately turned into depth slice maps on site in minutes as shown below. In this system the vector nature of the measurement is critical. Imaging makes use of vector information to generate pseudoscalar depth slice maps.



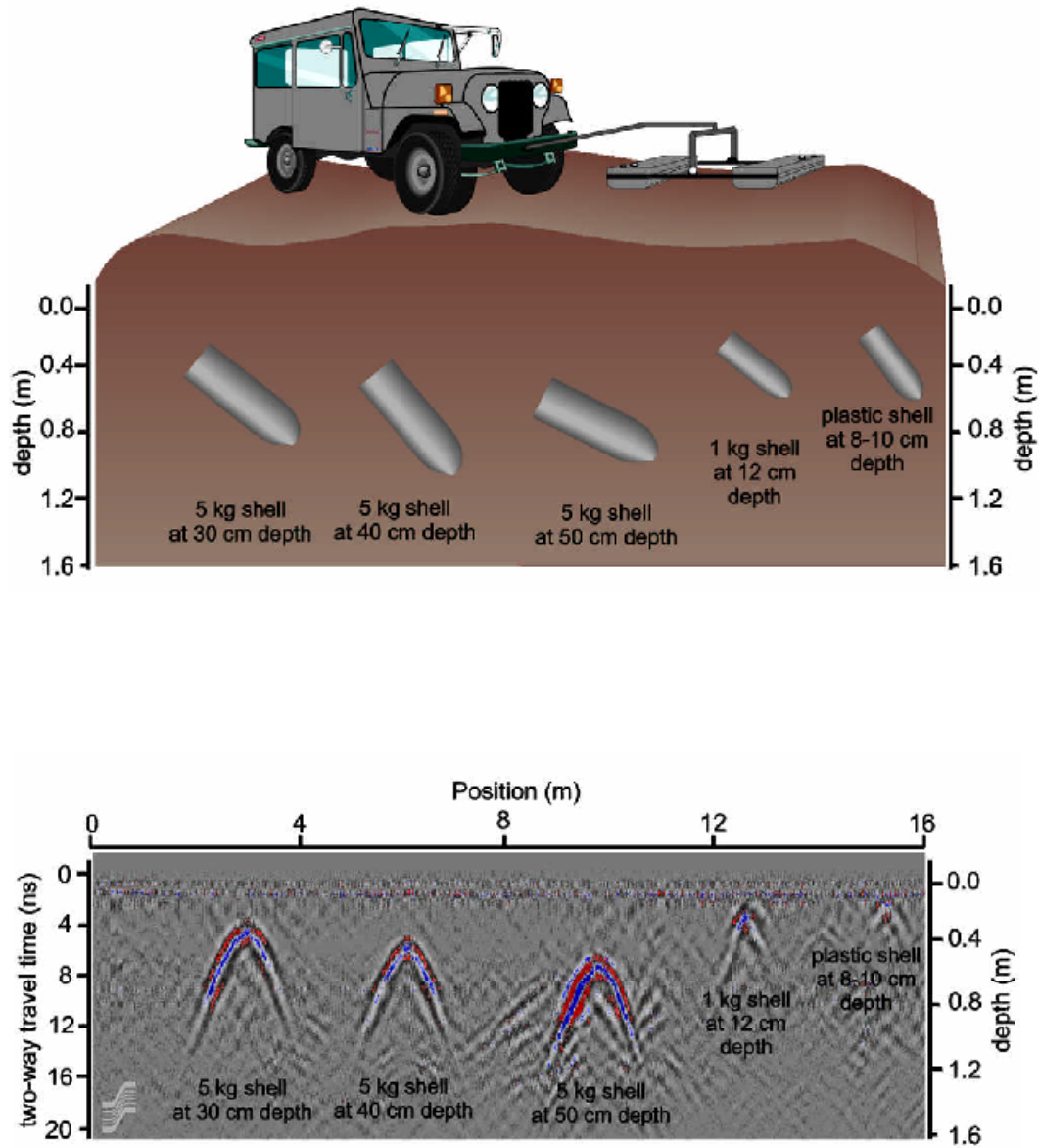
Photo of Conquest GPR system designed specifically for imaging concrete. Data are acquired on a predefined survey grid.



Example of depth slice output of a Conquest system showing rebar and an electrical conduit. Conquest generates depth slice maps of a concrete structure enabling the location of embedded objects such as rebar, post tension cables and utility conduits. The slices show two depth images from the same location. The left sees a rebar grid and an electrical conduit meeting at a junction box. The right shows another conduit at a greater depth.

10.6 MILITARY, LAW ENFORCEMENT & ESPIONAGE

UXO DETECTION



Data display of buried artillery shells.

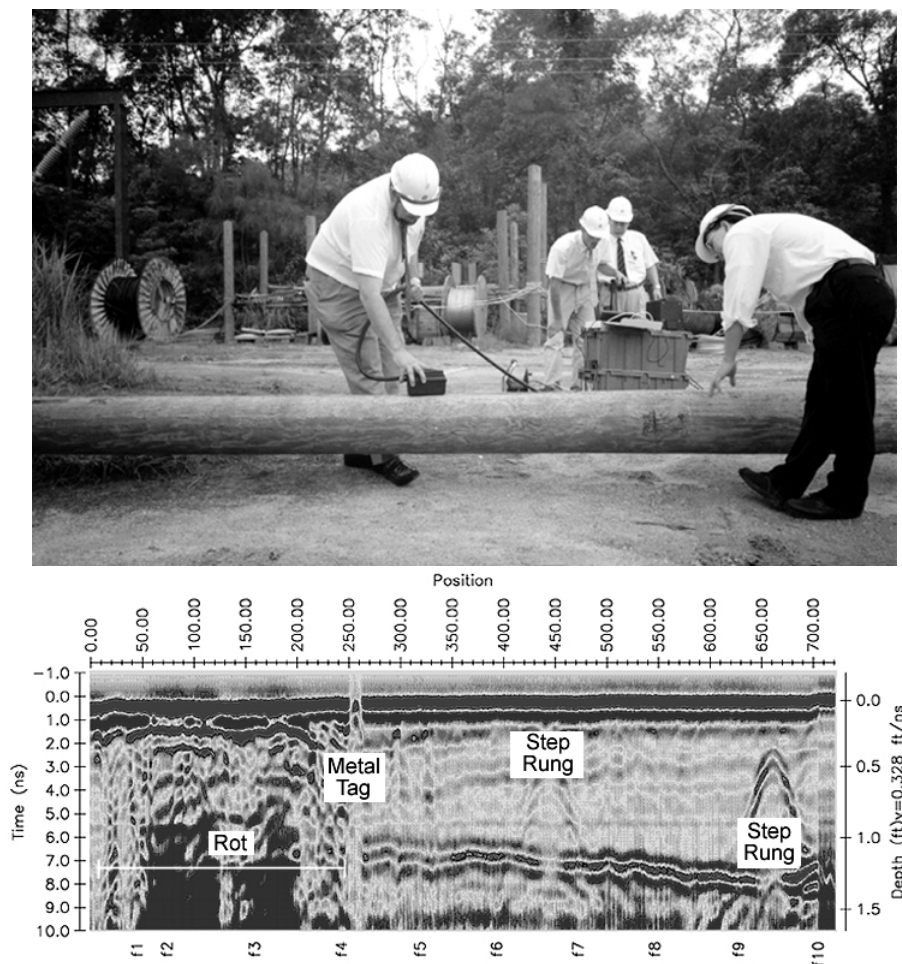
10.7 BIO APPLICATIONS

WOODEN POLE & TREE MAPPING

A unique but extremely effective use of ground penetrating radar (GPR) is mapping the internal structure of wooden poles and trees. GPR has proven to be a powerful means to locate anomalies in wood, primarily associated with changes in water content. Variations in water content most often indicate that rot or insect infestation is present.

This survey was conducted in Hong Kong to determine whether or not rot was present in wooden hydro poles. The study was easily carried out by one person using a pulseEKKO 1000 GPR system with 1200 MHz antennas to obtain a high-definition image of the poles. This information is very important in ascertaining the stability of poles supporting telephone and hydro cabling.

The above data section clearly shows the rot present in the first 200 cm of the pole. The GPR information indicated that the rot was extensive, making the pole unsuitable for further use.



10.8 SNOW & ICE

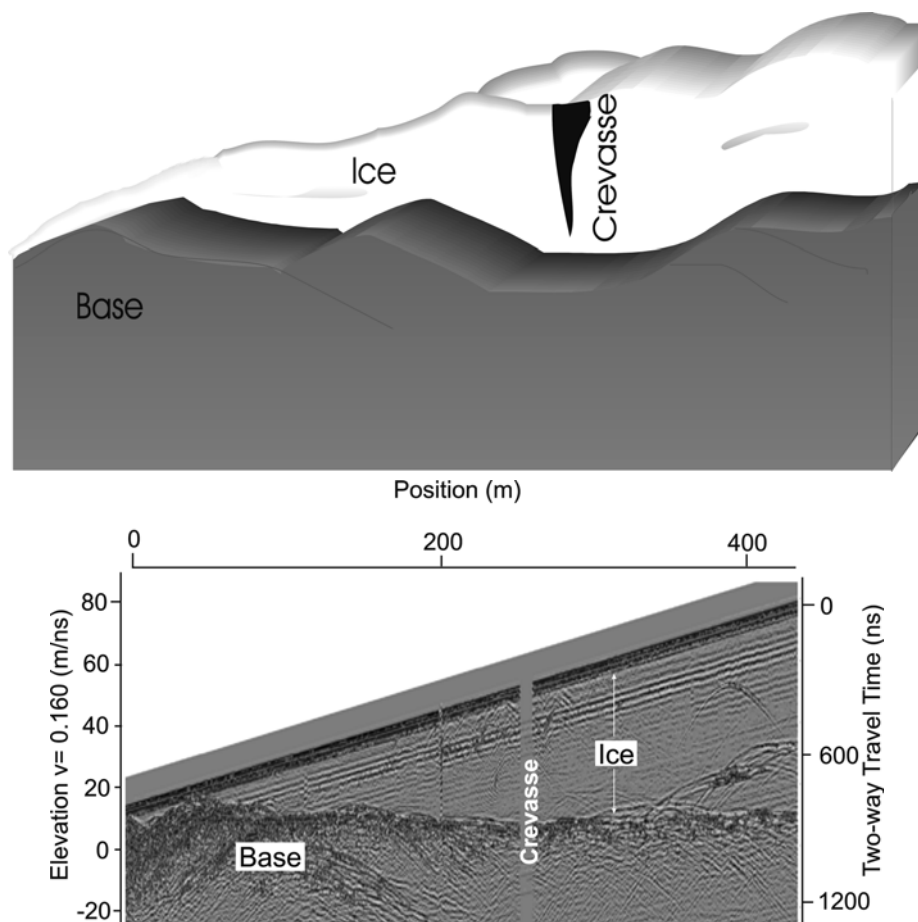
GLACIOLOGY

Ground penetrating radar (GPR) is an ideal method for glaciology as ice is very transparent to GPR signals.

This study was conducted on Bylot Island, NWT, Canada, using a pulseEKKO GPR system with 50 MHz antennas. In ice covered areas, knowledge of ice thickness and permafrost condition is important for land use management and resource exploitation planning.

The data above were quickly and easily collected by a two man team, using sleds to expedite the process. The pulseEKKO GPR data above provide a graphic view of the ice conditions. Note the clear definition of the glacier base and the cracks in the ice above.

Data compliments of Carleton University, Department of Geology, Canada



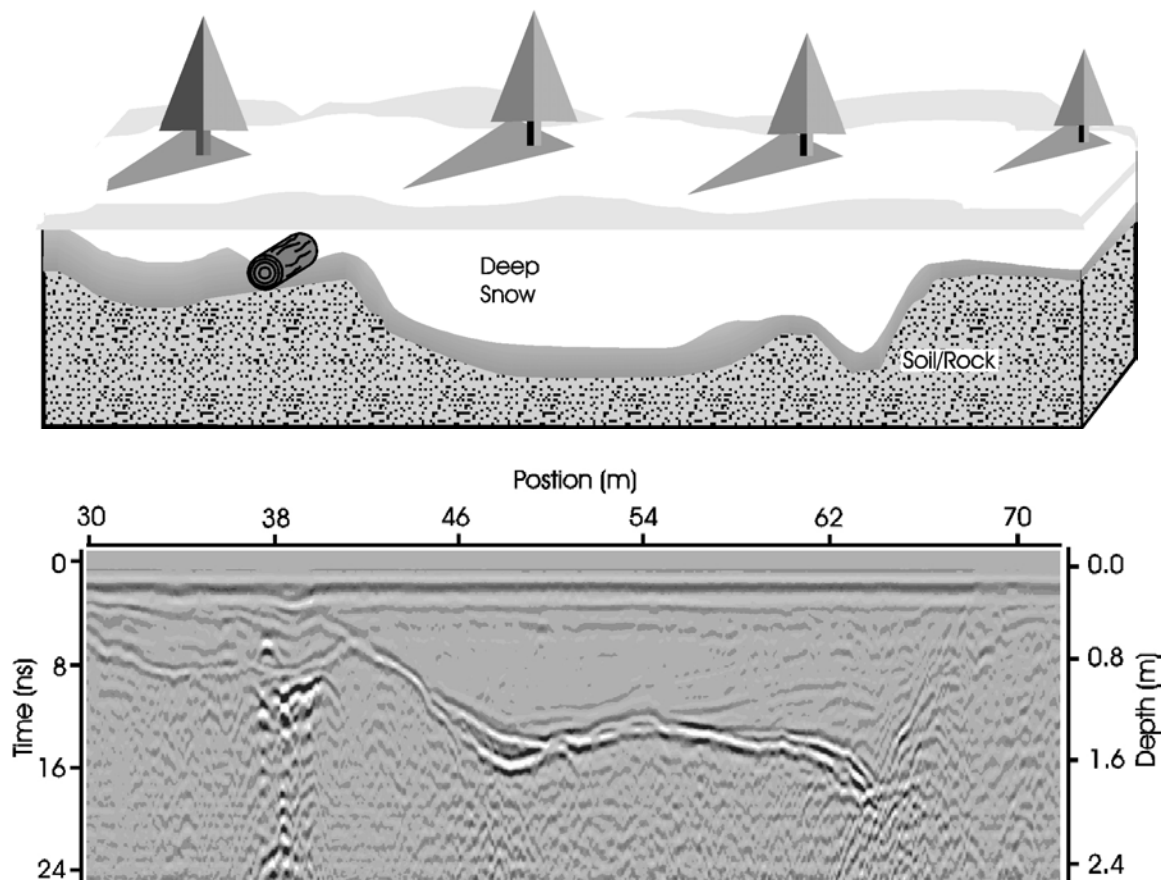
WATER CONTENT IN SNOW

Measuring snow thickness is a fairly straightforward application for ground penetrating radar (GPR). Portable GPR systems mounted on sleds, vehicles, or towed by skiers can quickly profile snow depth. GPR also gives users the power to estimate water content of snow, making it an optimal tool for snow studies.

These data were obtained using a pulseEKKO 1000 system with 900 MHz antennas during a survey at a hydroelectric power generation research area in Svalbard, Norway. In this case the water content of the snow was the information required to estimate the availability of water for hydro power generation. The data collected distinctly show the snow thickness and the location of buried objects. Water content was found by acquiring CMP velocity soundings through the snow and combining these with the reflection profiles shown above, using the integrated pulseEKKO software.

The speed of snow pack mapping combined with the ability to estimate water content are used in hydroelectric flow models, which help plan reservoir capacity for power generation. The ability to detect buried objects can be very useful in avalanche areas, where time is of the essence when locating buried victims.

Data compliments of TS Geokonsult, Sweden



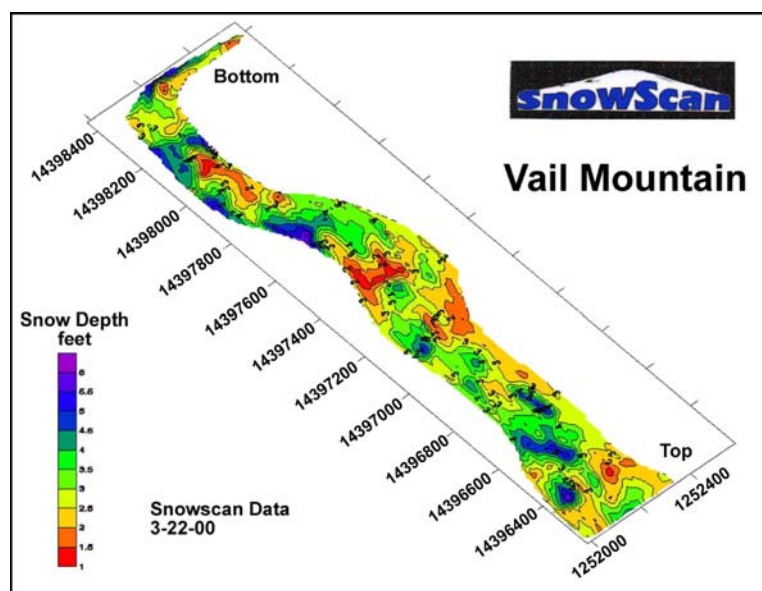
SKI SLOP SNOW THICKNESS MAPPING

Historically, GPR practitioners have looked at GPR cross sections as the fundamental information. Some applications no longer look at GPR sections but treat them as a given and only display derived data. This is a sign of increasing maturity and eventually one will seldom see raw GPR sections used for presentation or interpretation. More and more derived products of various attributes (reflectivity impedance) and quantitative numbers (depth, target size, etc.) will be extracted which are specific to a particular application.

A good example is the SnowScan snow thickness application. In the initial measurement process, the data were displayed as radar sections. Within months the application had auto picking and tracking capability which displayed a snow depth profile and could output the information as a single depth number versus position using GPS (global positioning system) location. In its current embodiment the system no longer needs to display radar data (or any data for that matter) but logs snow thickness along with the GPS coordinates. These data are normally transformed into maps without ever looking at the raw GPR cross section.



Photos of a compact, lightweight SnowScan GPR designed specifically to measure snow depth and combine with GPS positioning.



Example of a snow depth map created using a SnowScan GPR system.

ICE ROADS & GPR

GPR for ice thickness measurements on glaciers is well known. Less well known is that measuring ice thickness for roads is another GPR application. Ice roads are a common transportation link in northern regions of Canada, Alaska and northern Europe. Quite often ice roads provide the only economical way to get materials to-and-from remote mining communities and petroleum exploration sites.

The history of GPR ice road thickness goes back to the 1970's. In the early days of oil and gas developments in Alaska and in Canada's Northwest Territories, GPR was used for an umber of applications, one of which was measuring ice thickness. Sensors & Software's staff was actively involved in pioneering activities which demonstrated the viability of GPR for ice road evaluation in the Arctic.

For those not familiar with ice roads, these roads are constructed on natural bodies of water such as lakes, rivers, and streams after the onset of natural bodies of freezing occurs in the winter. The major question, of course, is how safe is the ice for a vehicle? Often the snow cover is plowed off the ice to encourage thickening of the ice so it has the strength to carry larger trucks and other heavy vehicles.

In addition to roads, temporary aircraft runways are constructed on ice. As with the roads, it is important to know ice thickness and to determine if degradation is occurring. Thinning ice occurs because of change in current patterns, warming weather conditions or ice movement.

Recently surges in oil and gas prices have stimulated exploration and development in northern areas again. As a result, this has stirred interest in GPR for construction of safe ice roads and monitoring their condition during winter operations.



Figure 1: GPR mounted behind a truck on the Mackenzie River delta near Inuvik, Canada.

Figure 1 shows a recent installation on a truck. This system was mounted on a vehicle for regular evaluation of ice thickness on an ice road in the Mackenzie River delta. In this case, the sensor is towed behind a pick-up truck; sometimes a lighter vehicle such as skidoo is used. In some risky applications, the operators prefer to push the transducer ahead of the vehicle rather than trail it behind for obvious safety reasons.



Figure 2: The ice thickness monitor mounted in the cab of the pick-up truck gives the operator a real time read-out of ice thickness.

Figure 2 shows the operation and control part of the system which provides a monitor of ice thickness in real time. The display is mounted in the truck cab right beside the driver so a view of ice thickness is available at all times.

Positioning of the data can be done in a number of manners. One can use an odometer wheel, landmarks or a GPS positioning system to get coordinates. The particular configuration is dependent on the particular needs of the application. The Sensors & Software Inc. DVL (digital video logger) is designed to readily accommodate all options.

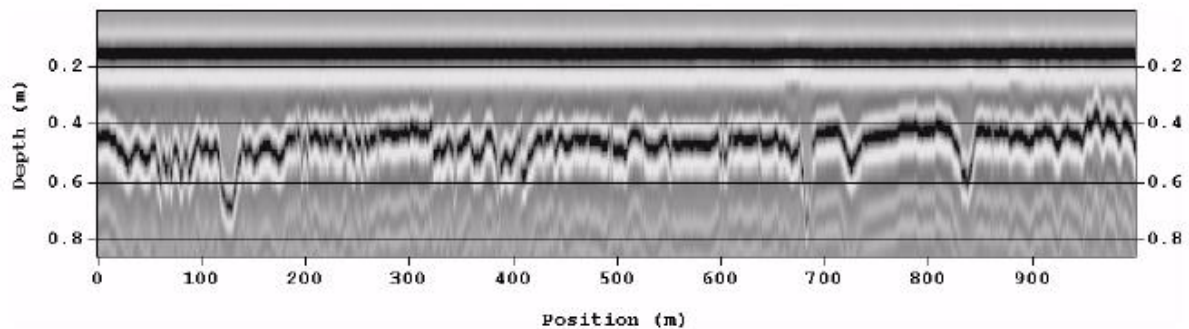


Figure 3: Example profile of ice thickness on a 1 km stretch of the Mackenzie River delta obtained in December 2000.

Figure 3 presents a sample profile of data from the Mackenzie River delta. Ice at this site was about 30 to 70 cm thick. A 500 MHz bandwidth GPR transducer was used for this particular survey operation. The data were acquired at about 30 km/hour.

This novel use of GPR is just another example of the breadth of GPR applications. The fascinating application of GPR will no doubt stimulate other applications for the technology in snow and ice as imaginations are put to work.

10.9 EDUCATIONAL MATERIAL

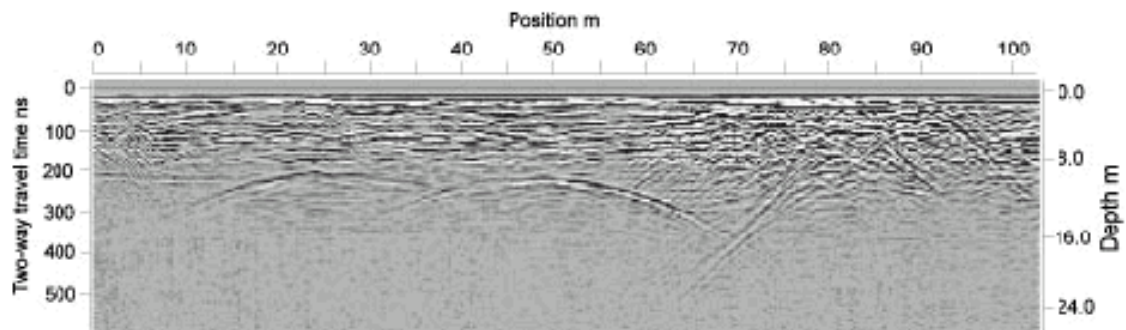
GPR FREQUENCY SELECTION

A major factor in the success of your ground penetrating radar (GPR) survey is the use of the correct antenna frequency. Defining a goal before you start will help ensure that you get the desired results. This case history demonstrates the effects of different antenna frequencies used on the same site.

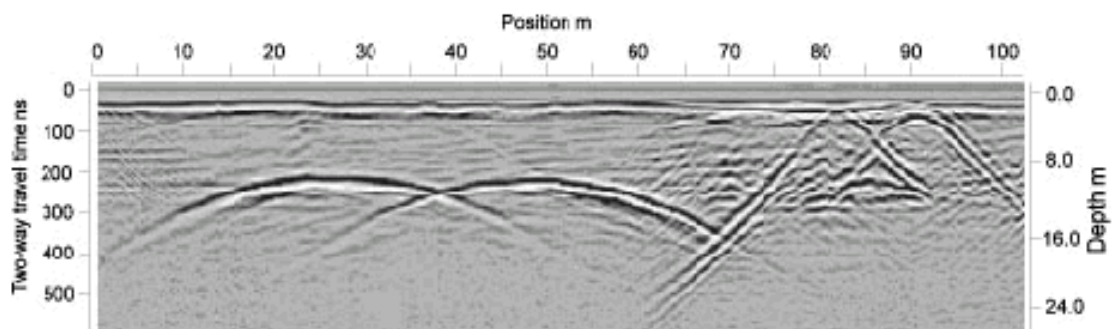
The pulseEKKO GPR data below were collected over two highway tunnels in Sweden. The first data set was collected with 100 MHz antennas. The data indicate the two road tunnels cut through the bedrock, and also shows bedrock stratigraphy. Note that the tunnel reflectors are weak and the gneissic bedrock texture events are strong.

The second data set, collected with 50 MHz antennas, show much stronger returns from the two tunnels. Note that these data more readily locate a culvert and a communications cable to the right of the tunnels, shown by arches on the right. Note that this data set is much less cluttered by the bedrock texture.

This is one example of how proper antenna frequency can effect the outcome of your survey. If the objective is large scale structure mapping, the 50 MHz data nicely define underground structures with minimal bedrock feature interference. On the other hand, if the purpose is to map mass stability, for tunnel maintenance and repair, the 100 MHz data will provide more information of potentially hazardous bedrock conditions.



100 MHz pulseEKKO data detect two highway tunnels plus finescale bedrock features.



50 MHz pulseEKKO data enhance major feature response and reduce clutter.

DATA MIGRATION

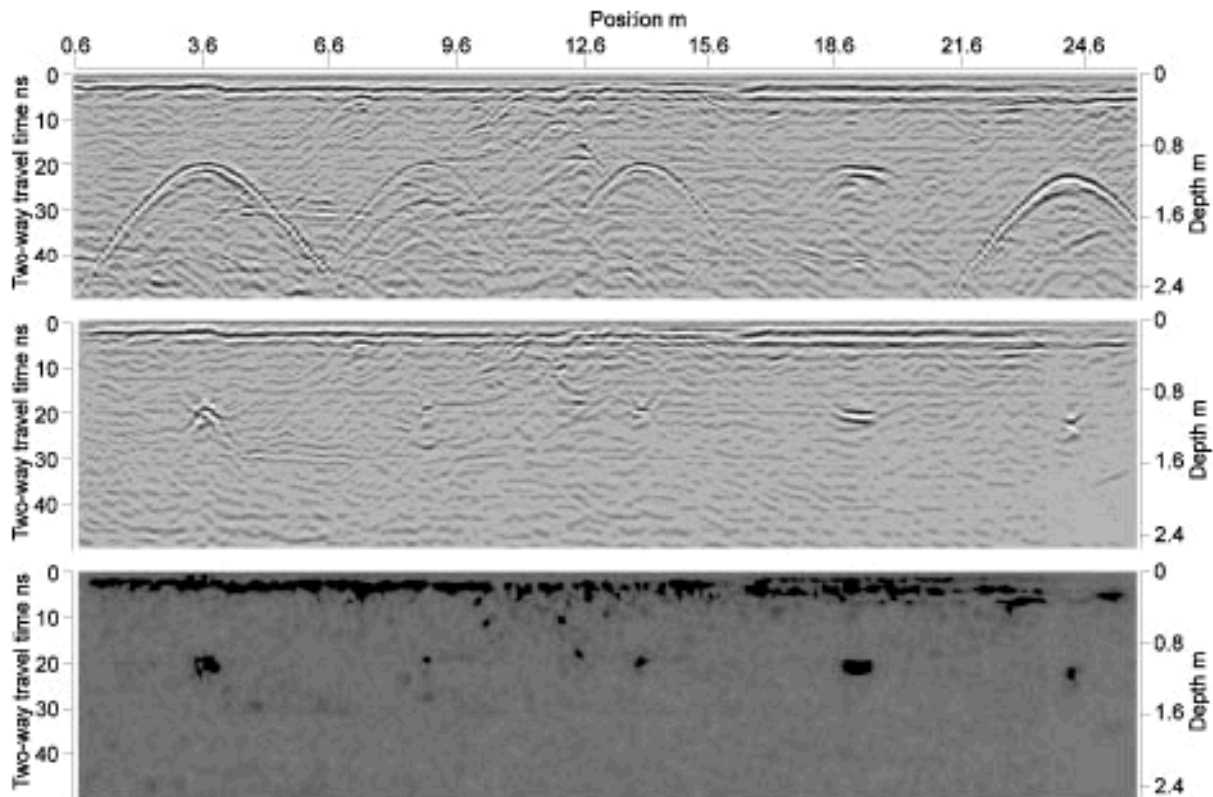
Once ground penetrating radar (GPR) profiles are obtained, migration of the image data can reconstruct the appearance of targets to more closely resemble the original geometry. The ability to display data in different forms helps in the interpretation of data.

The data below were acquired at a test site with buried pipes and barrels. The raw data in Figure 1 are what you would see without any migration. The pipes and barrels exhibit classic hyperbolic responses which are indicative of localized types of targets.

The data shown in Figure 2 is result of applying an F-K migration algorithm to the unmigrated data set assuming a constant background velocity. This migrated data shows a more correct representation of the ground.

The data displayed in Figure 3 are further processing of the migrated data set (Figure 2), which give a fuzzy image of the actual targets. The small pipes at nine and 14 meters are sharpened to point-like events. The 0.5 meter diameter pipe at 4 meters and the barrels at 19 and 24 meters remain extended in space.

Note that while the different displays of data are optimal for interpretation, most experienced GPR users find the classic hyperbolic shapes as shown in the first data set more readily identifiable.



11 REFERENCES

- Alumbaugh, D.L. and Newman, G.A., 1994, **Fast Frequency-Domain Electromagnetic Modeling of a 3-D Earth Using Finite Differences**: Extended Abstracts from the Society of Exploration Geophysicists 1994 Annual Meeting, Los Angeles, California, pp. 369-373.
- Annan, A.P., 1974, **The Equivalent Source Method for Electromagnetic Scattering**, Ph.D. Thesis, Memorial University.
- Annan, A.P. and Chua, L.T., 1992, **Ground Penetrating Radar Performance Predictions**: The Geological Survey of Canada, Paper 90-4, pp. 5-13.
- Annan, A.P. and Davis, J.L., 1976, **Impulse Radar Soundings in Permafrost**: Radio Science, Vol. 11, pp. 383-394.
- Annan, A.P. and Davis, J.L., 1977, **Radar range analysis for geological material**; Report of Activities, Part B, Geological Survey of Canada, Paper 77-1B, p. 117-124.
- Annan, A.P. and Davis, J.L., 1978, **Methodology for Radar Transillumination Experiments**: Report of Activities, Geological Survey of Canada, Paper, 78-1B, pp. 107-110.
- Annan, A.P., Davis, J.L., and Gendzwill, D., 1988, **Radar Sounding in Potash Mines: Saskatchewan, Canada**. Geophysics, Vol. 53, pp. 1556-1564.
- Annan, A.P. and Cosway, S.W., 1992, **Ground Penetrating Radar Survey Design**: Proceedings of the Symposium on the Application of Geophysics to Engineering and Environmental Problems, SAGEEP'92, April 26-29, 1992, Oakbrook, IL, pp. 329-351.
- Annan, A.P. and Cosway, S.W., 1994, **GPR Frequency Selection**: Proceedings of the Fifth International Conference on Ground-Penetrating Radar, Kitchener, Ontario, Canada, June 12-16, 1994, pp. 747-760.
- Annan, A.P. and Cosway, S.W., 1992, **Simplified GPR Beam Model for Survey Design**, Extended abstract of 62nd Annual International Meeting of the Society of Exploration Geophysicists, New Orleans, 1992.
- Annan, A.P., 1993, **Practical Processing of GPR Data**: Proceedings of the Second Government Workshop on Ground Penetrating Radar, October, 1993, Columbus, Ohio.
- Annan, A.P., Davis, J.L. and Johnston, G.B., 1997, **Maximizing 3D GPR Image Resolution: A Simple Approach**: Proceedings of the High Resolution Geophysics Workshop, University of Arizona, Tucson, AZ, January 6-9, 1997.
- Annan, A. P., 1996, **Transmission Dispersion and GPR**, JEEG, Vol. 0, January 1996, p. 125-136.
- Annan, A.P., 1973, **Radio Interferometry Depth Sounding: Part I - Theoretical Discussion**: Geophysics, Vol. 38, p. 557-580.
- Annan, A.P., Waller, W.M., Strangway, D.W., Rossiter, J.R., Redman, J.D., and Watts, R.D., 1975, **The Electromagnetic Response of a Low-Loss, 2-Layer Dielectric Earth for Horizontal Electric Dipole Excitation**: Geophysics V. 40 p. 285-298.
- Annan, A.P., Redman, J.D., Pilon, J.A., Gilson, E.W., and Johnston, G.B., 1997, **Crosshole GPR for Engineering and Environmental Applications**. Proceedings of the High Resolution Geophysics Workshop, University of Arizona, Tucson, AZ, January 6-9, 1997.
- Bailey, J.T., Evans, S. and Robin G. de Q., 1964, **Radio echo sounding in polar ice sheets**: Nature, Vol. 204, No. 4957, p. 420-421.
- Banos, A., 1962, **Dipole Radiation in the Presence of a Conducting Half-Space**, Pergamon Press.
- Barakat, N., Dolphin, L., et al., 1975, **Electromagnetic Sounder Experiments at the Pyramid of Giza**: Final Report, NSF Grant No. GF-38767, Stanford Research Institute, Menlo Park, California.

- Benson, R.C., Glaccum, R.A. and Noel, M.R., 1984, **Geophysical Techniques for Sensing Buried Wastes and Waste Migration**. US EPA Contract No. 68-03-3053. Environmental Monitoring Systems Laboratory. Office of R&D. US EPA, Las Vegas, Nevada 89114. 236p.
- Bentley, C.R., 1964, **The structure of Antarctica and its ice cover**: Research in Geophysics, Vol. 2: Solid Earth and Interface Phenomena, Cambridge Mass., Technology Press of Massachusetts Institute of Technology, p. 335-389.
- Bergmann, T., Blanch, J.O., Robertsson, J.O.A., Holliger, K., 1999, **A simplified Lax-Wendroff correction for staggered-grid FDTD modeling of electromagnetic wave propagation in frequency-dependent media**, Geophysics, Vol. 64, pp. 1369-1377.
- Bergmann, T., Robertsson, J.O.A., and Holliger, K., 1996, **Numerical properties of staggered finite-difference solutions of Maxwell's equations for ground-penetrating radar modeling**, Geophys. Res. Lett., 23, pp. 45-48.
- Berkhout, A. J., 1984, **Seismic Resolution: Resolving Power of Acoustical Echo Techniques**. Geophys. Press.
- Bevan, V. and Kenyon, J., 1975, **Ground-penetrating radar for historical archaeology**: MASCA Newsletter, Vol. II, No. 2, University of Pennsylvania Museum of Applied Science Center for Archaeology, Philadelphia, Pennsylvania.
- Bleistein, N. and Gray, S.H., 2001, **From the Hagedoorn imaging technique to Kirchhoff migration and inversion**, Geophysical Prospecting, Vol. 49, pp. 629-643.
- Born, M., & Wolf, E., 1980, **Principles of Optics**. 6th Edition, Pergamon Press.
- Brekhovskikh, L.M., 1960, **Waves in Layered Media**, New York, Academic Press.
- Brewster, M.L., 1993, **Observed migration of a controlled DNAPL release by ground penetrating radar**. M.Sc. Thesis, University of Waterloo.
- Brewster, M.L. and Annan, A.P., 1994, **Ground-penetrating radar monitoring of a controlled DNAPL release: 200 MHz radar**: Geophysics, Vol. 59, P. 1211-1221.
- Burhl, M., Vermeer, G.J.O., Kiehn, M., 1996, **Fresnel Zones for Broadband Data**, Geophysics, 61, No. 2, p 600 - 604.
- Cai, J. and McMechan, G.A., 1995, **Ray-based Synthesis of Bistatic Ground-Penetrating Radar Profiles**, Geophysics, Vol. 60, pp. 87-96.
- Carcione, J.M., 1996, **Ground-penetrating radar: Wave theory and numerical simulation in lossy anisotropic media**, Geophysics, Vol. 61, p. 1664-1677.
- Casper, D.A. and Kung, K-J.S., 1996, **Simulation of Ground-Penetrating Radar Waves in a 2-D Soil Model**, Geophysics, Vol. 61, pp. 1034-1049.
- Cook, J.C., 1973, **Radar Exploration Through Rock in Advance of Mining**, Trans. Society Mining Engineers, AIME, V. 254, pp. 140-146.
- Coon, J.B., Fowler, J.C. and Schafers, C.J., 1981, **Experimental Uses of Short Pulse Radar in Coal Seams**, Geophysics, Vol. 46, No. 8, pp. 1163-1168.
- Cerveny, V. and Ravindra, R., 1971, **Theory of Seismic head waves**, University of Toronto, Press, pp. 312
- Davis, J.L., and Annan, A.P., 1989, **Ground Penetrating Radar for High-Resolution Mapping of Soil and Rock Stratigraphy**, Geophysical Prospecting, 37 p. 531-551.
- Davis, J.L., and Annan, A.P., 1986, **Borehole Radar Sounding in CR-6, CR-7 and CR-8 at Chalk River, Ontario**, Technical Record TR-401, Atomic Energy of Canada Ltd.

- Davis, J.L., and Annan, A.P., 1989, **Ground Penetrating Radar for High-Resolution Mapping of Soil and Rock Stratigraphy**, Geophysical Prospecting, Vol. 37, pp. 531-551.
- Davis, J.L., Annan, A.P., Black, G., and Leggatt, C.D., 1985, **Geological sounding with low frequency radar**: in Extended Abstracts, 55th Annual International Meeting of the Society of Exploration Geophysicists, Washington, D.C.
- Davis, J.L., Annan, A.P., and Vaughan, C.J., 1985, **Placer Exploration Using Radar and Seismic Methods**, Canadian Institute of Mining Bulletin 80, (898), pp. 67-72.
- Davis, J.L., Heginbottom, J.A., Annan, A.P., Duncan, K.E., **Plan-View Presentation of GPR Data**, Proceedings of the Seventh International Conference on Ground Penetrating Radar (GPR '98), University of Kansas, Lawrence, KS
- Dix, C.H., 1956, **Seismic Prospecting of Oil**, Harper, New York.
- Dolphin, L.T., et al., 1978, **Radar Probing of Victorio Peak, New Mexico**: Geophysics, Vol. 43, No. 7, p. 1441-1448.
- Doolittle, J.A., and Asmussen, L.E., 1992, **Ten years of applications of Ground Penetrating Radar by United States Department of Agriculture**, Proceedings of the Fourth International Conference on Ground Penetrating Radar, Geological Survey of Finland, Special Paper 16, p. 139-147.
- El Said, M.A.H., 1956, **Geophysical prospection of underground water in the desert by means of electromagnetic interference fringes**, Pro. I.R.E., v. 44, p. 24-30 and 940.
- Endres, A. L. and Knight, R., 1992, **A theoretical treatment of the effect of microscopic fluid distribution on the dielectric properties of partially saturated rocks**, Geophysics Prospector, vol. 40, p. 307 - 324
- Evans, S., 1965, **Dielectric properties of ice and snow - a review**, Journal of Glaciology, Vol. 5, No. 42, p. 773-792.
- Fisher, E., McMechan, G.A., and Annan, A.P., 1992, **Acquisition and processing of wide-aperture ground penetrating radar data**: Geophysics, 57, p. 495.
- Fisher, E., McMechan, G.A., Annan, A.P., and Cosway, S.W., 1992, **Examples of reverse-time migration of single-channel, ground-penetrating radar profiles**, Geophysics, 57, p. 577-586.
- Friere, S.L.M., and Ulrych, T.J., 1988, **Application of singular decomposition to vertical seismic profiling**, Geophysics, v. 53, n. 6, p. 778-785.
- Gerlitz, K., Knoll, M.D., Cross, G.M., Luzitano, R.D., and Knight, R., 1993, **Processing ground penetrating radar data to improve resolution of near-surface targets**, Proceeding of the Symposium on the Application of Geophysics to Engineering and Environmental Problems, San Diego, California.
- Giannopoulos, A., 1997, **The investigation of Transmission Line Matrix and Finite-Difference Time-Domain Methods for the Forward Problem of Ground Probing Radar**, D. Phil thesis, Department of Electronics, University of York, UK.
- Gilson, E.W., Redman, J.D., Pilon, J.A., and Annan, A.P., 1996, **Near Surface Applications of Borehole Radar**. Proceedings of the Symposium on the Application of Geophysics to Engineering and Environmental Problems, April 28 - May 2, 1996, Keystone, Colorado, pp. 545-553.
- Goodman, D., 1994, **Ground-Penetrating Radar Simulation in Engineering and Archaeology**, Geophysics, Vol. 59, pp. 224-232.
- Grant, F.S. and West, G.F., 1965, **Interpretation Theory in Applied Geophysics**, McGraw-Hill.
- Grasmueck, M., 1996, **3-D Ground-Penetrating Radar Applied to Fracture Imaging in Gneiss**, Geophysics, Vol. 61, pp. 1050-1064.
- Greaves, R.J., Lesmes, D.P., Lee, J.M. and Toksoz, M.N, **Velocity Variation and Water Content Estimated from Multi-Offset, Ground Penetrating Radar**, Geophysics, Vol. 61, No. 3, May-June 1996, pp. 683-695.

- Greaves, R.J. and Toksoz, M.N., 1994, **Applications of Multi-Offset, Ground-Penetrating Radar**, Proceedings of the Symposium on the Application of Geophysics to Engineering and Environmental Problems, SAGEEP'94, pp. 775-793.
- Green, A., Holliger, K., Horstmeyer, H., Maurer, H., Tronicke, J., van der Kruk, J., 2002, **3D acquisition, processing and imaging of Ground Penetrating Radar Data**, GPR 2002 Tutorial 2 Notes, Proceedings of the Ninth International Conference on Ground Penetrating Radar (GPR 2002), Santa Barbara, California, April 29 – May 2, 2002.
- Hansen, S., 1942, **Electrical Wave Analysis**, US Patent 2,280,524.
- Hasted, J. B., 1972, **Liquid water -dielectric properties: in Water a comprehensive treatise**, v. 1, The physics and physical chemistry of water, F. Franks, ed., Plenum Press, NY, p.255-310
- Hohmann, 1987, **Numerical Modelling for Electromagnetic Methods of Geophysics**, Electromagnetic Methods in Applied Geophysics – theory: Volume 1, edited by M.N. Nabighian, Society of Exploration Geophysicists, pp. 313-361.
- Holliger, K. and Bergmann T., 2000, **Finite-difference modelling of borehole georadar data**, in press, Geophysics.
- Holser, W.T., Brown, R.J.S., Roberts, F.A., Fredriksson, O.A., and Unterberger, R.R., 1972, **Radar logging of a salt dome**: Geophysics, 37, P. 889-906.
- Holtzman, R. and Kastner, R., 2001, **The Time-Domain Discrete Green's Function Method (GFM) characterizing the FDTD Grid Boundary**, IEEE Transactions of Antennas and Propagation, Vol. 49, No. 7, July 2001, pp. 1079-1093.
- Jackson, J.D., 1962, **Classical Electrodynamics**, John Wiley and Sons.
- Jiracek, G.R., 1967, **Radio Sounding of Antarctic Ice**: Research Report Series 67-1, The University of Wisconsin, Geophysical & Polar Research Center, Department of Geology.
- Jol, H., 1996, **Digital Ground Penetrating Radar (GPR): A New Geophysical Tool for Coastal Barrier Research (Examples from the Atlantic, Gulf and Pacific Coasts U.S.A.)**, Journal of Coastal Research, Fall 1996.
- Kline, M. and Kay, I.W., 1965, **Electromagnetic Theory and Geometrical Optics**, Interscience Publishers, New York.
- Knapp, R. W., 1991, **Fresnel Zones in the Light of Broadband Data**: Geophysics, 56, P. 354 - 359.
- Lampe, B. and Holliger, K., 2000, **Finite-difference modelling of ground-penetrating radar antenna radiation**, 556 bis 560, Proceedings of the 8th International Conference on Ground Penetrating Radar, Gold Coast, Australia, May 23-26, 2000.
- Luneburg, R.K., 1964, **Mathematical Theory of Optics**, University of California, Press, Berkeley.
- Maijala, P., 1992, **Application of Some Seismic Data Processing Methods to Ground Penetrating Radar Data**, Fourth International Conference on Ground Penetrating Radar June 8-13, 1992, Rovaniemi, Finland. Geological Survey of Finland, Special Paper 16, 365 pages.
- McMechan, G.A., 1981, **Modeling of Zero-offset Profiles with Asymptotic Ray Theory**: Can J. Earth Sci., vol. 18, p. 551-560.
- Mooney, H. M. and Bleifuss, R., 1953, **Magnetic Susceptibility Measurements in Minnesota, Part II, Analysis of field results**, Geophysics, vol. 18, p 383-393.
- Moran, M.L. and Arcone, S.A., 2000, **GPR radiation pattern effects on 3D Kirchhoff Imaging**, Proceedings of the 8th International Conference on Ground Penetrating Radar, Gold Coast, Australia, May 23-26, 2000.

- Morey, R.M., 1974, **Continuous Subsurface Profiling by Impulse Radar**: Proceedings of Engineering Foundations Conference on Subsurface Exploration for Underground Excavations and Heavy Construction, Henniker, N.H. p. 213-232.
- Neuf, D., Brown, D., and Jaracz, R., 1973, **Multioctave Double Balanced Mixer**: Microwave Journal, Vol. 16, No. 1 (Jan. 1973), pp. 13-14,
- Noon, D.A., Longstaff, D., Yelf, R.J., 1994, **Advances in the development of step frequency ground penetrating radar**; Fifth International Conference on Ground Penetrating Radar (GPR '94), Kitchener, ON, Canada, June 12-16, 1994, Vol. 1 of 3, p. 117-131.
- Oguz, U. and Levent, G., 2001, **Modelling of Ground-Penetrating-Radar Antennas with Shields and Simulated Absorbers**, IEEE Transactions on Antenna and Propagation, Vol. 49, No. 11, November 2001, pp. 1560-1567.
- Olhoeft, G.R., 1975, **The Electrical Properties of Permafrost**, Ph.D. Thesis, University of Toronto, 172 pages.
- Olhoeft, G.R., 1981, **Electrical Properties of Rock and Minerals Short Course Notes**, Pers. Com., 196 pages.
- Olhoeft, G.R., 1987, **Electrical Properties from 10^{-3} to 10^{+9} Hz - Physics and Chemistry**, Proceedings of the 2nd International Symposium on the Physics and Chemistry of Porous Media, American Institute of Physics Conference Proceedings, Vol. 154, pp. 281-298.
- Olhoeft, G.R., 1988, **Interpretation of Hole-to-Hole Radar Measurements**, Proceedings of the Third Technical Symposium on Tunnel Detection, January 12-15, 1988, Golden, CO, pp. 616-629.
- Oldenburg, D.W., McGillivray, P.R., and Ellis, R.G., 1993, **Generalized subspace method for large scale inverse problems**, Geophys. J. Internat., Vol. 144, pp. 12-20.
- Olsson, O., Falk, L., Forslund, O., and Sandberg, E., 1987, **Crosshole Investigations - Results from Borehole Radar Investigations**, Stripa Project TR 87-11. SKB, Stockholm, Sweden.
- Olsen, O., Anderson, P., Carlsten, S., Falk, L., Niva, D., and Sandberg, E., 1992. **Fracture Characterization in Crystalline Rock by Borehole Radar**, Ground Penetrating Radar, Geological Survey of Canada, Paper 90-4, pp. 139-150.
- Owen, T.R., 1981, **Cavity Detection Using VHF Hole to Hole Electromagnetic Techniques**: Proceedings of the Second Tunnel Detection Symposium, Colorado School of Mines, Golden CO, July 21-23, 1981, U.S. Army MERA-DOM, Ft. Belvoir, VA, pp. 126-141.
- Ott, H., 1941, **Reflexion and Brechung von Kugelwellen**: Effekte Q. Ordnung: Ann. Physik, v. 41, p. 443-466
- Powers, M.H. and Olhoeft, G.R., 1994, **Modeling Dispersive Ground Penetrating Radar Data**: Proceedings of the Fifth International Conference on Ground-Penetrating Radar, Kitchener, Ontario, Canada, June 12-16, 1994.
- Redman, J.D., Kunert, Gilson, E.W., M., Pilon, J.A., Annan, A.P., 1996, **Borehole Radar for Environmental Applications: Selected Case Studies**: Proceedings of the Sixth International Conference on Ground Penetrating Radar (GPR'96), September 30-October 3, 1996, Sendai, Japan.
- Rees, H.V., and Glover, J.M., 1992, **Digital enhancement of ground probing radar data, in ground penetrating radar**, ed. J. Pilon; Geological Survey of Canada, Paper 90-4, p. 187-192.
- Reitz, J.R. and F.J. Milford, 1960, **Foundations of Electromagnetic Theory**, Addison-Wesley.
- Roberts, R.L. and Daniels, J.J., 1996, **Analysis of GPR Polarization Phenomena**, JEEG, vol. 1, no. 2, p. 139-157.
- Roddy, D., 1992, **Cepstral analysis of subsurface data, in ground penetrating radar**, ed. J. Pilon; Geological Survey of Canada, Paper 90-4, p. 193-198.
- Rogers, P.G., Edwards, S.A., Young, J.A., and Downey, M., 1987, **Geotomography for the Delineation of Coal Seam Structure**, Geoexploration, Vol. 24, pp. 301-328.

- Sanders, K.A., 1994, **Characterization of DNAPL Movement in Saturated Porous Media Using Ground Penetrating Radar**, M.E. Thesis ER-4336, Dept. of Geology, Colorado School of Mines, Golden, CO. 258.
- Scaife, J.E., & Annan, A.P., 1991, **Ground Penetrating Radar - A Powerful, High Resolution Tool for Mining Engineering and Environmental Problems**; Paper presented at 93rd CIM Annual General Meeting, Vancouver, B.C., April 29 - May 1, 1991.
- Schmitt, H.J., Harrison, C.W., Williams, C.S., 1996, **Calculated and Experimental Response of Thin Cylindrical Antennas to Pulse Excitation**; IEEE Trans. on Antennas & Propagation, AP14, p. 120-126.
- Sigurdsson, T., 1993, **Ground Penetrating Radar for Geological Mapping**, Thesis, Aarhus University, Department of Earth Sciences, Aarhus, Denmark, August, 1993.
- Sigurdsson, T. and Overgaard, T., 1996, **Application of GPR for 3D Visualization of Geological and Structural Variation in a Limestone Formation**, Proceedings of the Sixth International Conference on Ground Penetrating Radar (GPR'96), September 30-October 3, 1996, Sendai, Japan.
- Simmons, G., Strangway, D., Annan, A.P., Baker, R., Bannister, L., Brown, R., Cooper, W., Cubley, D., deBettencourt, J., England, A.W., Groener, J., Kong, J.A., LaTorraca, G., Meyer, J., Nanda, V., Redman, J.D., Rossiter, J., Tsang, L., Urner, J., Watts, R., 1973, **Surface Electrical Properties Experiment**, in Apollo 17: Preliminary Science Report, Scientific and Technical Office, NASA, Washington, D.C., pp. 15-1 - 15-4.
- Smith, G.S., 198, **Directive Properties of Antennas for Transmission into a Material Half-Space**, IEEE Trans. Antennas propagate, vol AP-32, p. 232-246.
- Smythe, W.R., 1989, **Static & Dynamic Electricity**, Taylor & Francis, A SUMMA book, 1989.
- Sommerfeld, A., 1949, **Partial Differential Equations in Physics**, New York, Academic Press.
- Stewart, R.D. and Unterberger, R.R., 1976, **Seeing through rock salt with radar**: Geophysics, 41, P. 123-132.
- Stickley, G.F., Noon, D.A., Cherniakov, M., Longstaff, I.D., Leat, C.J., Li, C.W., 1998, **Gated Stepped-Frequency GPR Field Demonstrations**, Seventh International Conference on Ground-Penetrating Radar (GPR '98), University of Kansas, Lawrence, Kansas, USA, May 27-30, 1998, Volume 1, p. 343-347.
- Tarantolo, P.J., and Unterberger, R.R., 1978, **Radar detection of boreholes in advanced mining**: Geophys Prosp. 26, P. 359-382.
- Tarantola, A., 1987, **Inverse Problem Theory**, Elsevier Science E.V., Amsterdam
- Telford, W.M., Geldart, L.P., Sheriff, R.E., Keys, D.A., 1976, **Applied Geophysics**, Cambridge University Press.
- Theirbach, R., 1974: **Electromagnetic Reflections in Salt Deposits**: J. Geophys. 40, P. 633-637.
- Tillard, T., and Dubois, J-C., 1992, **Influence and lithology on radar echoes: analysis with respect to electromagnetic parameters and rock anisotropy**: Fourth International Conference on Ground Penetrating Radar June 8-13, 1992. Rovaniemi, Finland. Geological Survey of Finland, Special Paper 16, 365 pages.
- Todoschuck, J.P., Lafleche, P.T., Jensen, O.G., Judge, A.S., and Pilon, J.A., 1992, **Deconvolution of ground probing radar data, in ground penetrating radar**, ed. J. Pilon; Geological Survey of Canada, Paper 90-4, p. 227-230.
- Turner, G., 1992, **Propagation deconvolution**, Fourth International Conference on Ground Penetrating Radar June 8-13, 1992. Rovaniemi, Finland. Geological Survey of Finland, Special Paper 16, 365 pages.
- Topp, G.C., Davis, J.L. and Annan, A.P., 1980, **Electromagnetic Determination of Soil Water Content: Measurements in Coaxial Transmission Lines**, Water Resources Research, Vol. 16, No. 3, p. 574-582.
- Ulriksen, C.P.F., 1982, **Application of Impulse Radar to Civil Engineering**, Unpublished Ph.D. Thesis, Dept. of Engr, Geol., U. of Technology, Lund, Sweden, p. 175.

- Unterberger, R.R., 1978, **Radar propagation in rock salt**: Geophys. Prosp., 26, P. 312-328.
- van der Kruk, J., 2001, **Three dimensional imaging of multi-component ground penetrating radar**, Ph.D. Thesis, Delft University of Technology, pp. 242.
- Vickers, R.S., 1978, **Application of Resistivity and Radar Techniques to Archaeological Surveys**: SRI Technical Memorandum.
- Vickers, R.S. and Bollen, R.S., 1974, **An Experiment in the Radio Echo Sounding of Temperate Glaciers**: Final Report, Contract 14-08-0001-14650 for U.X. Geological Survey, Denver, Stanford Research Institute, Menlo Park, California.
- Vozoff, K., Smith, G.H., Hatherly, P.J., and Thompson, S., 1993, **An Overview of the Radio Imaging Method in Australian Coal Mining**, First Break, Vol. 10, (January 1993), pp. 13-21.
- Von Hippel, A.R., ed., 1954, **Dielectric Materials and Applications**, John Wiley and Sons, New York, 438 p.
- Wait, J.R., 1962, **Electromagnetic Waves in Stratified Media**, Pergamon Press, (Revised edition, 1970).
- Waite, A.H. and Schmidt, S.J., 1961, **Gross errors in height indication from pulsed radar altimeters operating over thick ice or snow**, IRE International Convention Record, Part 5, p. 38-54.
- Walford, M.E.R., 1964, **Radio echo sounding through an ice shelf**: Nature, Vol. 204, No. 4956, p. 317-319.
- Wang, T. and Tripp, A.C. 1996, **FDTD Simulations of EM Waves Propagation in a 3-D Media**, Geophysics, Vol. 61, pp. 110-120.
- Ward, S.H., Phillips, R.J., Adams, G.F., Brown, Jr., W.E., Eggleton, R.E., Jackson, P., Jordan, R., Linlor, W.I., Peoples, W.J., Porcello, L.J., Ryu, J., Schaber, G., Sill, W.R., Thompson, S.H. and Zelenka, J.S., 1972, **Apollo Lunar Sounder Experiment**, in Apollo 17: Preliminary Science Report, Scientific and Technical Office, NASA, Washington, D.C., p. 22-1 - 22-26.
- Watts, R.D., and England, A.W., 1976, **Radio-echo Sounding of Temperate Glaciers: Ice Properties and Sounder Design Criteria**. Journal of Glaciology, Vol. 21, No. 85, pp. 39-48.
- Wedepohl, E., 1993, **Radio Wave Tomography - Imaging Ore Bodies Using Radio Waves**, Expanded Abstracts, 3rd Technical Meeting of the South African Geophysical Association, Capetown South Africa, pp. 85-88.
- Wharton, R. P., Hazen, G. A., Rau, R. N., and Best, D. L., 1980, **Advancements in electromagnetic propagation logging**: Society Petroleum Engineering, Paper 9041.
- White, R.E., 1991, **Properties of instantaneous seismic attributes**, Geophysics: The Leading Edge of Exploration.
- Wills, R.H., 1992, **A digital phase coded ground probing radar**; Ground penetrating radar, ed. J. Pilon; Geological Survey of Canada, Paper 90-4, p. 231-235.
- Wright, D.L., Bradley, J.A., Grover, T.P., 1994, **Data acquisition systems for ground penetrating radar with example applications from the air, the surface and boreholes**; Fifth International Conference on Ground Penetrating Radar (GPR '94), Kitchener, ON, Canada, June 12-16, 1994, Vol. 3 of 3, p. 1075-1089.
- Xu, T., and McMechan, G.A., 1977, **GPR attenuation and its numerical simulation in 2.5-dimensions**, Geophysics, Vol. 62, pp. 403-414.
- Yee, K.S., 1966, **Numerical solutions of initial boundary value problems involving Maxwell's equations in isotopic media**, IEEE Trans. Ant. Propag., Vol. 14, pp. 302-307.
- Yilmaz, O., 1987, **Seismic Data Processing Series: Investigations in Geophysics**, Vol. 2, Society of Exploration Geophysicists, Tulsa.

Young, J.L. and Nelson, R.O., 2001, **A Summary and Systematic Analysis of FDTD Algorithms for Linearly Dispersive Media**, IEEE Antennas and Propagation Magazine, Vol. 43, No. 1, February 2001, pp. 61-77.

Zeng, X., McMechan, G.A., Cai, J., and Chen, H.W., 1995, **Comparison of Ray and Fourier Methods for Modeling Monostatic Ground-Penetrating Radar Profiles**, Geophysics Vol. 60, pp. 1727-1734.

GPR CONFERENCE REFERENCES

Proceedings of the International Workshop on the Remote Estimation of Sea Ice Thickness Centre for Cold Ocean Resources Engineering (C-CORE), St. John's Newfoundland, Sept. 25-26, 1979.

Proceedings of the Ground Penetrating Radar Workshop, Geological Survey of Canada, Ottawa, Ontario, Canada, May 24-26, 1988.

Abstracts of the Third International Conference on Ground Penetrating Radar, United States Geological Survey, Lakewood, Colorado, USA May 24-26, 1990.

Proceedings of the Fourth International Conference on Ground Penetrating Radar, Geological Survey of Finland, Rovaniemi, Finland, June 8-13, 1992.

Proceedings of the Fifth International Conference on Ground Penetrating Radar (GPR'94), Kitchener, Ontario, Canada, June 12-16, 1994.

Proceedings of the Sixth International Conference on Ground Penetrating Radar (GPR '96), Sendai, Japan, Sept. 30- Oct. 3, 1996.

Proceedings of the Seventh International Conference on Ground Penetrating Radar (GPR '98), Lawrence, Kansas, USA, May 27-30, 1998.

Proceedings of the Eighth International Conference on Ground Penetrating Radar (GPR 2000), Goldcoast, Australia, May 23-26, 2000, SPIE vol. 4084.

Proceedings of the Ninth International Conference on Ground Penetrating Radar (GPR 2002), Santa Barbara, California, Apr 29 - May 2, 2002.